

國立臺灣大學理學院化學研究所

碩士論文

Department of Chemistry
College of Science

National Taiwan University

Master Thesis



設計與合成人類胸苷酸激酶之抑制劑

Design and Synthesis of

Inhibitors against

Human Thymidylate Kinase

黃夢若

Meng-Ruo Huang

指導教授：方俊民 博士

Advisor: Jim-Min Fang, Ph.D.

中華民國 102 年 7 月

July, 2013



謝誌

時光飛逝，轉眼間研究所的兩年就這樣匆匆過了。想當初還只是個懵懵懂懂的大學畢業生，一腳踏進台大這個國內首屈一指的學術殿堂，還真怕自己程度跟不上大家。所幸在老師與學長姐們的協助下總算慢慢熬了過來，雖然過程歷經不少挫折，現在回首望去，也許那些都是磨練我們具備更佳抗壓性的必經之路吧！真的非常感謝指導教授方俊民老師在這兩年時間的諄諄教誨，每當我實驗遇到困難時，您總是非常有耐心的替我想辦法解決問題，才讓我得以順利的將實驗完成。此外，也很感謝您每年大方提供的出遊計畫和各種聚餐活動，讓我們在實驗之餘也能享受到精神上的調劑。陽明大學的張智芬老師，謝謝您提供我們生物活性實驗協助以及相關研究方向的建議，利用 TMPK 的抑制來對癌症進行治療真的是一項偉大的新發現。同為陽明大學的許世宜老師，感謝您替我們做的分子動態模擬實驗，也謝謝您親切的為我解答實驗不懂的地方。羅禮強老師，這麼晚才向您敲定口試時間深感抱歉，謝謝您提出的論文改進方向，讓我能將論文整理得更加完整。另外，實驗部份要特別感謝詹迺立老師替我們做蛋白質的結晶，效率超群的趙玉正小姐的 ESI-HRMS 分析，以及親切的蘇仁寬先生在 NMR 上的協助，每次都要麻煩你測 overnight 真是非常不好意思。

除了老師之外，實驗室的同仁也幫了我許多忙。個性穩健的怡禎學長，生化專家大溫學長，唱歌很有感情的公政學長，笑容親切的珈男學長，總是能提出很多問題的農森學長，充滿親和力又有趣的銘祥學長，以及又會唱歌又會招呼學弟妹的紹宏學長，希望你們在就業的路上都能平安順遂，財源滾滾。為人親切的俊霖學長，感謝你在我需要打 HPLC 時冒著吸到 chloroform 的危險教我純化技術。幽默風趣的志安哥哥，謝謝你在 meeting 時提出的建議，讓我獲益良多。生活作息超規律的北濤學長，每次看到你認真做實驗的態度總是自嘆不如，相信付出一定會有代價的！超級帥氣的正台灣男兒小彬彬學長，雖然剛開始覺得你像流氓(好像本來就是)，不過熟了之後真的覺得你人超 nice！感謝你在我碩一時像保母一樣的將我拉拔長大，讓我學到不少實驗知識和技巧，現在想起當初作伙「買涼的」都覺得格外懷念呢！希望你能趕快找到合適對象，來個閃電結婚也不錯唷。外表看起來超年輕的育禎學姐，雖然覺得你就這樣休學有點可惜，不過相信你也是做了一番評估才下定決心，祝福你和親愛的白頭偕老喔！飛到荷蘭從此成為脫韁野馬一去不復返的乳焜同學，很懷念當初和你一邊做報告一邊暢快聊天的感覺，希望你早日回國讓我們砲一下。總是很搞笑的密友佩琪姊姊，我的手機跟我說沒有你玩它的日子有些落寞耶，是否該回來露臉一下呢？希望你在台積能夠繼續奮鬥下去，不過錢要賺肝也要顧喔！笑容靦腆的瑋霖學長，每次看你報進度都覺得你真的好認真，相信這樣的態度到業界一定是備受肯定的，希望你感情事業都順順利利。盡責又會照顧學弟妹的蔡 MOMO，你的開朗個性總能讓實驗室活潑熱鬧許多，希望你能順利完成實驗，早日畢業。善解人意的凱哥，每次被你逼問八卦都有點招架不住的感覺，不過你真人很 nice 又很風趣，祝你實驗順利。體貼又美麗的思涵姊姊，從剛進實驗室一直

到畢業都麻煩你很多事情，謝謝你總是不厭其煩的幫我，相信現在實驗上的辛苦一定會有代價，再撐一下以後就是高薪貴婦了，期待被你丟紅色炸彈的那天，不過滷肉飯桌可以加點配菜嗎？人超 nice 的鵬皓學長，雖然沒有跟你聊很多，不過幾次接觸下來覺得你人很好，希望你能順利推上理想的學校。認真的哲哲學長，希望你實驗一切順利，早日畢業。外表看似嚴肅內心卻很幽默的氣象專家俞瑞哥，感謝你常常請我們吃美食，可惜我還是不爭氣的沒長胖，看樣子你乾脆列個美食清單給我比較快，祝你實驗順利，TG 組的大家長要 hold 住團隊唷！親愛的阿王，謝謝你這兩年來的陪伴，不論何時，你總能看出我的低潮並且陪我一起走過，今天之所以能順利畢業有一半的功勞都要歸功於你，真的很感謝。雖然你的題目時常遇到瓶頸，不過你的認真程度是大家有目共睹的，相信老天不會辜負這樣努力的你，要堅持下去唷！有點冒失唱歌卻很好聽的子瑋，一直覺得你是個很樂觀開朗的人，但是太過大而化之是優點也是缺點，你要自己好好衡量一下，然後實驗要加油喔，現在有學妹陪你奮鬥更要好好努力，fighting！實驗超厲害的隆誌學長，感覺你真的是念博班的料，要繼續加油下去！同為 TMPK 組的怡瑄學姊，有你加入之後讓我覺得自己終於不是孤軍奮鬥，謝謝你教了我很多生物方面的知識，以後實驗就靠你了，有問題歡迎與我聯絡。幽默的程健哥，很可惜你沒能繼續唸下去，不過現在有了愛情的滋潤加上不錯的工作，應該算是愛情事業兩得意吧，先跟你說聲恭喜囉！

很有自己規劃的小宥宥，兩年下來受你不少幫助，希望你口試和就業順利，和女朋友也能愛情長跑下去。認真又很有責任感的翊瑋，總覺得你常常給自己太大壓力，要記得適度的放鬆才能保持身心健康，祝你未來一切順遂。活潑又有原則的小單，剛開始覺得你酷酷的，久了才知道其實你是外冷內熱，雖然你很想承認，但我們終究是密友對吧，希望以後有機會還能分享彼此的心情跟想法唷！很有自己想法的乃維，看得出你對自己的要求以及堅持，不過努力之餘還是要記得放鬆一下，朝著自己的理想邁進吧！個性隨和又健談的宛蓁，感覺你也是蠻容易緊張的人，不過相信以你的能力應該能在畢業前做出不少 final，要對自己有信心！開朗風趣的日平，謝謝你以前常常在我忙不過來的時候幫我代班，實驗方面再加把勁就可以發 paper 了，加油，你可以的。自戀又多愁善感的年加，其實越跟你相處就越覺得你人不錯又搞笑，做事也很盡責，只是發條要上緊點，還有個性要再硬一些，然後少講些冷笑話，才不會常常句點，加油好嗎？常常放空卻又帶點喜感的昱婷，生物背景來做有機合成真是辛苦你了，雖然覺得休學有點可惜，不過既然你有自己的轉換目標就好好堅持下去吧！新進的碩一，苓瑋、哲瑄、仁堯、若綺、晏靈，以及助理子禎，每次到實驗室都覺得你們很認真，以後實驗室就靠你們這些新血了，加油！專題生哲凡、昱泓，和曹一包，看到你們對自己未來的規劃就很替你們開心，希望你們繼續朝夢想努力下去。蒼蒼、王婷、薇立，以及欣傳，希望你們不論是推甄和考試都能一切順利，早日成為研究生，享受做實驗的樂趣。

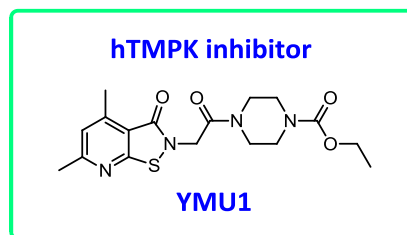
最後要感謝我的家人，願意一路支持我走到現在並且給予關心，還要忍受我的壞脾氣。沒有你們我就無法順利從這裡畢業，謝謝你們。同時也祝 JMF 的大家都實驗順利，日日有 data，月月發 paper，年年出專利！

摘要



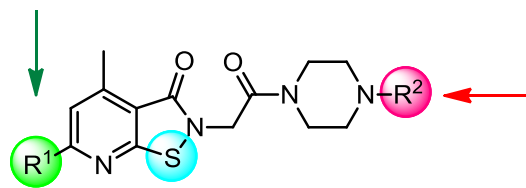
癌症一直以來是造成國人死亡率居高不下的原因，如何有效對抗癌症因此成為科學家致力研究的方向。目前醫療上廣泛應用的化療藥物小紅莓(doxorubicin)雖具有良好抑制效果，然而其嚴重的副作用也使得這個藥物的發展受到限制。因此找尋小分子抑制劑來敏化小紅莓對癌症的毒殺能力，進而降低其藥劑量便成為一個開發方向。

根據高通量藥物篩選的結果，YMU1 被發現對人類胸苷酸激酶(hTMPK)具有良好的抑制效果，同時在低劑量小紅莓的共同作用下，能選擇性對癌症細胞造成毒殺作用。因此在本篇論文裡，我將 YMU1 結構中的硫原子置換成其他原子，進而比較其結構與活性的關係。另外，為了改善 YMU1 的水溶性問題，設計一系列親水性 YMU1 衍生物也是我們研究的方向。最後，由於二聚體(dimer)結構的化合物具有比 YMU1 更好的抑制活性，我們合成不同的二聚體衍生物並測試其活性。



由目前合成的 30 個類似物來看，有 7 個衍生物已證實具有和 YMU1 相同，甚至更好的抑制活性。此外，我們也透過這些衍生物歸納出結構與活性之關係，包含硫原子確實在 YMU1 中扮演重要角色、環上的氫氧基能大幅提升 YMU1 衍生物之抑制活性，以及二聚體結構普遍具有良好的活性等，希冀能有助於未來的人類胸苷酸激酶抑制劑之開發。

Hydroxyl functional group may enhance the inhibition,
but amino group is ineffective.



Dimeric analogs show better
inhibition, whereas carboxylic
acid is unfavorable.

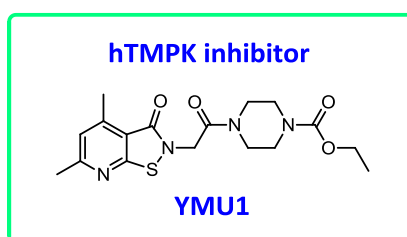
Sulfur atom is crucial
in heterocyclic core.



Abstract



Cancer has become one of the most fatal diseases in recent 30 years. Anti-cancer drugs such as doxorubicin, which can inhibit the function of type II topoisomerase, have been used extensively. However, doxorubicin treatment causes many side effects including vomit, hair loss, myelosuppression and cardiotoxicity. Searching for new drugs to cure cancer with reduced side effects from doxorubicin has become an important task. After screening a series of compounds, YMU1 was found to inhibit the activity of human thymidylate kinase (hTMPK), which plays an important role in synthesis of DNA. YMU1 could sensitize cancer cells to chemotherapeutic agent such as doxorubicin. The combined use of YMU1 and doxorubicin substantially inhibits tumor growth and reduces the side effect of doxorubicin.

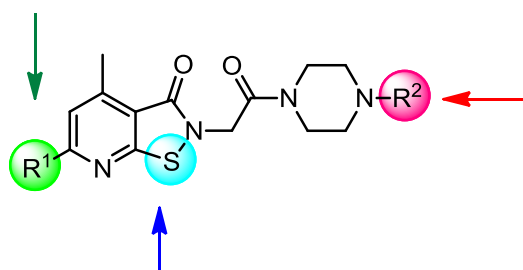


My research aims to modify the structure of YMU1 to find derivatives showing better inhibition against hTMPK. In order to test the importance of sulfur atom in YMU1,

the sulfur atom was replaced by other atoms and the inhibitory activities of such derivatives were compared with the sulfur-containing structure. To solve the low solubility of YMU1 in water, I also prepared YMU1 derivatives having high hydrophilicity good for animal experiments. Because dimeric compound has a potential to show better inhibition than YMU1, different cores of dimeric derivatives were synthesized.

Among the above-prepared derivatives, 7 compounds were proved to have either comparable or better inhibition than YMU1. We also made several conclusions for the relationship between structure and activity, including the crucial role of the sulfur atom in the heterocyclic core, the enhanced hTMPK inhibition with a hydroxyl group in the core structure, and better inhibition of the dimeric compounds. This study will be useful for the development of anticancer therapy.

Hydroxyl functional group may enhance the inhibition, but amino group is ineffective.



Dimeric analogs show better inhibition, whereas carboxylic acid is unfavorable.

Sulfur atom is crucial in heterocyclic core.

Table of Contents



Abstract in Chinese.....	I
Abstract in English.....	III
Table of Contents.....	V
Index of Figures.....	VIII
Index of Schemes.....	XII
Index of Tables.....	XIII
Abbreviations.....	XIV
Chapter 1. Introduction.....	1
1.1. Brief introduction of cancer.....	1
1.2. Inhibition of topoisomerase	2
1.3. Mechanism of DNA repair	5
1.4. Biosynthetic pathway of dTTP in cells.....	7
1.5. Antimetabolite agents targeting dTTP formation	8
1.6. Structure and physiology of TMPK	10
1.7. The relationship between the doxorubicin sensitization by TMPK inhibition to p53 status	13
1.8. Confirming the characteristic role of hTMPK during DNA repair.....	15

1.9. Screening inhibitors against hTMPK	21
Chapter 2. Results and Discussion	27
2.1.1. Structural feature of YMU1.....	27
2.1.2. Molecular dynamic simulation of YMU1 with TMPK.....	28
2.1.3. Specific YMU1 derivatives proposed in this study	29
2.1.4. Luciferase-coupled TMPK assay	30
2.1.5 General synthetic scheme.....	32
2.2.1. Replacement of the sulfur atom in heterocyclic core.....	32
2.2.2. Synthesis of piperazine linkers	34
2.2.3. Synthesis of YMU1 derivatives 13–17	35
2.2.4. Structure–activity relationship of compounds 3–7, 9 and 13–18.....	36
2.3.1. Hydrophilic YMU1 derivatives	38
2.3.2. Synthesis of hydrophilic derivatives	40
2.3.3. Structure–activity relationship of compounds 3, 20, 22–29, and 33–34.....	46
2.4.1. Dimeric inhibitors.....	52
2.4.2. Synthetic schemes for dimeric inhibitors	52
2.4.3. SAR of dimeric compounds 35, 38–39, and 42.....	55
2.5. Molecular docking of YMU1 derivatives.....	58
2.6. Conclusion	61



Chapter 3. Experimental Section.....	63
3.1. General part	63
3.2. Expression and purification of enzymes	64
3.3. Luciferase-coupled TMPK assay	64
3.4. NADH-coupled TMPK assay	65
3.5. Molecular docking	65
3.6. Synthetic procedures and characterization of compounds.....	66
References	99
Appendixes ¹H and ¹³C NMR spectra	109

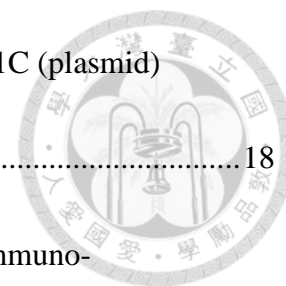


Index of Figures



Figure 1. Chemical structures of drugs targeting topoisomerases I and II	3
Figure 2. Mechanism of DNA homologous recombination.....	6
Figure 3. Biosynthetic pathways of cellular dTTPs.....	7
Figure 4. Chemical structures of drugs targeting thymidylate kinase (TS)	8
Figure 5. Mechanism of TS inhibition by 5-FU.....	9
Figure 6. Ribbon structure of human TMPK (PDB ID: 1E2F).....	11
Figure 7. Movement of human TMPK structures	12
Figure 8. dTTP pool size measurement of lentiviral TMPK ^{shRNA} and scramble ^{shRNA} in p53-proficient and p53-null HCT-116 cells.....	14
Figure 9. Comparison of TMPK and TS knockdown on doxorubicin-induced apoptosis in p53(+/+) and p53(-/-) HCT-116 cells	15
Figure 10. Combined treatment of doxorubicin and hTMPK inhibitor to trigger cell apoptosis	16
Figure 11. (a) γ H2AX foci staining of MDA-MB231 cells with or without TMPK silencing after recovery from doxorubicin	18
(b) XRCC1 foci staining of LacZ or UNG lentivirus infected cells recovered from doxorubicin treatment for 24 h	18

Figure 12. (a) pCMV2-YFP-Nuc (vector) or pCMV2-YFP-Nuc-R1C (plasmid)	
transfected into TMPK or TMPK knockdown cells	18
(b) Laser-micro-irradiation of HeLa cells followed by immuno-	
fluorescence staining.....	18
(c) γ H2AX foci staining of MCF-7 cells with TMPK, R2 and	
TMPK/R2 knockdown at the indicated time points.....	19
Figure 13. γ H2AX foci staining of MCF-7, H184B5F5/M10, and MCF-10A cells	
transfected with TMPK siRNA after DNA damage recovery	20
Figure 14. Flow cytometry of cells at the indicated time points after recovery from	
doxorubicin	20
Figure 15. Principles of NADH- and luciferase-coupled TMPK assays.....	22
Figure 16. Chemical structure of YMU1	24
Figure 17. (a) H184B5F5/M10, MCF10A, MCF-7, and HCT-116 $p53^{(-/-)}$ cells	
were treated with YMU1 or 5-FU at different concentration, and stained	
by crystal violet after 14 days	25
(b) γ H2AX foci staining of cells after treated with vehicle or YMU1	
along with doxorubicin exposure.....	25
Figure 18. (a) On treatment with vehicle or YMU1 for 72 h, followed by 4 h	
doxorubicin exposure, cells were incubated for colony formation over	



14 days	25
(b) Comparison of tumor growth in mice with combined treatment of YMU1 and doxorubicin or doxorubicin/YMU1 alone	25
Figure 19. Structure of YMU1	27
Figure 20. Some structural features of YMU1 derivatives	28
Figure 21. MD simulation of the mechanism of TMPK with or without YMU1	29
Figure 22. Stabilization of YMU1 in hTMPK via the π - π stacking interaction with Arg16.....	29
Figure 23. Specific YMU1 derivatives	30
Figure 24. Protocol of luciferase-coupled TMPK assay.....	31
Figure 25. Chemical structures of benzo[<i>d</i>]isothiazol-3(2 <i>H</i>)-one (BT), compounds 3–7, 9, 13–18 and YMU1	37
Figure 26. Chemical structures of compounds 3, 20, 22–29, 33 and 34.....	47
Figure 27. Dosage-dependent TMPK inhibition of YMU1, compounds 22, 29 and 33.	50
Figure 28. The chemical structure of dimeric TMPK inhibitor 35.....	52
Figure 29. Chemical structures of dimeric inhibitors 35, 38, 39, and 42 as well as suicide inhibitors 40 and 41	55
Figure 30. Dosage-dependent inhibition of YMU1 and dimeric compounds 35, 38, 39 and 42 against TMPK.....	57

Figure 31. Selected compounds for molecular docking.....	58
Figure 32. Docking of compounds 22 and 42 with hTMPK.....	60
Figure 33. Chemical structures of efficient hTMPK inhibitors	61
Figure 34. Structural features of YMU1 derivatives against hTMPK	62



Index of Schemes



Scheme 1. General synthetic scheme for YMU1 derivatives.....	32
Scheme 2. Synthesis of compound 12	35
Scheme 3. Synthesis of compounds 13–17	35
Scheme 4. Synthesis of compounds 20 and 22	41
Scheme 5. Synthesis of compounds 23 and 24	42
Scheme 6. Synthesis of compounds 25 and 26	42
Scheme 7. Synthesis of compounds 27 and 28	43
Scheme 8. Attempted synthesis of compound 29	43
Scheme 9. Synthesis of compound 29	45
Scheme 10. Synthesis of derivatives 33 and 34	46
Scheme 11. Synthesis of dimeric inhibitors 35 , 38 and 39	53
Scheme 12. Synthesis of compounds 40–42	54

Index of Tables

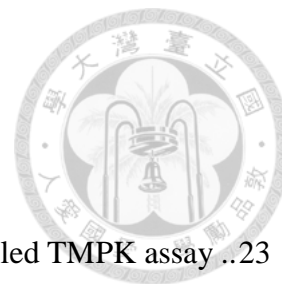


Table 1. Comparison of sensitivity in NADH- and luciferase-coupled TMPK assay ..	23
Table 2. Reaction conditions for the synthesis of compound 16	36
Table 3. Normalized TMPK inhibition of compounds BT, 3–7, 9, 13–18 and YMU1.	37
Table 4. Attempted protection of compound 22	44
Table 5. Synthesis of compound 34	46
Table 6. cLog P values and TMPK inhibition of compounds 3, 20, 22–29, 33 and 34	48
Table 7. Dosage-dependent assays of YMU1, compounds 22, 29 and 33 against TMPK	50
Table 8. Normalized TMPK inhibition of dimeric compounds 35 and 38–42 at 2 μ M	55
Table 9. Dosage-dependent assays of YMU1 and dimeric compounds 35, 38, 39 and 42 against TMPK	56
Table 10. K_i values of compounds 22 and 42 for hTMPK	59

Abbreviations



5-FU	5-fluorouracil
Ac	acetyl
ADP	adenosine 5'-diphosphate
Ala	alanine
AMP	adenosine 5'-monophosphate
AppNHp	adenosine 5'-(β,γ -imido)triphosphate lithium
Arg	arginine
Asp	aspartate
ATP	adenosine 5'-triphosphate
Bn	benzyl
Boc	<i>tert</i> -butoxycarbonyl
BSA	bovine serum albumin
BT	benzo[<i>d</i>]isothiazol-3(2 <i>H</i>)-one
CH₂THF	5,10-methylene tetrahydrofolate
cLog P	calculated lipophilicity
CPT	camptothecin
dADP	deoxyadenosine diphosphate
dCDP	deoxycytidine diphosphate

DIEA	diisopropylethylamine
DMAP	4-dimethylaminopyridine
DMF	<i>N,N</i> -dimethyl formamide
DMSO	dimethyl sulfoxide
DNA	deoxyribonucleic acid
dNTP	deoxyribonecleotide
dTDP	deoxythymidine diphosphate
dTMP	deoxythymidine monophosphate
DTNB	5,5'-dithiobis(2-nitrobenzoic acid)
dTTP	deoxythymidine triphosphate
dUDP	deoxyuridine diphosphate
dUMP	deoxyuridine monophosphate
dUTP	deoxyuridine triphosphate
EDTA	ethylenediaminetetraacetic acid
ESI	electrospray ionization
Et	ethyl
EtOAc	ethyl acetate
EtOH	ethanol
FdUMP	fluorodeoxyuridine monophosphate



FdUTP	fluorodeoxyuridine triphosphate
FITC	fluorescein isothiocyanate
FUTP	fluorouridine triphosphate
Glu	glutamate
Gly	glycine
HB	hydrogen bond
HJ	Holliday junction
HPLC	high-performance liquid chromatography
HR	homologous recombination
HRMS	high-resolution mass spectrum
hTMPK	human thymidylate kinase
IC₅₀	half maximal inhibitory concentration
IPTG	isopropyl-β-D-thiogalactopyranoside
IR	infrared
K_i^{app}	apparent inhibition constant
MD	molecular dynamics
Me	methyl
MeOH	methanol
mp	melting point



MW	molecular weight
NADH	nicotinamide adenine dinucleotide
NEt₃	triethylamine
NHEJ	non-homologous end joining
NMP	nucleotide monophosphate
NMR	nuclear magnetic resonance
PBS	phosphate buffered saline
Pd/C	palladium on carbon
PEP	phosphoenol pyruvate
PG	protecting group
Piv	pivaloyl
PPi	pyrophosphate
PTSA	<i>p</i> -toluenesulfonic acid
RNA	ribonucleic acid
RNR	ribonucleotide reductase
rt	room temperature
SAR	structure–activity relationship
shRNA	small hairpin RNA
siRNA	small interfering RNA



SSBs	single-strand breaks
TBAI	tetrabutylammonium iodide
TBDMS	<i>tert</i> -butyldimethylsilyl
TFA	trifluoroacetic acid
THF	tetrahydrofuran
TK	thymidine kinase
TLC	thin-layer chromatography
TOP2	topoisomerase II
TS	thymidylate synthase
UDG	uracil-DNA-glycosylase
UMP	uridine monophosphate
YFP	yellow fluorescent protein



Chapter 1. Introduction



1.1. Brief introduction of cancer

Cancer has remained top spot among the ten leading causes of death in Taiwan for 31 years. It is estimated that one person died of cancer in an average of every 3 minutes and 25 seconds, indicating the severe damage to human beings. Cancers usually arise from genomic instability,¹ making cells become uncontrolled in proliferation and differentiation. By genome evolution, cancer cells have potential to proceed metastasis to other locations in body through blood and lymphatic systems, endangering one's health enormously.

Oncogenes and tumor-suppressor genes have been confirmed to correlate with the production of cancers.² The former are genes that has the potential to cause cancer, while the latter are, as its name, the genes which help to restrain formation of cancers. Once the function of tumor-suppressor genes such as *Tp53* is disrupted, genomic instability drives cancer cell formation.³

Substances causing genomic mutation are called carcinogens, and can be roughly divided into three categories: chemical carcinogens, physical carcinogens, and biological carcinogens. Chemical carcinogens include organic and inorganic compounds, physical carcinogens contain radiation, especially ultraviolet and X-ray exposure, and biological

carcinogens comprise viruses and other microorganisms.



1.2. Inhibition of topoisomerase

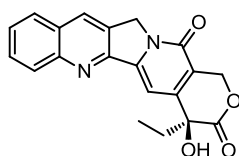
Each human cell contains DNA with approximately 1.8 m long, winding around the nucleus tightly.⁴ Due to the double-helix structure of DNA, it is crucial for DNA to unwind its double strands in order to obtain information from genes. Topoisomerase is an extremely important enzyme which contains a conserved tyrosine residue to react with phosphodiester bond in DNA, forming phosphotyrosine to cut the double strands. Once the break has formed, DNA can be untangled or unwound, followed by reconnecting DNA backbone to alter the topology.⁵

Topoisomerase can be divided into two types according to the number of strands cut in one round of performance.⁶ Type I topoisomerase cleaves one strand of DNA, making the other strand rotate around to release the stress from supercoiled and reanneal the break site. On the other hand, type II topoisomerase cleaves both strands in DNA double helix; thus, the unbroken DNA duplex can pass through the breakage. After religation, DNA loop may be able to increase or decrease the tension.

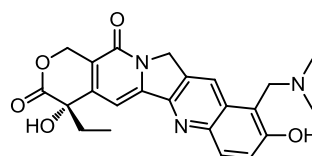
Since topoisomerase is essential for DNA functionality, several drugs and treatments are designed to target this enzyme (Figure 1). For example, camptothecin (CPT) and topotecan are widely used in clinical treatment against topoisomerase I.⁷

Chemotherapeutic agents targeting topoisomerase II (TOP2) are classified into two categories. The first class of compounds, which trap the enzyme intermediate, a TOP2–DNA covalent complex, resulting in permanent DNA lesion are called TOP2 poisons. The second class of compounds, which diminish enzymatic activity of TOP2 and lead to cell death pathway, are called TOP2 inhibitors. Most of the clinically active drugs are TOP2 poisons, including etoposide, mitoxantrone, and doxorubicin.⁸

Topoisomerase I inhibitors

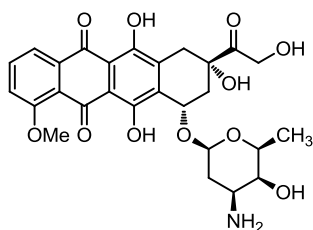


Camptothecin
(CPT)

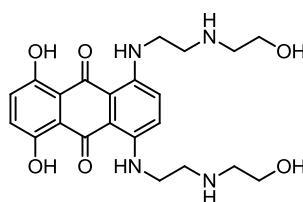


Topotecan

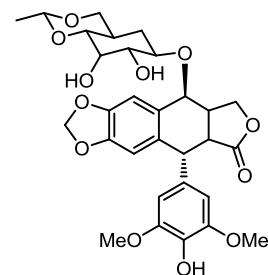
Topoisomerase II poisons



Doxorubicin

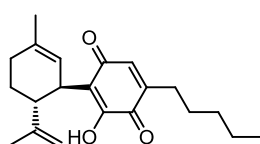


Mitoxantrone

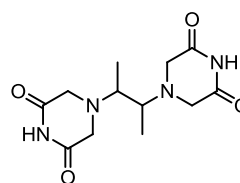


Etoposide

Topoisomerase II inhibitors

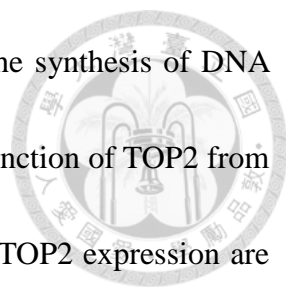


HU-331



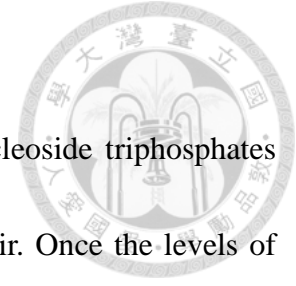
ICRF-193

Figure 1. Chemical structures of drugs targeting topoisomerases I and II.



Doxorubicin (adriamycin) is an antibiotic agent that blocks the synthesis of DNA by intercalating into DNA double strands, and further inhibits the function of TOP2 from religation. Cancer cells with rapid proliferation and high levels of TOP2 expression are most sensitive to doxorubicin. Doxorubicin is widely used for treating leukemias as well as cancers in breast, ovaries, multiple myeloma, and others.^{4, 9} However, the radical oxygen species (ROS) generated by interaction of doxorubicin with irons may result in severe side effects, such as cardiotoxicity,⁹ acute infection of bowels,¹⁰ and secondary malignancies.¹¹ Moreover, cancer cells showing resistance to doxorubicin has emerged by alteration of NADPH metabolism,¹² variation in cellular glutathione levels, and regulation of gene expression and TOP2 activity.¹³ Finding new drugs in combination with low dosage of doxorubicin to trigger cell apoptosis is a promising approach to cancer therapy.

1.3. Mechanism of DNA repair



To regulate the cellular concentrations of four deoxyribonucleoside triphosphates (dNTPs) is critical for DNA synthesis during replication and repair. Once the levels of dNTP pool are too high or too low, DNA may be prone to mutation. Ribonucleotide reductase (RNR), which catalyzes the reduction of ribonucleotides into the corresponding deoxyribonucleotides (dADP, dUDP, dCDP, and dGDP) through radical reaction, is composed of two different dimeric subunits often called R1 and R2. These two subunits are regulated by different cell cycles, with RNR controlled by the level of R2.¹⁴ Besides, R2 may be able to collaborate with multiple oncogenes for malignant transformation and tumorigenesis.¹⁵ R2 is often overexpressed in tumor cells,¹⁶ suggesting that R2 mediates the activity of DNA repair.

Double-strand breaks (DSB) can be repaired through non-homologous end joining (NHEJ) or homologous recombination (HR).¹⁷ NHEJ ligates the break ends directly without the assistance of homologous template, and mainly predominates in the G1 phase.¹⁸ Compared with NHEJ, HR repair takes place during S/G2 phases, and requires a long homologous strand (usually sister chromatids) to lead repair.^{18, 19} After DSB occurs, HR repair starts by resection at the 5' end on either side of the break, providing 3' overhangs of single strand DNA (Figure 2). Strand invasion then proceeds on a homologous template by 3' overhang strand to form a D-loop junction. Afterwards,

non-crossover and crossover products can be generated from synthesis-dependent strand annealing (SDSA) pathway or double-strand break repair (DSBR) pathway that forms an intermediate harboring two Holliday junctions (HJ).¹⁹ HR requires more than 10000 dNTPs for incorporation into DNA strands during DSB invasion.²⁰ Therefore, RNR that mediates the recruitment of dNTPs, with R2 expressing through S and G2/M phases,¹⁶ plays a significant role for HR repair.

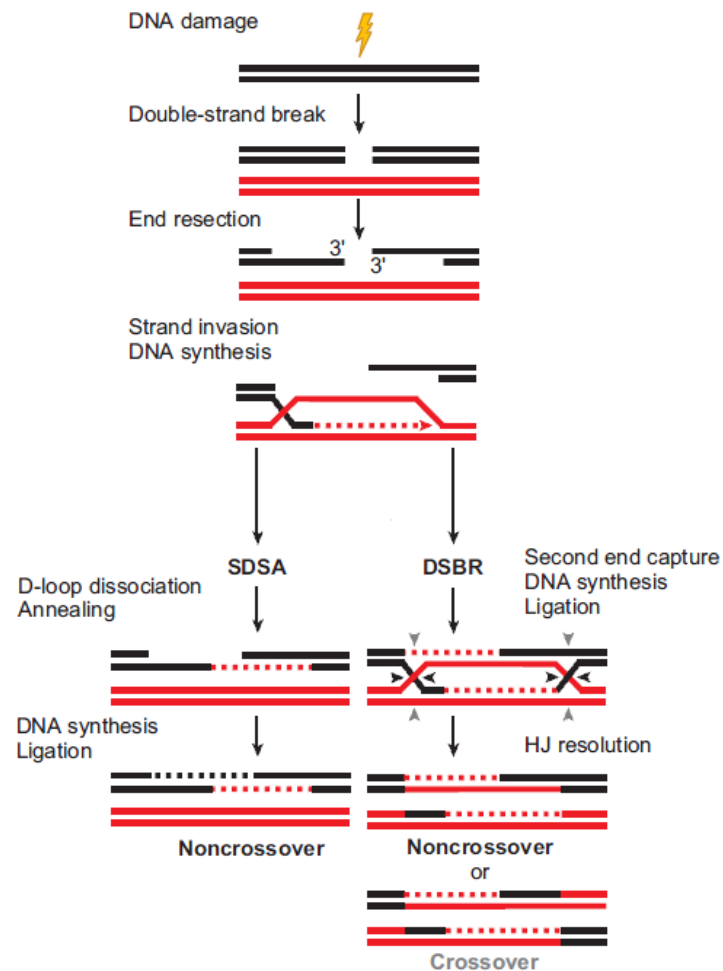
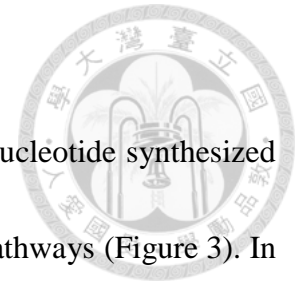


Figure 2. Mechanism of DNA homologous recombination.¹⁹

1.4. Biosynthetic pathway of dTTP in cells²¹



Among the four dNTPs in cells, dTTP is the only deoxyribonucleotide synthesized without RNR. The biosynthesis of dTTP can be divided into two pathways (Figure 3). In the *de novo* pathway, dUMP is catalyzed by rate-limiting enzyme thymidylate synthase (TS) to transform into dTMP. Thymidylate kinase (TMPK) then modifies dTMP to dTDP, followed by pyrophosphorylation through nucleotide diphosphate kinase to generate dTTP. For *salvage* pathway, dTMP is synthesized from thymidine with the help of thymidine kinase (TK). The subsequent phosphorylation steps are just the same as that in *de novo* pathway. Owing to the unique biosynthetic mechanism of dTTP, several cancer chemotherapeutic drugs are designed to focus on the inhibition of dTTP formation during DNA repair.

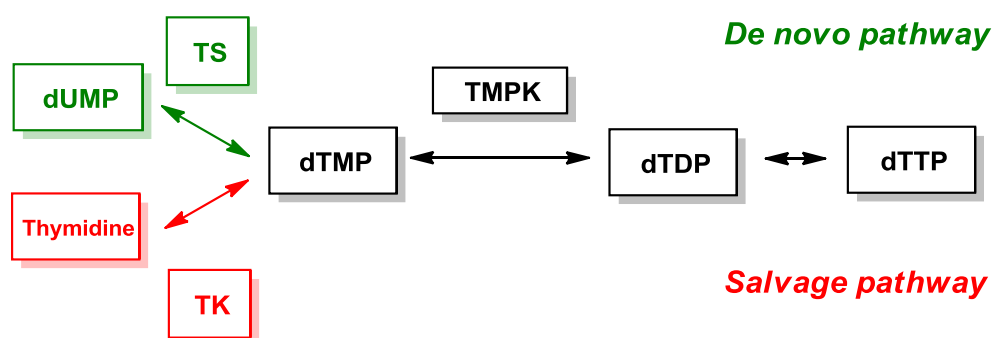
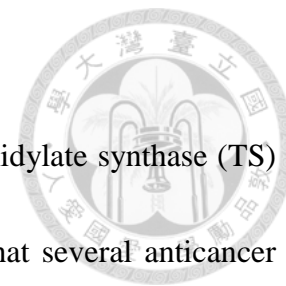


Figure 3. Biosynthetic pathways of cellular dTTPs.²²

1.5. Antimetabolite agents targeting dTTP formation



Among the enzymes involving in biosynthesis of dTTP, thymidylate synthase (TS) is a potential target for dTTP inhibition.²³ It has been reported that several anticancer drugs including 5-fluorouracil (5-FU)^{23, 24} and raltitrexed (Tomudex),²⁵ a folate analog, block the function of TS (Figure 4), thereby diminishing the production of dTMP and dTTP. Consequently, imbalanced recruitment of dNTPs mediated by RNR will induce DNA breakage during replication or repair to cause cells death.

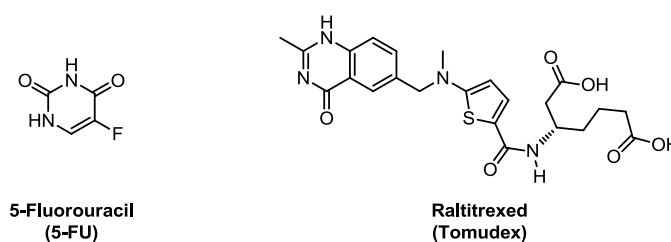


Figure 4. Chemical structures of drugs targeting thymidylate kinase (TS).

5-Fluorouracil (5-FU) is an analog of uracil with hydrogen atom at the C-5 position being replaced by fluorine. Once entering into cells, 5-FU can camouflage as uracil to convert into several active metabolites including fluorodeoxyuridine monophosphate (FdUMP), fluorodeoxyuridine triphosphate (FdUTP) and fluorouridine triphosphate (FUTP) (Figure 5). FdUMP binds irreversibly to TS that catalyzes the transformation of dUMP into dTMP with the help of the one-carbon methyl donor 5,10-methylenetetrahydrofolate (CH₂THF), thereby blocking the binding site of normal

dUMP.²⁴ The formation of dTMP in *de novo* pathway is inhibited, causing thymineless death. Moreover, inhibition of TS may result in accumulation of dUMP, and enhance the level of dUTP in cells. DNA polymerase is unable to distinguish between dUTP and dTTP,²⁶ therefore, excessive amount of dUTP and FdUTP can be misincorporated into DNA. Such a futile process of misincorporation will eventually lead to DNA damage-induced cell death.

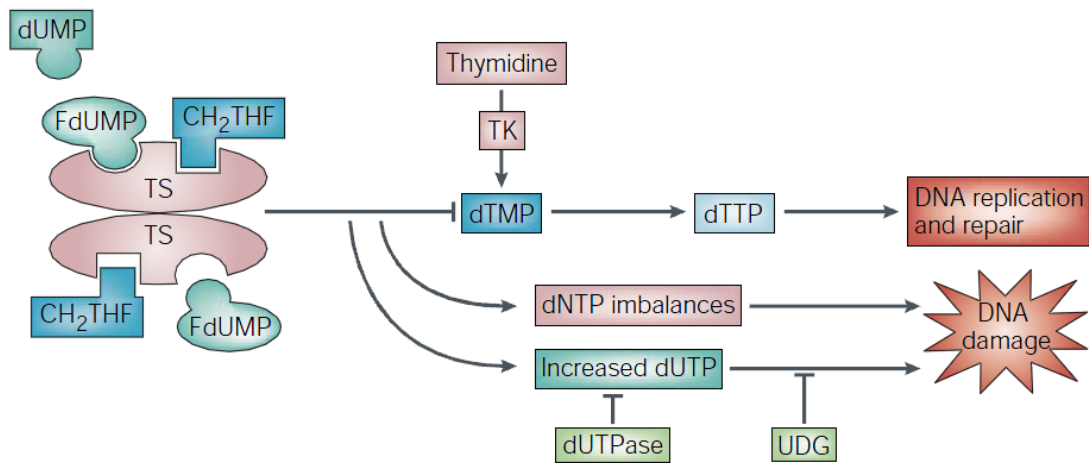
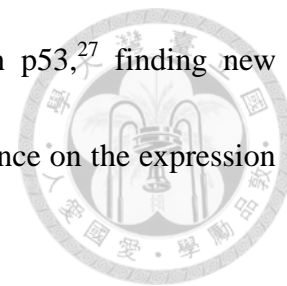


Figure 5. Mechanism of TS inhibition by 5-FU.²⁴

The treatment of 5-FU for cancer chemotherapy has been used more than 40 years. However, many of the therapies that use 5-FU alone or in combination with other agents show drug resistance. For instance, p53 disruption makes human colorectal cancer cells less sensitive to 5-FU.²⁷ TS deficiency only sensitizes the p53- deficient cells to doxorubicin to a limit extent, probably due to the compensation of *salvage* pathway

mediated by TK.²⁸ Since tumor cells are frequently mutated in p53,²⁷ finding new anticancer drugs to inhibit the formation of dTTP without dependence on the expression of p53 will be particularly important.



1.6. Structure and physiology of TMPK

Because targeting TS may be complemented by TK through *salvage* pathway, thereby diminishing the inhibition efficiency against TS,²⁴ the enzymes participating in both dTTP biosynthetic pathways will be more reliable targets for drug development. For example, TMPK is a good target because it stands at the junction of *de novo* and *salvage* pathways to catalyze the transfer of phosphate group from ATP to dTMP in the presence of Mg^{2+} .²⁹

Thymidylate kinase (TMPK) is a member of nucleoside monophosphate (NMP) kinase family.³⁰ The structure is usually a homodimer with each subunit composed of a central five-stranded β -sheet surrounded by α -helices (Figure 6).³¹ The enzymes are divided into three parts termed CORE domain, NMP binding site, and ligand-induced degradation (LID, residues 135-150) domain (Figure 6).^{31, 32} CORE domain is highly conserved among NMP kinases and contains the central parallel β -sheet as well as a phosphate binding loop (P-loop, residues 13-17) that controls the position of phosphate donor (ATP) for substrate recognition and catalysis. NMP binding region is largely

helical among most of the NMP kinases except guanylate monophosphate kinase. LID domain is flexible and covers a phosphate donor site partially for phosphate transfer.^{31, 32, 33}

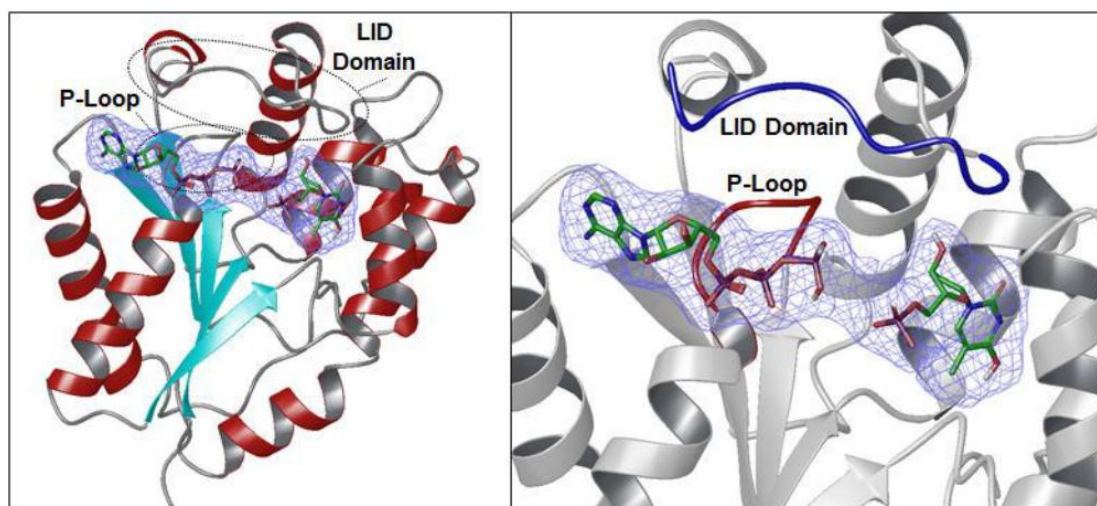


Figure 6. Ribbon structure of human TMPK (PDB ID: 1E2F). Left panel: central five-stranded β -sheet (light blue) surrounded by α -helices (red). Right panel: The P-loop (red) and LID domain (blue).³¹

When both the nucleotide binding sites are occupied, the active site of TMPK will exist as a globally closed conformation.^{34, 35} Several conformational changes of adenine-base binding loop (residue 178-188 for human TMPK), P-loop, and LID loop in the globally closed conformation of TMPK have been confirmed to correlate with the phosphorylation activity. The structure of TMPK in the presence of TMP and ADP is termed P-loop open form, and the partially closed form is observed in combination with TMP and AppNHp (an ATP analog). When TDP and ADP bind to TMPK, P-loop is

situated in a fully closed state.^{32, 34, 35} Among the catalytic process, the conformation of TMPK will change from open into closed form according to the movement of P-loop, and bring the phosphoryl donor close to the acceptor.^{31, 35} It is noted that the distance between Arg16 (P-loop) and the β,γ -phosphate bridging atom of ATP in the partially and fully closed conformation is closer than that in the open form. This is important for stabilizing the negative charge occurring during the phosphoryl transfer. Besides, the side chain of Asp15 that is essential in TMPK catalysis is too far away to interact with the 3'-hydroxyl group of TMP or the Arg97 residue in the open form.³⁵ Thus, the partially closed and fully closed conformations with P-loop may be structurally relevant to the catalytically active conformation, whereas the P-loop open form is an inactive state.^{34, 35}

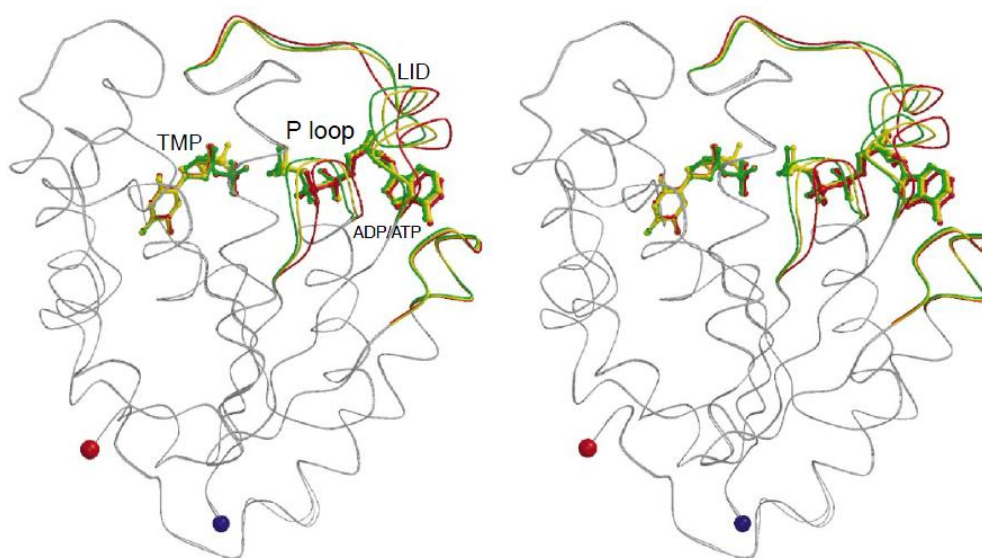
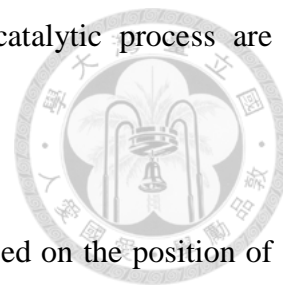


Figure 7. Movement of human TMPK structures: P-loop open (red), partially closed (yellow), and fully closed conformation (green) in response to binding of substrates.

P-loop, LID loop, and NMP binding site that change during catalytic process are colored.³⁵

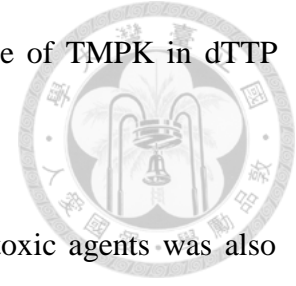


Lavie and coworkers³⁶ classified TMPKs into two classes based on the position of basic residues (mostly Arg) in the active site. Type I TMPKs are mainly from eukaryotes (e.g. human and yeast). A basic residue occurs at position 10 in the P-loop that can interact with ATP; however the LID domain lacks this residue. In contrast, type II TMPKs are mainly from prokaryotes (e.g. *E. coli*). The basic residue is situated in the LID region (Arg153) rather than P-loop, which has a replacement of glycine.^{30, 31, 36} By understanding the classification and mechanism of TMPK, one can better control the activity of enzyme for further drug discovery.

1.7. The relationship between the doxorubicin sensitization by TMPK inhibition to p53 status

In order to confirm the relationship between human TMPK and *p53* status, Chang and coworkers have generated lentivirus shRNA for hTMPK knockdown, and assessed the effect on dTTP pools in either isogenic *p53* (+/+) or *p53* (-/-) HCT-116 colon cancer cells.³⁷ After infected by lentivirus for 3 days, the steady state level of dTTP diminished gradually up to 50% in TMPK silenced cells compared with normal cancer cells (scramble shRNA) in both *p53* (+/+) and *p53* (-/-) types, with the dTTP amount of *p53*

(+/+) cells higher than *p53* (-/-) cells, indicating the essential role of TMPK in dTTP formation (Figure 8).



Additionally, the combination of TMPK silencing and genotoxic agents was also examined. As shown in Figure 9A, neither low dosage (0.5 $\mu\text{mol/L}$) of doxorubicin nor TMPK knockdown alone showed apparent effect on apoptotic induction. Nevertheless, TMPK silencing followed by doxorubicin treatment led to cell death (Annexin V-positive) in both *p53* (+/+) and *p53* (-/-) cells. On the other hand, 1 $\mu\text{mol/L}$ administration of doxorubicin after TS deletion led to apoptosis with *p53* (+/+) rather than *p53* (-/-) cells (Figure 9B). These evidences revealed that low-dose doxorubicin in combination with TMPK knockdown was *p53* independent, and was more effective than that with TS depletion (*p53* dependent) to induce apoptosis of *p53* deficient cells.

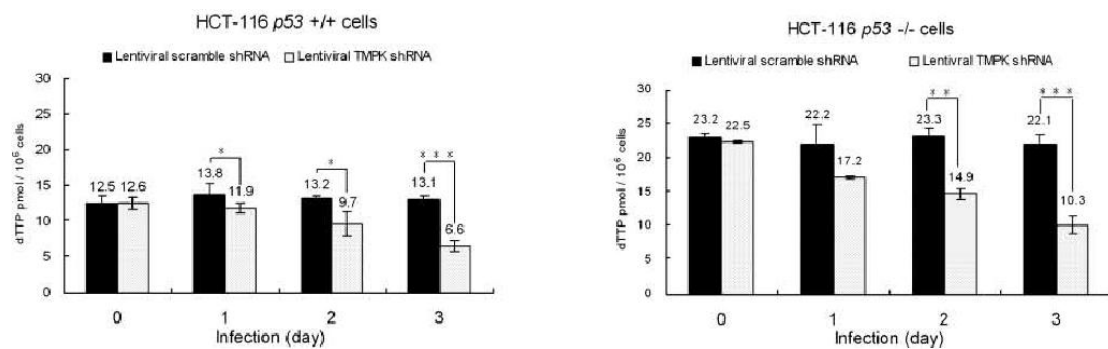


Figure 8. dTTP pool size measurement of lentiviral TMPK^{shRNA} and scramble^{shRNA} in *p53*-proficient and *p53*-null HCT-116 cells. (*, $P = 0.06$; **, $P = 0.01$; ***, $P < 0.001$ based on a two-tailed Student's t test.)

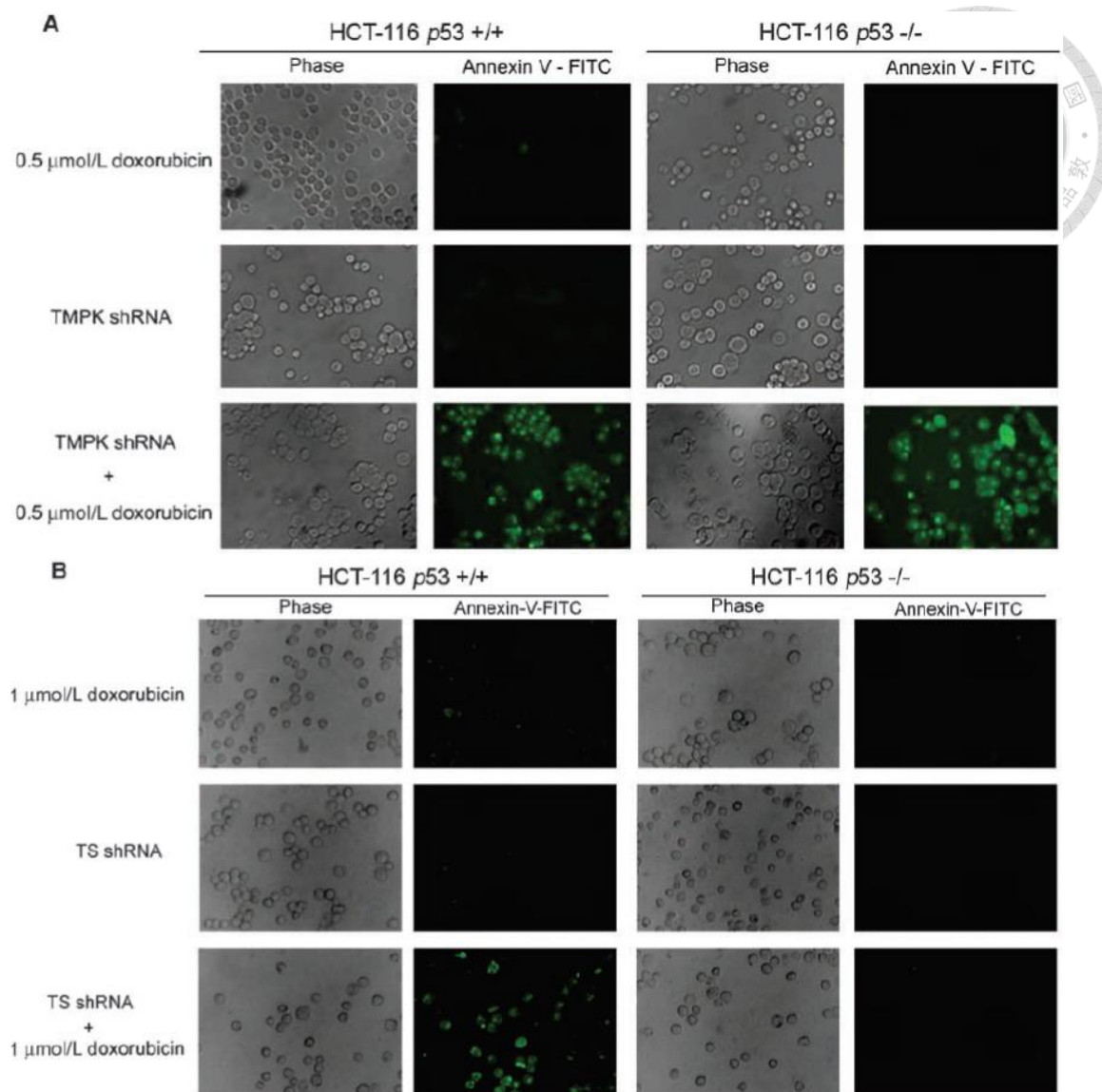


Figure 9. Comparison of TMPK and TS knockdown on doxorubicin-induced apoptosis in *p53*(+/+) and *p53*(-/-) HCT-116 cells by FITC-labeled Annexin V apoptosis assay.

1.8. Confirming the characteristic role of hTMPK during DNA repair

Based on the aforementioned information, it is hypothesized that reducing the formation of dTTPs by inhibiting TMPK function will sensitize tumor cells to doxorubicin. As the DNA breakage occurs after doxorubicin treatment, DNA repair will start by incorporating dNTPs into DSB site. Since HR requires more than 10000 dNTPs

to repair each DSB, the supply of dNTPs mediated by RNR is highly demanded. Blocking TMPK function reduces the level of dTTP at damage site, and causes the imbalanced incorporation of four dNTPs during HR repair. Since DNA polymerase is unable to differentiate between dUTP and dTTP, surpluses amount of dUTP will misincorporate into DNA and trigger cell death finally (Figure 10).

R2, which is a subunit of RNR, is cell-cycle regulated and usually expresses during G2/M phases. Malignant tumor cells are cell-cycle checkpoint defected,³⁸ and thus show high G2/M-phase population after recovery from DNA damage, during which HR repair takes place along with R2 overexpression. On the other hand, the intact checkpoint functionality in normal cells reduces the population during S phase, and triggers cell quiescence into G0 phase, leading to low expression of R2 and less dUDP formation thereafter. Hence, TMPK knockdown will sensitize DNA damage only in tumor cells rather than normal cells.³⁹

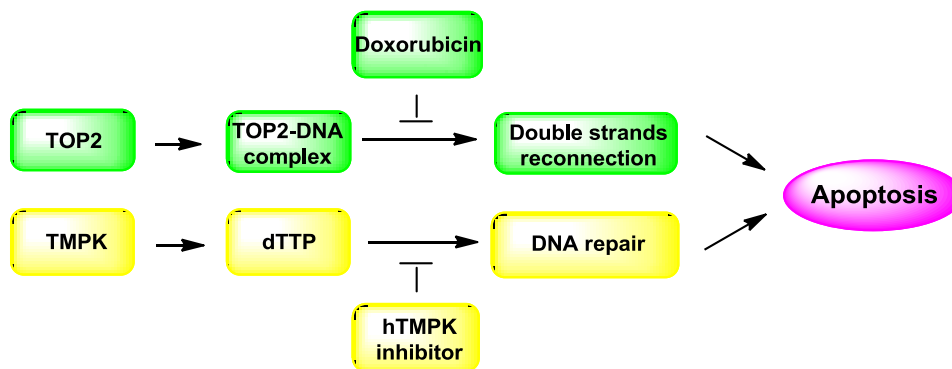
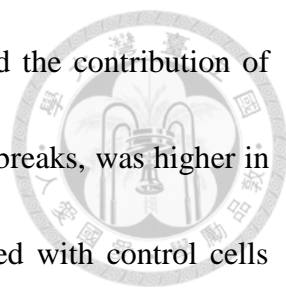


Figure 10. Combined treatment of doxorubicin and hTMPK inhibitor to trigger cell apoptosis.²²



To confirm the hypotheses, Hu and Chang³⁹ first investigated the contribution of TMPK during DNA repair. γ H2AX, the indicator of double-strand breaks, was higher in the TMPK knockdown MDA-MB231 breast cancer cells compared with control cells after recovery from a low-dosage doxorubicin treatment for 24 h, demonstrating that TMPK is essential for DNA repair in cancer cells (Figure 11a). Thereafter, uracil misincorporation test was conducted by inhibiting uracil *N*-glycosylase (UNG), an enzyme which removes erroneous uracil from DNA and forms single-strand breaks (SSBs) subsequently. After 24 h recovery from DNA damage, XRCC1 foci (SSBs marker) was reduced apparently by UNG knockdown in TMPK-knockdown cells (Figure 11b).

In order to make sure RNR will generate dUDP for incorporation during DNA repair in the absence of TMPK, the recruitment of RNR to DNA damage site was blocked by yellow fluorescent protein (YFP) fusion. The results showed that decline of RNR recruitment abolished the effect of TMPK knockdown during recovery from doxorubicin treatment (Figure 12a). Besides, TMPK and RNR were proved to co-localize and bind to the damage site of DNA, where is the place needed for dNTPs balance (Figure 12b). Furthermore, reducing the expression of R2 generated DNA repair in spite of TMPK silencing in tumor cells (Figure 12c). These evidences indicated that DNA repair required the cooperation of TMPK and R2 in RNR at the damage site.

TMPK is essential to DNA repair by preventing dUTP misincorporation.

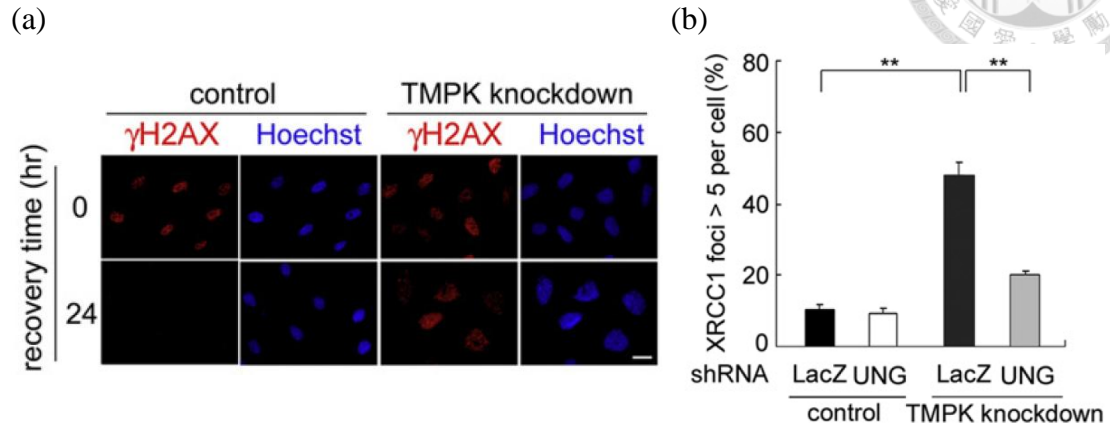
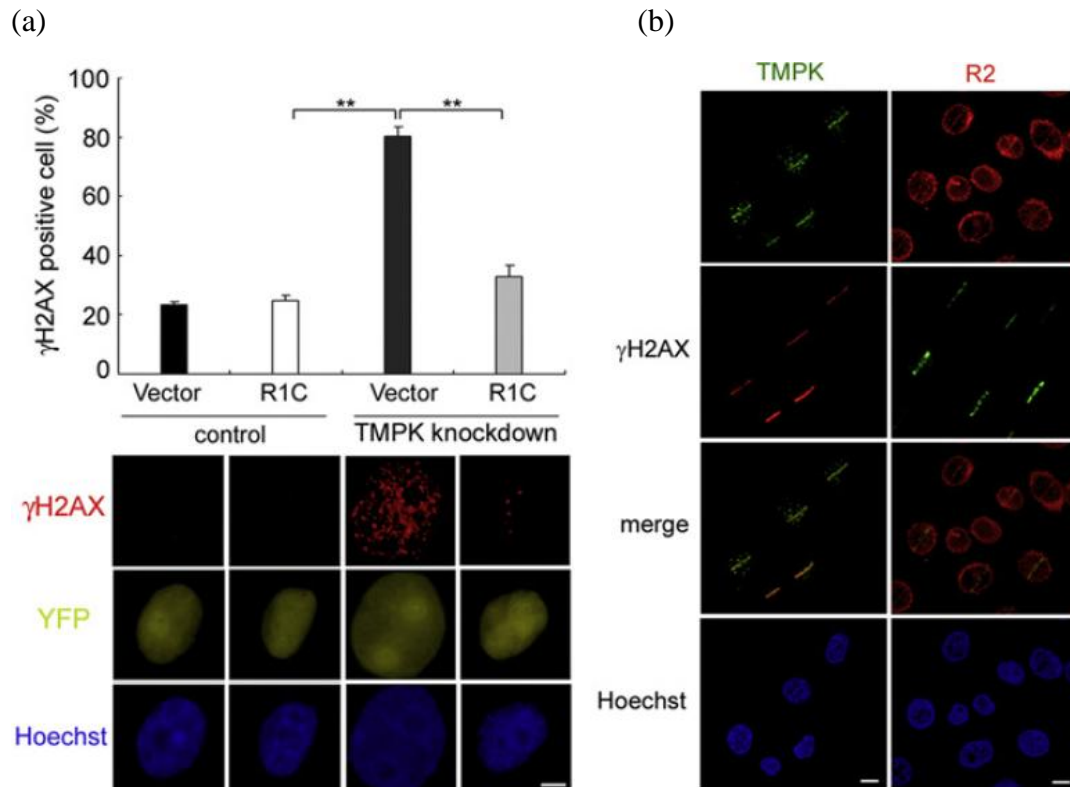


Figure 11. (a) γ H2AX foci staining of MDA-MB231 cells with or without TMPK silencing after recovery from doxorubicin. (b) XRCC1 foci staining of LacZ or UNG lentivirus infected cells recovered from doxorubicin treatment for 24 h.



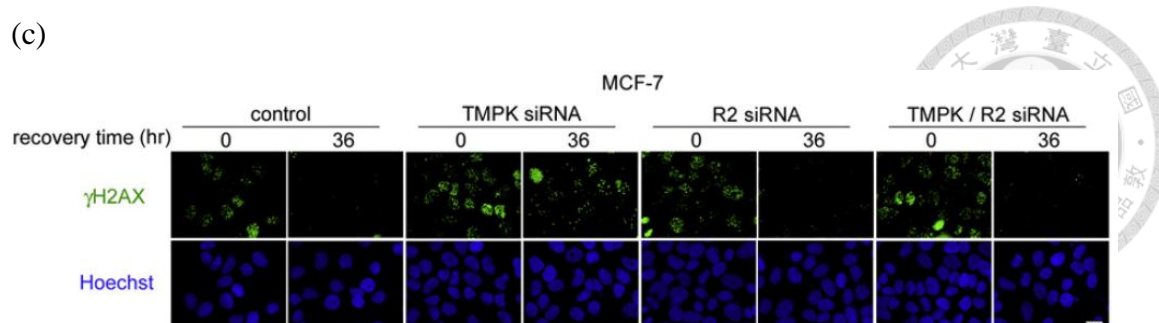


Figure 12. (a) pCMV2-YFP-Nuc (vector) or pCMV2-YFP-Nuc-R1C (plasmid) transfected into TMPK or TMPK knockdown cells. (b) Laser-micro-irradiation of HeLa cells followed by immunofluorescence staining. (c) γ H2AX foci staining of MCF-7 cells with TMPK, R2 and TMPK/R2 knockdown at the indicated time points.

Given that TMPK knockdown will trigger apoptosis of tumor cells with low-dosage doxorubicin treatment, it is worthwhile to investigate the selectivity between cancer and normal cells. Breast cancer cell line MCF-7 as well as nontumorigenic H184B5F5/M10 and MCF10A were tested for the influence of TMPK silence during DNA repair. After recovery from DNA damage, γ H2AX foci remained in MCF-7 cells but not H184B5F5/M10 or MCF10A cell lines, indicating the nontoxicity of TMPK knockdown toward normal cells (Figure 13). To further understand the reason for selectivity, Chang and coworkers used flow cytometry analysis to study the cell-cycle population of cell lines after doxorubicin treatment. H184B5F5/M10 and MCF10A cells showed higher population in G0/G1 phases compared with MCF-7 and MDA-MB231 cancer cells, which possessed larger S and G2/M phase populations after DNA damage (Figure 14), demonstrating lower integrity of checkpoint function in these cancer cells.

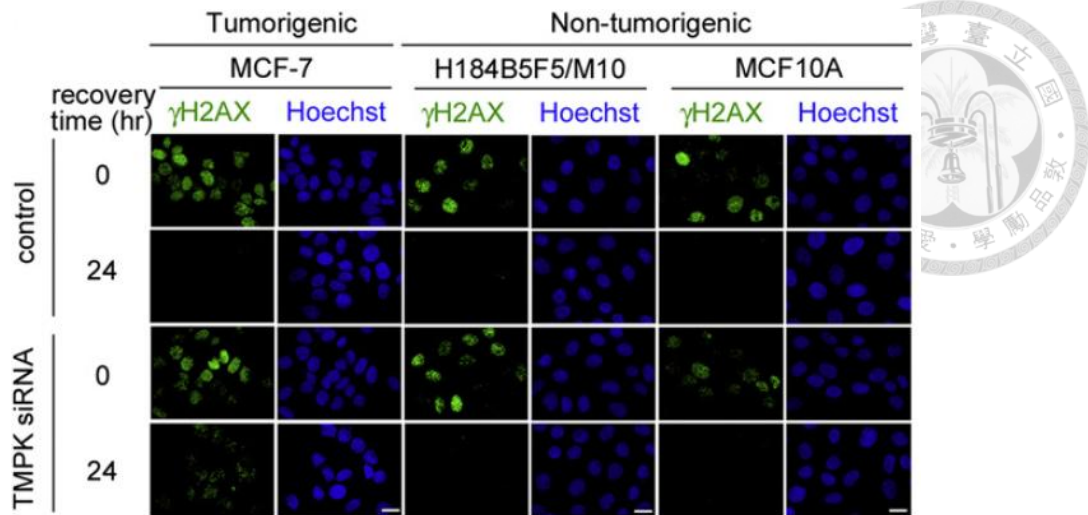


Figure 13. γ H2AX foci staining of MCF-7, H184B5F5/M10, and MCF-10A cells transfected with TMPK siRNA after DNA damage recovery.

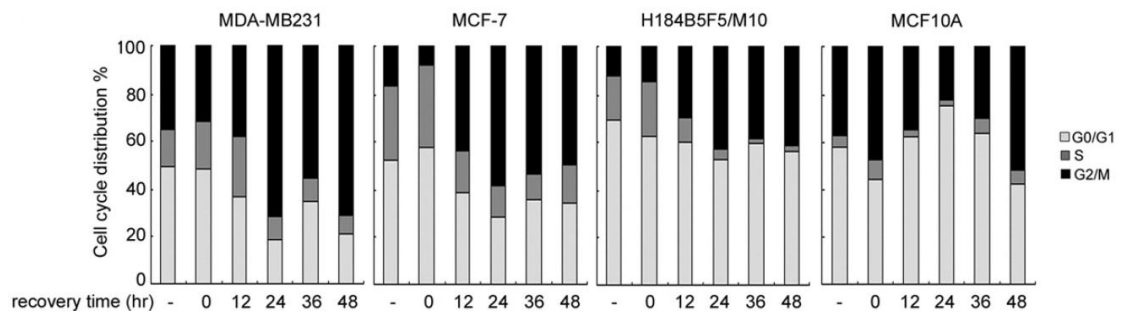
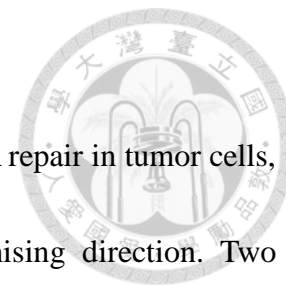


Figure 14. Flow cytometry of cells at the indicated time points after recovery from doxorubicin.

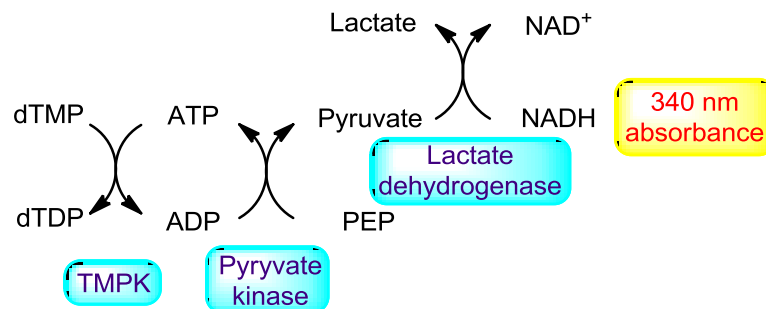
1.9. Screening inhibitors against hTMPK



Based on the significant characteristics of TMPK during DNA repair in tumor cells, searching for small molecules targeting TMPK will be a promising direction. Two methods have been developed for TMPK enzymatic assay.^{31, 40} The first method uses isotope labeled dTMP as the substrate. After incubation with TMPK, dTMP acquires a phosphate group from ATP, and the ratio between dTMP and dTDP are evaluated by the radiative intensities for calculation of enzymatic activity. However, this method requires long time and is not suitable for high-throughput screening even though it is accurate by using only one enzyme. Another widely used method is NADH-coupled enzymatic assay. This method comprises three enzymes, TMPK, pyruvate kinase, and lactate dehydrogenase (Figure 15). TMPK phosphorylates dTMP into dTDP along with the generation of ADP. The ADP then turns back to ATP by reacting rapidly with phosphoenolpyruvate (PEP) in the presence of pyruvate kinase. Pyruvate formed from PEP turns into lactate by lactate dehydrogenase with the cofactor NADH oxidized into NAD⁺. Since NADH shows absorbance at 340 nm, the activity of TMPK can be inferred from measurement of the absorbance at 340 nm. Two additional enzymes are required in this assay, and the sensitivity is limited by the low extinction coefficient of NADH. In addition, the accuracy of this assay may be interfered with any substrate absorbs near the region of 340 nm.

To circumvent the disadvantage of NADH-coupled enzymatic assay, Chang and coworkers⁴⁰ develop a new method termed luciferase-coupled TMPK assay, which has been used for screening hTMPK inhibitors. Luciferase catalyzes the oxidation of luciferin in the presence of ATP and generates luminescence. Hence, inhibiting TMPK will decrease the amount of ATP for luciferase. According to the intensity of luminescence, ATP remains after TMPK consumption can be determined accordingly. Compared with the conventional assays, this method measures luminescence intensity which is more sensitive and rapid in determining the activity of hTMPK without the interference of substrate absorption (Table 1).

NADH-coupled enzymatic assay



Luciferase-coupled TMPK assay

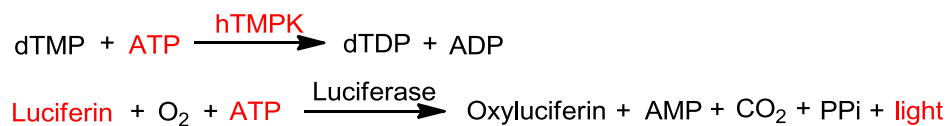


Figure 15. Principles of NADH- and luciferase-coupled TMPK assays.

Table 1. Comparison of sensitivity in NADH- and luciferase-coupled TMPK assays.⁴⁰

hTMPK protein (μg)	Luciferase-coupled assay	NADH-coupled assay
0.01	3.8 ± 0.2^a	Not detectable
0.05	18.2 ± 0.9^a	Not detectable
0.10	36.5 ± 1.1^a	33.8 ± 7.4^a
1.00	89.3 ± 4.7^a	85.7 ± 6.1^a
0.50	177.3 ± 6.4^a	166.1 ± 4.0^a
1.00	373.4 ± 5.1^a	387.5 ± 9.7^a

^aMean value (pmol of dTDP formation /min) of five independent experiments. Different concentrations (0.01 to 1 μg) of purified hTMPK protein were tested. In the luciferase-coupled assay, TMPK activity ($\Delta\text{RLU}/\text{min}$) was converted to the amount of dTDP formation per minute. In the NADH-coupled assay, TMPK activity ($\Delta A_{340\text{nm}}/\text{min}$) was estimated by the following equation: dTDP formation ($\text{pmol}/\text{min } 100\mu\text{l}^{-1}$) = $\Delta A_{340\text{nm}} 6.22 \times 10^5 / \text{reaction time (min)}$.

Using luciferase-coupled TMPK assay for high-throughput screening, a library of 21,120 small molecules was screened to find YMU1 as a potent compound (Figure 16), with $\text{IC}_{50} 0.061 \pm 0.02 \mu\text{M}$ and $K_i 0.22 \pm 0.03 \mu\text{M}$ against TMPK.³⁹ As shown in Figure 17a, YMU1 itself did not give rise to genome toxicity in cells, unlike 5-FU which caused cell death without selectivity between normal and tumor cells. However, pretreatment of YMU1 followed by treatment with low-dosage doxorubicin demonstrated apparent DNA damage in tumor cells rather than normal cells (Figure 17b), indicating that YMU1 impaired DNA repair as effective as TMPK silencing.

To further verify that the combined use of doxorubicin and YMU1 was also verified to inhibit the growth of tumor cells, HCT-116 and MCF-7 cells were test and all showed

growth suppression (Figure 18a). Moreover, the size of tumor in mice treated with both YMU1 and doxorubicin was significantly smaller than that individually treated with YMU1 or doxorubicin (Figure 18b). Taken together, these results indicate that YMU1 has high potential in targeting human TMPK for tumor suppression. Therefore, YMU1 is a promising lead compound for development in cancer chemotherapy.

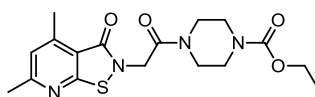


Figure 16. Chemical structure of YMU1.

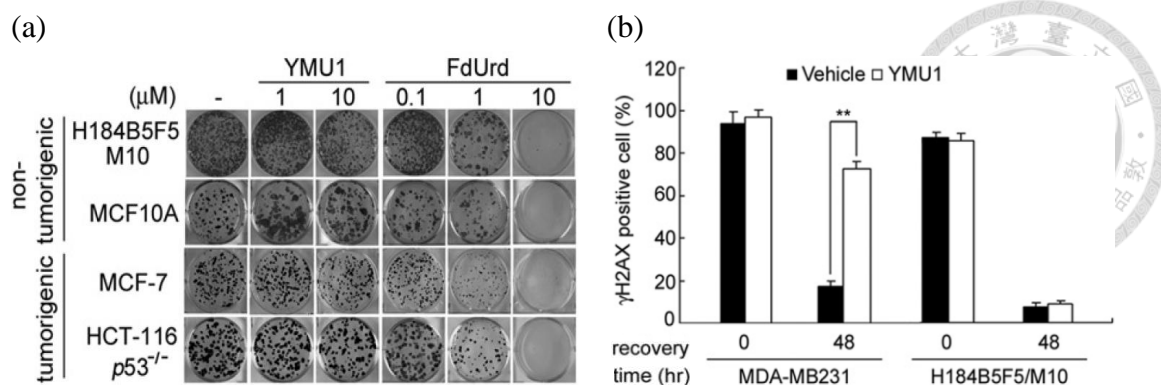


Figure 17. (a) 5000 cells of H184B5F5/M10, 3000 cells of MCF10A, MCF-7, and HCT-116 *p53*^(-/-) were treated with YMU1 or 5-FU at different concentration, and stained by crystal violet after 14 days. (b) γ H2AX foci staining of cells after treated with vehicle or YMU1 along with doxorubicin exposure.

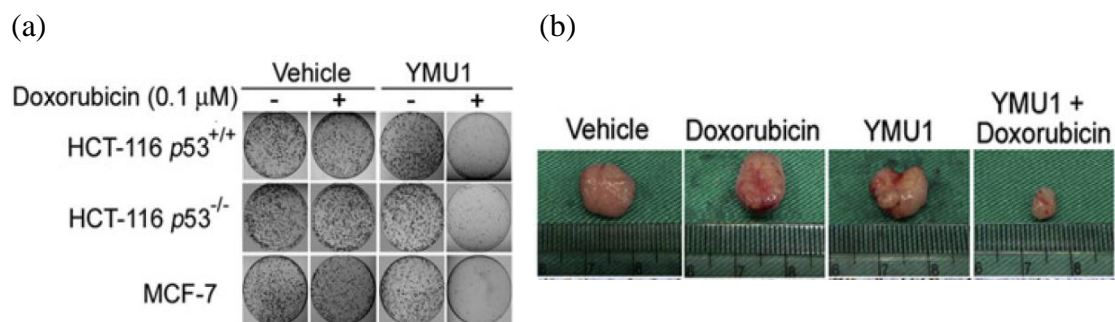


Figure 18. (a) On treatment with vehicle or YMU1 for 72 h, followed by 4 h doxorubicin exposure, cells were incubated for colony formation over 14 days. (b) Comparison of tumor growth in mice with combined treatment of YMU1 and doxorubicin or doxorubicin/YMU1 alone for two weeks.



Chapter 2. Results and Discussion



2.1.1. Structural feature of YMU1

Chemical structure of YMU1 can be divided into three parts: The heterocyclic core, linker containing a six member ring, and the end group R (Figure 19). Based on the derivatives synthesized previously by Yeh,²² several structure features are considered to maintain the inhibitory activity against hTMPK, including the role of sulfur atom in core structure, the importance of *N*-alkylation with linker over *O*-alkylated analogs, the appropriate length of linker with a six member ring, and the alteration of the end group R. (Figure 20).

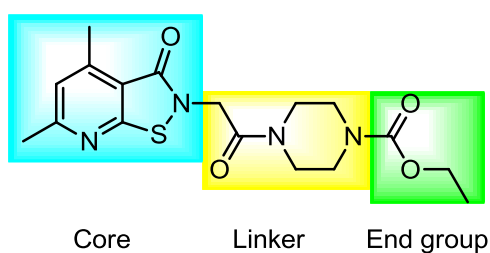


Figure 19. Structure of YMU1.

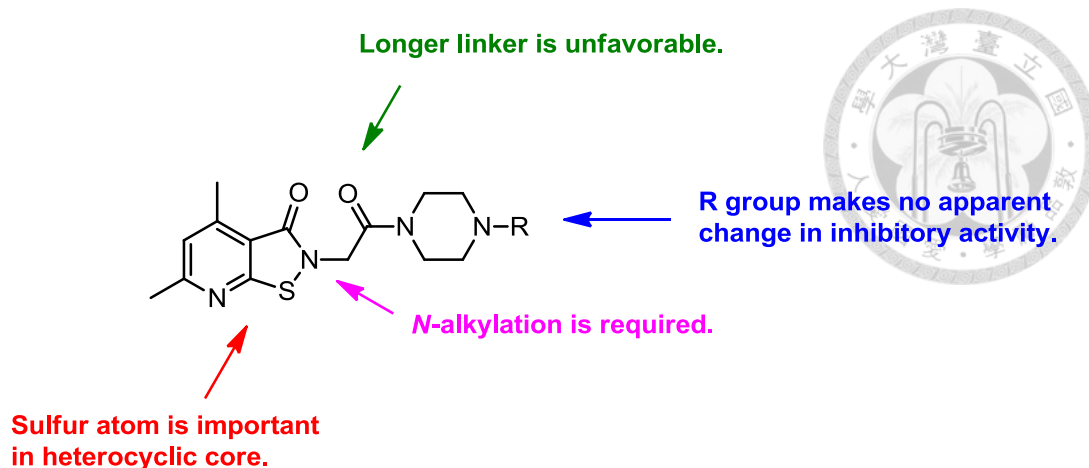


Figure 20. Some structural features of YMU1 derivatives.²²

2.1.2. Molecular dynamic simulation of YMU1 with TMPK

By means of molecular dynamic (MD) simulations of YMU1 with the crystal structure of TMPK, the inhibition mechanism can be further investigated. As shown in Figure 21, P-loop and LID region are connected by several residues including Arg16, Gly144, Ala145, Glu152, Asp15, Arg143, Ala17, and Ala180 via hydrogen-bond network. When YMU1 is incubated, the connection between LID and P-loop is disrupted, and the LID region is pushed outward. Arg16 in P-loop is supposed to interact with the heterocyclic core part of YMU1 by a π - π stacking, which can stabilize the disposition of YMU1 (Figure 22). In addition, YMU1 is able to dock into the ATP binding site and thus prevents Mg^{2+} from interacting with Asp15, a residue that is crucial for the activity of TMPK. *O*-alkylation derivatives cannot prevent this interaction, thus show poor inhibition against TMPK.³⁹ Moreover, the two carbonyl groups of YMU1 can chelate

one Mg^{2+} ion, therefore, a long linker will be disfavored. Further modification of YMU1 can be performed more practically with the assistance of the simulation results.

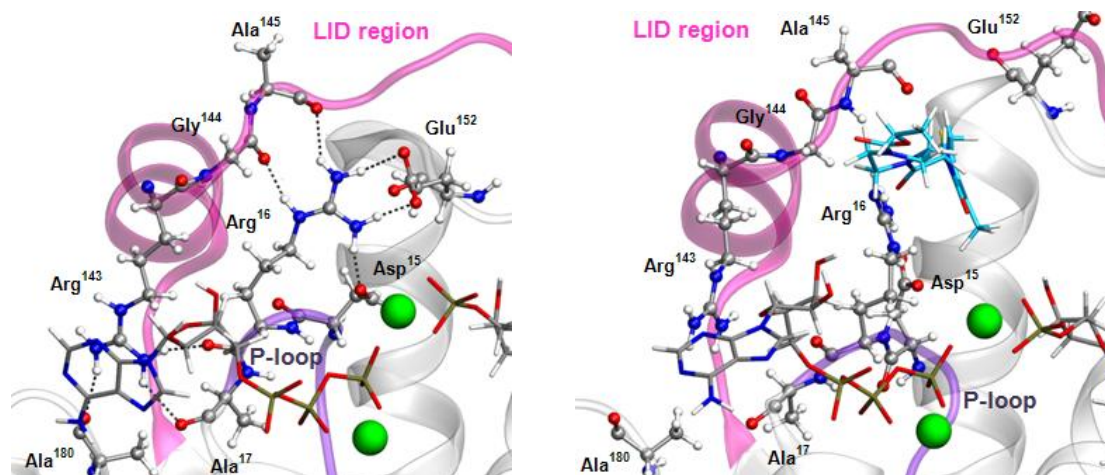
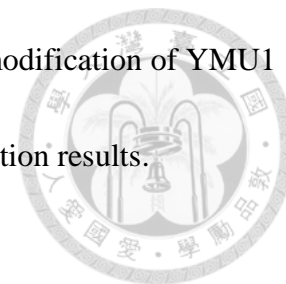


Figure 21. MD simulation of the mechanism of TMPK with or without YMU1. Hydrogen bonds were indicated with dash lines and YMU1 was shown as bright blue structure.

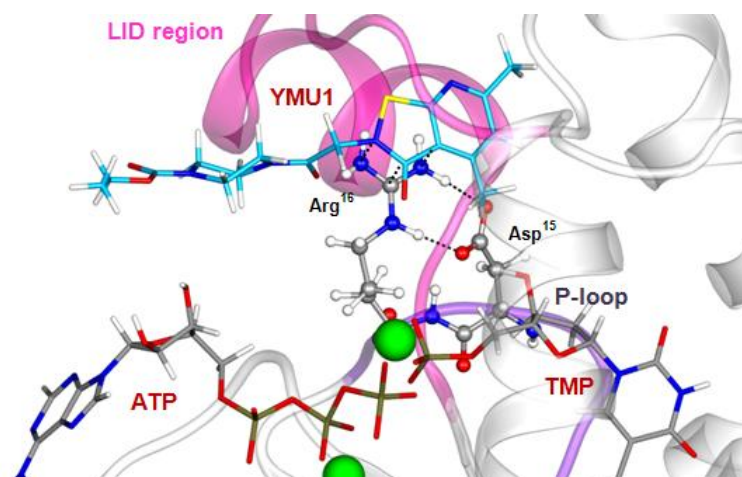


Figure 22. Stabilization of YMU1 in hTMPK via the π - π stacking interaction with Arg16.

2.1.3. Specific YMU1 derivatives proposed in this study

Although the previous study²² indicated that the end group R in YMU1 made no

apparent difference in TMPK inhibition, I still plan to synthesize the dimeric compounds having the R group containing another heterocyclic core structure to test their inhibitory activity against TMPK. Besides, I further modified the structure of YMU1 to investigate the importance of the sulfur atom in the heterocyclic core, and to enhance the hydrophilicity by changing substituents in the core structure and the R group.

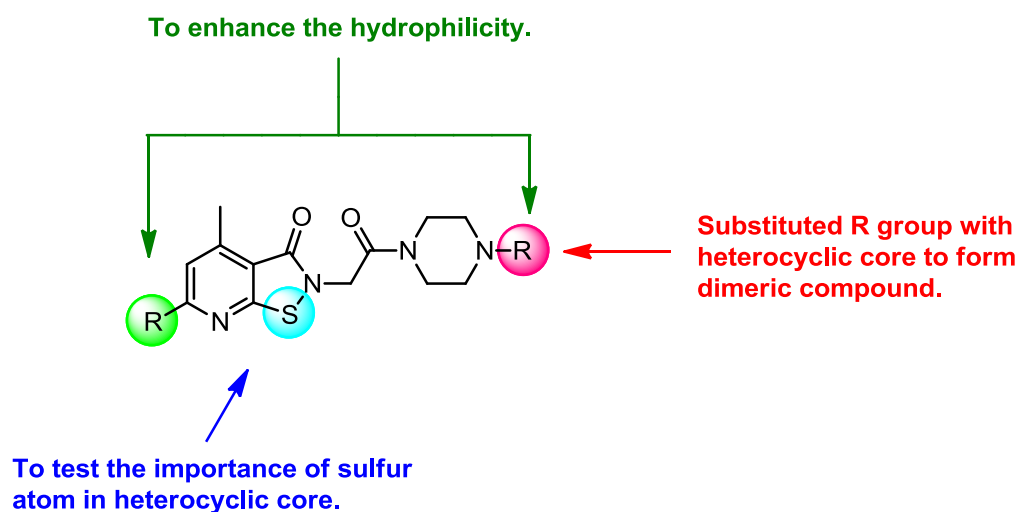


Figure 23. Specific YMU1 derivatives.

2.1.4. Luciferase-coupled TMPK assay

After setting the research target, the next step is to identify the inhibitory activity of YMU1 derivatives against hTMPK in cancer cells with the combined use of low-dosage doxorubicin. In order to screen inhibitors more efficiently and accurately, Chang and coworkers have established a convenient protocol of luciferase-coupled TMPK assay (Figure 24).⁴⁰ Each test compound was dissolved in DMSO to a concentration of 5 mM,

and then diluted into different concentrations for tests. For example, a drug (10 μM) was transferred to a 96-well plate containing 10 μL of 0.5 μg TMPK for 10-min preincubation. Then, 30 μL of buffer solution containing 100 mM Tris-HCl (pH 7.5), 100 mM KCl, 10 mM MgCl_2 , 50 μM ATP and 100 μM dTMP were added to initiate the reaction. After 10 min, 200 μL of 100 μM 5,5'-dithiobis(2-nitrobenzoic acid) (DTNB) was added to stop the reaction. The sample solution (10 μL) was transferred to a 96-well plate, followed by adding 90 μL of luciferase assay buffer containing 50 mM Gly (pH 7.0), 0.1 μg luciferase, 0.5 mM EDTA, 50 μM luciferin, 5 mM MgCl_2 and 0.1 % bovine serum albumin (BSA) into each well to measure the luminescence.

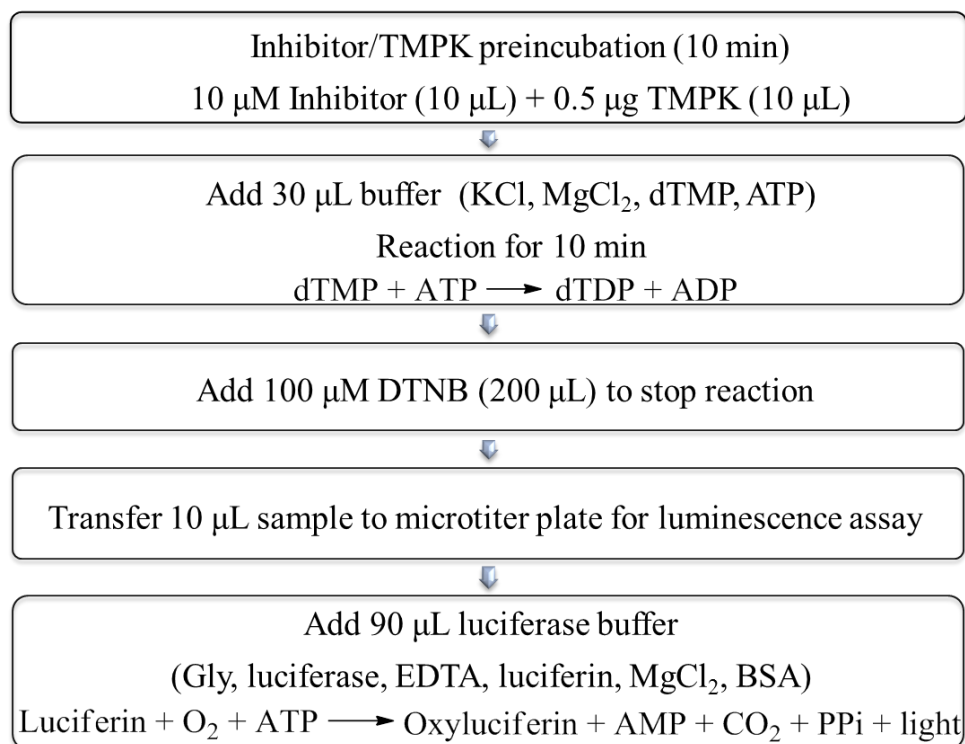
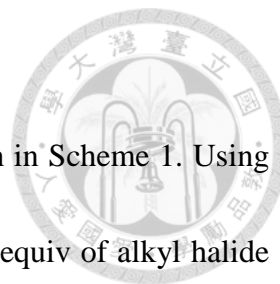


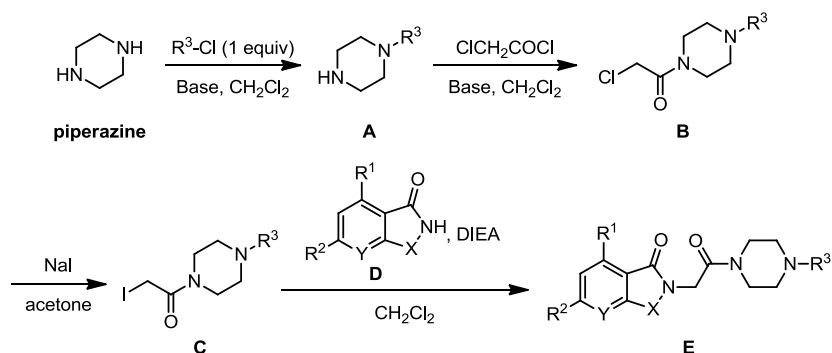
Figure 24. Protocol of luciferase-coupled TMPK assay.²²



2.1.5. General synthetic scheme

The general synthetic strategy for YMU1 derivatives is shown in Scheme 1. Using piperazine as the starting material, the substitution reaction with 1 equiv of alkyl halide (R^3Cl) would generate a mono-substituted piperazine **A**. The substitution reaction of chloroacetyl chloride would be performed via addition–elimination mechanism to form disubstituted piperazine derivative **B**. Further substitution of the chlorine atom with iodine atom would be conducted by using sodium iodide as a nucleophile in acetone. Finally, diverse heterocyclic compounds **D** would be introduced by coupling with the iodo-substituted **C** to give a series of the desired YMU1 derivatives **E**.

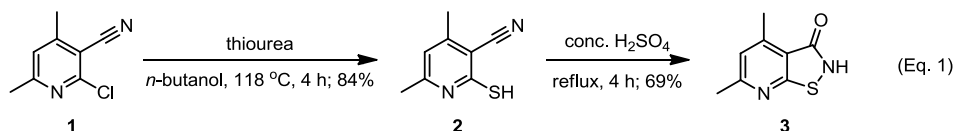
Scheme 1. General synthetic scheme for YMU1 derivatives.



2.2.1. Replacement of the sulfur atom in heterocyclic core

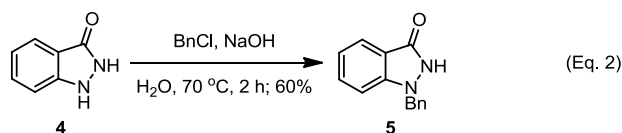
Heterocyclic core **2** was synthesized from the commercially available 2-chloro-4,6-dimethylnicotinonitrile (**1**) and thiourea in *n*-butanol at 118 °C. The

oxidative cyclization reaction was then performed in conc. H₂SO₄ at 100 °C for 4 h to afford compound **3** (Eq. 1).



In the first part, we aimed to test the significance of the sulfur atom in heterocyclic core for TMPK inhibition. Yeh has changed the sulfur atom of YMU1 into sulfone, and found the derivative did not show inhibition against hTMPK. We further replaced the sulfur atom with oxygen, nitrogen, carbon, carbonyl, and *N*-benzyl group to investigate the role of sulfur atom in the heterocyclic core.

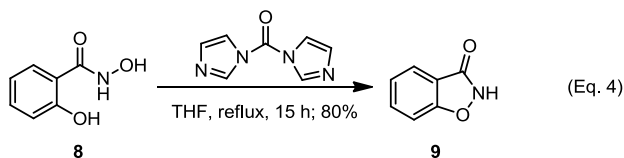
We first focused on constructing the heterocyclic core having an *N*-benzyl group. The commercially available 1*H*-indazol-3(2*H*)-one (**4**) was treated with benzyl chloride and sodium hydroxide in H₂O at 70 °C for 2 h. The precipitates were collected and purified to afford compound **5** (Eq. 2).⁴¹



Using cyclohexane as the reducing agent, reduction of phthalimide (**6**) was promoted by aluminum chloride to afford phthalimidine **7**⁴² as the carbon-substituted YMU1 derivative (Eq. 3).



The oxygen-containing heterocyclic core **9**⁴³ was synthesized from salicylhydroxamic acid (**8**) with carbonyl diimidazole in THF at 70 °C (Eq. 4).

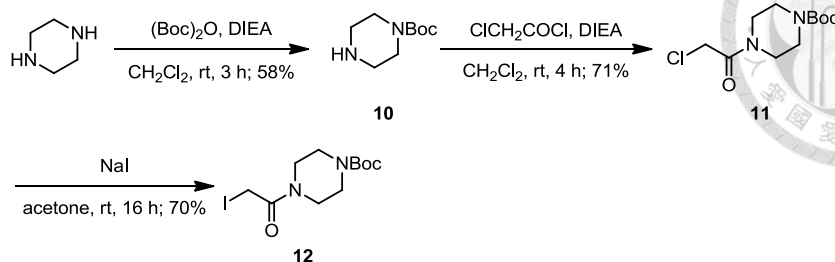


2.2.2. Synthesis of piperazine linkers

The commercially available piperazine was treated with Boc-anhydride (1 equiv) in the presence of a base DIEA to form the mono-Boc-protected piperazine **10** (Scheme 2).

The reaction of 2-chloroacetyl chloride with **10** provided compound **11**, which underwent a substitution reaction with sodium iodide in acetone to give the iodo compound **12**.

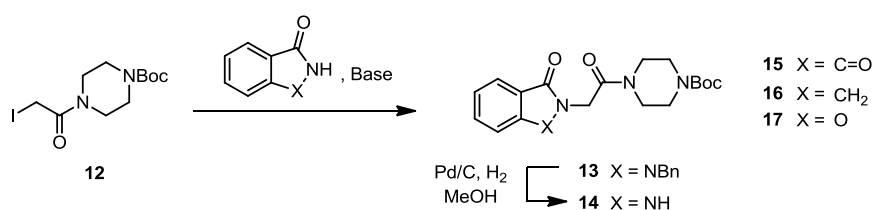
Scheme 2. Synthesis of compound **12**.²²



2.2.3. Synthesis of YMU1 derivatives **13–17**

The heterocyclic compounds **5–7** and **9** underwent substitution reactions with the iodo compound **12** in the presence of appropriate base to give the YMU1 derivatives **13** and **15–17**, respectively (Scheme 3). Removal of the benzyl group from **13** was carried out by hydrogenation over Pd/C in MeOH to give compound **14**.

Scheme 3. Synthesis of compounds **13–17**.

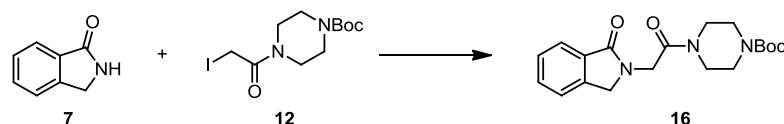


Noteworthy, the substitution reaction of phthalimidine **7** with **12** could not be realized by using DIEA as shown in the general synthetic procedure. We thus tested different bases, including NaH, LiH and Cs₂CO₃, and solvents, including DMF, THF and CH₃CN, for this transformation (Table 2). The reaction using Cs₂CO₃ in CH₃CN at

50 °C showed the highest yield (entry 4).



Table 2. Reaction conditions for the synthesis of compound **16**.



Entry	Conditions	Results
1	DIEA, CH ₂ Cl ₂ , rt, 5 d	No reaction
2	NaH, DMF, rt, 5 d	16 (41%)
3	LiH, THF, reflux, 3 d	16 (16%)
4	Cs ₂ CO ₃ , CH ₃ CN, 50 °C, 36 h	16 (49%)

2.2.4. Structure–activity relationship of compounds **3–7**, **9** and **13–18**

After synthesizing a variety of derivatives by replacement of the sulfur atom in YMU1, we started to study the relationship between the structure and inhibitory activity. As shown in Figure 25, benzo[*d*]isothiazol-3(2*H*)-one (BT) and **3** was used to compare with compounds **4–7** and **9** having heterocyclic cores, whereas compound **18** was used to compare with compounds **13–17**.

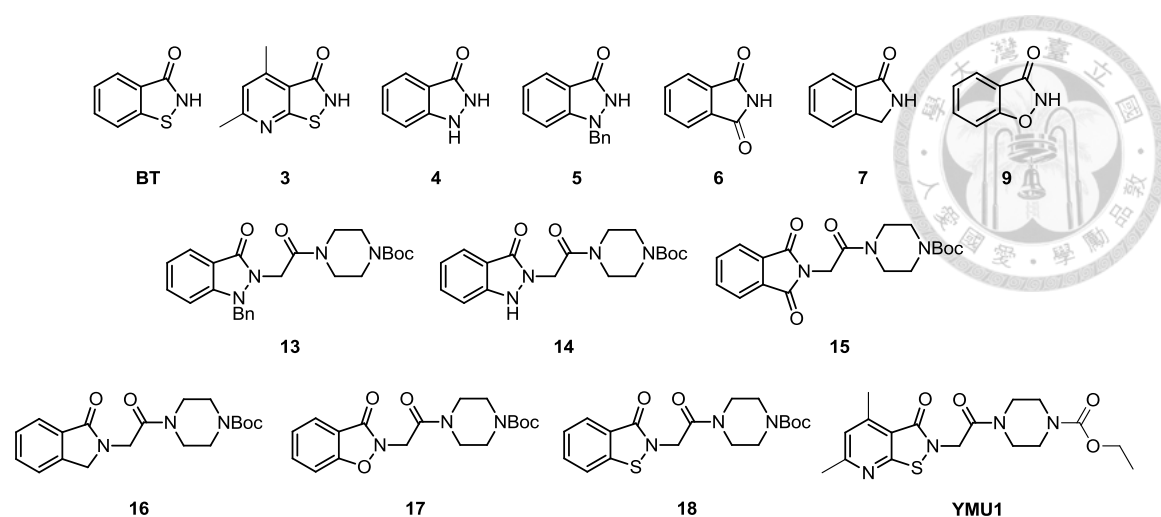


Figure 25. Chemical structures of benzo[*d*]isothiazol-3(2*H*)-one (BT), compounds **3–7**, **9**, **13–18** and YMU1.

Table 3. Normalized TMPK inhibition of compounds BT, **3–7**, **9**, **13–18** and YMU1.⁴⁴

Compound	Inhibition (%) ^a	Compound	Inhibition (%) ^a
BT	51.8	13	8.4 ± 2.5 ^b
3	19.6	14	0.6 ± 1.5 ^b
4	−3.3	15	18.7 ± 3.4 ^b
5	−4.5	16	2.2 ± 5.4 ^b
6	13.1	17	10.6 ± 7.6 ^b
7	−6.0	18	91.3 ± 5.7 ^b
9	−3.3	YMU1	70.0 ± 7.0 ^b

^aNormalized TMPK inhibition of the test compound compared with YMU1 as 70% inhibition at 2 μM.

^bData of quadruplicate experiments.

Table 3 shows the inhibitory activity of compounds at 2 μM using luciferase-coupled TMPK assay as the preliminary test. The normalized inhibition value was calculated according to a formula:

$$(\text{inhibitory activity of compound}) \div (\text{inhibitory activity of YMU1}) \times 100\%.$$

Though BT and **3** still possessed moderate TMPK inhibition, compounds **4–7** and **9** having different heterocyclic cores without sulfur atom revealed poor activity against TMPK. Moreover, compounds **13–17** without sulfur atom were also inactive to TMPK, whereas the sulfur-containing derivative **18** was highly active with 91% normalized inhibition against TMPK. These results confirmed that the sulfur atom placed in the heterocyclic core of YMU1 indeed played an important role in the TMPK inhibition activity. Once the sulfur atom is replaced by other atom or functional group, the efficiency of inhibition against TMPK will decrease dramatically.

2.3.1. Hydrophilic YMU1 derivatives

Lipophilicity refers to the ability of chemical compound to partition between organic and polar aqueous phases (two immiscible solvents).⁴⁵ Molecules with high capacity to form hydrogen bonds are more hydrophilic and tend to dissolve in high polar substances such as water. On the other hand, compounds having less hydrogen bonds often interact within themselves with London dispersion force, and are more favorable

to hydrophobic (non-polar) solvent. Understanding the lipophilicity is important in drug discovery for oral administration because hydrophilic compounds are unable to pass through lipid bilayers of intestinal epithelium of hydrophobic nature. In contrast, compounds with high lipophilicity are hydrophobic enough to enter lipid bilayers. The lipophilicity of a drug still needs to be in an adequate range for solubility in water medium in body.

The logarithm partition coefficient P ($\log P$) is commonly used to represent the lipophilicity of un-ionized compounds.⁴⁶ As shown in equation 5, $\log P$ refers to the ratio of concentrations of an un-ionized compound in two immiscible phases (often using octanol as an organic phase and water as the aqueous phase). The higher the value of $\log P$, the more hydrophobic the compound is, with an upper limit of value 5 for bioavailability. For ionizable compounds, the logarithm distribution coefficient D ($\log D$), which is the ratio of the concentration of the sum of both ionized and un-ionized forms of the compound in two phases,⁴⁷ is used (Equation 6). Compared with $\log P$ that is pH independent, $\log D$ changes as the function of pH values. For an acidic compound, high pH promotes the ionization and thus the value of $\log D$ is decreased. In contrast, $\log D$ value of a basic compound increases at higher pH due to less ionization.

$$\log P_{\text{oct/wat}} = \log \left(\frac{[\text{solute}]_{\text{oct}}}{[\text{solute}]_{\text{wat}}} \right) \quad (\text{Eq. 5})$$

$$\log D_{\text{oct/wat}} = \log \left(\frac{[\text{solute}]_{\text{oct}}}{[\text{solute}]_{\text{wat}}^{\text{unionized}} + [\text{solute}]_{\text{wat}}^{\text{ionized}}} \right) \quad (\text{Eq. 6})$$



In order to measure the lipophilicity of a compound, calculated log P (clog P) is used for prediction. YMU1, with the clog P value of 1.59, showed poor solubility in doing animal assay. To promote the bioavailability of hTMPK inhibitor, we modified the structure of YMU1 by two approaches to increase the hydrophilicity. First, we added a hydrophilic substituent, such as amine and hydroxyl groups, to the heterocyclic core. Second, carboxylic acid was used to replace R group at the end position of YMU1 to increase water solubility. Noteworthy, such modifications may also provide extra hydrogen bondings to interact with the amino acid residues located in hTMPK active site to render enhanced inhibitory activity.

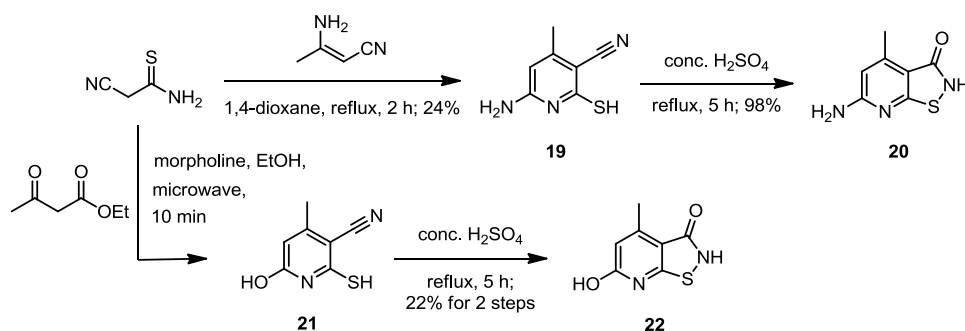
2.3.2. Synthesis of hydrophilic derivatives

The synthetic methods of hydrophilic derivatives were described in this section (Scheme 4). The commercially available 2-cyanothioacetamide and 3-aminocrotononitrile in 1,4-dioxane underwent condensation reaction under refluxing condition to afford a pyridine structure **19**.⁴⁸ The oxidative cyclization reaction was then performed in conc. H₂SO₄ at 100 °C for 5 h to afford **20**, by a procedure similar to that

for compound **3**.

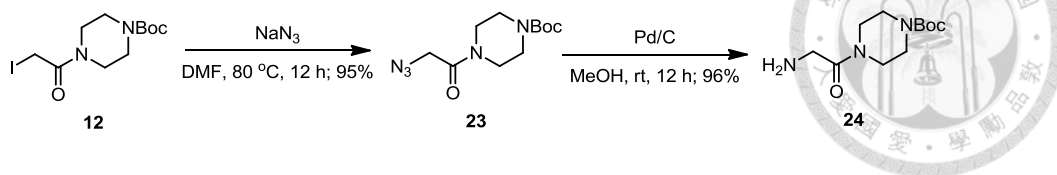
To synthesize compound **22** with a hydroxyl-substituted heterocyclic core, 2-cyanothioacetamide was treated with ethyl acetoacetate in the presence of morpholine at 160 °C by microwave irradiation to provide an intermediate **21**.⁴⁹ Further oxidative cyclization of **21** was similarly performed in conc. H₂SO₄ to give **22**.

Scheme 4. Synthesis of compounds **20** and **22**.^{48, 49}



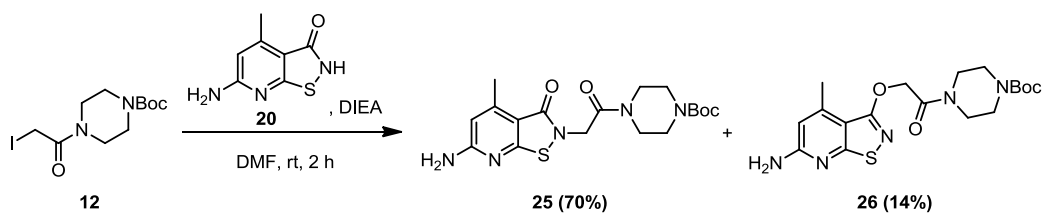
We also modified the linker fragment of YMU1 with a hydrophilic amino group (Scheme 5). Sodium azide acted as a nucleophile to replace the iodide atom in **12** through an S_N2 reaction in the presence of DMF, giving compound **23**. The azido group in **23** was then reduced under an atmosphere of hydrogen by catalysis of Pd/C in MeOH to generate amino derivative **24**.

Scheme 5. Synthesis of compounds **23** and **24**.



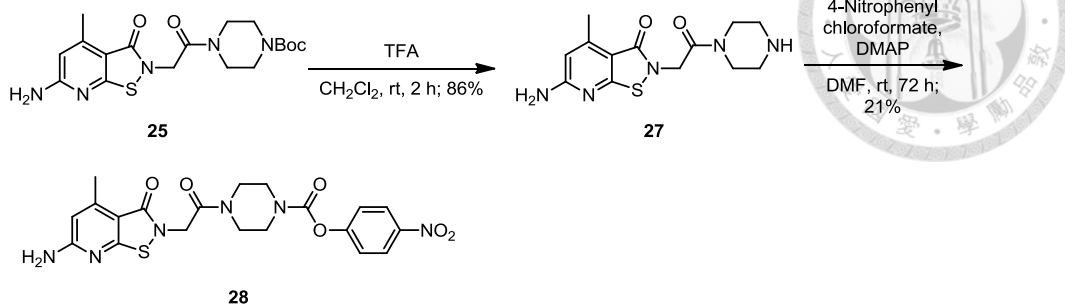
Due to the poor solubility of derivative **20** in CH_2Cl_2 , we used DMF as an alternative solvent to connect **20** with the previously synthesized compound **12** in the presence of DIEA, producing the amine-containing compounds **25** and **26** in a ratio of 5:1 (Scheme 6). The reaction in polar DMF solvent apparently reduced the selectivity of *N*-alkylation. It was noted that the alkylation with the primary amine did not occur because it was conjugated to the heterocyclic core to show poor nucleophilicity.

Scheme 6. Synthesis of compounds **25** and **26**.



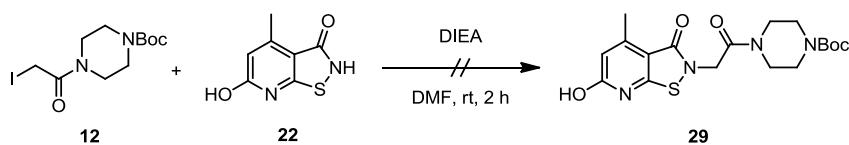
Compound **25** was reacted with TFA in CH_2Cl_2 for 2 h to remove the Boc protecting group (Scheme 7). With the assistance of DMAP, compound **27** reacted with 4-nitrophenyl chloroformate to form derivative **28**.

Scheme 7. Synthesis of compounds **27** and **28**.



For synthesis of hydroxyl-substituted derivative, we first tried to couple compounds **22** and **12** directly by using DIEA as the base and DMF as the solvent (Scheme 8), similar to that for **25**. Unexpectedly, the hydroxyl group showed sufficient nucleophilicity to react with the iodo compound **12**. Therefore, alkylations at the hydroxyl group as well as the *N*- and *O*- sites of amido group occurred along with di-alkylation products. Isolation of the desire product **29** became difficult and tedious.

Scheme 8. Attempted synthesis of compound **29**.

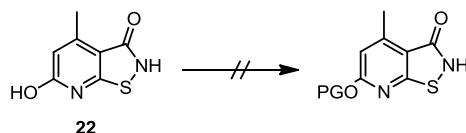


To prevent the unwanted side reactions, we tried to protect the hydroxyl group of **22** by benzyl (Bn), silyl (TBDMS), acyl (Ac and Piv), and THP groups. Unfortunately, all of these protecting groups could not be successfully introduced to **22** due to poor

selectivity and solubility (Table 4).



Table 4. Attempted protection of compound **22**.



Entry	Conditions ^a	Results
1	BnBr, K ₂ CO ₃ , DMF, 2 h	Multiple products
2	TBDMSCl, imidazole, DMF, 1 d	No reaction
3 ⁵⁰	Ac ₂ O, H ⁺ resin, benzene, 1 d	No reaction
4	Ac ₂ O, NEt ₃ , DMF, 1 d	No reaction
5	PivCl, NEt ₃ , DMF, rt, 1 d	No reaction
6	Dihydropyran, PTSA, DMF, 1 d	No reaction

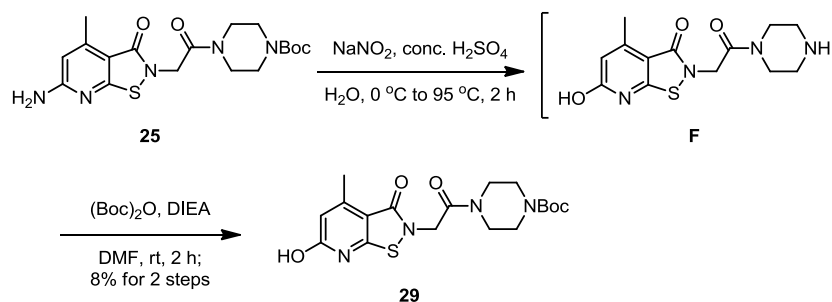
^aFor entry 1, the reaction was conducted only at room temperature. For other entries, the reactions were conducted at room temperature as well as at 70 °C.

Alternatively, we prepared **29** from the amino compound **25** via Sandmeyer reaction (Scheme 9). Using sodium nitrite, the amino group was transformed into diazonium ion in acidic condition, and the intermediate was attacked by water at 95 °C to form hydroxyl group.⁵¹ Nevertheless, the Boc group will be deprotected inevitably in the presence of conc. H₂SO₄. Therefore, after neutralization of the reaction mixture, Boc

anhydride was added with DIEA to reprotect the piperazine moiety, giving derivative **29**.



Scheme 9. Synthesis of compound **29**.⁵¹



To replace the end R group with carboxylic acid, methyl 1-(piperidin-4-yl)carboxylate (**30**) was used as a starting material to react with 2-chloroacetyl chloride to form a disubstituted-piperazine **31** (Scheme 10). Further substitution was processed by sodium iodide in acetone to change the chloride into iodide, which was a better leaving group. BT then acted as a nucleophile to attack compound **32** in the presence of DIEA to give **33** having an ester substituent. It was found that the piperidine amide was also susceptible to hydrolysis in basic conditions (Table 5). In entry 1, we used NaOH as the base and MeOH/THF (1:1) as cosolvent to hydrolyze the ester bond. However, the amide bond was also cleaved within 1 h at room temperature. Using excess NEt_3 as the base in entry 2, no desired product was obtained. Finally, we treated **33** with LiOH as an appropriate base in cosolvent THF/EtOH/ H_2O (2:2:1) at room temperature for 1 h to acquire 11% yield of **34** (Table 5, entry 3).

Scheme 10. Synthesis of derivatives **33** and **34**.

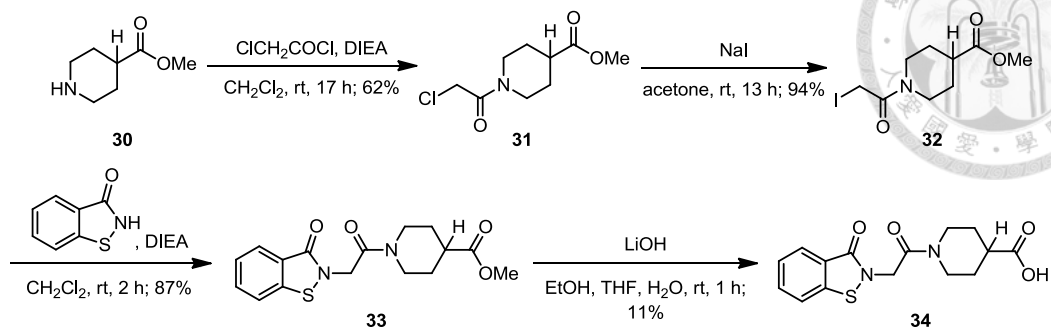
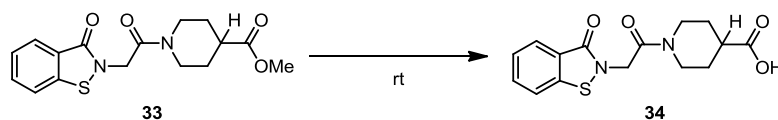


Table 5. Synthesis of compound **34**.



Entry	Conditions	Results
1	NaOH (5 equiv), MeOH/THF = 1:1, 1 h	34 (7.1%)
2	NEt ₃ (40 equiv), THF/H ₂ O = 1:1, 12 h	Messy compound
3	LiOH (1.5 equiv), THF/EtOH/H ₂ O = 2:2:1, 1 h	34 (11%)

2.3.3. Structure–activity relationship of compounds **3**, **20**, **22–29**, and **33–34**

We have synthesized a number of hydrophilic derivatives. Compounds **3**, **20**, and **22** were designed to study the influences of different substituents on the heterocyclic core. The comparison of TMPK activity will be made for disubstituted piperazine **23** and

24 having azido and amino substituents, respectively. The TMPK inhibition of the *N*-alkylated coupling compounds **25** and *O*-alkylated analog **26** will be investigated, though the previous research indicated that the *O*-alkylated compound might not show appreciable inhibitory activity. Compound **27** involves a hydroxy-modified heterocyclic core linked to the piperazine ring with Boc group, **28** and **29** contain amine-substituted heterocyclic core linked to the piperazine ring with different end groups (H and CO₂C₆H₄-*p*-NO₂), whereas methyl ester **33** and carboxylic acid **34** comprise a piperidine-ring instead of piperazine.

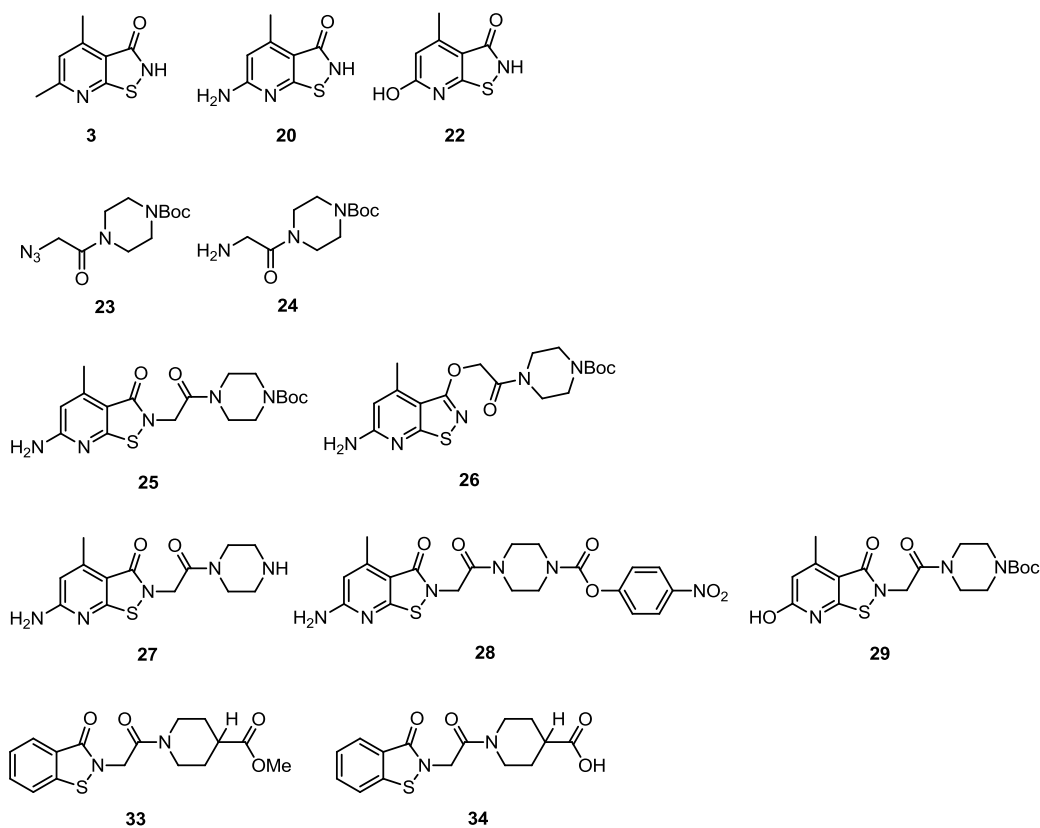


Figure 26. Chemical structures of compounds **3**, **20**, **22–29**, **33** and **34**.

Table 6. cLog P values and TMPK inhibition of compounds **3**, **20**, **22–29**, **33** and **34** at 2 μ M. (n = 9)^{a, 44}

Compound	cLog P ^b	Inhibition (%) ^c
3	1.20	19.6 \pm 14.8
20	0.63	3.6 \pm 3.7
22	0.63	90.5 \pm 3.7
23	ND ^d	11.6
24	0.66	-5.9
25	1.43	26.4 \pm 5.1
26	2.27	5.3 \pm 6.0
27	-0.46	10.8 \pm 5.8
28	0.56	17.2 \pm 7.8
29	0.17	98.8 \pm 6.9
33	1.64	62.1 \pm 12.1
34	1.17	21.8 \pm 5.4
YMU1	1.59	70.0 \pm 7.0

^aEach of the data were obtained from 3 independent experiments and each assay was performed in triplicate except for **23** and **24**.

^bCalculated values of octanol–water partition coefficients at pH 7.4 using Advanced Chemistry Development (ACD/Labs) Software V12.01.

^cNormalized TMPK inhibition based on YMU1 (70% inhibition) at 2 μ M.

^dNot determined.



As shown in Table 6, most derivatives showed lower clog P values than YMU1 (clog P = 1.59) except for the *O*-alkylated product **26** and methyl ester **33**. These results revealed that incorporation of amino, hydroxyl, and carboxylic groups indeed enhanced the hydrophilicity.

Each of the compounds in Figure 26 was tested by luciferase-coupled assay in three independent experiments, with data processed in triplicate at a final concentration of 2 μ M. Compounds **22** and **29** possessing a hydroxyl substituted heterocyclic core revealed promising inhibitory activity against TMPK, whereas compounds **20** and **25–28** having an amino group on the heterocyclic core greatly diminished the inhibitory activity. The azido and amino-containing compounds **23** and **24** were also ineffective to TMPK. Methyl ester **33** showed a higher inhibitory activity than the carboxylic acid **34**. The dosage-dependent experiments using five different concentrations of 0.1, 0.2, 0.5, 1, and 2 μ M were conducted to evaluate the differences of TMPK inhibition by YMU1, **22**, **29** and **33** (Table 7 and Figure 27)

Table 7. Dosage-dependent assays of YMU1, compounds **22**, **29** and **33** against TMPK. (n = 9)^{a, 44}

Compound	Normalized inhibition (%) ^b				
	0.1 μ M	0.2 μ M	0.5 μ M	1 μ M	2 μ M
22	9.0 \pm 6.9	24.0 \pm 1.8	61.5 \pm 5.7	85.4 \pm 3.9	90.5 \pm 3.7
29	0.3 \pm 3.3	2.6 \pm 3.6	49.4 \pm 0.9	87.1 \pm 2.4	98.8 \pm 6.9
33	8.7 \pm 5.4	18.7 \pm 6.9	42.5 \pm 11.4	66.3 \pm 6.4	62.1 \pm 12.1
YMU1	1.6 \pm 1.1	7.6 \pm 2.5	17.4 \pm 0.9	44.9 \pm 12.2	70.0 \pm 7.0

^aEach of the data were obtained from 3 independent experiments and each assay was performed in triplicate.

^bBased on YMU1 (70% TMPK inhibition) at 2 μ M.

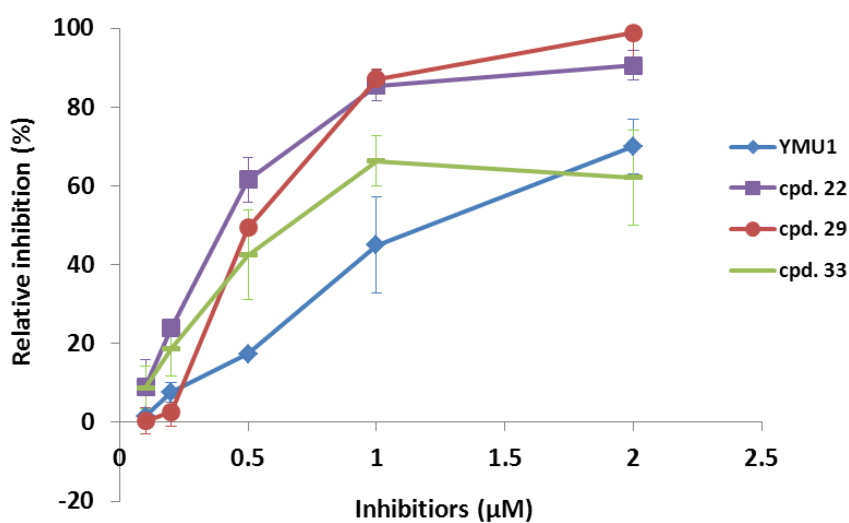
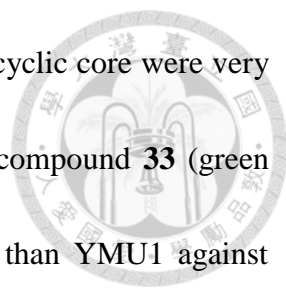


Figure 27. Dosage-dependent TMPK inhibition of YMU1, compounds **22**, **29** and **33**.



Compounds **22** and **29** containing hydroxyl-substituted heterocyclic core were very effective against hTMPK, even better than YMU1. Methyl ester compound **33** (green line) containing a piperidine ring demonstrated higher inhibition than YMU1 against hTMPK at low dosages, though slightly less inhibition at 2 μ M. The results indicated that the hydroxyl group of inhibitors might provide specific interactions with the residues in the TMPK active sites. Taken together, the TMPK active site favors the binding with the compounds having hydroxyl-substituted heterocyclic core, but not amino substituent. Installation of an anionic carboxylic group as the end group seems to disfavor the binding with TMPK.

2.4.1. Dimeric inhibitors

In the previous study, the symmetric dimeric compound **35** bearing two heterocyclic cores has been found to possess appreciable inhibition against hTMPK (Figure 28).²² However, the yield of **35** was very low due to difficulty in purification using flash chromatography on a silica gel column. In this study, we thus explored an improved method to purify compound **35**. We also synthesized dimeric analogs **38** and **39** to examine their inhibitory activities. Because symmetric dimeric compounds displayed poor water solubility we further designed an asymmetric dimeric derivative **42** to enhance the water solubility.

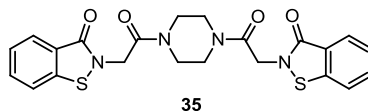


Figure 28. The chemical structure of dimeric TMPK inhibitor **35**.

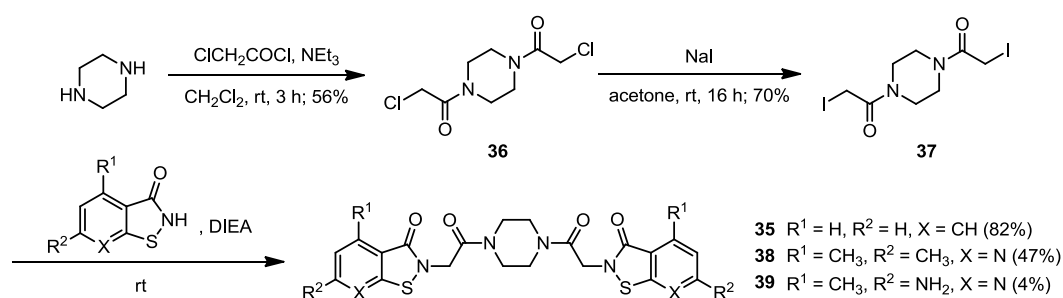
2.4.2. Synthetic schemes for dimeric inhibitors

To construct dimeric derivatives, piperazine was used as the starting material and reacted with 2 equiv of chloroacetyl chloride to produce a symmetric disubstituted-piperazine linker **36** (Scheme 11). On treatment with sodium iodide in acetone, the chlorine atoms were replaced to give the diiodo analog **37**.²²

BT, **3**, and **22** were then used as nucleophiles to undergo substitution reactions with

37 in appropriate solvents to afford symmetric dimeric derivatives **35**, **38**, and **39**, respectively. Purification of **35** by silica gel chromatography was not favored due to its poor solubility in most solvents except DMSO. We thus used MeOH to wash off the impurities in the crude reaction mixture, and collected practically pure dimeric product **35** in a respectable yield (82%). By using this procedure, compound **38** was also obtained in a convenient manner. However, the amine-substituted compound **39** was synthesized in DMF solution along with *O*-alkylated side products which were hard to be removed by MeOH. Further purification by reverse-phase chromatography was applied to separate the *O*-alkylated dimeric side products.

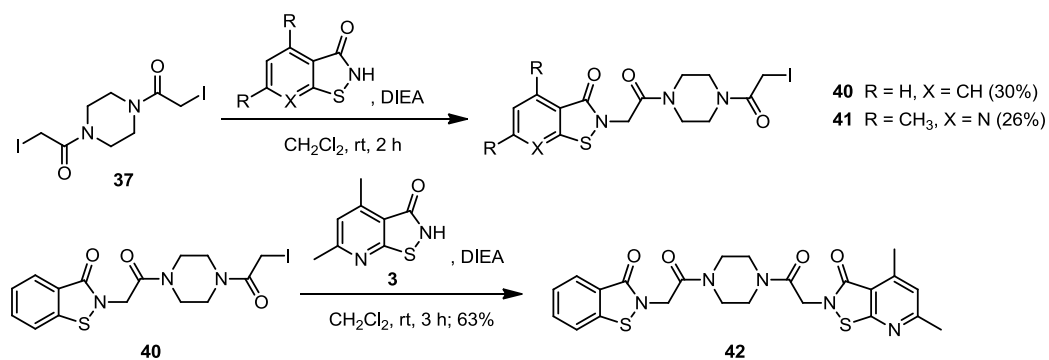
Scheme 11. Synthesis of dimeric inhibitors **35**, **38** and **39**.



For synthesizing asymmetric dimeric compound **42**, diiodo compound **37** was first reacted with 1 equiv of BT in the presence of DIEA for 2 h to give a mono-coupling derivative **40** (Scheme 12). Further substitution reaction was then performed with **3** to afford the asymmetric dimeric product **42**. To our anticipation, asymmetric dimeric

compound **42** showed a better solubility in polar solvents than symmetric dimeric analogs **35**, **38**, and **39**. Therefore, **42** was purified by recrystallization from MeOH. We noted that the intermediate iodo-compound **40** had the potential to act as a suicide inhibitor by forming irreversible covalent bonds with the amino acid residues in the active site of hTMPK.⁵² We also prepared another mono-coupling derivative **41** by the reaction of **3** with **37**.

Scheme 12. Synthesis of compounds **40–42**.



2.4.3. SAR of dimeric compounds 35, 38, 39, and 42

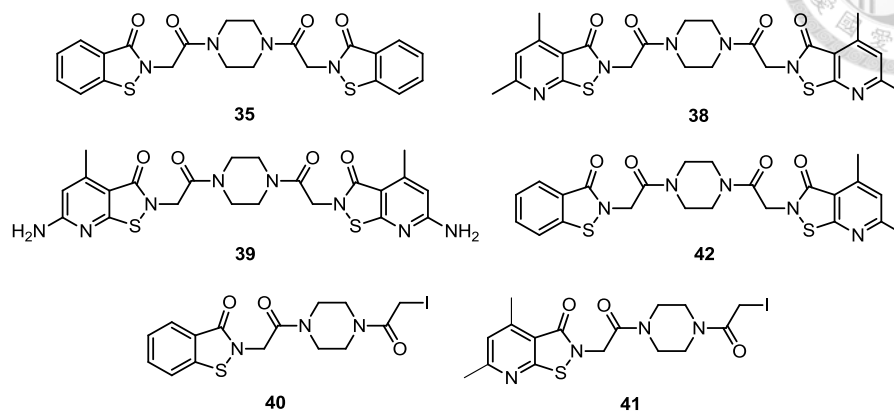


Figure 29. Chemical structures of dimeric inhibitors **35**, **38**, **39**, and **42** as well as suicide inhibitors **40** and **41**.

Table 8. Normalized TMPK inhibition of dimeric compounds **35** and **38–42** at 2 μM . ($n = 6$)^{a, 44}

Compound	Inhibition (%) ^b
35	80.7 \pm 2.1
38	81.5 \pm 3.8
39	79.1 \pm 5.0
42	84.0 \pm 1.2
40	51.3 \pm 5.5
41	47.8 \pm 3.3

^aEach of the data were obtained from 2 independent experiments and each assay was performed in triplicate.

^bNormalized TMPK inhibition based on YMU1 (70% inhibition) at 2 μM .

The luciferase-coupled TMPK assays (Table 8) indicated that all of the dimeric compounds at 2 μ M revealed potent inhibitory activity, whereas, the iodo-substituted analogs **40** and **41** presented moderate inhibition against TMPK. The dimeric compounds **35**, **38**, **39**, and **42** with decent inhibitory activity were chosen for the dosage-dependent inhibition experiments (Table 9).

Table 9. Dosage-dependent assays of YMU1 and dimeric compounds **35**, **38**, **39** and **42** against TMPK. (n = 9)^{a, 44}

Compound	Normalized inhibition (%) ^b				
	0.1 μ M	0.2 μ M	0.5 μ M	1 μ M	2 μ M
35	3.9 \pm 4.5	19.9 \pm 17.3	57.9 \pm 18.3	84.8 \pm 1.4	85.3 \pm 2.1
38	0.9 \pm 2.0	11.6 \pm 7.0	26.0 \pm 7.1	65.3 \pm 3.1	86.0 \pm 2.7
39	5.3 \pm 4.3	7.0 \pm 1.9	24.1 \pm 14.2	46.2 \pm 11.9	83.6 \pm 5.0
42	12.9 \pm 0.5	40.9 \pm 0.6	74.5 \pm 4.5	83.9 \pm 3.6	88.9 \pm 1.2
YMU1	1.6 \pm 1.1	7.6 \pm 2.5	17.4 \pm 0.9	44.9 \pm 12.2	70.0 \pm 7.0

^aEach of the data were obtained from 3 independent experiments and each assay was performed in triplicate.

^bBased on YMU1 (70% TMPK inhibition) at 2 μ M.

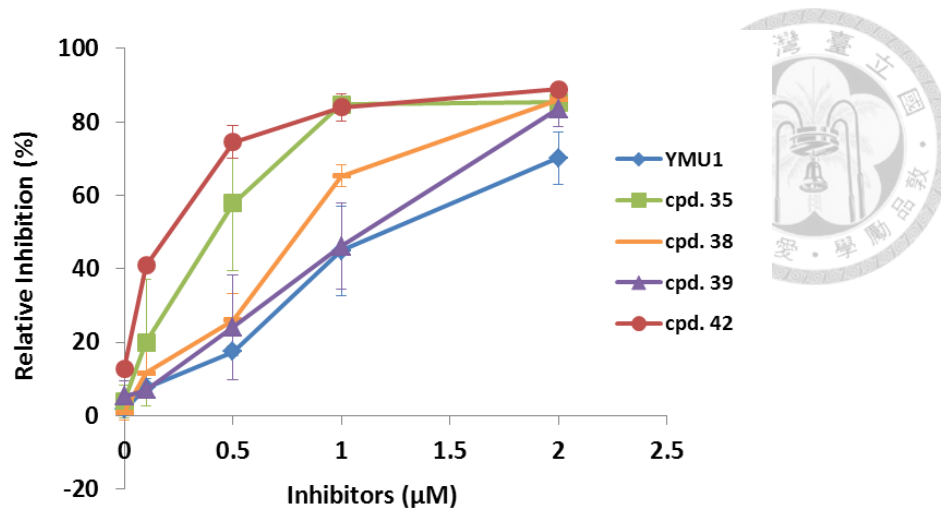


Figure 30. Dosage-dependent inhibition of YMU1 and dimeric compounds **35**, **38**, **39** and **42** against TMPK.

All of the dimeric derivatives showed dosage-dependent inhibition with superior activity than YMU1 (blue line) at the indicated concentrations. In particular, the asymmetric dimer **42** (red line) demonstrated a great inhibitory activity at low concentrations (0.2–1 μM). The asymmetric dimer **42** also improved the water solubility, an Achilles' heel of symmetric dimers.

2.5. Molecular docking of YMU1 derivatives

To further have an insight into the SAR, we chose compound **22** with a hydroxyl-substituted heterocyclic core and the asymmetric dimer **42** for molecular docking experiments as well as inhibition constant (K_i) calculations (Figure 31). The docking experiments were performed by Sheu and coworkers at National Yang Ming University.

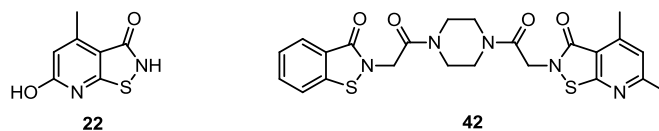


Figure 31. Selected compounds for molecular docking.

By using the NADH-coupled TMPK assay (Table 10), different concentrations of compounds **22** and **42** (0.1–2 μM) were preincubated with TMPK to measure the initial velocity. The K_m and V_{\max} were obtained from nonlinear regression analysis, and the K_i values of compounds **22** and **42** were calculated by the equation of

$$K_i = [I] / (V_{\max}/V_{\max'} - 1)$$

wherein V_{\max} is the maximal velocity without treatment of compound, $[I]$ and $V_{\max'}$ are the concentration of compound and maximal velocity in the presence of compound,³⁹ to give 0.12 ± 0.03 and 0.18 ± 0.15 μM , respectively. Compared with YMU1 ($K_i = 0.22 \pm 0.03$ μM), the hydroxyl-substituted core **22** and asymmetric dimer **42** indeed showed

better inhibition against hTMPK.



Table 10. K_i values of compounds **22** and **42** for hTMPK (n = 4)^a

Cpd. 22 (μM)	K_m for ATP (μM)	V_{max} (nmol / min / mg)	K_i (μM)
0	7.8 \pm 1.5	175.4 \pm 32.4	0.12 \pm 0.03
0.1	9.9 \pm 4.5	102.1 \pm 17.5	
0.2	7.9 \pm 1.1	69.9 \pm 16.7	
0.5	4.9 \pm 5.4	31.3 \pm 14.0	
1.0	6.2 \pm 2.8	22.1 \pm 9.5	
2.0	7.7 \pm 1.4	14.2 \pm 3.3	

Cpd. 42 (μM)	K_m for ATP (μM)	V_{max} (nmol / min / mg)	K_i (μM)
0	9.1 \pm 1.3	163.9 \pm 36.0	0.18 \pm 0.15
0.1	8.3 \pm 1.7	98.0 \pm 33.6	
0.2	2.6 \pm 7.4	55.2 \pm 30.6	
0.5	5.0 \pm 3.3	30.4 \pm 20.2	
1.0	2.9 \pm 7.0	29.5 \pm 18.3	
2.0	12.9 \pm 7.1	22.6 \pm 5.2	

For the K_i value determination, the initial velocity of compound **22** and **42** were measured at different concentrations of ATP (7.8–1000 μM) in the presence of TMP (200 μM). Data obtained from nonlinear regression analysis were used to calculate the V_{max} and K_m . The K_i values represent mean values derived from five different concentrations of compounds **22** and **42**.

^aEach of the data were obtained from 3 independent experiments.

As shown in Figure 32, three small molecules of **22** will be prone to insert into TMPK, with two bound at ATP pocket and one situated in YMU1 binding site according to the binding affinity of docking results. This may explain the superior inhibition of analog **22** at high concentration since the higher level of small molecules present, the more potential of these inhibitors to enter into the binding pocket of TMPK. On the

other hand, two molecules of dimeric compounds **42** may bind with TMPK, with one located at YMU1 binding site and the other covers the LID domain. Noteworthily, the dimeric analog contains two heterocyclic cores similar to the structure of adenine, one of the core fragments may bind to ATP pocket and the other one may situate at the original TMP binding site. Therefore, a dimeric compound will bind with TMPK more tightly to reveal higher inhibitory activity than YMU1 at either low or high concentrations.

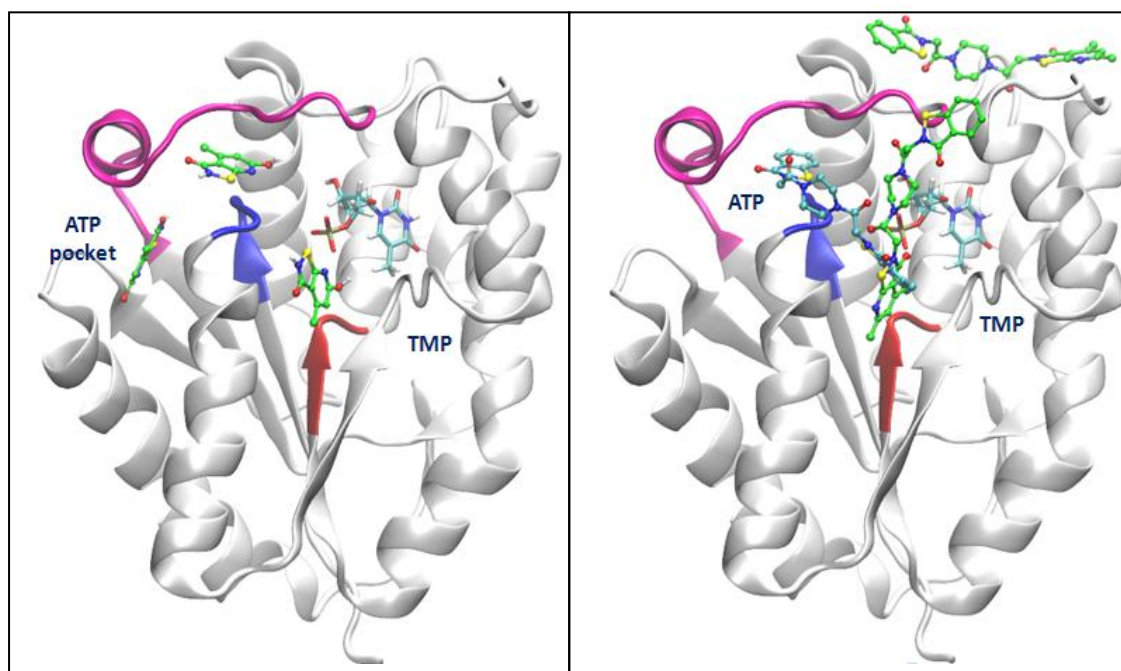


Figure 32. Docking of compounds **22** (left) and **42** (right) with hTMPK. Inhibitors (green), ATP, TMP (light blue), LID domain (pink), and P-loop (blue) are shown.⁵²

2.6. Conclusion

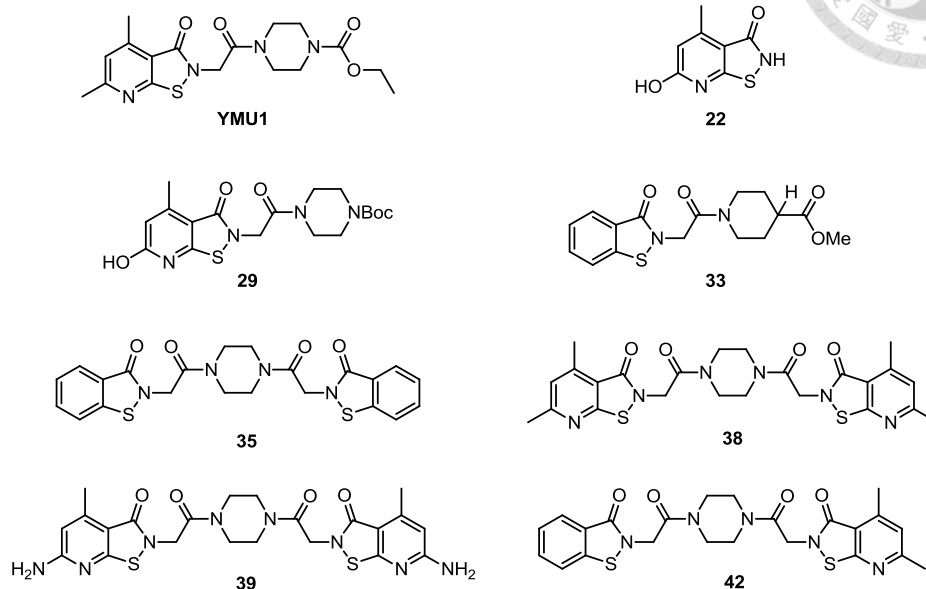
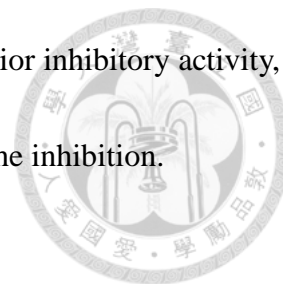


Figure 33. Chemical structures of efficient hTMPK inhibitors.

In summary, we have synthesized 30 YMU1 derivatives and tested for their inhibitory activity against hTMPK. Among these compounds, 7 analogs were proved to exhibit comparable or even better inhibitory activity than YMU1 (Figure 33). Based on the structure–activity relationships, we can establish a general structural feature as shown in Figure 34. First of all, the sulfur atom in bicyclic core plays an important role to maintain the inhibition potency. Second, additional hydroxyl functional group in the heterocyclic core can exert hydrogen bondings with the residues in hTMPK active site to promote the binding affinity. Third, more than one hydrophilic substituted bicyclic cores may be incorporated into the hTMPK binding site to attain good inhibitory activity.

Finally, dimeric analogs with diverse heterocyclic cores show superior inhibitory activity, whereas changing the end group R^2 to a carboxylic acid decreases the inhibition.



Hydroxyl functional group may enhance the inhibition, but amino group is ineffective.

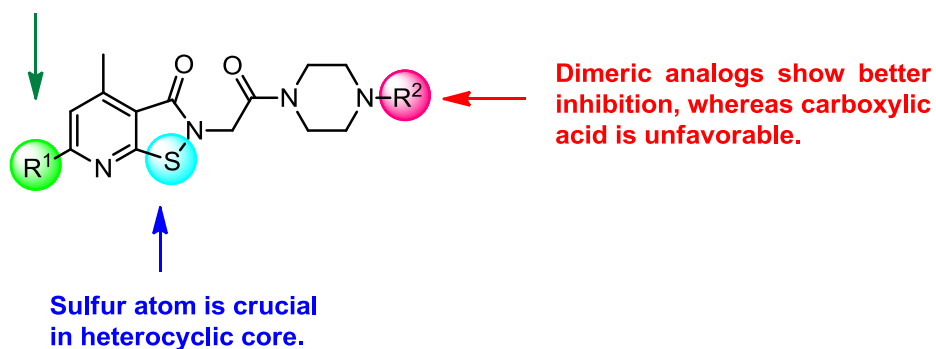


Figure 34. Structural features of YMU1 derivatives against hTMPK.

For further research, symmetric and asymmetric dimeric derivatives with hydrophilic functional groups at the R^1 position will be promising targets to enhance the inhibitory activity against hTMPK. In addition to co-crystallization of hTMPK–inhibitor for X-ray analysis, photoaffinity probe such as changing the R^1 into an azido group and introducing biotin at the R^2 position may be a prospective way to study the binding site.

Chapter 3. Experimental Section

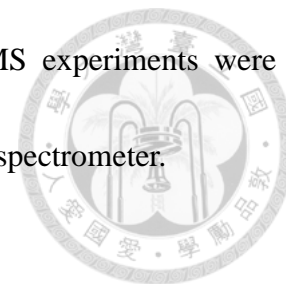


3.1. General part

All reagents and solvents were reagent grade and used without further purification unless indicated otherwise. All solvents were anhydrous grade unless otherwise specified. Dichloromethane (CH_2Cl_2) was distilled from CaH_2 . All air or moisture sensitive experiments were performed under the atmosphere of argon. Reactions were tracked by analytical thin-layer chromatography (TLC) on 0.25 mm E. Merck silica gel 60 F₂₅₄ glass plates. Compounds were visualized by UV, or using ninhydrine, *p*-anisaldehyde, KMnO_4 , and phosphomolybdic acid (PMA) as visualizing agent. Flash chromatography was carried out by using E. Merck silica gel 60 (0.040–0.063 mm particle sizes).

Melting points were recorded on a Yanco micro apparatus. Infrared (IR) spectra were recorded on Nicolet Manga 550-II. Nuclear magnetic resonance (NMR) spectra were obtained on Varian Unity Plus-400 (400 MHz) and chemical shifts (δ) were recorded in parts per million (ppm) relative to δ_{H} 7.24/ δ_{C} 77.0 (central line of t) for $\text{CHCl}_3/\text{CDCl}_3$, δ_{H} 3.31/ δ_{C} 49.0 for $\text{CH}_3\text{OH}/\text{CD}_3\text{OD}$, and δ_{H} 2.50 (m)/ δ_{C} 39.5 (m) for $(\text{CH}_3)_2\text{SO}/(\text{CD}_3)_2\text{SO}$. The splitting patterns are reported as s (singlet), d (doublet), t (triplet), dd (double of doublets), ddd (double of double of doublets), m (multiplet), and

br (broad). Coupling constants (J) are given in Hz. The ESI-MS experiments were conducted on a Bruker Daltonics BioTOF III high-resolution mass spectrometer.



3.2. Expression and purification of enzymes

Human TMPK cloned in pGEX-2T was transformed in *E coli* JM 109 strain and treated with 0.1 mM isopropyl- β -D-thiogalactopyranoside (IPTG) at 37 °C for 4 h to produce GTS-hTMPK fusion protein. After affinity purification by glutathione 4B beads (Amersgam Pharmacia Biotech), hTMPK protein was cleaved from GST-fusion protein bound to glutathione beads by thrombin digestion at 4 °C overnight.

3.3. Luciferase-coupled TMPK assay

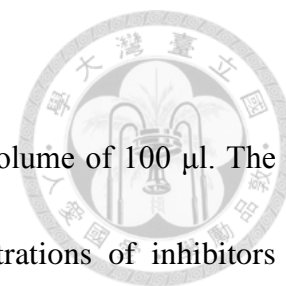
The TMPK reaction was started by adding 0.01–1 μ g of purified hTMPK in 50 μ L of TMPK assay buffer (100 mM Tris-HCl, pH 7.5, 100 mM KCl, 10 mM MgCl₂, 50 μ M ATP and 100 μ M dTMP) in 96-well plate at 25 °C, and then terminated by adding 200 μ L of DTNB (100 μ M). Afterwards, 10 μ L of reaction solution was transferred to a white 96-well plate containing 90 μ L of luciferase assay buffer (50 mM glycine, 0.5 mM EDTA and 5 mM MgCl₂, pH 7.0, 0.1 μ g of luciferase, 50 μ M luciferin and 0.1% BSA). The luminescence was measured with a luminescence counter (Packard).

3.4. NADH-coupled TMPK assay

All reactions were performed in 96-well plates in an assay volume of 100 μ l. The activity of hTMPK was measured at 25 °C. Different concentrations of inhibitors (0.1–2 μ M) with 10 μ l and the purified hTMPK with 10 μ l were preincubated for 10 min, and then 70 μ l of the buffer containing 100 mM Tris–HCl, pH 7.5, 100 mM KCl, 10 mM MgCl₂, 0.5 mM phosphoenol pyruvate, 0.25 mM NADH, 5 units of lactate dehydrogenase, 4 units of pyruvate kinase, and 200 μ M dTMP were added, followed by 10 μ l of ATP with different concentrations (7.8–1000 μ M) to undergo the reaction. The change in NADH concentration was measured by reading the absorbance at 340 nm.

3.5. Molecular docking

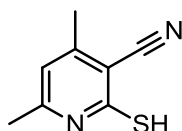
The initial structure of TMPK for YMU1 MD simulation was taken from PDB 1E2D and subjected to energy minimization. The crystal structure of hTMPK for compounds **22** and **42** molecular docking was provided from Nei-Li Chan's team. YMU1 was built and the charge was assigned using Gaussian03 package. AutoDock program was used to identify the binding sites and the interactions of YMU1 with TMPK. This study involved MD simulation performed by the NAMD program with the CHARMM27 force field.



3.6. Synthetic procedures and characterization of compounds

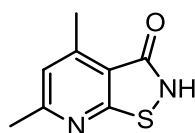


2-Mercapto-4,6-dimethylnicotinonitrile (**2**)²²



A mixture of 2-chloro-4,6-dimethylnicotinonitrile **1** (400 mg, 2.42 mmol) and thiourea (600 mg, 7.89 mmol) in *n*-butanol (12 mL) was heated at reflux (118 °C) for 4 h. After cooling to room temperature, the solution turned to a suspension containing light yellow solids. The solids were collected by filtration, rinsed with *n*-butanol, and dried under reduced pressure to give compound **2** (333 mg, 84% yield). C₈H₈N₂S; light yellow powder; ¹H NMR (400 MHz, CDCl₃); δ 6.40 (1 H, s), 2.45 (3 H, s), 2.43 (3 H, s); ESI–HRMS calcd for C₈H₉N₂S: 165.0486, found: *m/z* 165.0484 [M + H]⁺.

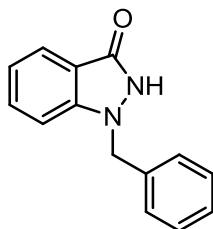
4,6-Dimethylisothiazolo[5,4-*b*]pyridin-3(2*H*)-one (**3**)²²



A solution of compound **2** (310 mg, 1.89 mmol) in conc. H₂SO₄ (2.1 mL) was

stirred at 100 °C for 4 h. The mixture was then cooled and adjusted to pH 5–6 by addition of saturated NaHCO_{3(aq)}, producing white solids in suspension. The solids were then collected by filtration, rinsed with H₂O, and dried in vacuo to give compound **3** (237 mg, 69% yield). C₈H₈N₂OS; pale yellow powder; ¹H NMR (400 MHz, CDCl₃); δ 6.95 (1 H, s), 2.75 (3 H, s), 2.62 (3 H, s); ¹³C NMR (100 MHz, CDCl₃) δ 168.3, 166.5, 163.3, 149.9, 122.5, 115.0, 25.0, 18.3; ESI–HRMS calcd for C₈H₉N₂OS: 181.0436, found: *m/z* 181.0437 [M + H]⁺.

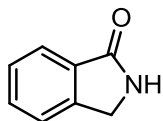
Benzyl-1*H*-indazol-3(2*H*)-one (5**)**⁴¹



A mixture of 1*H*-indazol-3(2*H*)-one **4** (400 mg, 2.98 mmol) and NaOH (120 mg, 2.98 mmol) in H₂O (3 mL) was heated at 35 °C until it became a clear solution. Benzyl chloride (0.34 mL, 2.98 mmol) was then added slowly to the solution at 70 °C. The mixture was stirred for 2 h to give a suspension containing beige solids. After cooling to room temperature, the solids were collected by filtration, and then recrystallized from EtOAc to give compound **5** (40 mg, 60% yield). C₁₄H₁₂N₂O; white powder; ¹H NMR

(400 MHz, CD₃OD); δ 7.68 (1 H, dt, $J = 8.4, 1.0$ Hz), 7.36–7.39 (2 H, m), 7.21–7.27 (3 H, m), 7.16–7.7.18 (2 H, m), 7.05 (1 H, ddd, $J = 7.8, 6.4, 1.4$ Hz), 5.25 (2 H, s); ¹³C NMR (100 MHz, CD₃OD) δ 158.8, 145.1, 138.3, 130.2, 129.7 (2 \times), 128.9, 128.7 (2 \times), 122.3, 121.1, 115.6, 111.2, 53.4; ESI–HRMS calcd for C₁₄H₁₃N₂O: 225.1028, found: m/z 225.1026 [M + H]⁺.

Isoindolin-1-one (7)⁴²

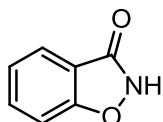


Phthalimide **6** (2 g, 13.5 mmol) was added to a suspension of AlCl₃ (9 g, 67.50 mmol) in cyclohexane (50 mL) at 110 °C for 15 h. The solids were removed by filtration, and the residue was extracted with CHCl₃ and H₂O. The organic phase was dried over MgSO₄, filtered, and concentrated to give yellow solids which were recrystallized from EtOAc to give compound **7** (1 g, 57% yield). C₈H₇NO; white powder; ¹H NMR (400 MHz, CDCl₃); δ 8.83 (1 H, s), 7.76 (1 H, d, $J = 8.4$ Hz), 7.42–7.45 (1 H, m), 7.33–7.36 (2 H, m), 4.36 (2 H, s); ¹³C NMR (100 MHz, CDCl₃) δ 171.6, 143.1, 131.6, 130.9, 127.2, 122.8, 122.5, 45.9; ESI–HRMS calcd for C₈H₈NO: 134.0606, found: m/z 134.0602 [M +

H]⁺.

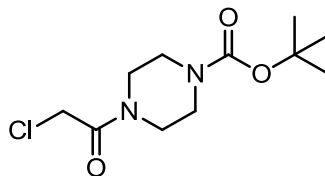


Benzo[*d*]isoxazol-3(2*H*)-one (9)⁴³



A mixture of salicylhydroxamic acid **8** (100 mg, 0.65 mmol) and carbonyldiimidazole (127 mg, 0.78 mmol) in anhydrous THF (5 mL) was stirred for 15 h at 70 °C. The solution was concentrated under reduced pressure, and washed successively with 1 M HCl_(aq) and saturated NaHCO_{3(aq)}. The organic phase was dried over MgSO₄, filtered, and concentrated to give pink solids which were recrystallized from EtOAc to give compound **9** (70 mg, 80% yield). C₇H₅NO₂; white powder; ¹H NMR (400 MHz, CD₃OD); δ 7.63 (1 H, dd, *J* = 8.8, 1.2 Hz), 7.34–7.36 (1 H, m), 6.85–6.91 (2 H, m); ¹³C NMR (100 MHz, CD₃OD) δ 168.5, 160.3, 134.6, 128.4, 120.2, 118.3, 115.5; ESI–HRMS calcd for C₇H₄NO₂: 134.0242, found: *m/z* 134.0240 [M – H][–].

***Tert*-butyl 4-(2-chloroacetyl)piperazine-1-carboxylate (**11**)²²**



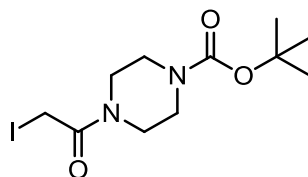
A mixture of piperazine (1.10 g, 12.8 mmol) and DIEA (2.24 mL, 12.8 mmol) in anhydrous CH₂Cl₂ (60 mL) was stirred at room temperature, and a solution of di-*tert*-butyl dicarbonate (1.46 mL, 6.4 mmol) in anhydrous CH₂Cl₂ (80 mL) was added slowly via a separatory funnel over a period of 3 h. The mixture was extracted with CH₂Cl₂ and H₂O. The organic phase was dried over MgSO₄, filtered, and concentrated to give compound **10** (1.39 g, 58% yield).

Chloroacetyl chloride (0.63 mL, 7.32 mmol) was added slowly to a solution of compound **10** (1.24 g, 6.64 mmol) and DIEA (3.5 mL, 19.94 mmol) in anhydrous CH₂Cl₂ at 0 °C. The mixture was then stirred at room temperature for 4 h and extracted with CH₂Cl₂ and H₂O. The organic phase was dried over MgSO₄, filtered, and purified by flash chromatography on a silica gel column with elution of EtOAc/hexane (1:2) to give compound **11** (1.14 g, 71% yield). C₁₁H₁₉ClN₂O₃; white solid; ¹H NMR (400 MHz, CDCl₃) δ 4.05 (2 H, s), 3.56–3.58 (2 H, m), 3.47 (4 H, s), 3.42–3.43 (2 H, m), 1.45 (9 H, s); ¹³C NMR (100 MHz, CDCl₃) δ 164.8, 154.0, 80.1, 45.9, 43.1 (2 ×), 41.8, 40.7, 28.2

(3 ×); ESI–HRMS calcd for C₁₁H₂₀ClN₂O₃: 263.1162, found: *m/z* 263.1165 [M + H]⁺.

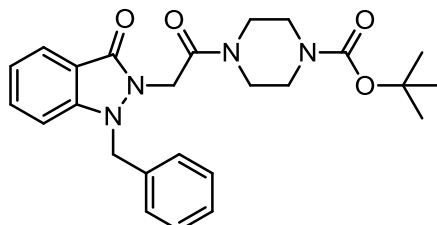


***Tert*-butyl 4-(2-iodoacetyl)piperazine-1-carboxylate (**12**)**²²



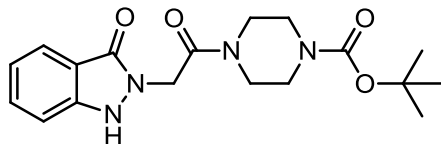
A mixture of compound **11** (297 mg, 1.13 mmol) and sodium iodide (514 mg, 3.43 mmol) in acetone (12 mL) was stirred at room temperature for 16 h. The solids were removed by filtration, and the solution was concentrated under reduced pressure. The residue was extracted with CH₂Cl₂ and H₂O. The organic phase was dried over MgSO₄, filtered, and concentrated to give compound **12** (353 mg, 88% yield). C₁₁H₁₉IN₂O₃; brown solid; ¹H NMR (400 MHz, CDCl₃) δ 3.74 (2 H, s), 3.56–3.59 (2 H, m), 3.51–3.53 (2 H, m), 3.40–3.42 (4 H, m), 1.46 (9 H, s); ¹³C NMR (100 MHz, CDCl₃) δ 166.2, 153.9, 80.1, 46.8, 42.6 (2 ×), 41.7, 28.2 (3 ×), –4.0; ESI–HRMS calcd for C₁₁H₂₀IN₂O₃: 355.0519, found: *m/z* 355.0515 [M + H]⁺.

Tert-butyl 4-[2-(1-benzyl-3-oxo-1H-indazol-2(3H)-yl)acetyl]piperazine-1-carboxylate (13)



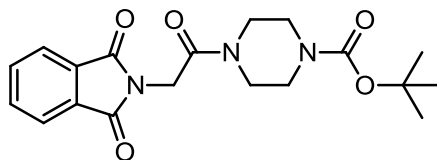
A mixture of compound **5** (100 mg, 0.45 mmol), compound **12** (189 mg, 0.54 mmol) and DIEA (0.39 mL, 2.23 mmol) in anhydrous CH_2Cl_2 (2 mL) was stirred for 8 h at room temperature. The solution was concentrated under reduced pressure, and then purified by flash chromatography on a silica gel column with elution of EtOAc/hexane (1:1) to give compound **13** (82 mg, 41% yield). $\text{C}_{25}\text{H}_{30}\text{N}_4\text{O}_4$; transparent liquid; TLC (EtOAc/hexane = 1:1) $R_f = 0.2$; IR ν_{max} (neat) 2976, 2929, 2864, 1704, 1462, 1417, 1366, 1235, 1168, 1030, 996, 919, 862, 754, 730, 700, 645, 542 cm^{-1} ; ^1H NMR (400 MHz, CDCl_3) δ 7.84 (1 H, d, $J = 8.0$ Hz), 7.51–7.55 (1 H, m), 7.15–7.25 (6 H, m), 7.10 (1 H, br, s), 4.94 (2 H, br, s), 4.57 (2 H, s), 3.43–3.46 (2 H, m), 3.22–3.31 (6 H, m), 1.43 (9 H, s); ^{13}C NMR (100 MHz, CDCl_3) δ 165.1, 154.4, 150.2, 135.2, 132.7, 128.7 (2 \times), 128.2 (2 \times), 127.7 (2 \times), 124.4, 122.3, 117.8, 111.8, 80.3, 54.3, 45.9, 44.9, 43.4 (2 \times), 41.9, 28.3 (3 \times); ESI-HRMS calcd for $\text{C}_{25}\text{H}_{31}\text{N}_4\text{O}_4$: 451.2345, found: m/z 451.2341 [$\text{M} + \text{H}$] $^+$.

***Tert*-butyl 4-[2-(3-oxo-1*H*-indazol-2(3*H*)-yl)acetyl]piperazine-1-carboxylate (**14**)**



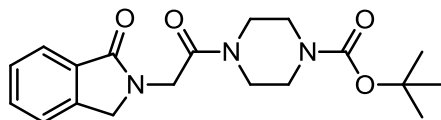
Compound **13** (28 mg, 0.06 mmol) and Pd/C (10%, 3 mg, 0.02 mmol) in MeOH (1 mL) was stirred at room temperature for 24 h under an atmosphere of hydrogen. After filtrated through a pad of Celite, the filtrate was concentrated, and purified by flash chromatography on a silica gel column with elution of EtOAc/hexane (1:1) to give compound compound **14** (12 mg, 53% yield). C₁₈H₂₄N₄O₄; yellow liquid; TLC (EtOAc/hexane = 1:1) *R_f* = 0.1; IR ν_{\max} (neat) 3453, 2974, 2929, 1638, 1634, 1469, 1462, 1422, 1365, 1238, 1170, 1031, 996, 757, 679 cm⁻¹; ¹H NMR (400 MHz, CDCl₃) δ 7.77 (1 H, d, *J* = 8.0 Hz), 7.56 (1 H, ddd, *J* = 8.4, 7.2, 1.2 Hz), 7.29 (1 H, d, *J* = 8.4 Hz), 7.18 (1 H, td, *J* = 8.4, 0.8 Hz), 4.89 (2 H, s), 3.58–3.61 (4 H, m), 3.53 (2 H, s), 3.46 (2 H, s), 1.48 (9 H, s); ¹³C NMR (100 MHz, CDCl₃) δ 167.3, 164.4, 156.4, 148.7, 133.4, 124.3, 123.0, 118.2, 113.6, 81.9, 46.8, 46.0, 43.2, 28.7 (3 ×); ESI–HRMS calcd for C₁₈H₂₃N₄O₄: 359.1719, found: *m/z* 359.1719 [M – H]⁻.

***Tert*-butyl 4-[2-(1,3-dioxoisindolin-2-yl)acetyl]piperazine-1-carboxylate (**15**)**



A mixture of phthalimide **6** (33 mg, 0.23 mmol), compound **12** (81 mg, 0.32 mmol), TBAI (84 mg, 2.30 mmol) and DIEA (0.2 mL, 1.14 mmol) in anhydrous CH₂Cl₂ (10 mL) was stirred at 40 °C for 24 h. The solution was concentrated under reduced pressure, and the residue was extracted with CH₂Cl₂ and H₂O. The organic phase was dried over MgSO₄, filtered, concentrated, and purified by flash chromatography on a silica gel column with elution of EtOAc/hexane (1:1) to give compound **15** (57 mg, 67% yield). C₁₉H₂₃N₃O₅; white solid; mp 243–244 °C; TLC (EtOAc/hexane = 1:1) *R_f* = 0.2; IR ν_{\max} (neat) 2922, 2852, 1774, 1726, 1458, 1420, 1395, 1236, 1169, 1115, 957, 716, 666 cm⁻¹; ¹H NMR (400 MHz, CDCl₃) δ 7.85 (2 H, dd, *J* = 5.6, 3.2 Hz), 7.70 (2 H, dd, *J* = 5.6, 3.2 Hz), 4.48(2 H, s), 3.51–3.57 (6 H, m), 3.43–3.45 (2 H, m), 1.47 (9 H, s); ¹³C NMR (100 MHz, CDCl₃) δ 167.9 (2 ×), 164.1, 154.3, 134.0 (2 ×), 132.1 (2 ×), 123.4 (2 ×), 80.3, 44.5, 43.1 (2 ×), 41.9, 38.9, 28.2 (3 ×); ESI–HRMS calcd for C₁₉H₂₄N₃O₅: 374.1716, found: *m/z* 374.1712 [M + H]⁺.

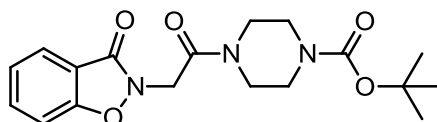
Tert-butyl 4-[2-(1-oxoisindolin-2-yl)acetyl]piperazine-1-carboxylate (16)



A mixture of compound **7** (30 mg, 0.23 mmol), compound **12** (96 mg, 0.27 mmol) and Cs₂CO₃ (220 mg, 0.68 mmol) in anhydrous CH₃CN (1 mL) was stirred at 50 °C for 36 h. The solution turned to a suspension containing white solids. After concentrated under reduced pressure, the residue was extracted with CH₂Cl₂ and H₂O. The organic phase was dried over MgSO₄, filtered, concentrated, and purified by flash chromatography on a silica gel column with elution of EtOAc/hexane (1:1) to give compound **16** (40 mg, 49% yield). C₁₉H₂₅N₃O₄; yellow solid; mp 212–214 °C; TLC (EtOAc/hexane = 1:1) *R_f* = 0.1; IR *v*_{max} (neat) 2974, 2924, 2856, 1684, 1663, 1458, 1413, 1365, 1238, 1166, 1031, 996, 736 cm⁻¹; ¹H NMR (400 MHz, CDCl₃); δ 7.84 (1 H, d, *J* = 7.6 Hz), 7.52–7.56 (1 H, m), 7.44 (2 H, t, *J* = 7.6 Hz), 4.54 (2 H, s), 4.44 (2 H, s), 3.54–3.59 (4 H, m), 3.40–3.45 (4 H, m), 1.45 (9 H, s); ¹³C NMR (100 MHz, CDCl₃) δ 168.5, 166.3, 154.2, 141.5, 131.6, 131.5, 127.9, 123.8, 122.7, 80.4, 50.8, 45.5, 45.1, 44.1 (2 ×), 41.9, 28.4 (3 ×); ESI–HRMS calcd for C₁₉H₂₆N₃O₄: 360.1923, found: *m/z* 360.1919 [M + H]⁺.

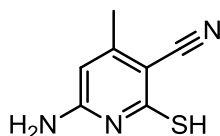
***Tert*-butyl 4-[2-(3-oxobenzo[*d*]isoxazol-2(3*H*)-yl)acetyl]piperazine-1-carboxylate**

(17)



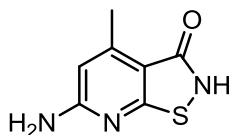
A mixture of compound **9** (120 mg, 0.89 mmol), compound **12** (376 mg, 1.06 mmol) and DIEA (0.92 mL, 5.30 mmol) in anhydrous CH₂Cl₂ (5 mL) was stirred for 72 h at room temperature. The solution was concentrated under reduced pressure, and then purified by flash chromatography on a silica gel column with elution of EtOAc/hexane (1:2) to give compound **17** (20 mg, 6% yield). C₁₈H₂₃N₃O₅; white solid; mp 221–223 °C; TLC (EtOAc/hexane = 1:1) *R_f* = 0.5; IR *v*_{max} (neat) 2976, 2929, 2865, 1791, 1695, 1668, 1489, 1461, 1419, 1366, 1241, 1168, 1022, 919, 754, 690 cm⁻¹; ¹H NMR (400 MHz, CDCl₃) δ 7.21 (1 H, d, *J* = 7.6 Hz), 7.14 (2 H, td, *J* = 13.4, 7.6 Hz), 6.99 (1 H, d, *J* = 7.6 Hz); 4.62 (2 H, s), 3.58–3.60 (2 H, m), 3.53–3.55 (2 H, m) 3.50 (2 H, s), 3.41–3.44 (2 H, m), 1.45 (9 H, s); ¹³C NMR (100 MHz, CDCl₃) δ 163.7, 154.2 (2 ×), 142.5, 130.9, 124.0, 122.8, 110.1, 109.1, 80.6, 45.2, 43.7 (2 ×), 43.3, 42.1, 28.5 (3 ×); ESI–HRMS calcd for C₁₈H₂₄N₃O₅: 362.1716, found: *m/z* 362.1716 [M + H]⁺.

6-Amino-2-mercapto-4-methylnicotinonitrile (**19**)⁴⁸



A mixture of 2-cyanothioacetamide (3.0 g, 30 mmol), 3-aminocrotononitrile (2.46 g, 30 mmol) in 1,4-dioxane (30 mL) was stirred at 100 °C for 2 h. After cooling to room temperature, the solids were collected and recrystallized from EtOH to give compound **19** (1.18 g, 24% yield). C₇H₇N₃S; light yellow solid; ¹H NMR (400 MHz, DMSO-*d*₆) δ 5.89 (1 H, s), 2.18 (3 H, s); ¹³C NMR (100 MHz, DMSO-*d*₆) δ 175.4, 155.2, 153.5, 118.1, 100.2, 99.0, 20.8; ESI–HRMS calcd for C₇H₈N₃S: 166.0439, found: *m/z* 166.0437 [M + H]⁺.

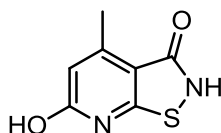
6-Amino-4-methylisothiazolo[5,4-*b*]pyridin-3(2*H*)-one (**20**)



A mixture of compound **19** (145 mg, 0.88 mmol) and conc.H₂SO₄ (1.5 mL) was stirred at 100 °C for 5 h. The mixture was cooled and adjusted to pH 5–6 by addition of

NaHCO_{3(s)}, producing white solids in suspension. The solids were collected by filtration, rinsed with H₂O, and dried in vacuo to give compound **20** (156 mg, 98% yield). C₇H₇N₃OS; pale yellow solid; mp 204–206 °C; TLC (CH₂Cl₂/MeOH = 9:1) *R_f* = 0.2; IR ν_{\max} (neat) 3421, 3344, 3069, 1632, 1600, 1550, 1453, 1375, 1209, 1170, 1028, 983, 838, 619, 550, 500 cm⁻¹; ¹H NMR (400 MHz, DMSO-*d*₆) δ 6.82 (2 H, s), 6.19 (1 H, s), 2.45 (3 H, s); ¹³C NMR (100 MHz, DMSO-*d*₆) δ 168.0, 166.0, 161.8, 147.5, 107.2, 106.9, 17.4; ESI–HRMS calcd for C₇H₈N₃OS: 182.0388, found: *m/z* 182.0395 [M + H]⁺.

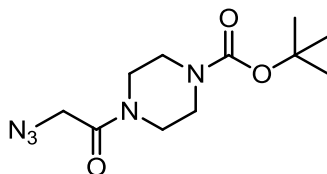
6-Hydroxy-4-methylisothiazolo[5,4-*b*]pyridin-3(2*H*)-one (22)⁴⁹



A mixture of 2-cyanothioacetamide (200 mg, 2.0 mmol) and morpholine (0.17 mL, 2.0 mmol) in EtOH (2 mL) was stirred in seal tube for 5 min. Once dissolved, ethyl acetoacetate (0.25 mL, 2.0 mmol) was added. The mixture was heated at 160 °C by microwave irradiation for 10 min. After cooling to room temperature, the solution was concentrated under reduced pressure to give dark red oil. The oil mixture was treated with CH₂Cl₂ at reflux for 10 min. Once cooling, the yellow solids of compound **21** (141 mg) were collected by filtration and dried in vacuo.

The above-prepared compound **21** (141 mg) was added to conc.H₂SO₄ (1 mL) and stirred under 80°C for 5 h. After cooling, the solution was modulated to pH 5–6 by NaHCO_{3(s)}, producing yellow solids in suspension. The solids were collected by filtration, rinsed with H₂O, and dried in vacuo to give compound **22** (78 mg, 22% yield for 2 steps). C₇H₆N₂O₂S; pale yellow solid; TLC (CH₂Cl₂/MeOH = 9:1) *R_f* = 0.2; ¹H NMR (400 MHz, DMSO-*d*₆) δ 6.13(1 H, s), 2.41 (3 H, s); ¹³C NMR (100 MHz, DMSO-*d*₆) δ 164.1, 163.0, 160.8, 148.6, 114.3, 106.5, 18.2; ESI–HRMS calcd for C₇H₇N₂O₂S: 183.0228, found: *m/z* 183.0231 [M + H]⁺.

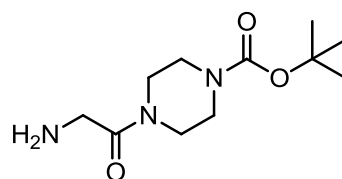
***Tert*-butyl 4-(2-azidoacetyl)piperazine-1-carboxylate (**23**)**



A mixture of compound **12** (67 mg, 0.14 mmol) and sodium azide (20 mg, 0.40 mmol) in DMF (0.5 mL) was stirred at 80 °C for 12 h. The solution was concentrated under reduced pressure and then extracted with CH₂Cl₂ and H₂O. The organic phase was dried over MgSO₄, filtrated, and concentrated to give compound **23** (36 mg, 95% yield). C₁₁H₁₉N₅O₃; yellow solid; mp 226–228 °C; TLC (EtOAc/hexane = 2:1) *R_f* = 0.2; IR

ν_{\max} (neat) 3518, 2977, 2929, 2865, 2098, 1684, 1650, 1459, 1421, 1366, 1285, 1236, 1169, 1127, 995, 863, 770, 553 cm^{-1} ; ^1H NMR (400 MHz, CDCl_3) δ 3.93 (2 H, s), 3.60 (2 H, s, br), 3.44 (4 H, s), 3.34–3.345 (2 H, m), 1.46 (9 H, s); ^{13}C NMR (100 MHz, CDCl_3) δ 165.4, 154.0, 80.3, 50.5, 44.8, 43.4 (2 \times), 41.7, 28.3 (3 \times); ESI–HRMS calcd for $\text{C}_{11}\text{H}_{20}\text{N}_5\text{O}_3$: 270.1566, found: m/z 270.1564 $[\text{M} + \text{H}]^+$.

***Tert*-butyl 4-(2-aminoacetyl)piperazine-1-carboxylate (**24**)**



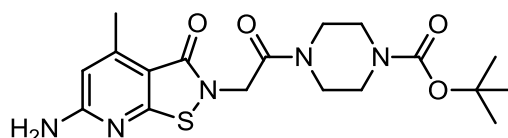
Compound **23** (33 mg, 0.12 mmol) and Pd/C (10%, 7 mg, 0.05 mmol) in MeOH (1.2 mL) was stirred at room temperature for 12 h under an atmosphere of hydrogen. The mixture was filtrated through a pad of Celite, and the filtrate was concentrated under reduced pressure to give compound **24** (28 mg, 96% yield). $\text{C}_{11}\text{H}_{21}\text{N}_3\text{O}_3$; pale yellow solid; mp 226–228 $^{\circ}\text{C}$; TLC (EtOAc/hexane = 1:2) R_f = 0.1; IR ν_{\max} (neat) 3014, 2980, 2687, 2600, 1681, 1654, 1504, 1434, 1364, 1244, 1179, 1009, 763, 545 cm^{-1} ; ^1H NMR (400 MHz, CD_3OD) δ 3.96 (2 H, s), 3.59–3.62 (2 H, m), 3.42–3.50 (6 H, m), 1.48 (9 H, s); ^{13}C NMR (100 MHz, CD_3OD) δ 166.1, 156.1, 81.8, 45.8, 43.1, 41.3, 28.8 (3 \times);

ESI–HRMS calcd for C₁₁H₂₂N₃O₃: 244.1661, found: *m/z* 244.1660 [M + H]⁺.



***Tert*-butyl 4-[(6-amino-4-methyl-3-oxoisothiazolo[5,4-*b*]pyridin-2(3*H*)-2-yl)acetyl]**

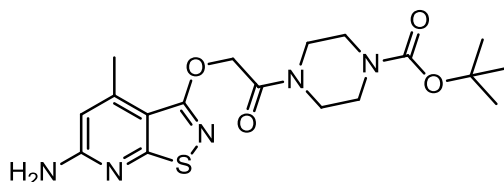
piperazine-1-carboxylate (25)



A mixture of compound **20** (100 mg, 0.55 mmol), compound **12** (98 mg, 0.28 mmol) and DIEA (0.38 mL, 2.27 mmol) in anhydrous DMF (3.8 mL) was stirred for 3 h at room temperature. The solution was concentrated under reduced pressure, and then purified by flash chromatography on a silica gel column with elution of EtOAc/hexane (1:1 to 3:1) to give compound **25** (78 mg, 68% yield). C₁₈H₂₅N₅O₄S; white solid; mp 226–228 °C; TLC (EtOAc/hexane = 1:1) *R_f* = 0.1; IR *v*_{max} (neat) 3260, 3109, 2944, 2887, 1708, 1603, 1568, 1495, 1379, 1298, 1194, 1142, 1080, 928, 795, 667, 432 cm⁻¹; ¹H NMR (400 MHz, CD₃OD) δ 6.29 (1 H, s), 4.70 (2 H, s), 3.56–3.57 (4 H, m), 3.53 (2 H, br, s), 3.45 (2 H, s), 2.54 (3 H, s), 1.48 (9 H, s); ¹³C NMR (100 MHz, CDCl₃) δ 167.8, 167.7, 166.5, 163.8, 156.4, 150.9, 109.1, 108.1, 81.9, 45.9, 45.3, 43.2, 28.8 (3 ×), 18.1; ESI–HRMS calcd for C₁₈H₂₆N₅O₄S: 408.1706, found: *m/z* 408.1706 [M + H]⁺.

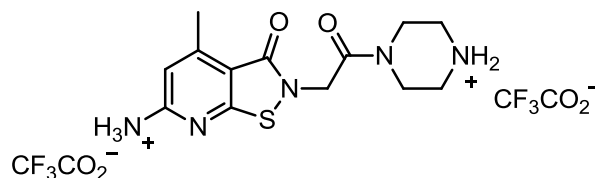
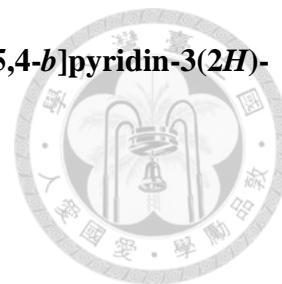
***Tert*-butyl 4-(2-[(6-amino-4-methylisothiazolo[5,4-*b*]pyridin-3-yl)oxy]acetyl]**

piperazin-1-carboxylate (26)



A mixture of compound **20** (52 mg, 0.29 mmol), compound **12** (51 mg, 0.14 mmol) and DIEA (0.2 mL, 1.19 mmol) in anhydrous DMF (2 mL) was stirred for 2 h at room temperature. The solution was concentrated under reduced pressure, and then purified by flash chromatography on a silica gel column with elution of EtOAc/hexane (1:1) to give compound **26** (9 mg, 16% yield). $C_{18}H_{25}N_5O_4S$; white solid; mp 206–208 °C; TLC (EtOAc/hexane = 1:1) R_f = 0.2; IR ν_{max} (neat) 3530, 3366, 3190, 2975, 2931, 1691, 1643, 1593, 1422, 1383, 1255, 1206, 1163, 1133, 1017, 840, 684, 590 cm^{-1} ; H NMR (400 MHz, CD_3OD) δ 6.36 (1 H, s), 5.23 (2 H, s), 3.57–3.58 (4 H, m), 3.54 (2 H, s, br), 3.46 (2 H, s, br), 2.58 (3 H, s), 1.48 (9 H, s); ^{13}C NMR (100 MHz, CD_3OD) δ 168.5 (2 \times), 162.6, 162.2, 156.1, 147.7, 111.1, 109.1, 81.8, 65.9, 45.8, 43.0, 28.8 (3 \times), 19.7; ESI–HRMS calcd for $C_{18}H_{26}N_5O_4S$: 408.1706, found: m/z 408.1705 [$M + H$] $^+$.

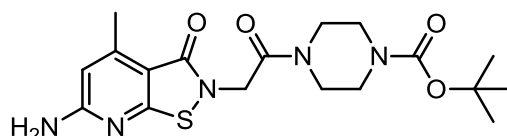
6-Amino-4-methyl-2-[2-oxo-2-(piperazin-1-yl)ethyl]isothiazolo[5,4-*b*]pyridin-3(2*H*)-one (27)



Compound **25** (48 mg, 0.12 mmol) and TFA (1.9 mL, 24.40 mmol) in anhydrous CH_2Cl_2 (14 mL) was stirred for 2 h at room temperature. The solution was concentrated under reduced pressure and washed successively with Et_2O and MeOH to give compound **27** as the TFA salt (55 mg, 86% yield). $\text{C}_{13}\text{H}_{17}\text{N}_5\text{O}_2\text{S}$; white powder; mp 214–216 °C; TLC ($\text{CH}_2\text{Cl}_2/\text{MeOH} = 9:1$) $R_f = 0.1$; IR ν_{max} (neat) 3414, 3335, 3228, 2924, 1680, 1648, 1598, 1543, 1444, 1375, 1340, 1249, 1203, 1145, 1026, 799, 723, 545, 465 cm^{-1} ; ^1H NMR (400 MHz, CD_3OD) δ 6.31(1 H, s), 4.72 (2 H, s), 3.84 (4 H, s, br), 3.37–3.84 (2 H, m), 3.25–3.26 (2 H, m), 2.55 (3 H, s); ^{13}C NMR (100 MHz, CD_3OD) δ 167.9 (2 \times), 166.4, 163.9, 151.0, 109.2, 108.0, 45.1, 44.5 (2 \times), 43.1, 40.2, 18.0; ESI–HRMS calcd for $\text{C}_{13}\text{H}_{18}\text{N}_5\text{O}_2\text{S}$: 308.1181, found: m/z 308.1179 $[\text{M} + \text{H}]^+$.

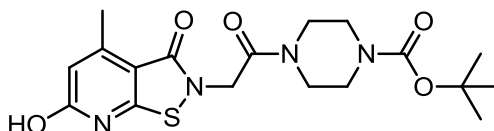
4-Nitrophenyl-4-[2-(6-amino-4-methyl-3-oxoisothiazolo[5,4-*b*]pyridin-2(3*H*)-yl)

acetyl]piperazine-1-carboxylate (28**)**



A mixture of compound **27** (55 mg, 0.10 mmol), 4-nitrophenyl chloroformate (22 mg, 0.11 mmol) and DMAP (37 mg, 0.30 mmol) in anhydrous DMF (0.5 mL) was stirred for 72 h at room temperature. The solution was concentrated under reduced pressure, and washed with MeOH to give brown solids. The solids were removed and the supernatant was purified by flash chromatography on a silica gel column with elution of CH₂Cl₂/MeOH (30:1 to 20:1) to give compound **28** (10 mg, 21% yield). C₂₀H₂₀N₆O₆S; white solid; mp 232–234 °C; TLC (EtOAc) *R_f* = 0.3; IR ν_{\max} (neat) 3321, 3211, 2923, 2852, 2486, 1731, 1638, 1593, 1523, 1442, 1422, 1344, 1028, 1158, 1109, 1018, 858, 746, 542 cm⁻¹; ¹H NMR (400 MHz, DMSO-*d*₆) δ 8.29(2 H, d, *J* = 8.8 Hz), 7.47 (2 H, d, *J* = 8.8 Hz), 6.93 (2 H, br, s), 6.22 (2 H, s), 4.67 (2 H, s), 2.46 (3 H, s); ¹³C NMR (100 MHz, DMSO-*d*₆) δ 165.3, 164.9, 164.3, 161.7, 155.9, 151.6, 147.9, 144.3, 125.0 (2 ×), 122.8 (2 ×), 107.1, 105.6, 43.8, 17.2; ESI–HRMS calcd for C₂₀H₂₁N₆O₆S: 473.1243, found: *m/z* 473.1237 [M + H]⁺.

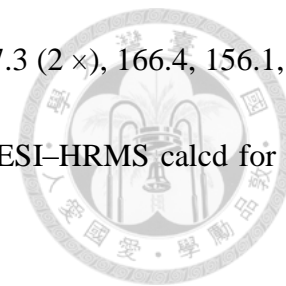
***Tert*-butyl 4-[(6-hydroxy-4-methyl-3-oxoisothiazolo[5,4-*b*]pyridin-2(3*H*)-2-yl)acetyl]piperazine-1-carboxylate (**29**)**



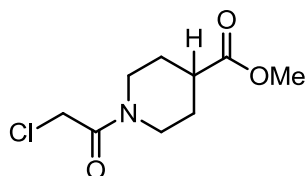
Compound **25** (133 mg, 0.33 mmol) was added to a solution of conc. H₂SO₄ (0.04 mL, 0.7 mmol) and H₂O (0.5 mL) below 0°C. The resultant solution was treated with a solution of NaNO₂ (24.1 mg, 0.35 mmol) in H₂O (0.5 mL) below 5 °C and stirred for 45 min. After then, the mixture was heated to 95°C for 1 h and turned into transparent solution. Once cooling, the solution was neutralized by NaHCO_{3(aq)} to pH 6–7, and dried under reduced pressure to give pale solids.

The crude solids were then treated with di-*tert*-butyl dicarbonate (0.1 mL, 0.5 mmol) and DIEA (0.3 mL, 1.63 mmol) in anhydrous DMF (1 mL), and stirred at room temperature for 2 h. The solution was concentrated under reduced pressure and purified by flash chromatography on a silica gel column with elution of CH₂Cl₂/MeOH (40:1 to 9:1) to give compound **29** (10 mg, 8% yield). C₁₈H₂₄N₄O₅S; white solid; mp 195–197 °C; TLC (EtOAc/hexane = 4:1) *R_f* = 0.1; IR *v*_{max} (neat) 3455, 3241, 2975, 2928, 2855, 1703, 1644, 1546, 1464, 1418, 1384, 1287, 1230, 1170, 1127, 1030, 860, 765, 556 cm⁻¹; ¹H NMR (400 MHz, CD₃OD) δ 6.25 (1 H, s), 4.73 (2 H, s), 3.54–3.60 (6 H, m), 3.46 (2 H,

s), 2.56 (3 H, s), 1.48 (9 H, s); ^{13}C NMR (100 MHz, CD_3OD) δ 167.3 (2 \times), 166.4, 156.1, 153.1, 115.3, 81.8, 45.9, 45.3, 44.1 (2 \times), 43.2, 28.8 (3 \times), 18.6; ESI-HRMS calcd for $\text{C}_{18}\text{H}_{25}\text{N}_4\text{O}_5\text{S}$: 409.1546, found: m/z 409.1547 $[\text{M} + \text{H}]^+$.

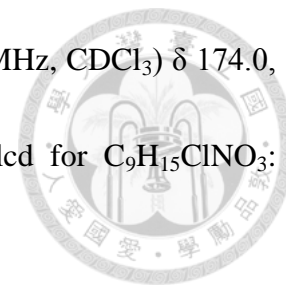


Methyl 1-(2-chloroacetyl)piperidine-4-carboxylate (**31**)

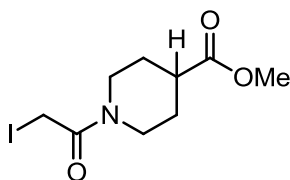


Chloroacetyl chloride (0.31 mL, 3.90 mmol) was added slowly to a solution of methyl piperidine-4-carboxylate **30** (0.48 mL, 3.54 mmol) and DIEA (1.9 mL, 10.63 mmol) in anhydrous CH_2Cl_2 at 0 $^\circ\text{C}$. The mixture was stirred at room temperature for 17 h, and extracted with CH_2Cl_2 and H_2O . The organic phase was dried over MgSO_4 , filtered, and purified by flash chromatography on a silica gel column with elution of EtOAc/hexane (1:2) to give compound **31** (482 mg, 62% yield). $\text{C}_9\text{H}_{14}\text{ClNO}_3$; yellow oil; TLC (EtOAc/hexane = 1:2) R_f = 0.1; IR ν_{max} (neat) 2954, 2863, 1731, 1650, 1452, 1320, 1204, 1178, 1040, 956, 788, 654 cm^{-1} ; ^1H NMR (400 MHz, CDCl_3) δ 4.31 (1 H, dt, J = 13.2, 3.6 Hz), 4.05 (2 H, s), 3.81 (1 H, dt, J = 7.0, 3.4 Hz), 3.69 (3 H, s), 3.20 (1 H, ddd, J = 13.6, 10.8, 2.8 Hz), 2.90 (1 H, ddd, J = 13.6, 10.8, 2.8 Hz), 2.56 (1 H, tt, J = 10.4,

4.0 Hz), 1.93–2.00 (2 H, m), 1.66–1.82 (2 H, m); ^{13}C NMR (100 MHz, CDCl_3) δ 174.0, 164.7, 51.8, 45.5, 41.5, 41.0, 40.4, 28.2, 27.6; ESI–HRMS calcd for $\text{C}_9\text{H}_{15}\text{ClNO}_3$: 220.0740, found: m/z 220.0739 $[\text{M} + \text{H}]^+$.

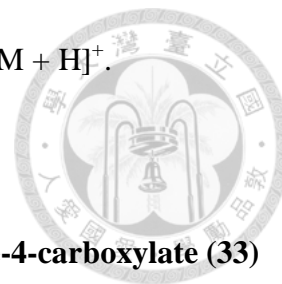


Methyl 1-(2-iodoacetyl)piperidine-4-carboxylate (**32**)

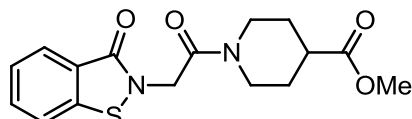


A solution of compound **31** (482 mg, 2.19 mmol) and sodium iodide (985 mg, 6.57 mmol) in acetone (23 mL) was stirred at room temperature for 13 h. The solids were removed by filtration, and the filtrate was concentrated under reduced pressure. The residue was extracted with CH_2Cl_2 and H_2O . The organic phase was dried over MgSO_4 , filtered, concentrated to give compound **32** (642 mg, 94% yield). $\text{C}_9\text{H}_{14}\text{INO}_3$; brown oil; IR ν_{max} (neat) 2998, 2951, 2860, 1730, 1644, 1454, 1374, 1323, 1173, 1040, 899, 606 cm^{-1} ; ^1H NMR (400 MHz, CDCl_3) δ 4.29–4.34 (1 H, m), 3.73 (2 H, t, $J = 4.0$ Hz), 3.69 (3 H, s), 3.13 (1 H, ddd, $J = 13.6, 10.8, 2.8$ Hz), 2.89 (1 H, ddd, $J = 13.6, 10.8, 2.8$ Hz), 2.6 (1 H, tt, $J = 10.4, 4.0$ Hz), 1.9–2.0 (2 H, m), 1.77–1.87 (1 H, m), 1.60–1.70 (2 H, m); ^{13}C NMR (100 MHz, CDCl_3) δ 173.6, 165.6, 52.0, 46.7, 41.7, 40.7, 28.0, 27.9, –3.5;

ESI–HRMS calcd for C₉H₁₅INO₃: 312.0093, found: *m/z* 312.0097 [M + H]⁺.



Methyl 1-[2-(3-oxobenzothiazol-2(3*H*)-yl)acetyl]piperidine-4-carboxylate (33**)**

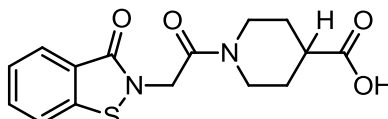


A mixture of BT (188 mg, 1.24 mmol), compound **32** (425 mg, 1.37 mmol) and DIEA (1.1 mL, 6.21 mmol) in anhydrous CH₂Cl₂ (5.6 mL) was stirred for 2 h at room temperature. The solution was concentrated under reduced pressure, and then purified by flash chromatography on a silica gel column with elution of EtOAc/hexane (1:1) to give compound **33** (360 mg, 87% yield). C₁₆H₁₈N₂O₄S; white solid; mp 148–150 °C; TLC (EtOAc/hexane = 1:1) *R_f* = 0.1; IR *v*_{max} (neat) 2951, 2859, 1730, 1650, 1448, 1340, 1314, 1174, 1039, 783, 743, 673 cm⁻¹; ¹H NMR (400 MHz, CDCl₃) δ 8.02 (1 H, dd, *J* = 8.0, 1.0 Hz), 7.54 (1 H, dt, *J* = 7.2, 0.8 Hz), 7.60 (1 H, ddd, *J* = 8.0, 7.0, 1.0 Hz), 7.37 (1 H, ddd, *J* = 8.0, 7.0, 1.0 Hz), 4.69 (2 H, d, *J* = 8.0 Hz), 4.32–4.35 (1 H, m), 3.90 (1 H, d, *J* = 13.2 Hz), 3.67 (3 H, s), 3.22 (1 H, ddd, *J* = 13.6, 10.8, 2.8 Hz), 2.89–2.96 (1 H, m), 2.56 (1 H, tt, *J* = 10.4, 4.0 Hz), 1.94–1.97 (2 H, m), 1.63–1.75 (2 H, m); ¹³C NMR (100 MHz, CDCl₃) δ 173.5, 165.0, 164.1, 140.1, 131.6, 126.3, 124.9, 123.0, 119.9, 52.0, 45.0, 44.6, 41.7, 40.7, 28.5, 27.9; ESI–HRMS calcd for C₁₆H₁₉N₂O₄S: 335.1066, found: *m/z*

335.1067 [M + H]⁺.

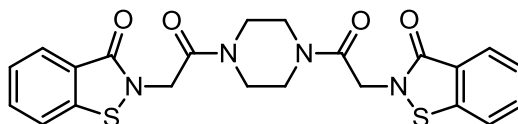


1-[2-(3-Oxobenzo[*d*]isothiazol-2(3*H*)-yl)acetyl]piperidine-4-carboxylic acid (34**)**



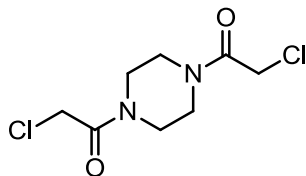
A mixture of compound **33** (100 mg, 0.30 mmol) and LiOH (18 mg, 0.44 mmol) in a mixed solvent of EtOH (0.34 mL), THF (0.34 mL) and H₂O (0.17 mL) was stirred for 1 h at room temperature. The solution was neutralized with 1M HCl_(aq), and then concentrated under reduced pressure. The residue was purified by flash chromatography on a silica gel column with elution of CH₂Cl₂/MeOH (4:1) to give compound **34** (10 mg, 11% yield). C₁₅H₁₆N₂O₄S; white solid; mp 259–261 °C; TLC (CH₂Cl₂/MeOH = 4:1) *R_f* = 0.3; IR *v*_{max} (neat) 3194, 2983, 1778, 1681, 1668, 1566, 1471, 1395, 1312, 1182, 1033, 942, 575, 455 cm⁻¹; ¹H NMR (400 MHz, CD₃OD) δ 8.02 (1 H, d, *J* = 7.6 Hz), 7.40–7.43 (1 H, m), 7.26–7.34 (2 H, m), 4.25 (1 H, t, *J* = 15.0 Hz), 3.90 (1 H, t, *J* = 13.4 Hz), 3.14–3.22 (1 H, m), 2.79 (1 H, t, *J* = 12.0), 2.34–2.36 (1 H, m), 1.87–1.97 (2 H, m), 1.49–1.67 (2 H, m); ¹³C NMR (100 MHz, CD₃OD) δ 168.0, 167.2, 135.0, 133.8, 130.6, 130.1, 128.5, 127.7, 127.0, 53.3, 46.9, 46.7, 43.8, 43.2, 29.9; ESI–HRMS calcd for C₁₅H₁₇N₂O₄S: 321.0909, found: *m/z* 321.0910 [M + H]⁺.

1,4-Bis[(3-oxo-benzo[d]isothiazol-2-yl)acetyl]piperazine (35)²²



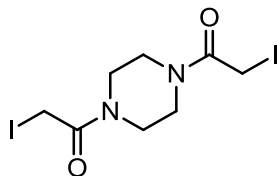
A mixture of BT (63 mg, 0.46 mmol), compound **37** (80 mg, 0.19 mmol) and DIEA (0.16 mL, 0.95 mmol) in anhydrous CH₂Cl₂ (2.2 mL) was stirred at room temperature for 12 h to give a suspension containing white solids. The suspension was concentrated under reduced pressure and washed with MeOH. The residual solids were collected by centrifugation, rinsed successively with CH₂Cl₂ and EtOAc, and dried in vacuo to give compound **35** (72 mg, 82% yield). C₂₂H₂₀N₄O₄S₂; white solid; TLC (CH₂Cl₂/MeOH = 30:1) *R_f* = 0.1; ¹H NMR (400 MHz, DMSO-*d*₆) δ 7.99 (2 H, d, *J* = 8.0 Hz), 7.88 (2 H, d, *J* = 8.0 Hz), 7.70 (2 H, t, *J* = 7.6 Hz), 7.43 (2 H, t, *J* = 7.6 Hz), 4.80–4.82 (4 H, m), 3.63 (2 H, br s), 3.57 (4 H, br s), 3.48 (2 H, br s); ¹³C NMR (100 MHz, CDCl₃) δ 165.2 (2 ×), 165.0 (2 ×), 141.4 (2 ×), 132.0 (2 ×), 125.7 (2 ×), 125.4 (2 ×), 123.5 (2 ×), 121.7 (2 ×), 44.5 (2 ×), 44.0 (2 ×); ESI–HRMS calcd for C₂₂H₂₁N₄O₄S₂: 469.1004, found: *m/z* 469.1003 [M + H]⁺.

1,4-Bis(chloroacetyl)piperazine (**36**)²²



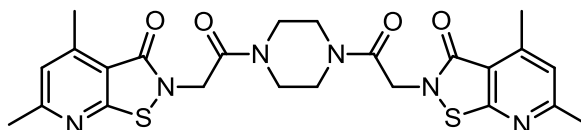
Chloroacetyl chloride (0.63 ml, 7.31 mmol) was added slowly to a solution of piperazine (300 mg, 3.48 mmol), Et₃N (1.9 ml, 13.93 mmol) in anhydrous CH₂Cl₂ at 0 °C. The mixture was then stirred at room temperature for 3 h. After washed with 1 M HCl_(aq) and extracted with CH₂Cl₂ and H₂O, the organic phase was dried over MgSO₄, filtered, and concentrated under reduced pressure to give compound **36** (419 mg, 56% yield). C₈H₁₂Cl₂N₂O₂; brown solid; ¹H NMR (400 MHz, CDCl₃) δ 4.07 (4 H, s), 3.69–3.70 (3 H, m), 3.61–3.64 (3 H, m), 3.54–3.55 (2 H, m); ¹³C NMR (100 MHz, CDCl₃) δ 165.2 (2 ×), 46.2, 45.8, 42.0, 41.7, 40.7 (2 ×); ESI–HRMS calcd for C₈H₁₃Cl₂N₂O₂: 239.0354, found: *m/z* 239.0356 [M + H]⁺.

1,4-Bis(iodoacetyl)piperazine (**37**)²²



A mixture of compound **36** (968 mg, 4.06 mmol) and sodium iodide (2.44 g, 16.25 mmol) in acetone (12 mL) was stirred at room temperature for 16 h. The solids were removed by filtration, and the solution was concentrated under reduced pressure. The residue was extracted with CH₂Cl₂ and H₂O. The organic phase was dried over MgSO₄, filtered, and concentrated to give compound **37** (1.21 g, 70% yield). C₈H₁₂I₂N₂O₂; white solid; ¹H NMR (400 MHz, CDCl₃) δ 3.76 (4 H, s), 3.72–3.74 (2 H, m), 3.62 (2 H, s), 3.57 (2 H, s) 3.44–3.47 (2 H, m); ¹³C NMR (100 MHz, CDCl₃) δ 166.2, 165.9, 46.6, 46.5, 41.7, 41.5, –3.9, –4.0; ESI–HRMS calcd for C₈H₁₃I₂N₂O₂: 422.9067, found: *m/z* 422.9076 [M + H]⁺.

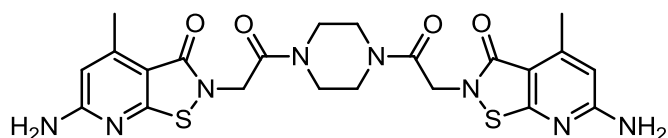
1,4-Bis[(3-oxo-4,6-dimethylisothiazolo[5,4-*b*]pyridin-2-yl)acetyl]piperazine (38)



A mixture of compound **3** (83 mg, 0.46 mmol), compound **37** (89 mg, 0.21 mmol) and DIEA (0.22 mL, 1.3 mmol) in anhydrous CH₂Cl₂ (2.2 mL) was stirred at room temperature for 1.5 h to give a suspension containing brown solids. The suspension was concentrated under reduced pressure and washed with MeOH. The residual solids were collected by centrifugation, rinsed successively with Et₂O, CH₂Cl₂, EtOAc, CH₃CN, and dried in vacuo to give compound **38** (52 mg, 47% yield). C₂₄H₂₆N₆O₄S₂; pale yellow solid; mp 258–261°C (decomposed); TLC (EtOAc/hexane = 1:1) *R_f* = 0.1; IR *v*_{max} (neat) 2922, 1656, 1649, 1562, 1478, 1441, 1356, 1236, 1033, 798 cm⁻¹; ¹H NMR (400 MHz, DMSO-*d*₆) δ 7.17 (2 H, s), 4.81–4.79 (4 H, m), 3.61 (2 H, br, s), 3.55 (4 H, br, s), 3.48 (2 H, br, s); 2.65 (6 H, s), 2.56 (6 H, s); ESI–HRMS calcd for C₂₄H₂₇N₆O₄S₂: 527.1535, found: *m/z* 527.1531 [M + H]⁺.

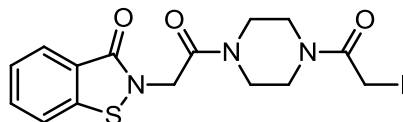
1,4-Bis[(6-amino-4-methyl-3-oxoisothiazolo[5,4-*b*]pyridin-2-yl)acetyl]piperazine

(39)



A mixture of compound **20** (55 mg, 0.30 mmol), compound **37** (59 mg, 0.14 mmol) and DIEA (0.15 mL, 0.84 mmol) in anhydrous DMF (1.5 mL) was stirred for 1 h at room temperature. The solution was concentrated under reduced pressure and washed with MeOH to give brown solids. The solids were then purified by C18 reverse-phase chromatography on a silica gel column (H₂O/MeOH = 70:30) to give compound **39** (3 mg, 4% yield). C₂₂H₂₄N₈O₄S₂; white solid; mp 266–268 °C; TLC (CH₂Cl₂/MeOH = 9:1) *R_f* = 0.4; IR ν_{\max} (neat) 3452, 3348, 3214, 2920, 1649, 1594, 1544, 1444, 1340, 1228, 1123, 1029, 980, 854, 792, 544 cm⁻¹; ¹H NMR (400 MHz, DMSO-*d*₆) δ 6.92(4 H, s), 6.20 (2 H, s), 4.64 (4 H, s), 2.46 (6 H, s); ESI–HRMS calcd for C₂₂H₂₅N₈O₄S₂: 529.1440, found: *m/z* 529.1444 [M + H]⁺.

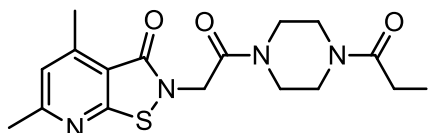
2-[2-(4-(2-Iodoacetyl)piperazin-1-yl)-2-oxoethyl]benzo[d]isothiazol-3(2H)-one (40)



BT (45 mg, 0.30 mmol) in anhydrous CH_2Cl_2 (2.7 mL) was added via syringe pump over a period of 2 h to a suspension of compound **37** (241 mg, 0.57 mmol) and DIEA (0.28 mL, 1.58 mmol) in anhydrous CH_2Cl_2 (0.8 mL) at room temperature. The mixture was washed with 1 M $\text{HCl}_{(\text{aq})}$, and extracted with CH_2Cl_2 and H_2O . The organic phase was dried over MgSO_4 , filtered, and concentrated under reduced pressure. The residual were then washed with MeOH and recrystallized from CH_2Cl_2 to give compound **40** (41 mg, 30% yield). $\text{C}_{15}\text{H}_{16}\text{IN}_3\text{O}_3\text{S}$; pale yellow solid; mp 210–212 °C; TLC (EtOAc/hexane = 8:1) R_f = 0.2; IR ν_{max} (neat) 2923, 2858, 1641, 1446, 1342, 1285, 1243, 1020, 985, 743, 673 cm^{-1} ; ^1H NMR (400 MHz, CDCl_3) δ 8.02 (1 H, d, J = 7.2 Hz), 7.62 (1 H, t, J = 7.2 Hz), 7.54–7.56 (1 H, m), 7.40 (1 H, t, J = 7.4 Hz), 4.71 (2 H, s), 3.74 (4 H, s), 3.60–3.65 (4 H, m), 3.46–3.49 (2 H, m); ^{13}C NMR (100 MHz, CDCl_3) δ 166.6, 165.2, 141.1, 132.2, 126.8, 125.5, 123.2, 120.3, 47.0, 46.7, 44.8, 41.9, 41.7, –4.4; ESI–HRMS calcd for $\text{C}_{15}\text{H}_{17}\text{IN}_3\text{O}_3\text{S}$: 446.0035, found: m/z 446.0033 $[\text{M} + \text{H}]^+$.

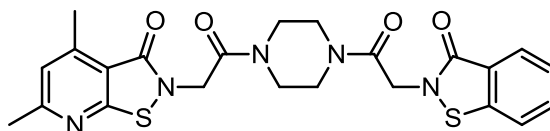
4,6-Dimethyl-2-[2-(4-(2-iodoacetyl)piperazin-1-yl)-2-oxoethyl]-isothiazolo[5,4-*b*]

pyridin-3(2*H*)-one (41)



A solution of compound **3** (105 mg, 0.58 mmol) in anhydrous CH₂Cl₂ (2.4 mL) was added via syringe pump over a period of 2 h to a suspension of compound **37** (245 mg, 0.58 mmol) and DIEA (0.5 mL, 2.90 mmol) in anhydrous CH₂Cl₂ (1.6 mL) at room temperature. The mixture was washed with 1 M HCl_(aq), and extracted with CH₂Cl₂ and H₂O. The organic phase was dried over MgSO₄, filtered, and concentrated under reduced pressure. The residual were then purified by chromatography on a silica gel column with elution of EtOAc/hexane (4:1) to CH₂Cl₂/MeOH (40:1) to give compound **41** (72 mg, 26% yield). C₁₆H₁₉IN₄O₃S; white solid; mp 100–102 °C; TLC (EtOAc/hexane = 8:1) *R_f* = 0.2; IR ν_{\max} (neat) 2923, 2857, 1644, 1584, 1568, 1441, 1332, 1284, 1244, 1021, 789, 681 cm⁻¹; ¹H NMR (400 MHz, CDCl₃) δ 6.93 (1 H, s), 4.66 (2 H, s), 3.74 (2H, s), 3.63–3.67 (4 H, m), 3.55–3.56 (2 H, m), 3.46–3.48 (2 H, m), 2.71 (3 H, s), 2.59 (3 H, s); ¹³C NMR (100 MHz, CDCl₃) δ 166.8, 165.3, 165.0, 163.4, 163.3, 150.1, 122.7, 114.0, 46.8, 44.6, 44.2, 41.8, 41.6, 24.6, 17.4, -4.7; ESI-HRMS calcd for C₁₆H₂₀IN₄O₃S: 475.0301, found: *m/z* 475.0299 [M + H]⁺.

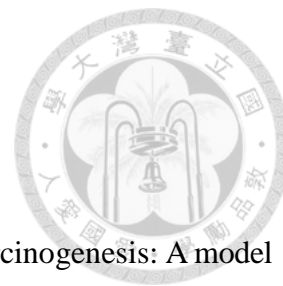
4-[(3-Oxo-benzo[*d*]isothiazol-2-yl)acetyl]-1-[(4,6-dimethyl-3-oxoisothiazolo
[5,4-*b*]pyridin-2-yl)acetyl]piperazine (42)



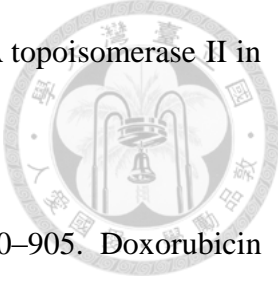
A mixture of compound **3** (19.5 mg, 0.11 mmol), compound **40** (44 mg, 0.98 mmol) and DIEA (0.1 mL, 0.54 mmol) in anhydrous CH₂Cl₂ (1 mL) was stirred for 3 h at room temperature. The mixture was washed with 1 M HCl_(aq) and extracted with CH₂Cl₂ and H₂O. The organic phase was dried over MgSO₄, filtered, and concentrated to give crude product as brown solids. The solids were washed with MeOH. The supernatant was recrystallized from MeOH and combined to give compound **42** (32 mg, 63% yield); C₂₃H₂₃N₅O₄S₂; white solid; mp 127–129 °C; TLC (EtOAc/hexane = 8:1) *R_f* = 0.1; IR ν_{\max} (neat) 2926, 2855, 1651, 1446, 1340, 1283, 1225, 986, 829, 781, 741, 669 cm⁻¹; ¹H NMR (400 MHz, CDCl₃) δ 8.01 (1 H, dd, *J* = 8.0 Hz), 7.61 (1 H, t, *J* = 7.4 Hz), 7.53–7.55 (1 H, m), 7.39 (1 H, t, *J* = 7.6 Hz), 6.92 (1 H, s), 4.69 (2 H, s), 4.64 (2 H, s), 3.58–3.65 (8 H, m), 2.71 (3 H, s), 2.59 (3 H, s); ¹³C NMR (100 MHz, CDCl₃) δ 165.5, 165.2, 165.0, 164.8, 163.1, 163.0, 150.0, 141.0, 132.2, 126.7, 125.5, 123.1, 122.6, 120.3, 114.0, 45.3, 44.8 (2 ×), 44.3, 42.0 (2 ×), 24.7, 17.6; ESI–HRMS calcd for C₂₃H₂₄N₅O₄S₂: 498.1270 found: *m/z* 498.1269 [M + H]⁺.

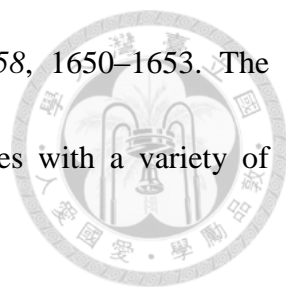


References

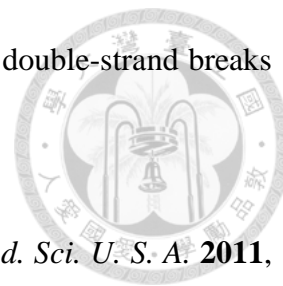


1. Rivera, M. C. A. *Int. J. Morphol.* **2012**, *30*, 309–314. 4NQO carcinogenesis: A model of oral squamous cell carcinoma.
2. Spandidos, D. A. *J. B. U. O. N.* **2007**, *12*, S9–S12. Oncogenes and tumor suppressor genes as paradigms in oncogenesis.
3. Kern, S. E.; Kinzler, K. W.; Bruskin, A.; Jarosz, D.; Friedman, P.; Prives, C.; Vogelstein, B. *Science* **1911**, *252*, 1708–1711. Identification of p53 as a sequence-specific DNA-binding protein.
4. Pommier, Y.; Leo, E.; Zhang, H.-L.; Marchand, C. *Chem. Biol.* **2010**, *17*, 421–433. DNA topoisomerases and their poisoning by anticancer and antibacterial drugs.
5. Wang, J. C. *J. Biol. Chem.* **1991**, *266*, 6659–6662. DNA topoisomerases: why so many?
6. Champoux J. J. *Annu. Rev. Biochem.* **2001**, *70*, 369–413. DNA topoisomerases: structure, function, and mechanism.
7. (a) Ewewuedo, R. B.; Ratain, M. J. *The Oncologist* **1997**, *2*, 359–364. Topoisomerase I inhibitors. (b) Cushman, M.; Pommier, Y. *Mol. Cancer Ther.* **2009**, *8*, 1008–1014. The indenoisoquinoline noncamptothecin topoisomerase I inhibitors: update and perspectives.

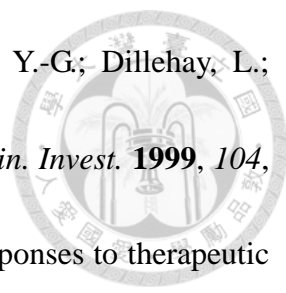
- 
8. Nitiss, J. L. *Nat. Rev. Cancer* **2009**, *9*, 338–350. Targeting DNA topoisomerase II in cancer chemotherapy.
9. Singal, P. K.; Iliskovic, N. *N. Engl. J. Med.* **1998**, *339*, 900–905. Doxorubicin induced cardiomyopathy.
10. Pestalozzi, B. C.; Sotos, G. A.; Choyke, P. L.; Fisherman, J. S.; Cowan, K. H.; O'Shaughnessy, J. A. *Cancer* **1993**, *71*, 1797–1800. Typhlitis resulting from treatment with taxol and doxorubicin in patients with metastatic breast cancer.
11. Chiuchetta, S. J. R.; Castro-Prado, M. A. A. *Braz. J. Microbiol.* **2002**, *33*, 255–259. Doxorubicin and etoposide induce somatic recombination in diploid cells of *Aspergillus nidulans*.
12. Ramu, A.; Cohen, L.; Glaubiger, D. *Cancer Res.* **1984**, *44*, 1976–1980. Oxygen radical detoxification enzymes in doxorubicin-sensitive and -resistant P388 murine leukemia cells.
13. Dunkern, T. R.; Wedemeyer, I.; Baumgärtner, M.; Fritz, G.; Kaina, B. *DNA Repair* **2003**, *2*, 49–60. Resistance of p53 knockout cells to doxorubicin is related to reduced formation of DNA strand breaks rather than impaired apoptotic signaling.
14. Engstrom, Y.; Eriksson, S.; Jildevik, I.; Skog, S.; Thelander, L.; Tribukai, B. *J. Biol. Chem.* **1985**, *260*, 9114–9116. Cell cycle-dependent expression of mammalian ribonucleotide reductase.

- 
15. Fan, H.-Z.; Villegas, C.; Huang, A.-P. *Cancer Res.* **1998**, *58*, 1650–1653. The mammalian ribonucleotide reductase R2 component cooperates with a variety of oncogenes in mechanisms of cellular transformation.
16. (a) Zhang, K.-Q.; Hu, S.-Y.; Wu, J.; Chen, L.-L.; Lu, J.-M.; Wang, X.,-C.; Liu, X.-Y.; Zhou, B.-S.; Yen, Y. *Mol. Cancer* **2009**, *8*, 11. Overexpression of RRM2 decreases thrombospondin-1 and increases VEGF production in human cancer cells in vitro and in vivo: implication of RRM2 in angiogenesis. (b) Kuo, M.-L.; Hwang, H.-S.; Sosnay, P. R.; Kunugi, K. A.; Kinsella, T. J.; Ohio, C. *Cancer J.* **2003**, *9*, 277–285. Overexpression of the R2 subunit of ribonucleotide reductase in human nasopharyngeal cancer cells reduces radiosensitivity.
17. Burkhalter, M. D.; Roberts, S. A.; Havener, J. M.; Ramsden, D. A. *DNA Repair* **2009**, *8*, 1258–1263. Activity of ribonucleotide reductase helps determine how cells repair DNA double strand breaks.
18. Hartlerode, A. J.; Scully, R. *Biochem. J.* **2010**, *423*, 157–168. Mechanisms of double-strand break repair in somatic mammalian cells.
19. Filippo, J. S.; Sung, P.; Klein, H. *Annu. Rev. Biochem.* **2008**, *77*, 229–257. Mechanism of eukaryotic homologous recombination.
20. Robert, T.; Vanoli, F.; Chiolo, I.; Shubassi, G.; Bernstein, K. A.; Rothstein, R.; Botrugno, O. A.; Parazzoli, D.; Oldani, A.; Minucci, S.; Foiani, M. *Nature* **2011**, *471*,

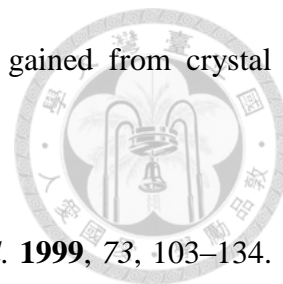
74–79. HDACs link the DNA damage response, processing of double-strand breaks and autophagy.



21. Anderson, D. D.; Quintero, C. M.; Stover, P. J. *Proc. Natl. Acad. Sci. U. S. A.* **2011**, *108*, 1–6. Identification of a de novo thymidylate biosynthesis pathway in mammalian mitochondria.
22. Yeh, M.-T. M.S. Thesis, 2011, National Taiwan University. Synthesis and identification of novel chemosensitizers against human thymidylate kinase.
23. Rose, M. G.; Farrell, M. P.; Schmitz, J. C. *Clin. Colorectal Cancer* **2002**, *4*, 220–229. Thymidylate synthase: A critical target for cancer chemotherapy.
24. Longley, D. B.; Harkin, D. P.; Johnston, P. G. *Nat. Rev. Cancer* **2003**, *3*, 330–338. 5-Fluorouracil: mechanisms of action and clinical strategies.
25. Widemann, B. C.; Balis, F. M.; Godwin, K. S.; McCully, C.; Adamson, P. C. *Cancer Chemother. Pharmacol.* **1999**, *44*, 439–443. The plasma pharmacokinetics and cerebrospinal fluid penetration of the thymidylate synthase inhibitor raltitrexed (TomudexTM) in a nonhuman primate model.
26. Bessman, M. J.; Lehman, I. R.; Adler, J.; Zimmerman, S. B.; Simms, E. S.; Kornberg, A. *Proc. Natl. Acad. Sci. U. S. A.* **1958**, *44*, 633–640. Enzymatic synthesis of deoxyribonucleic acid. III. The incorporation of pyrimidine and purine analogues into deoxyribonucleic acid.

- 
27. Bunz, F.; Hwang, P.-M.; Torrance, C.; Waldman, T.; Zhang, Y.-G.; Dillehay, L.; Williams, J.; Lengauer, C.; Kinzler, K. W.; Vogelstein, B. *J. Clin. Invest.* **1999**, *104*, 264–269. Disruption of p53 in human cancer cells alters the responses to therapeutic agents.
28. Lee, S.-J.; Kim, S.-Y.; Chung, J.-H.; Oh, S.-J.; Ryu, J.-S.; Hong, Y.-S.; Kim, T.-W.; Moon, D.-H. *Biochem. Pharmacol.* **2010**, *80*, 1528–1536. Induction of thymidine kinase 1 after 5-fluorouracil as a mechanism for 3'-deoxy-3'-[¹⁸F]fluorothymidine flare.
29. Kumar, M.; Sharma, S.; Srinivasan, A.; Singh, T. P.; Kaur, P. *J. Mol. Model.* **2011**, *17*, 1173–1182. Structure-based in-silico rational design of a selective peptide inhibitor for thymidine monophosphate kinase of mycobacterium tuberculosis.
30. Kotaka, M.; Dhaliwal, B.; Ren, J.-S.; Nochols, C. E.; Angell, R.; Lockyer, M.; Hawkins, A. R.; Stammers, D. K. *Protein Sci.* **2006**, *15*, 774–784. Structures of *S. aureus* thymidylate kinase reveal an atypical active site configuration and an intermediate conformational state upon substrate binding.
31. Cui, Q.; Shin, W.-S.; Luo, Y.; Tian, J.; Cui, H.; Yin, D. *Curr. Med. Chem.* **2013**, *20*, 1286–1305. Thymidylate kinase: An old topic brings new perspectives.
32. Ostermann, N.; Schlichting, L.; Brundiers, F.; Konrad, M.; Reinstein, J.; Veit, T.; Goody, R. S.; Lavie, A. *Structure* **2000**, *8*, 629–642. Insights into the

phosphoryltransfer mechanism of human thymidylate kinase gained from crystal structures of enzyme complexes along the reaction coordinate.



33. Yan, H.-G.; Tsai, M.-D. *Adv. Enzymol. Relat. Areas. Mol. Biol.* **1999**, *73*, 103–134.

Nucleoside monophosphate kinases: structure, mechanism, and substrate specificity.

34. Ostermann, N.; Segura-Peña, D.; Meier, C.; Veit, T.; Monnerjahn, V.; Konrad, M.;

Lavie, A. *Biochemistry* **2003**, *42*, 2568–2577. Structures of human thymidylate kinase in complex with prodrugs: Implications for the structure-based design of novel compounds.

35. Ostermann, N.; Lavie, A.; Padiyar, S.; Brundiars, R.; Veit, T.; Reinstein, J.; Goody,

R. S.; Konrad, M.; Schlichting, I. *J. Mol. Biol.* **2000**, *304*, 43–53. Potentiating AZT activation: Structures of wild-type and mutant human thymidylate kinase suggest reasons for the mutants' improved kinetics with the HIV prodrug metabolite AZTMP.

36. Lavie, A.; Ostermann, N.; Brundiars, R.; Goody, R. S.; Reinstein, J.; Konrad, M.;

Schlichting, I. *Proc. Natl. Acad. Sci. U. S. A.* **1998**, *95*, 14045–14050. Structural basis for efficient phosphorylation of 3'-azidothymidine monophosphate by *Escherichia coli* thymidylate kinase.

37. Hu, C.-M, Chang, Z.-F. *Cancer Res.* **2008**, *68*, 2831–2840. Synthetic lethality by

lentiviral short hairpin RNA silencing of thymidylate kinase and doxorubicin in

colon cancer cells regardless of the *p53* status.



38. Kastan, M. B.; Bartek, J. *Nature* **2004**, *432*, 316–323. Cell-cycle checkpoints and cancer.
39. Hu, C.-M.; Yeh, M.-T.; Tsao, N.; Chen, C.-W.; Gao, Q.-Z.; Chang, C.-Y.; Lee, M.-H.; Fang, J.-M.; Sheu, S.-Y.; Lin, C.-J.; Tseng, M.-C.; Chen, Y.-J.; Chang, Z.-F. *Cancer Cell* **2012**, *22*, 36–50. Tumor cells require thymidylate kinase to prevent dUTP incorporation during DNA repair.
40. Hu, C.-M.; Chang, Z.-F. *Anal. Biochem.* **2010**, *398*, 269–271. A bioluminescent method for measuring thymidylate kinase activity suitable for high-throughput screening of inhibitor.
41. Sokolenko, T. M.; Yagupolskii, L. M. *Chem. Heterocycl. Comp.* **2011**, *46*, 1649–1658. Polyfluoroalkylation and alkenylation of 1-benzyl-1H-indazol-3-ol.
42. Koltunov, K. Y.; Prakash, G. K. S.; Rasul, G.; Olah, G. A. *Eur. J. Org. Chem.* **2006**, *21*, 4861–4866. Superacidic activation of maleimide and phthalimide and their reactions with cyclohexane and arenes.
43. Yevich, J. P.; New, J. S.; Smith, D. W.; Lobeck, W. G.; Catt, J. D.; Minielli, J. L.; Eison, M. S.; Taylor, D. P.; Riblet, L. A.; Temple, D. L. *J. Med. Chem.* **1986**, *29*, 359–369. Synthesis and biological evaluation of 1-(1,2-benzisothiazol-3-yl)- and (1,2-benzisoxazol-3-yl)piperazine derivatives as potential antipsychotic agent.

44. Luciferase-coupled TMPK assays were conducted by Zee-Fang Chang's lab at National Yang Ming University.



45. Rutkowaka, E.; Pajak, K.; Józwiak, K. *Acta. Pol. Pharm.* **2013**, *70*, 3–18.

Lipophilicity-methods of determination and its role in medicinal chemistry.

46. Meylan, W. M.; Howard, P. H. *Persp. Drug. Disc. Des.* **2000**, *19*, 67-84. Estimating log P with atom/fragments and water solubility with log P.

47. Kah, M.; Brown, C. D. *Chemosphere* **2008**, *72*, 1401–1408. Log D: Lipophilicity for ionisable compounds.

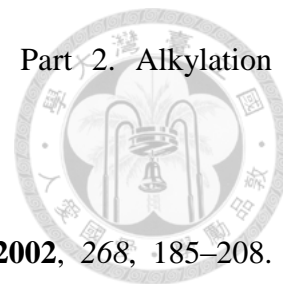
48. Elnagdi, M. H.; Erian, A. A. W. *Arch. Pharm.* **1991**, *324*, 853–858. New routes to polyfunctionally substituted pyridine, pyridopyridine, quinoline, and pyridazine derivatives.

49. Kennedy, J. P.; Bridges, T. M.; Gentry, P. R.; Brogan, J. T.; Brady, A. E.; Shirey, J. K.; Jones, C. K.; Conn, P. J.; Lindsley, C. W. *ChemMedChem.* **2009**, *4*, 1600–1607. Synthesis and structure-activity relationships of novel allosteric potentiators of the M₄ muscarinic acetylcholine receptor.

50. Srivastava, V.; Tandon, A.; Ray, S. *Synth. Commun.* **1992**, *22*, 2703–2710. Convenient and selective acetylations of phenols, amines and alcohols.

51. Adger, B. M.; Ayrey, P.; Bannister, R.; Forth, M. A.; Hajikarimian, Y.; Lewis, N. J.; O'Farrell, C.; Owens, N.; Shamji, A. *J. Chem. Soc., Perkin Trans. 1* **1998**, *10*,

2791–2796. Synthesis of 2-substituted 4-pyridylpropionates. Part 2. Alkylation approach.



52. Bogyo, M.; Wang, E.-W. *Curr. Top. Microbiol. Immunol.* **2002**, *268*, 185–208.

Proteasome inhibitors: complex tools for a complex enzyme.

53. Molecular docking of compounds 22 and 42 were conducted by Sheh-Yi Sheu's lab at National Yang Ming University.

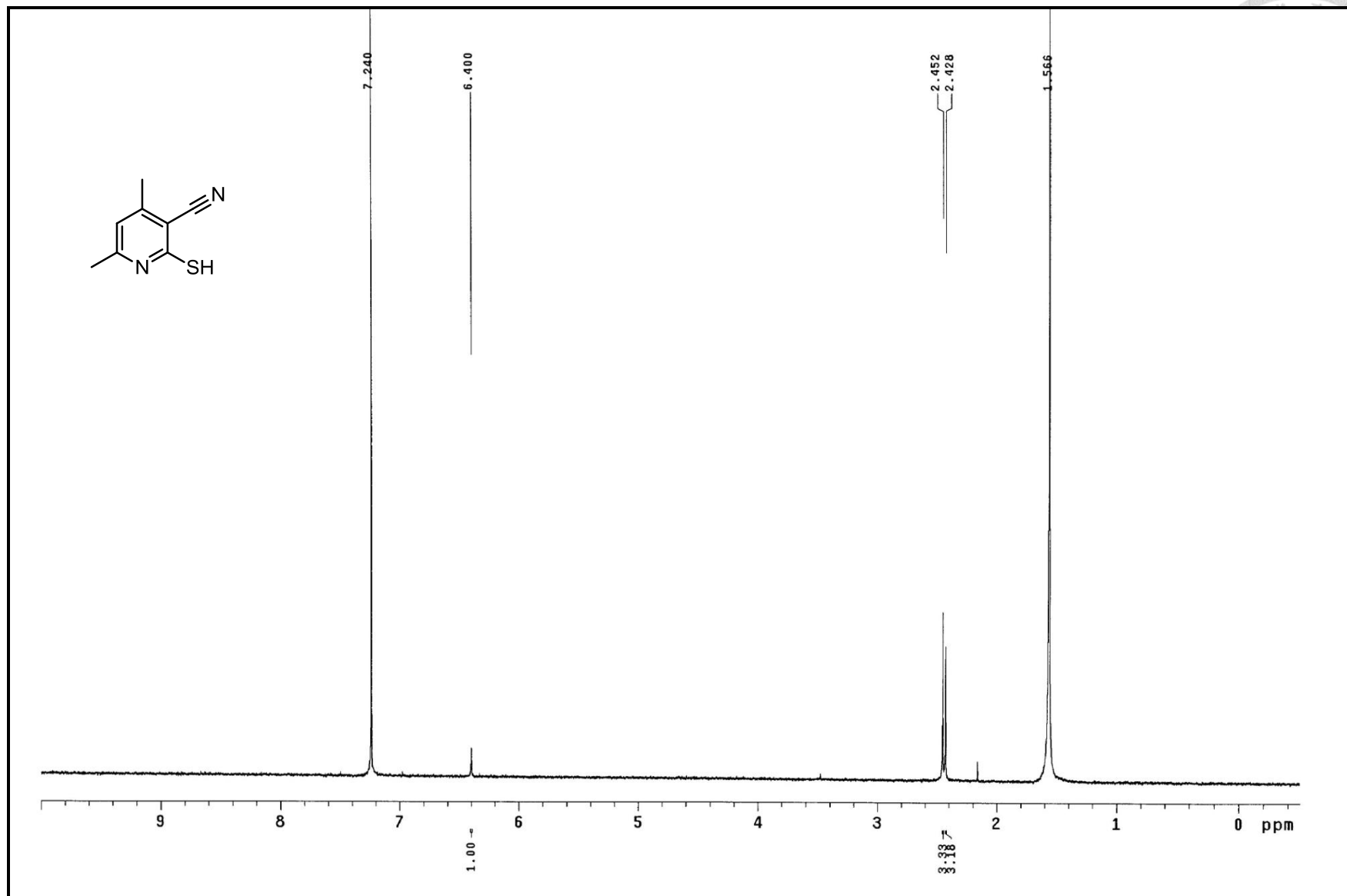
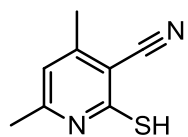




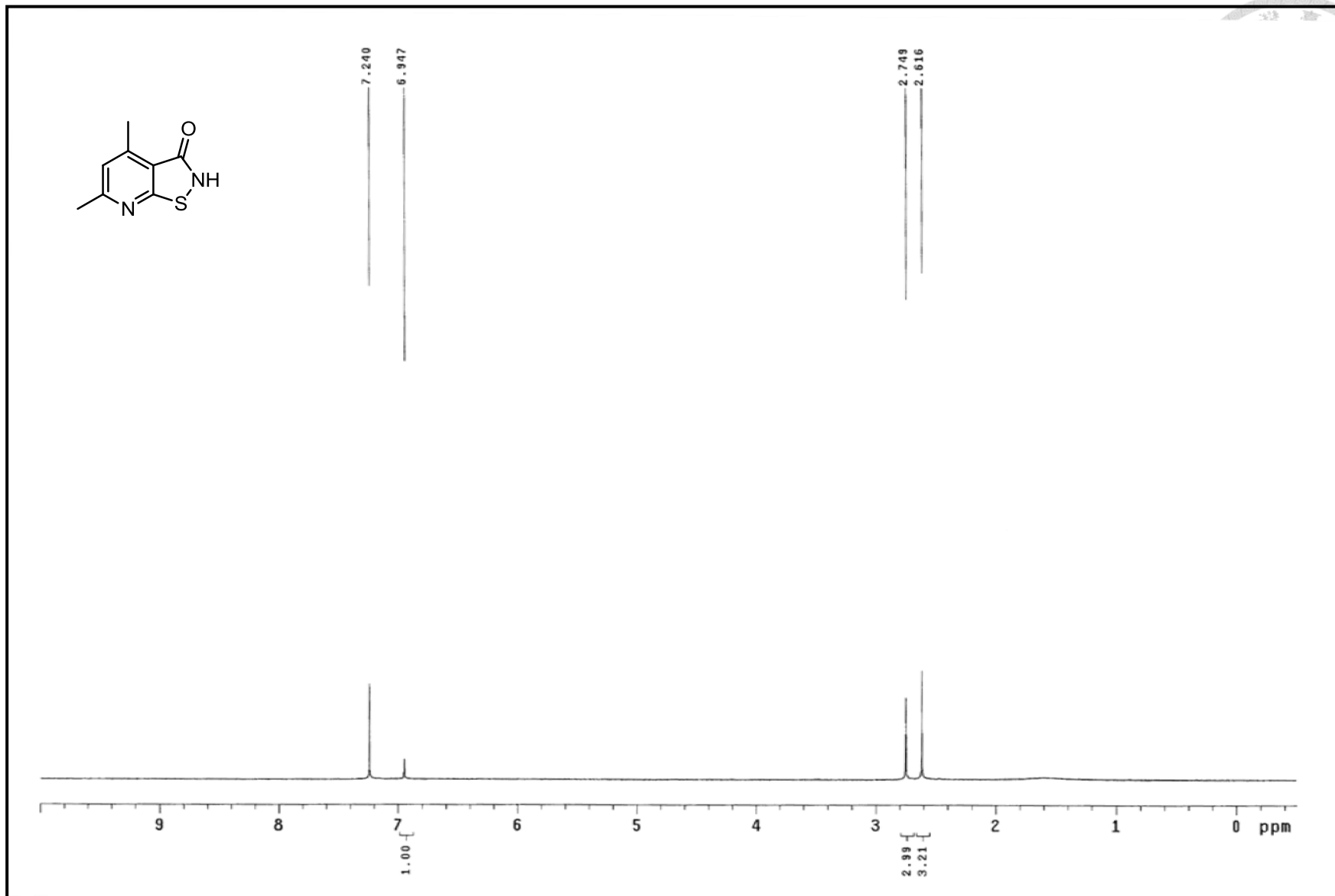
Appendixes

^1H and ^{13}C NMR Spectra

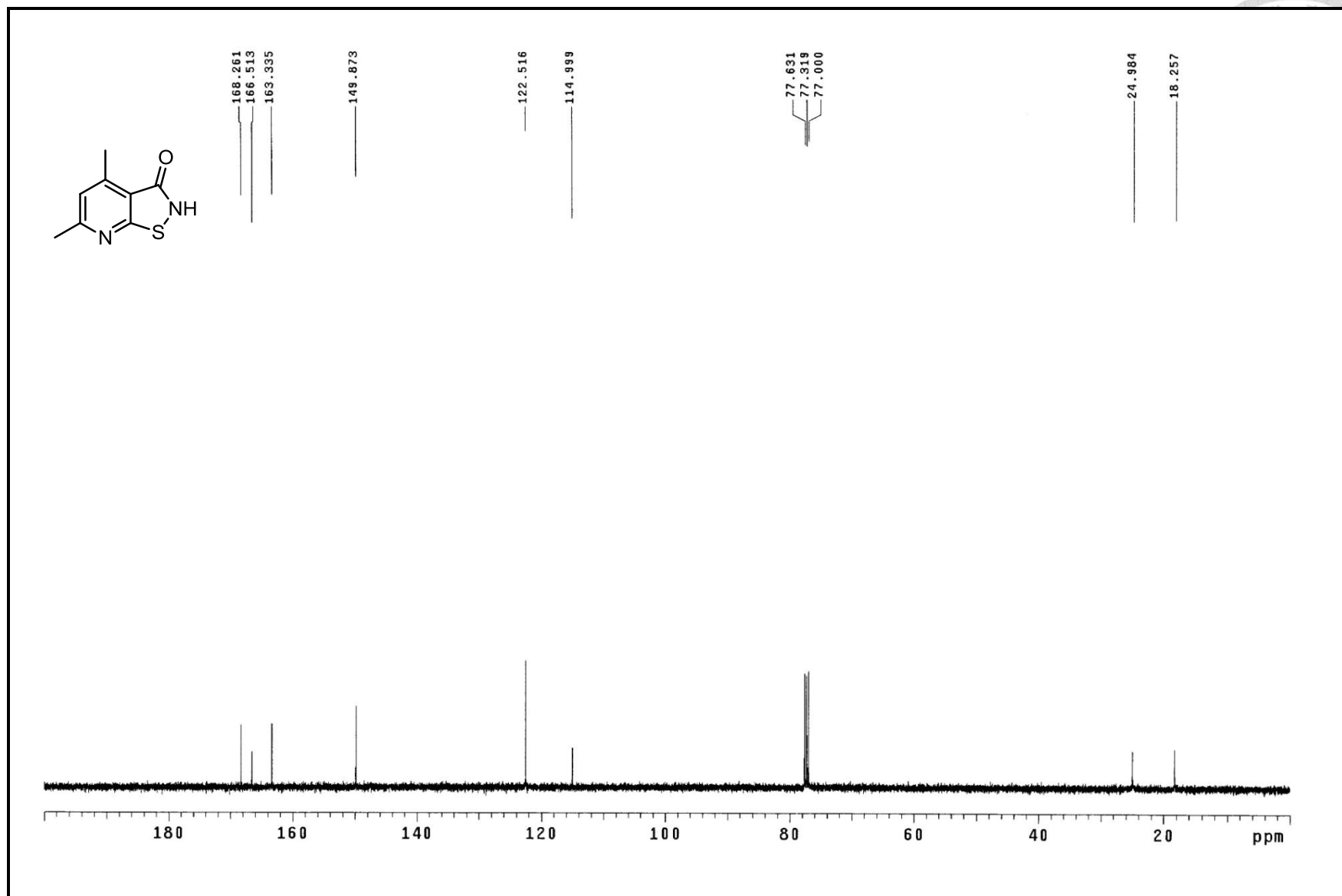




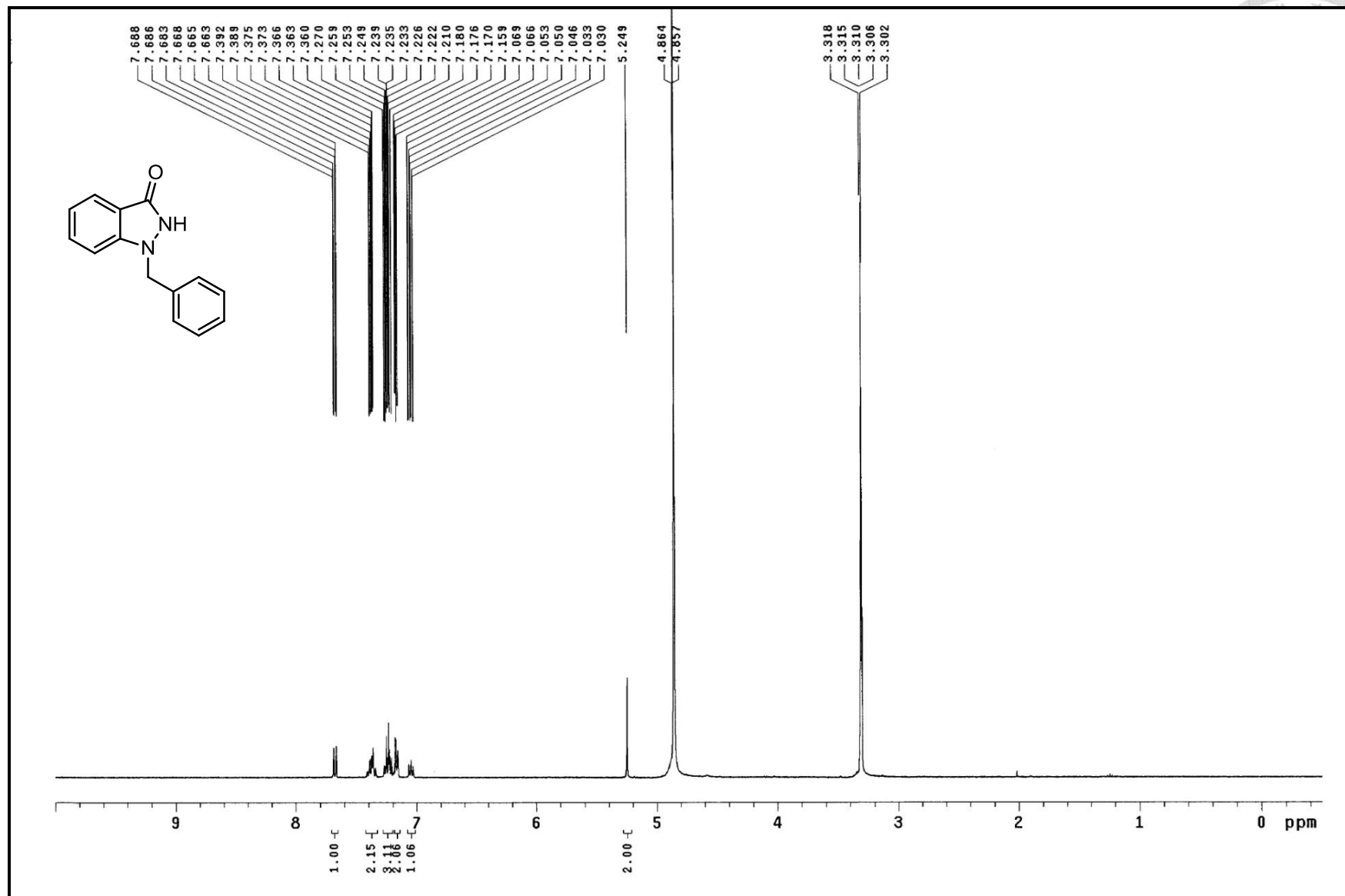
¹H NMR spectrum of compound 2 (400MHz, CDCl₃)

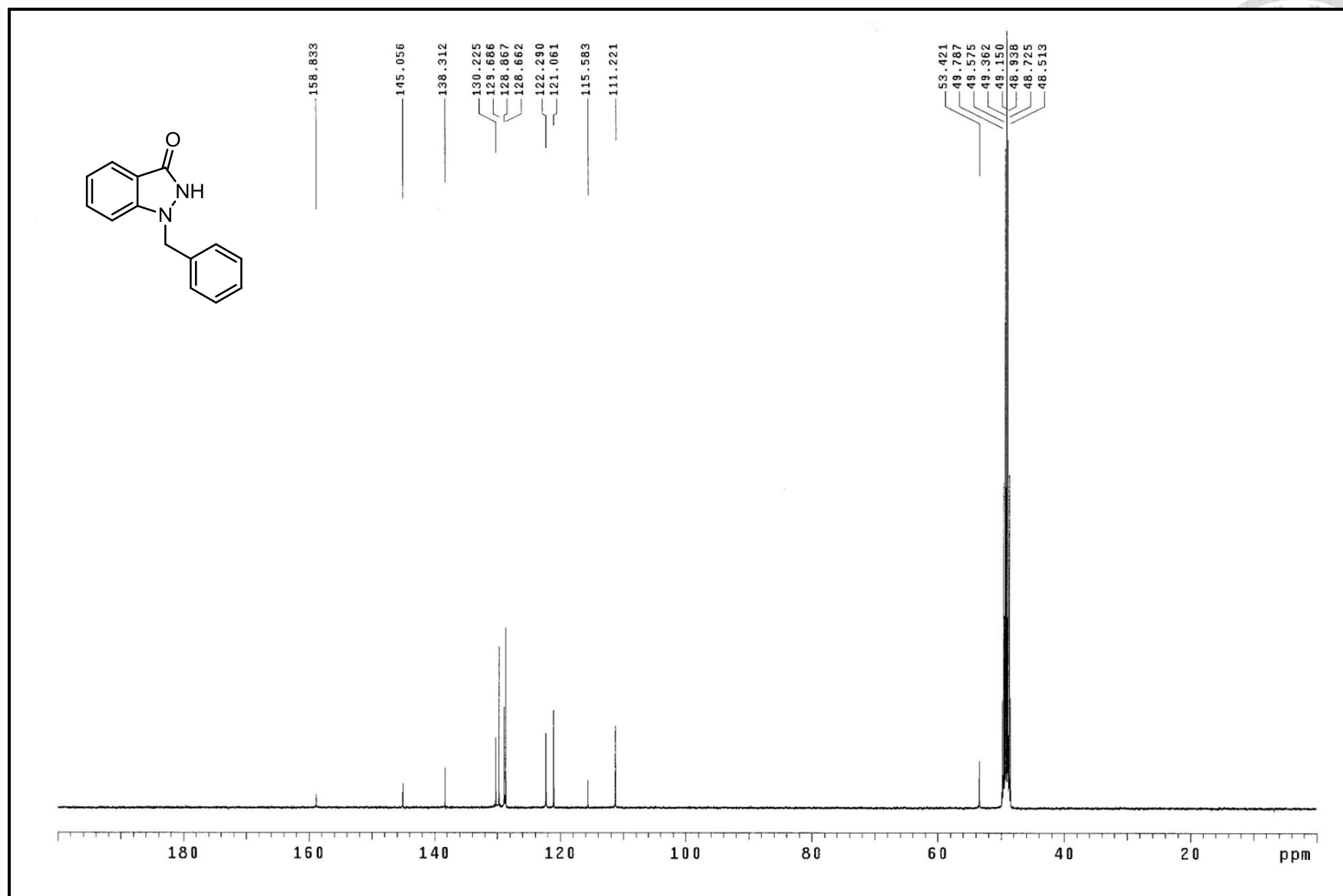


¹H NMR spectrum of compound 3 (400MHz, CDCl₃)

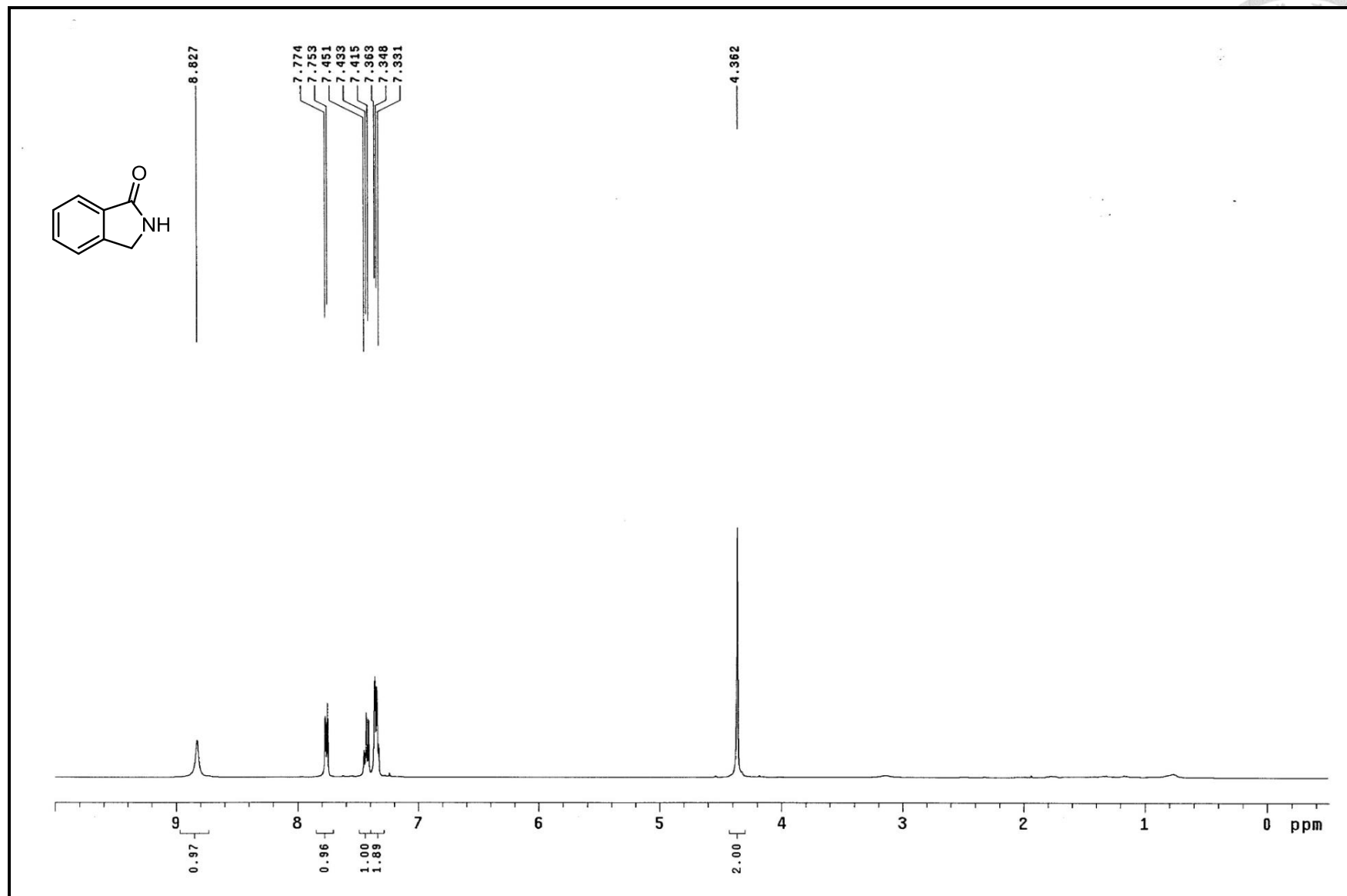


^{13}C NMR spectrum of compound 3 (100MHz, CDCl_3)

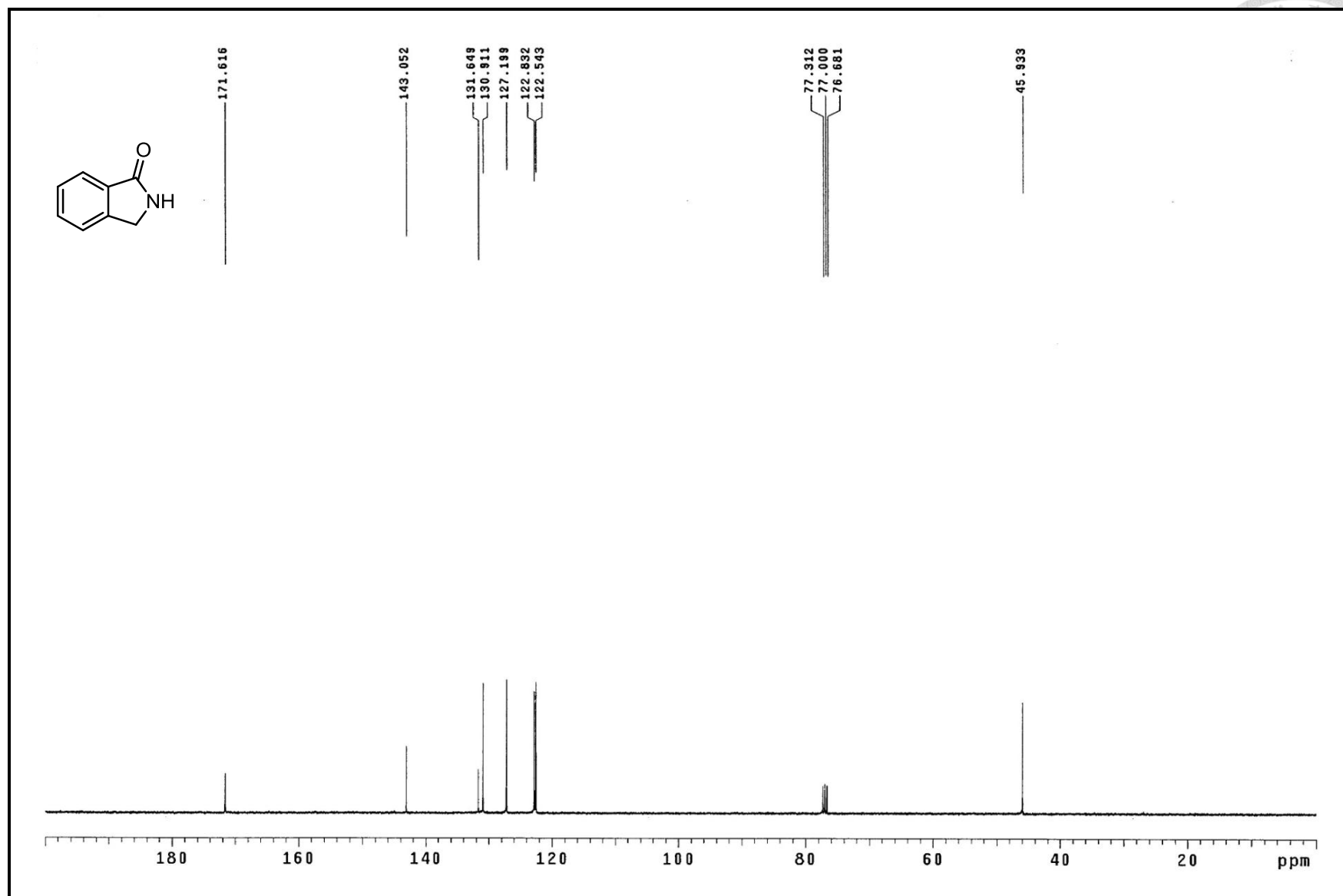
 ^1H NMR spectrum compound **5** (400MHz, CDCl_3)



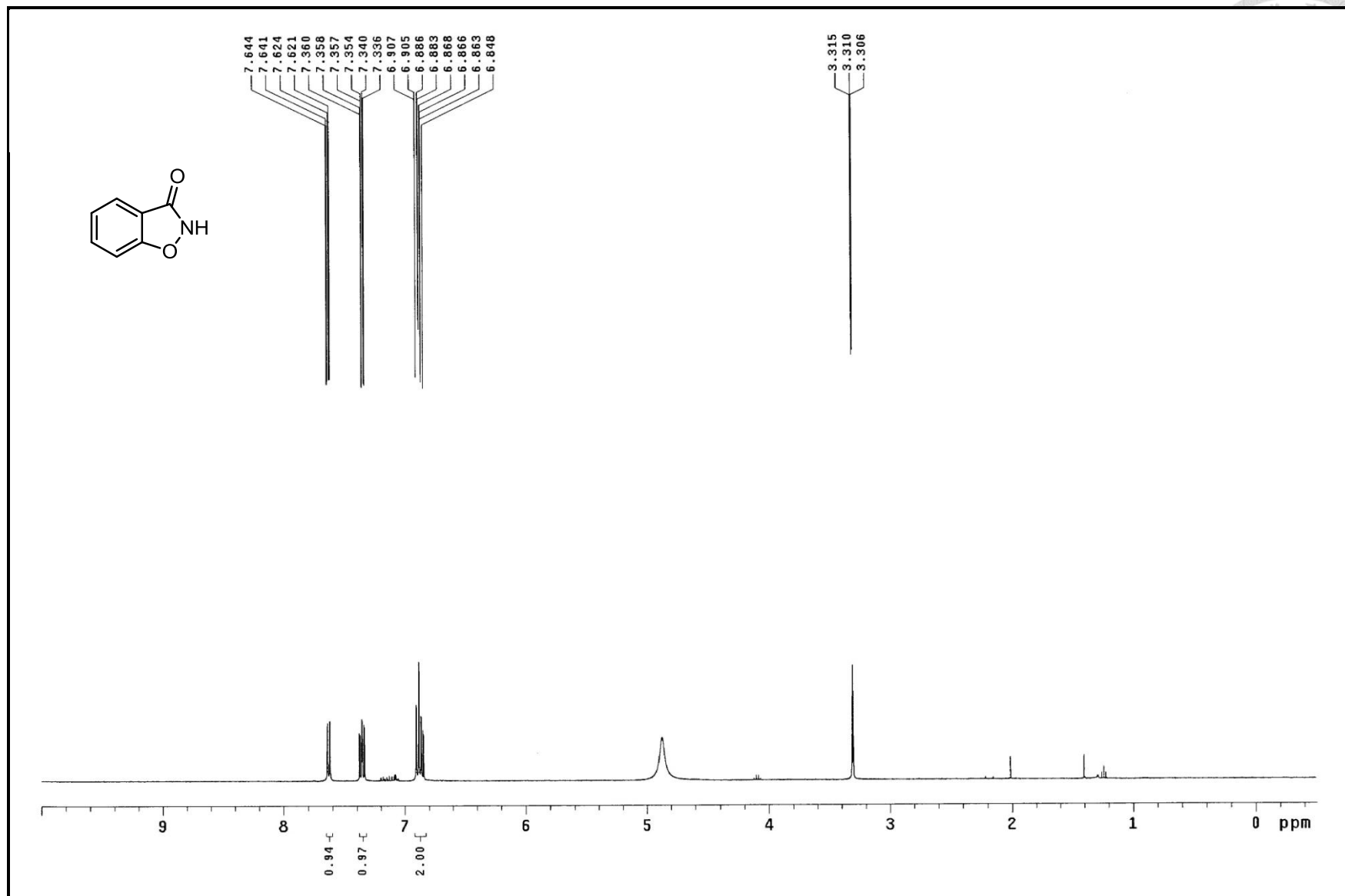
^{13}C NMR spectrum of compound **5** (100MHz, CDCl_3)



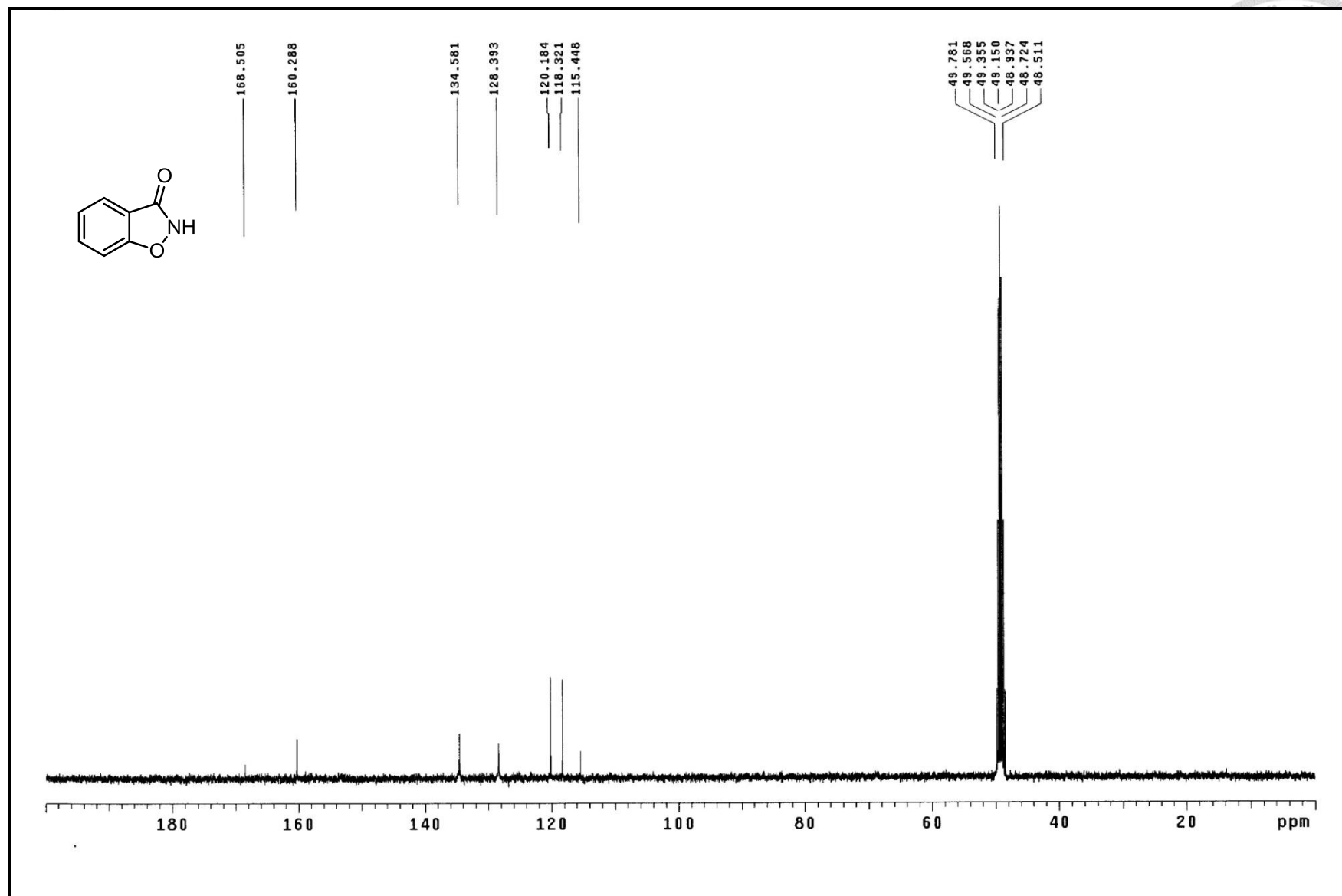
^1H NMR spectrum of compound **7** (400MHz, CDCl_3)



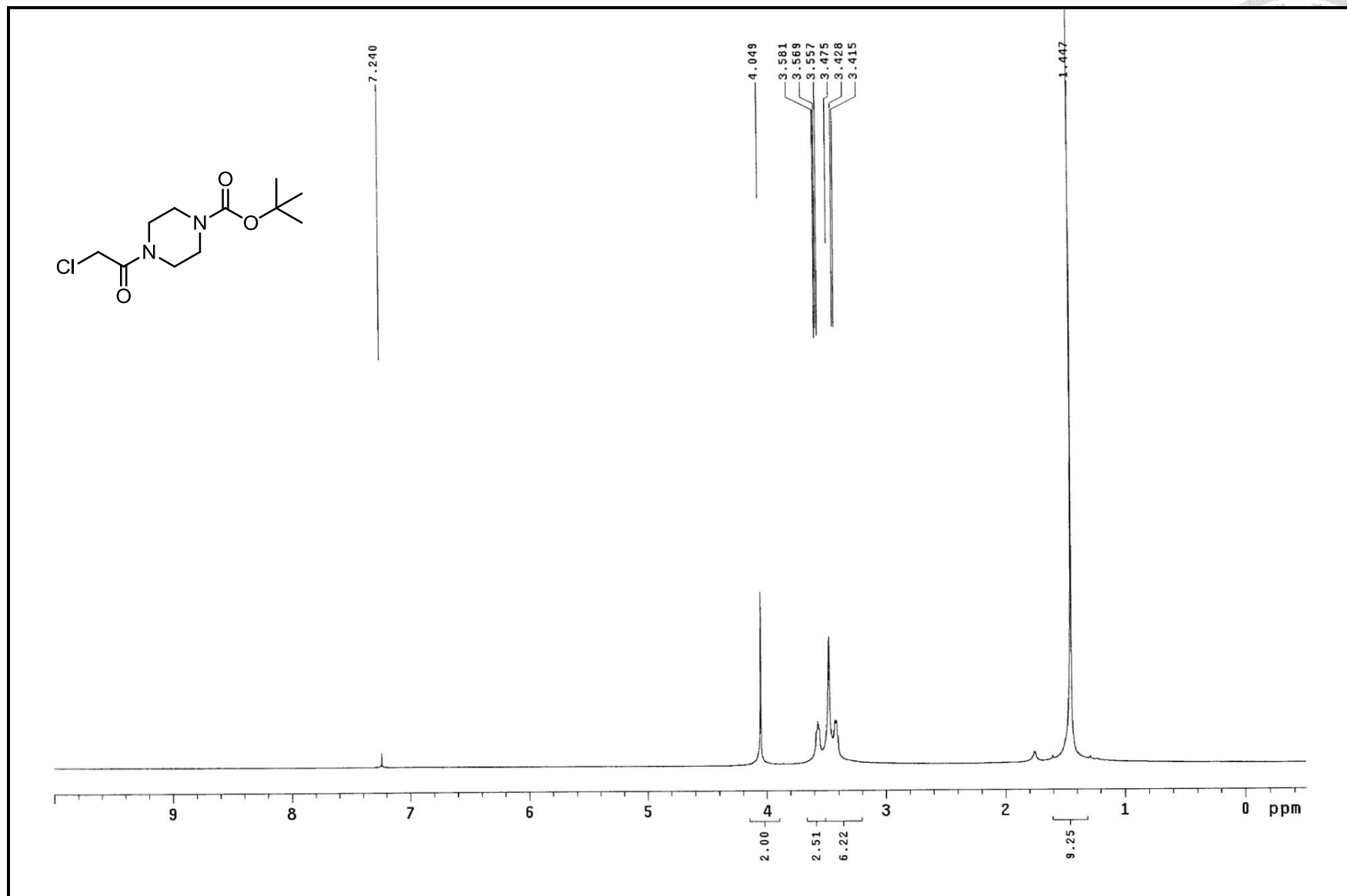
^{13}C NMR spectrum of compound 7 (100MHz, CDCl_3)



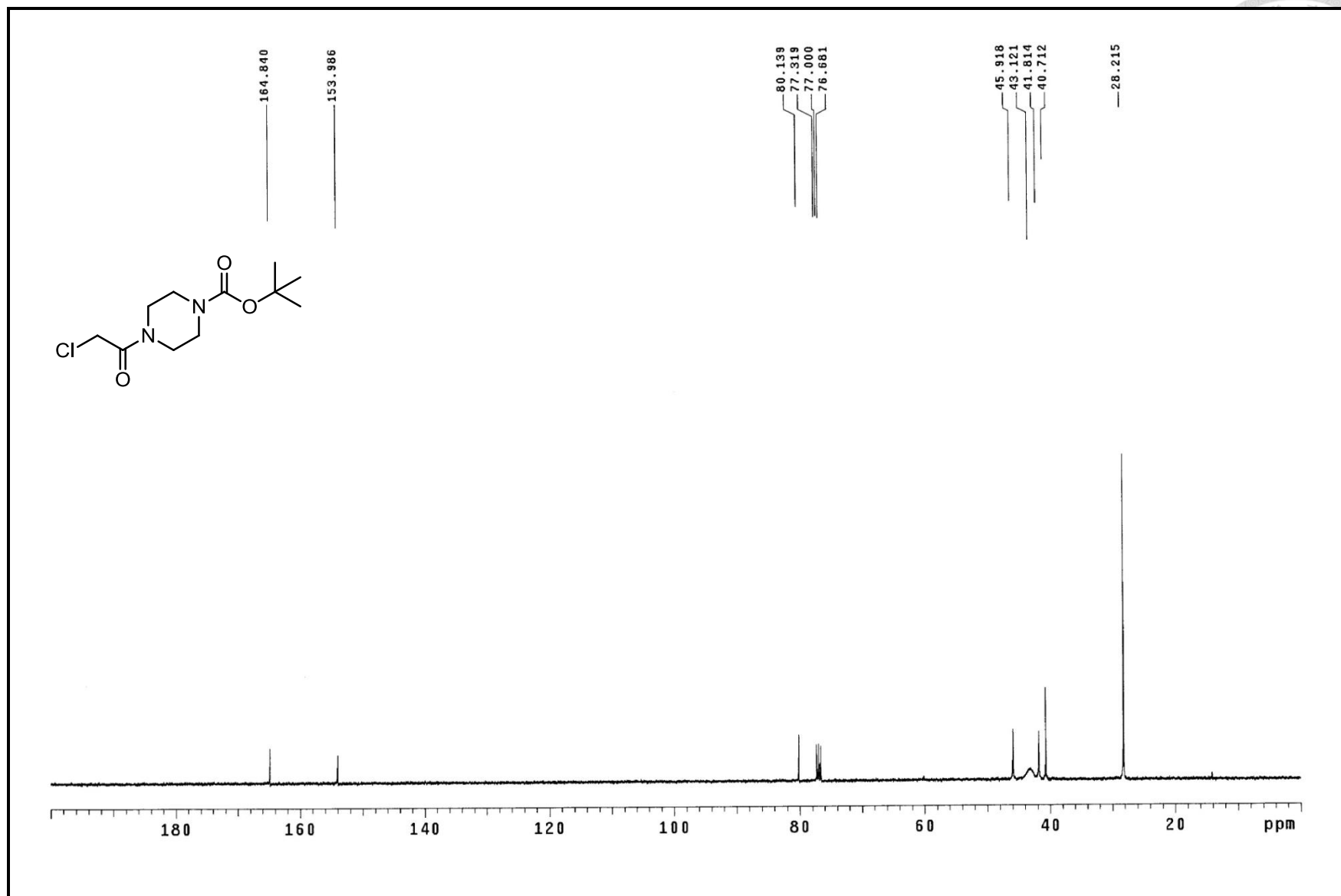
^1H NMR spectrum of compound **9** (400MHz, CD_3OD)



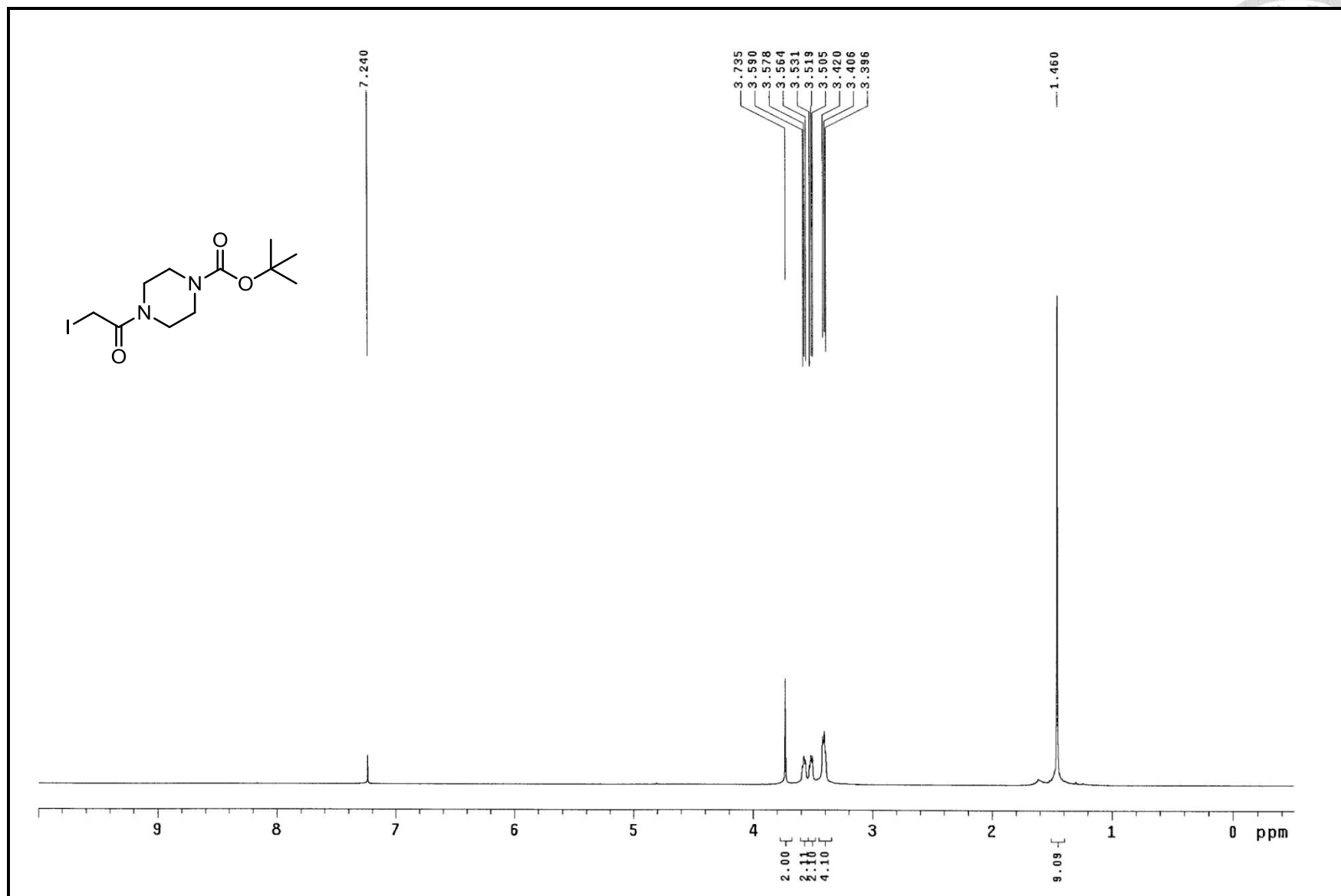
^{13}C NMR spectrum of compound **9** (100MHz, CD_3OD)



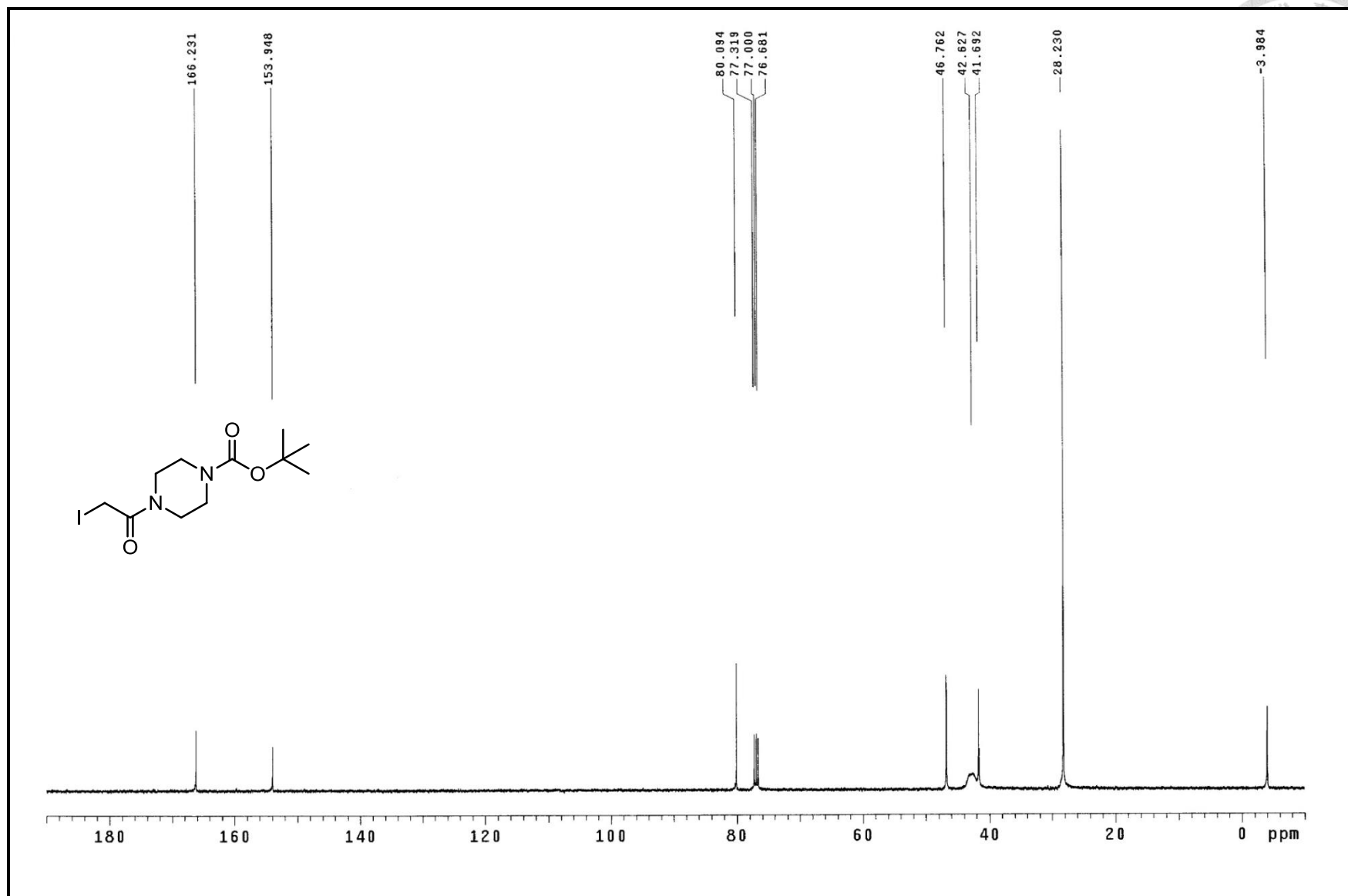
^1H NMR spectrum of compound **11** (400MHz, CDCl_3)



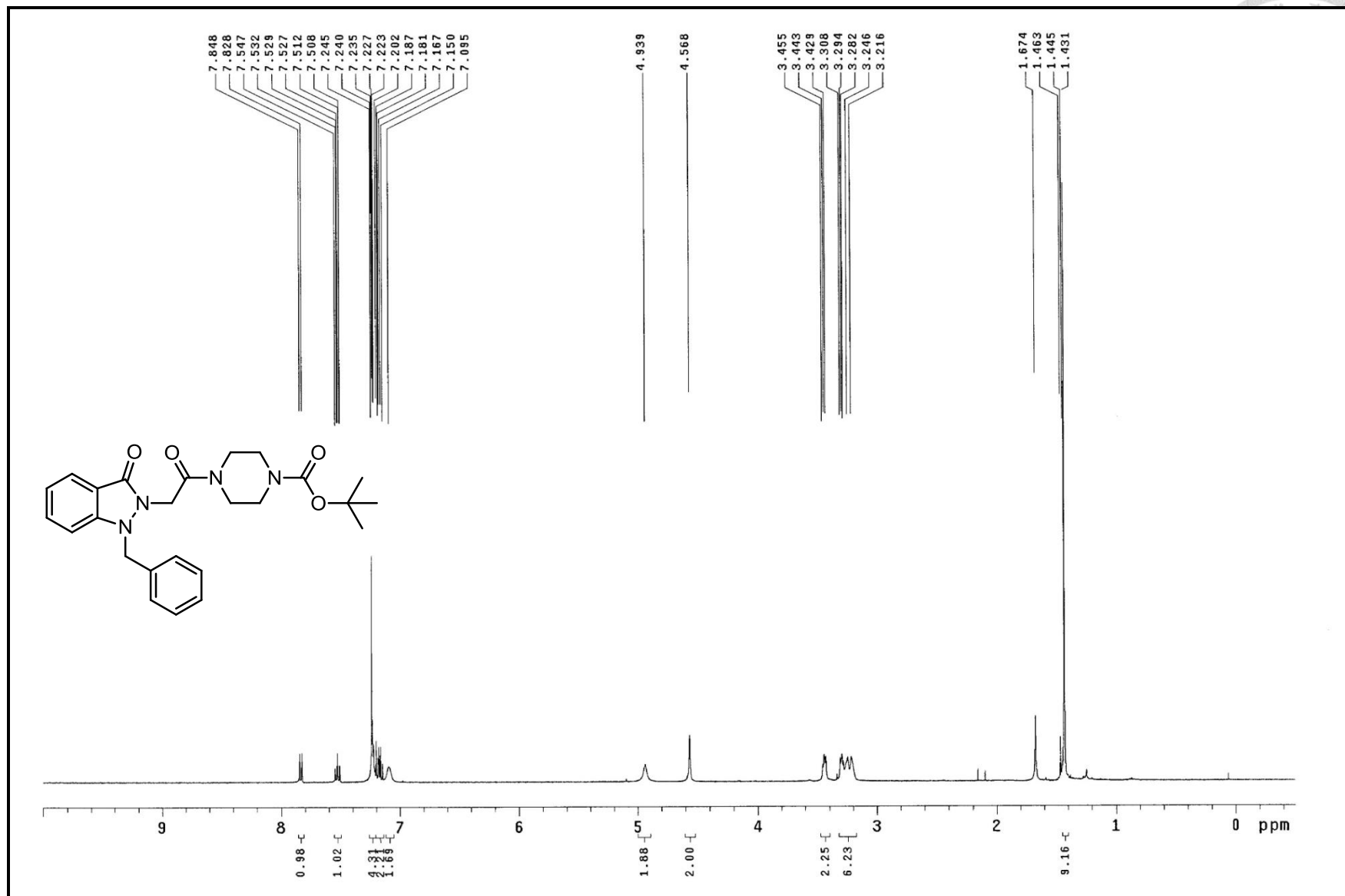
^{13}C NMR spectrum of compound **11** (100MHz, CDCl_3)



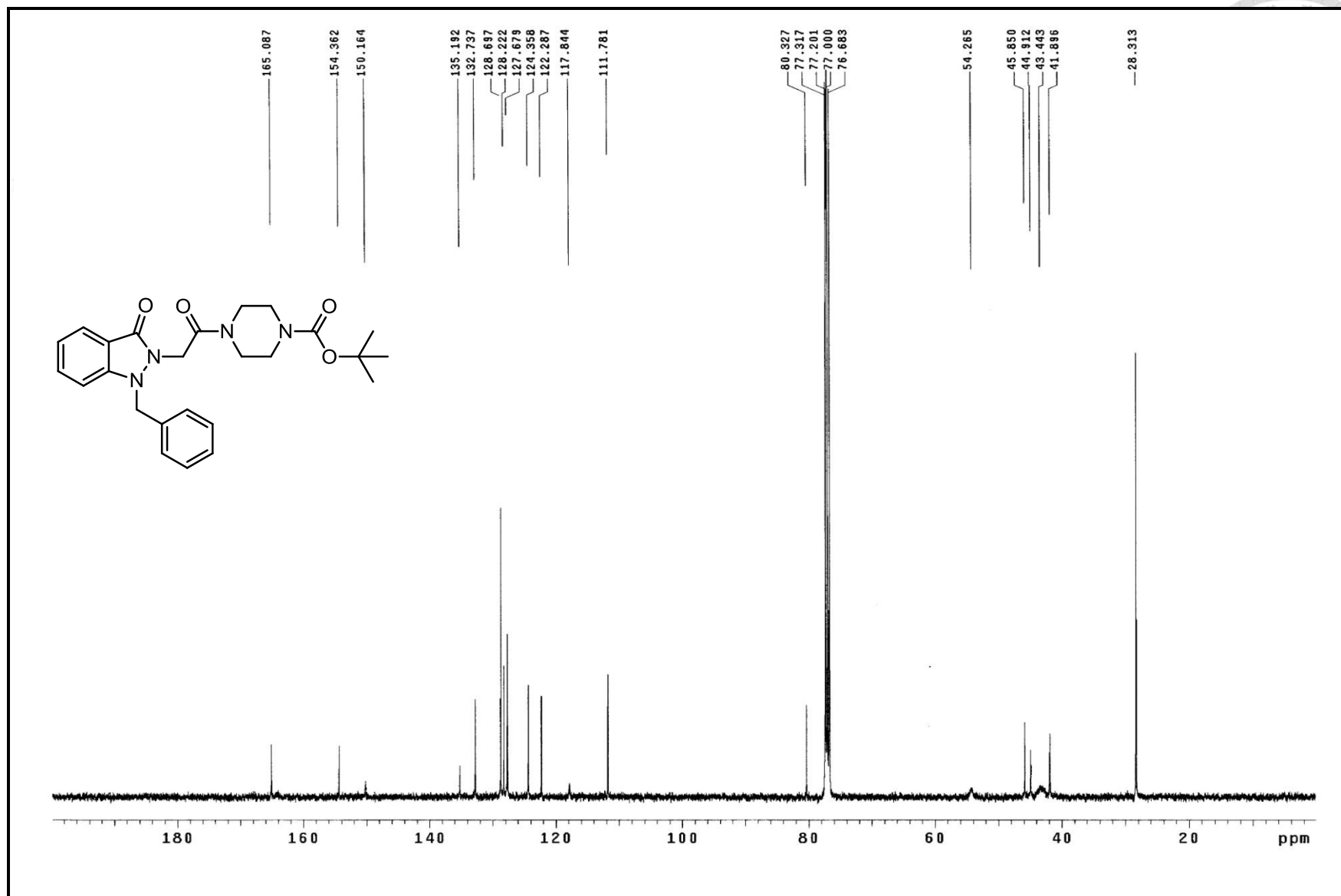
^1H NMR spectrum of compound **12** (400MHz, CDCl_3)



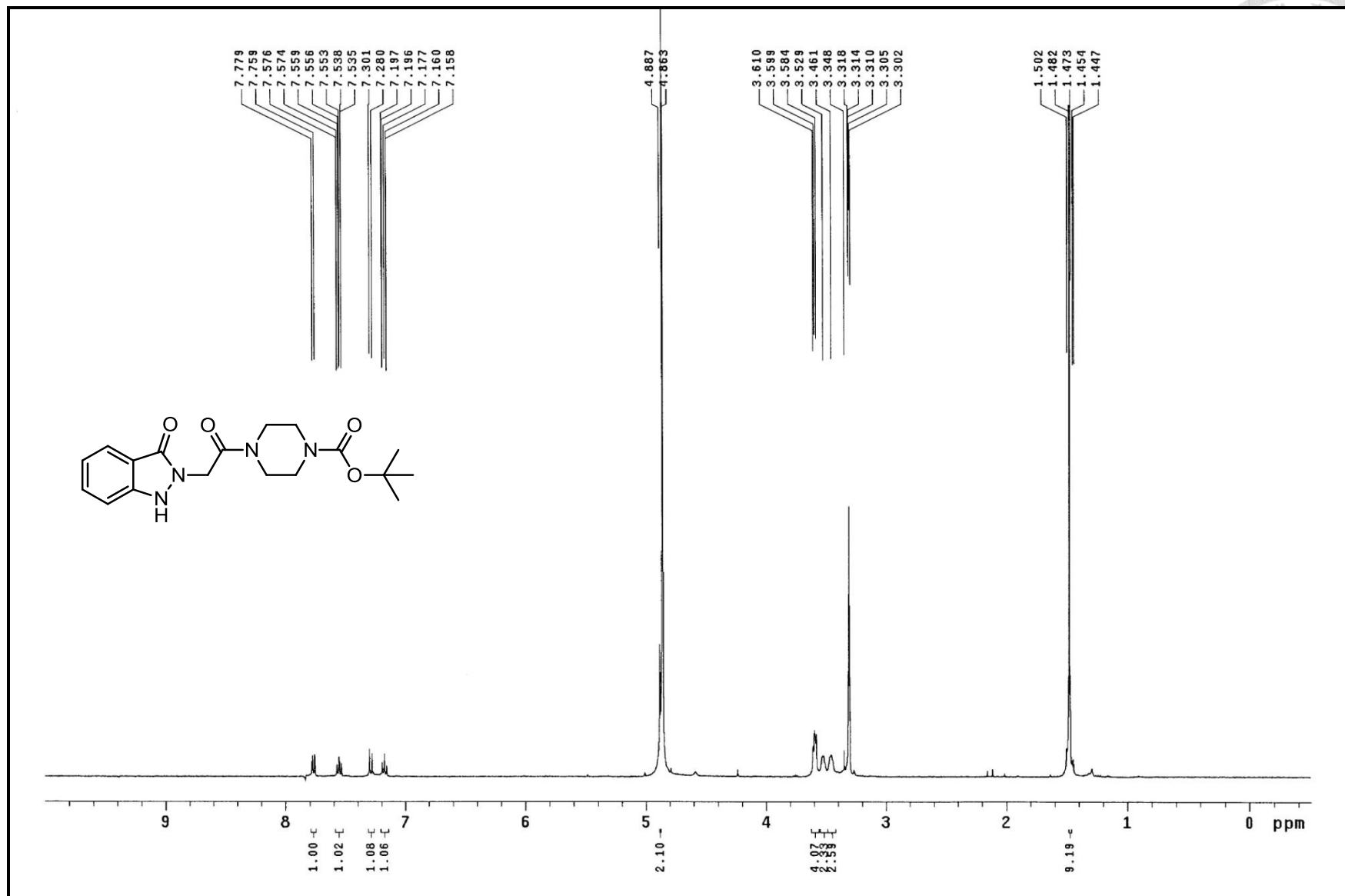
^{13}C NMR spectrum of compound **12** (100MHz, CDCl_3)



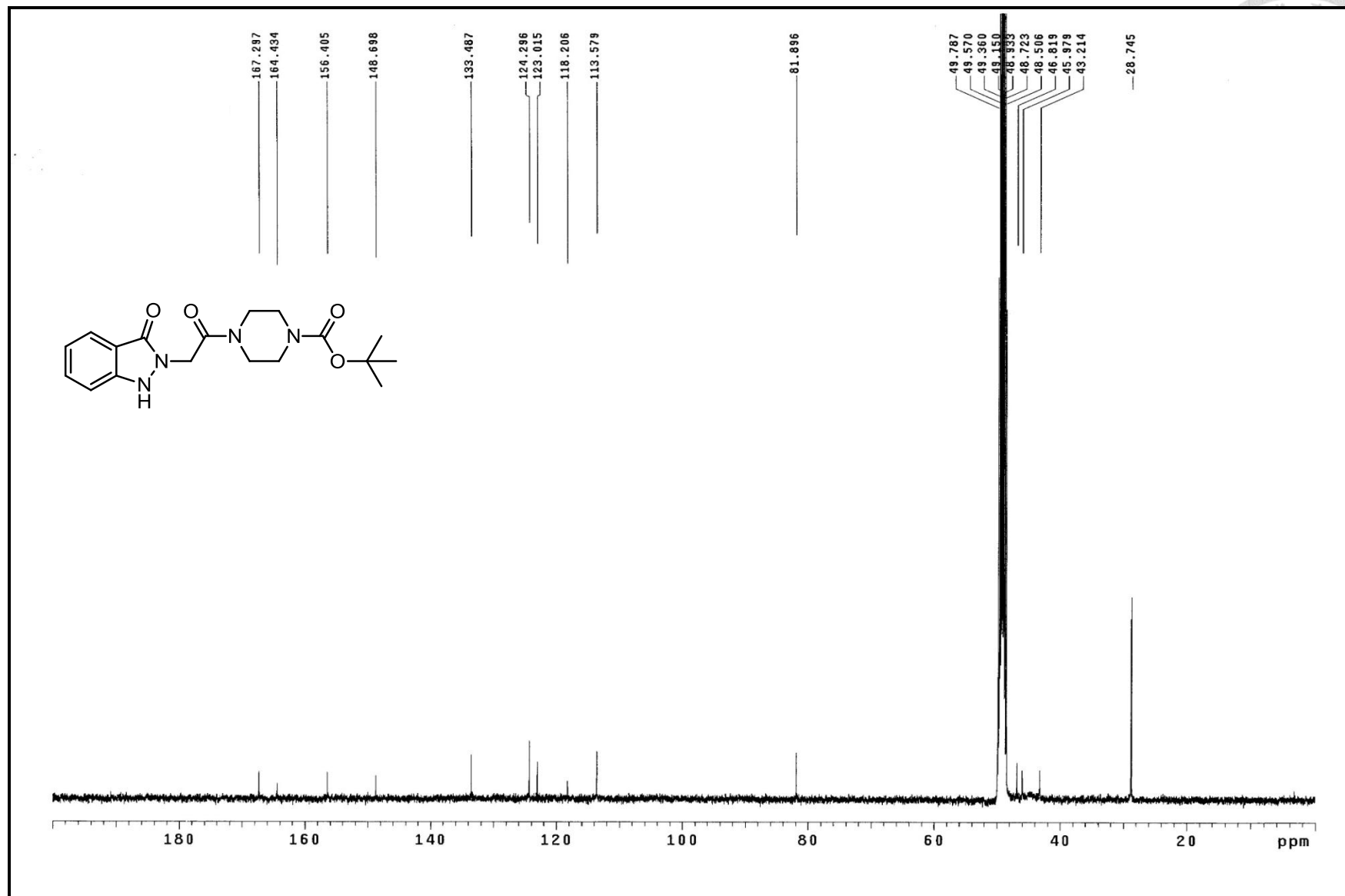
^1H NMR spectrum of compound **13** (400MHz, CDCl_3)



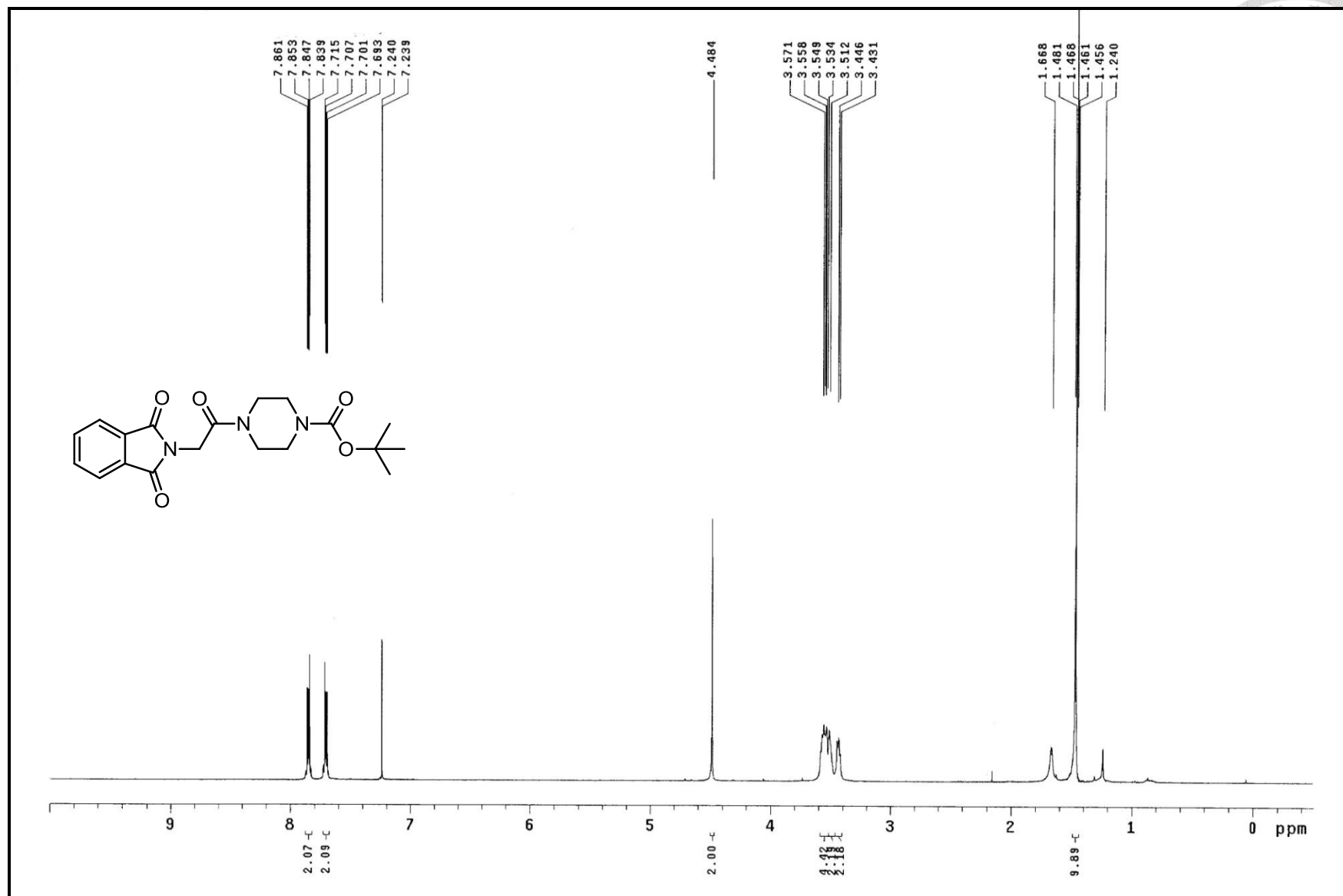
^{13}C NMR spectrum of compound **13** (100MHz, CDCl_3)



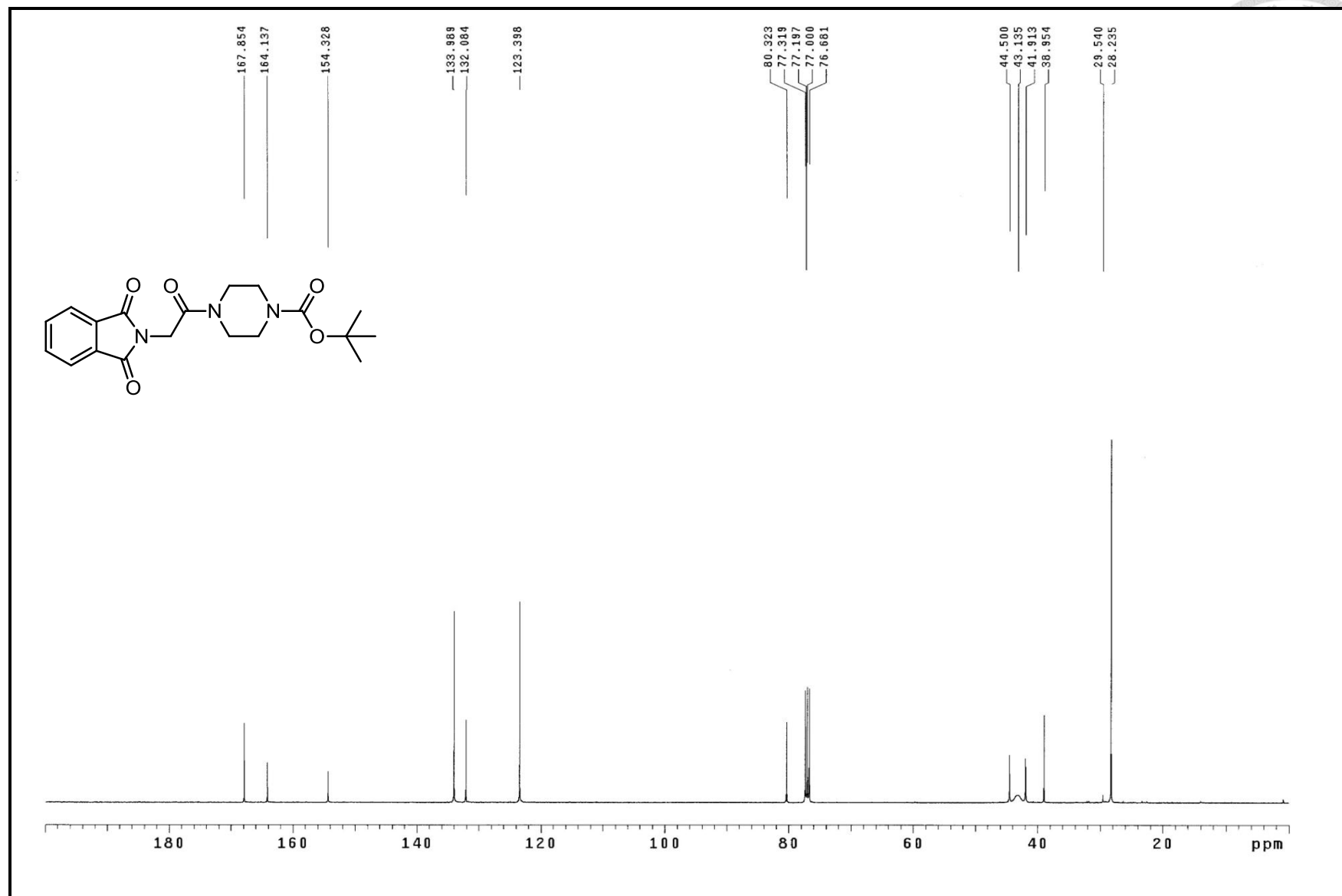
¹H NMR spectrum of compound **14** (400MHz, CD₃OD)



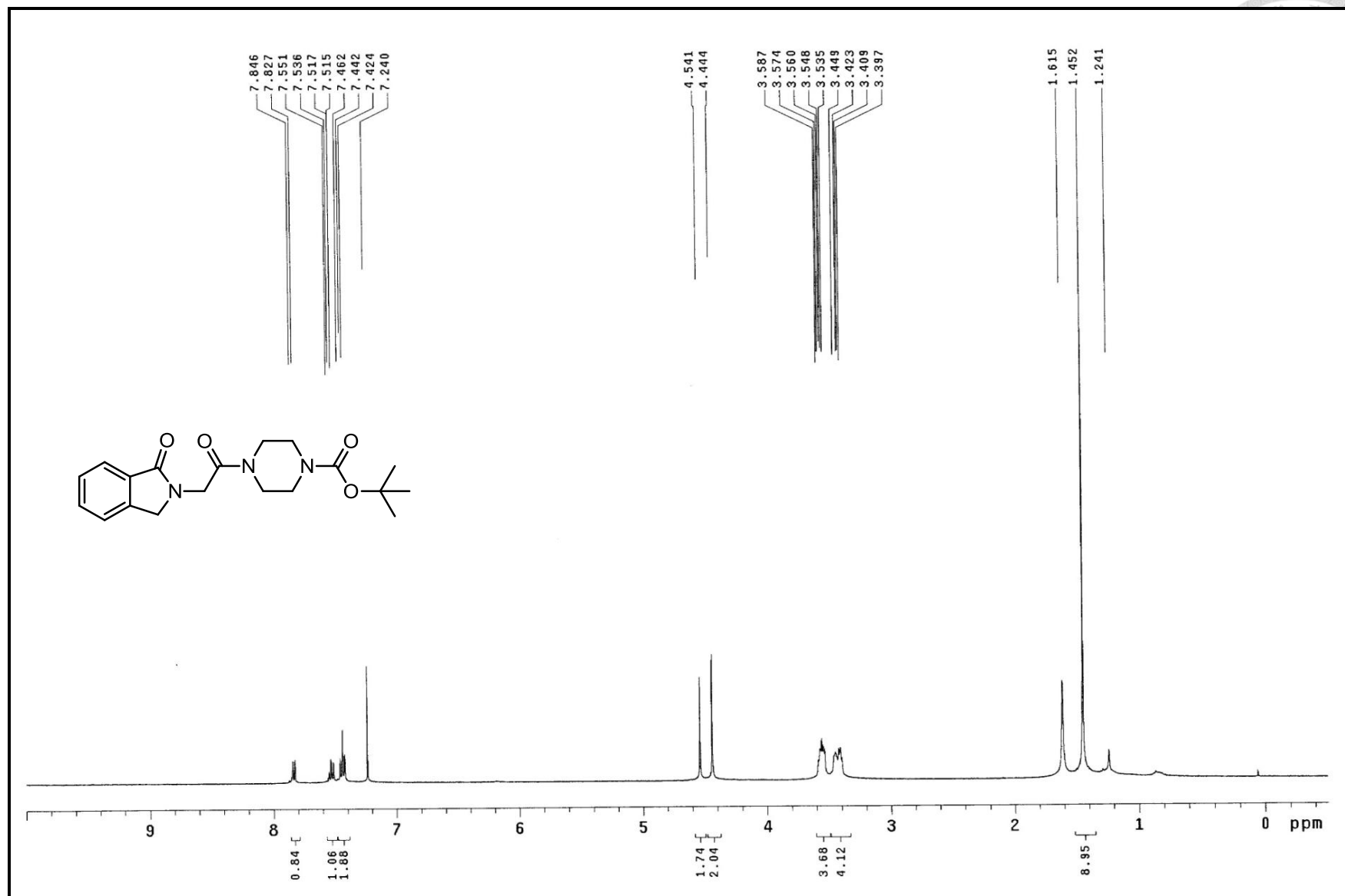
¹³C NMR spectrum of compound **14** (100MHz, CD₃OD)



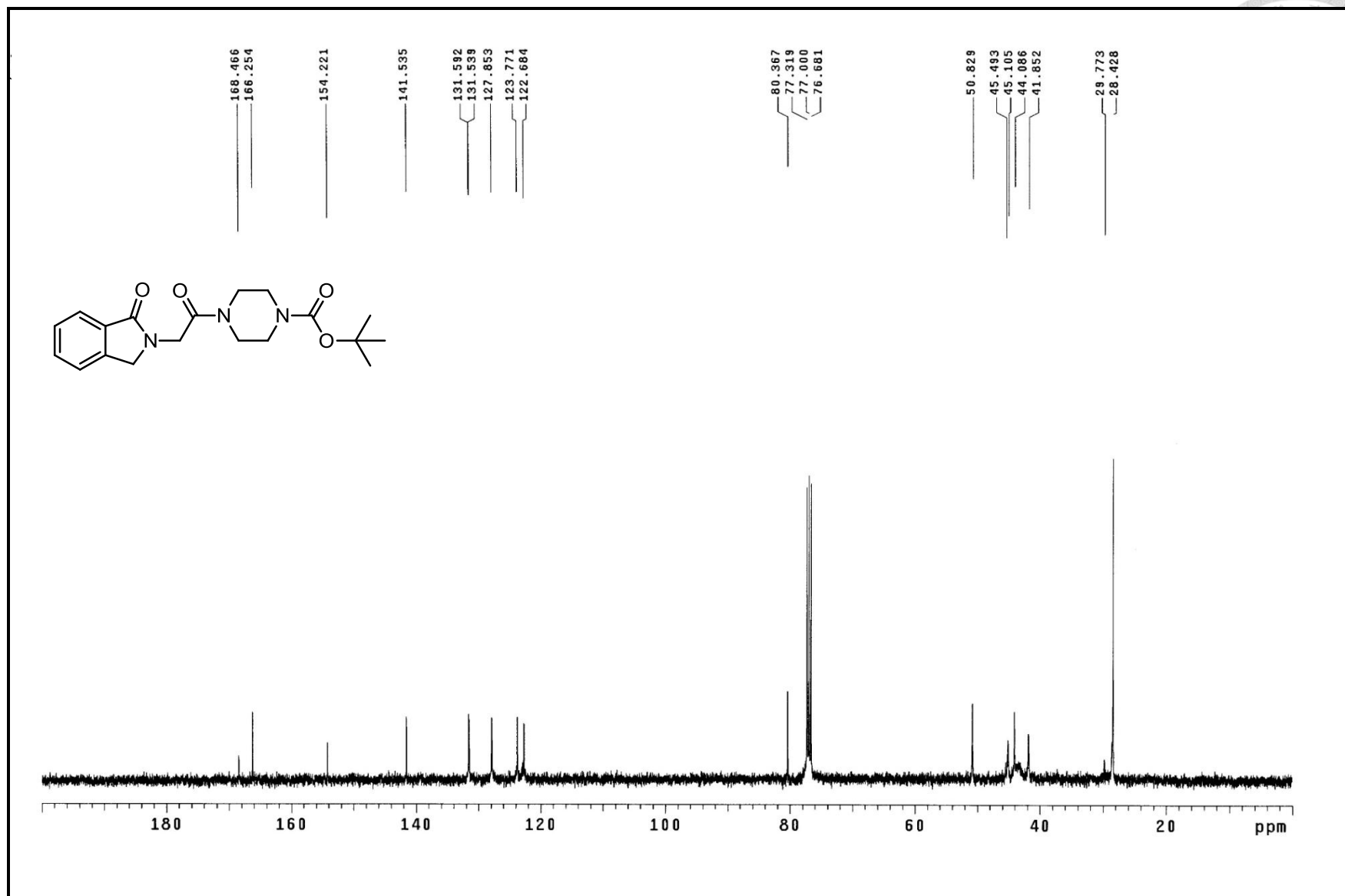
¹H NMR spectrum of compound **15** (400MHz, CDCl₃)



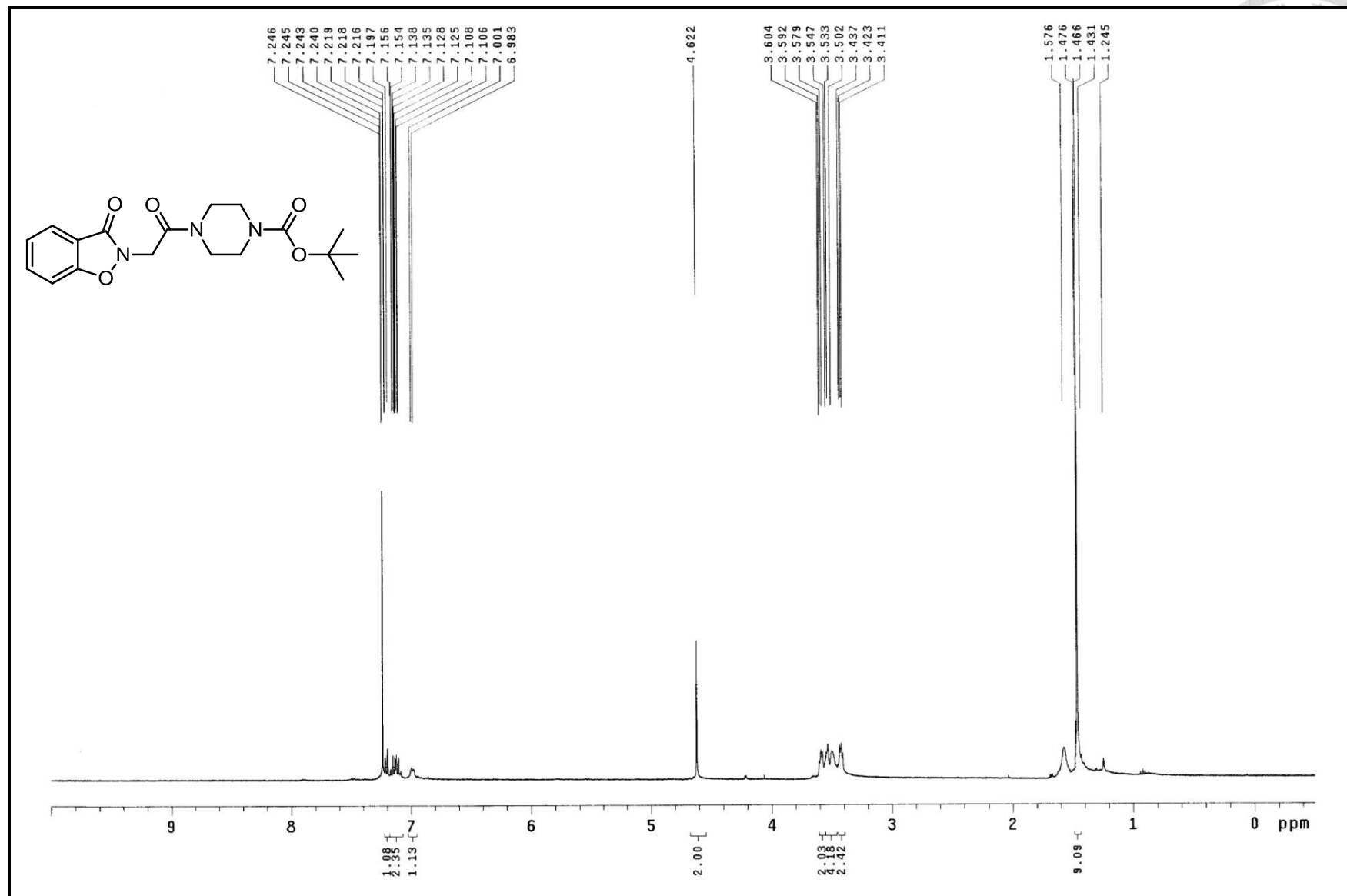
^{13}C NMR spectrum of compound **15** (100MHz, CDCl₃)



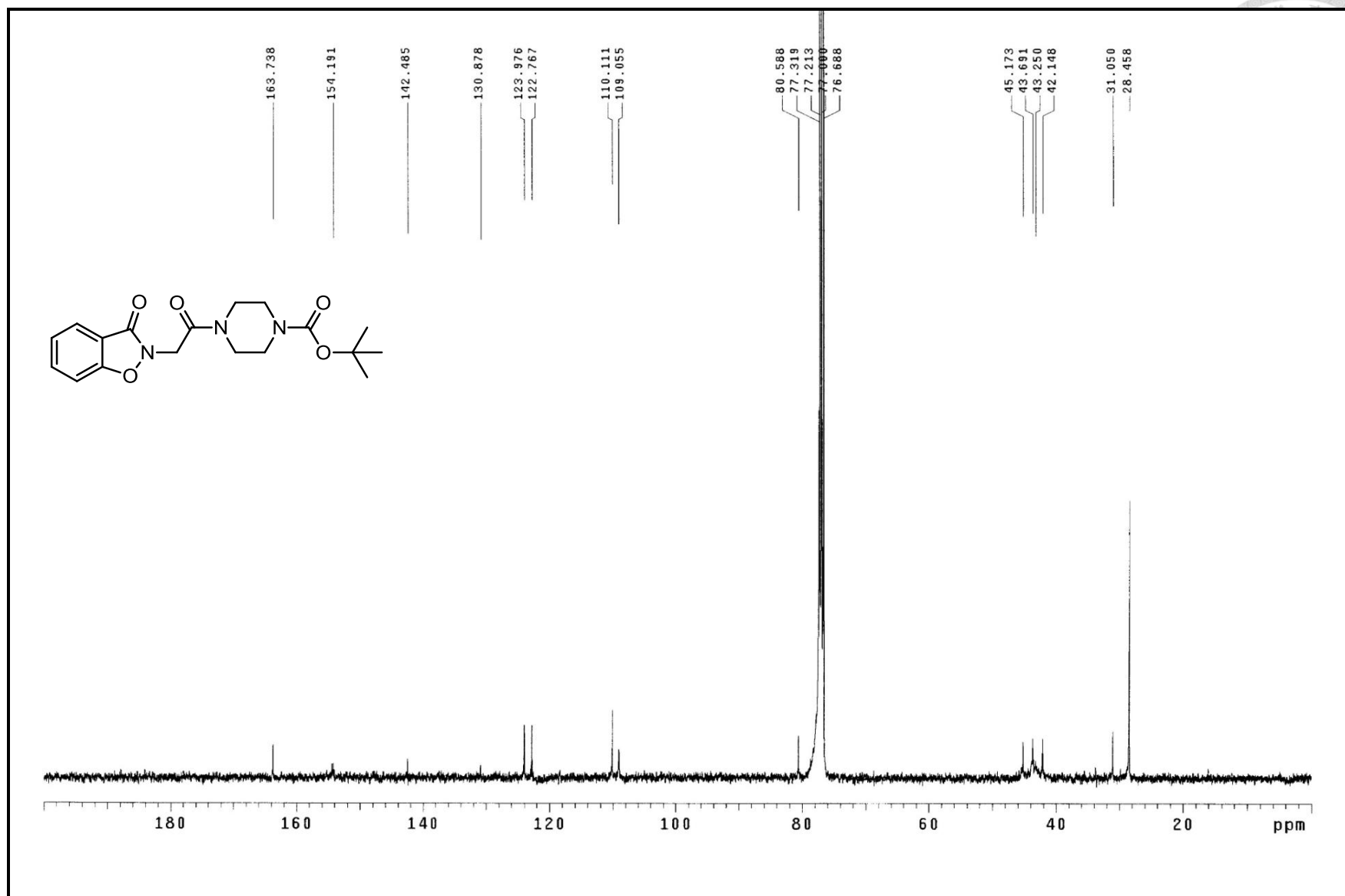
^1H NMR spectrum of compound **16** (400MHz, CDCl_3)



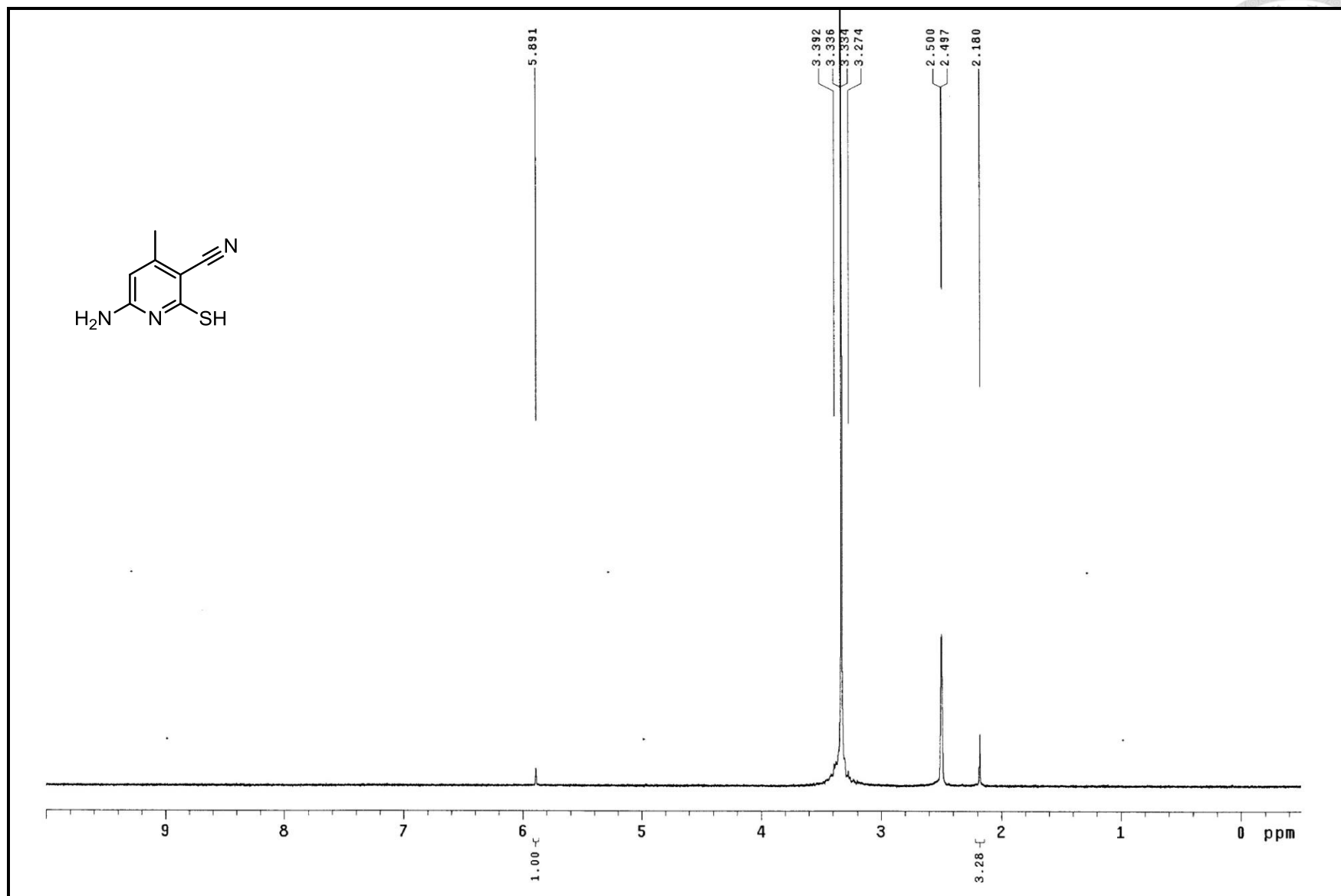
^{13}C NMR spectrum of compound **16** (100MHz, CDCl_3)



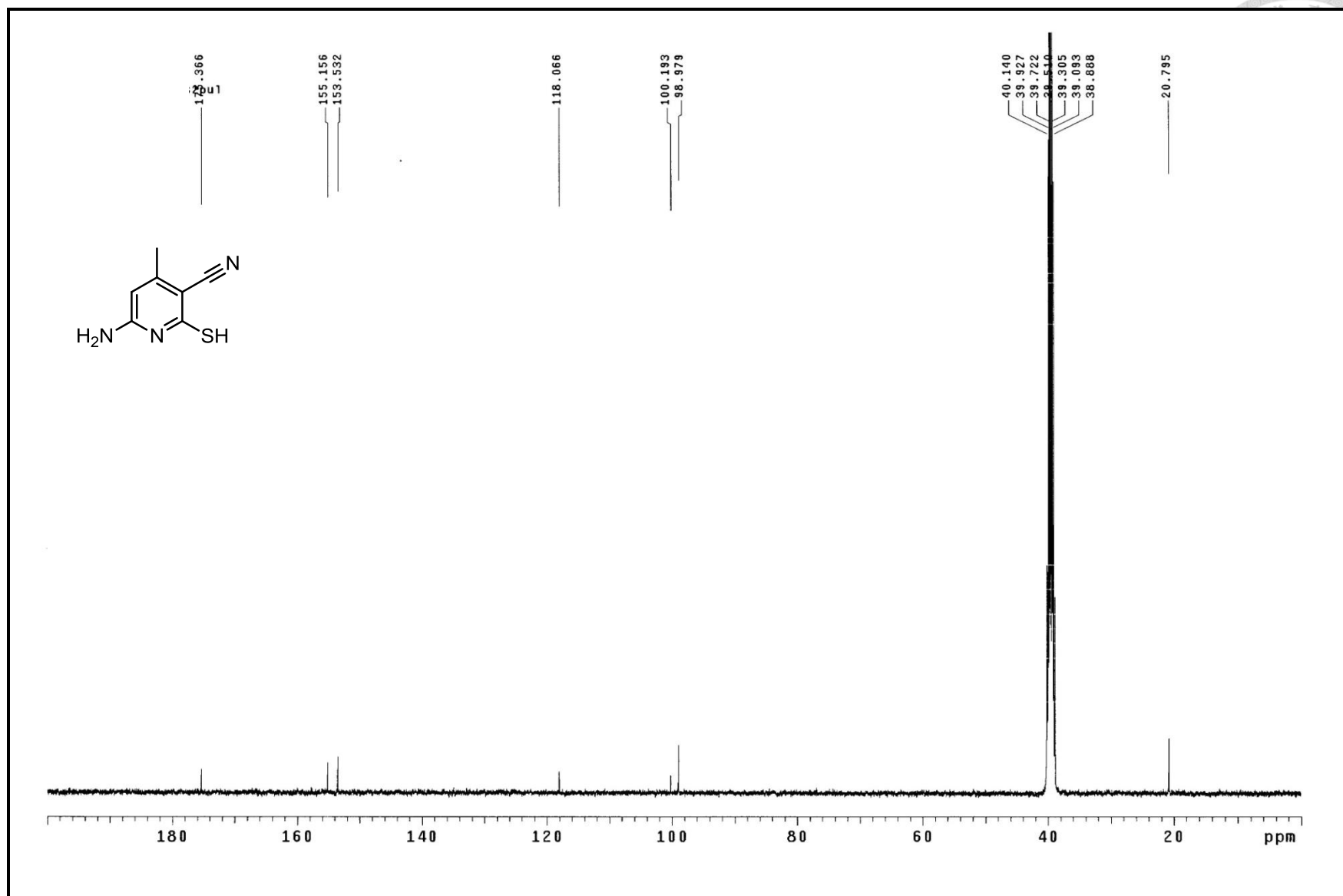
^1H NMR spectrum of compound **17** (400MHz, CDCl_3)



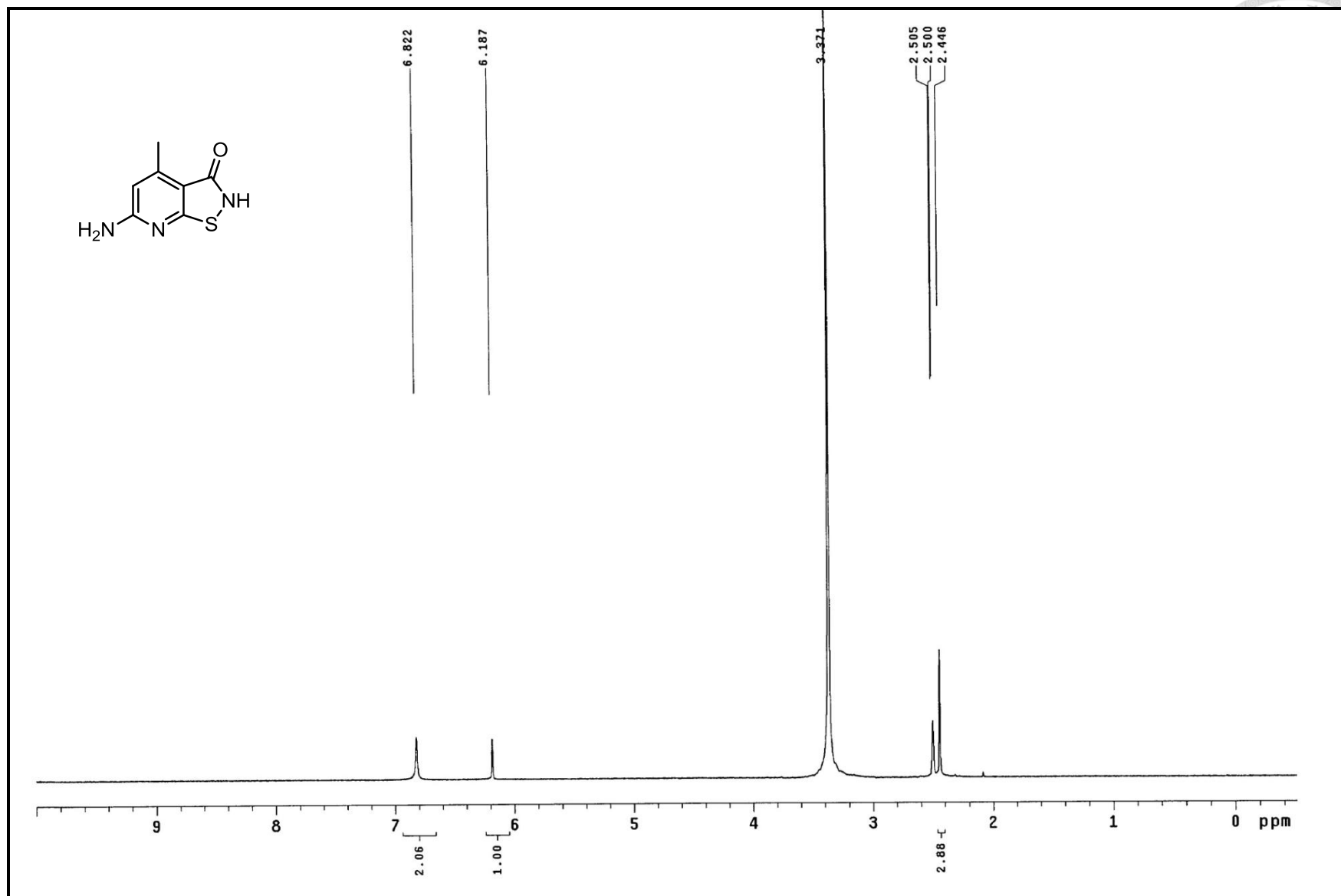
^{13}C NMR spectrum of compound **17** (100MHz, CDCl_3)



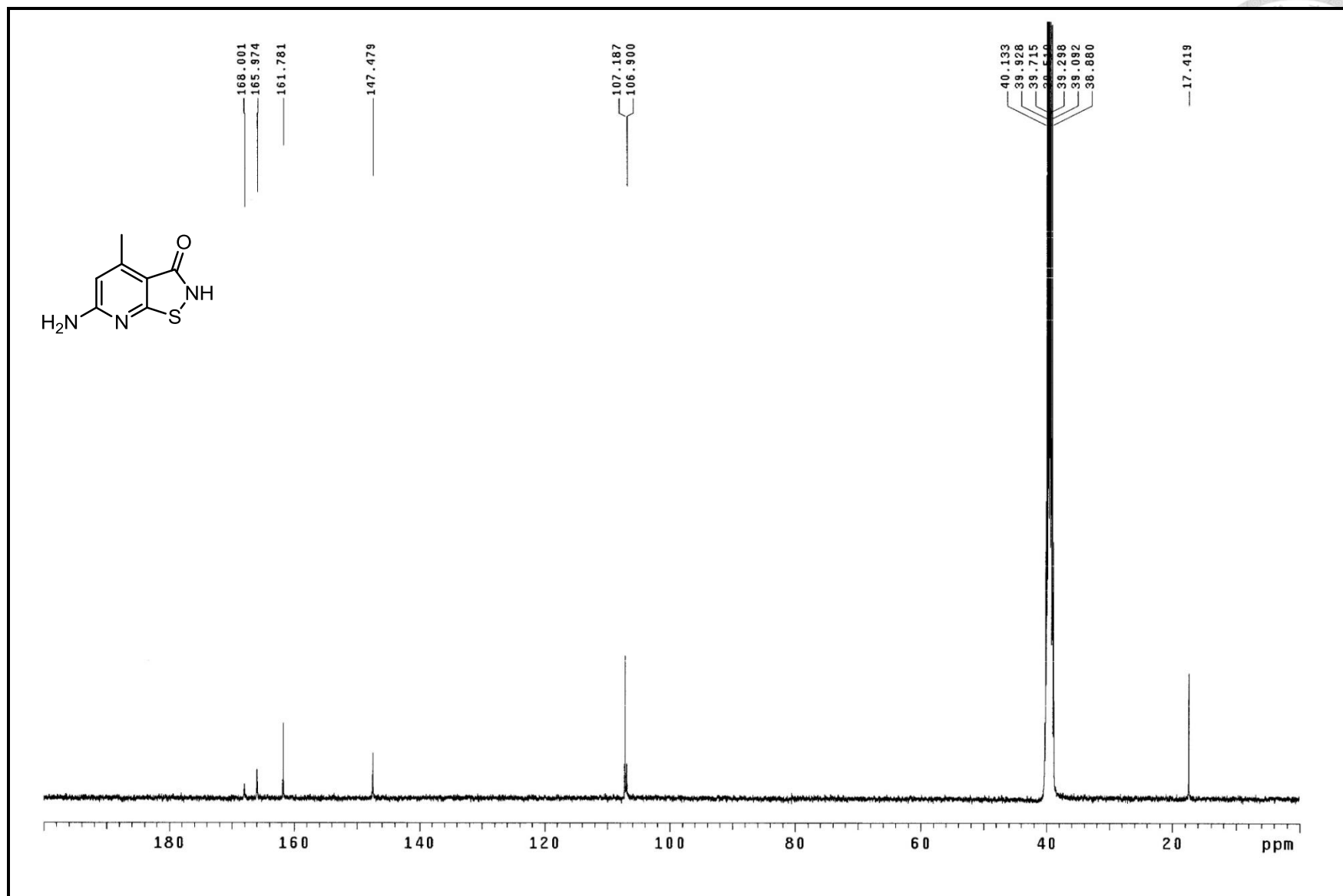
¹H NMR spectrum of compound **19** (400MHz, DMSO-d₆)



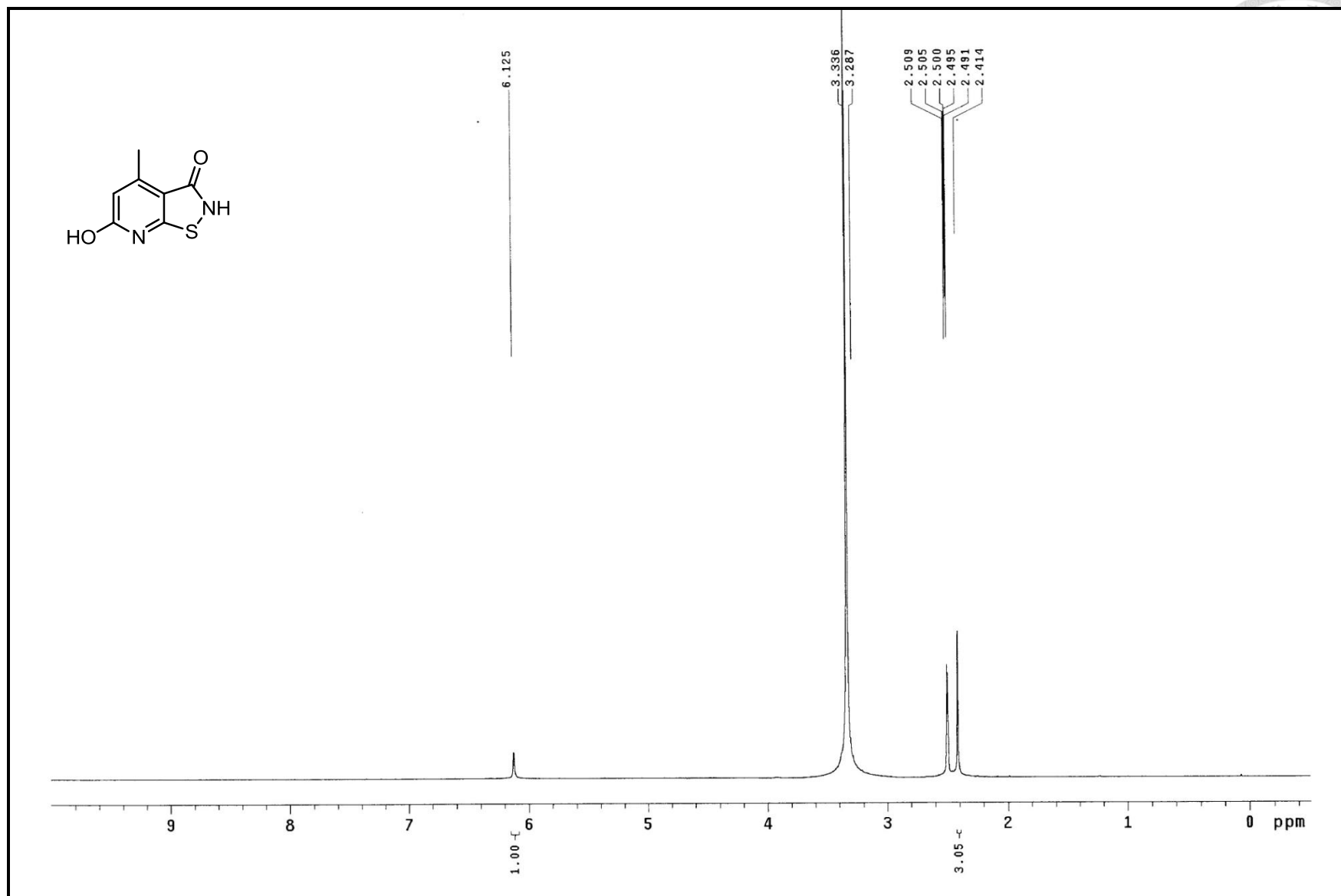
^{13}C NMR spectrum of compound **19** (100MHz, DMSO- d_6)



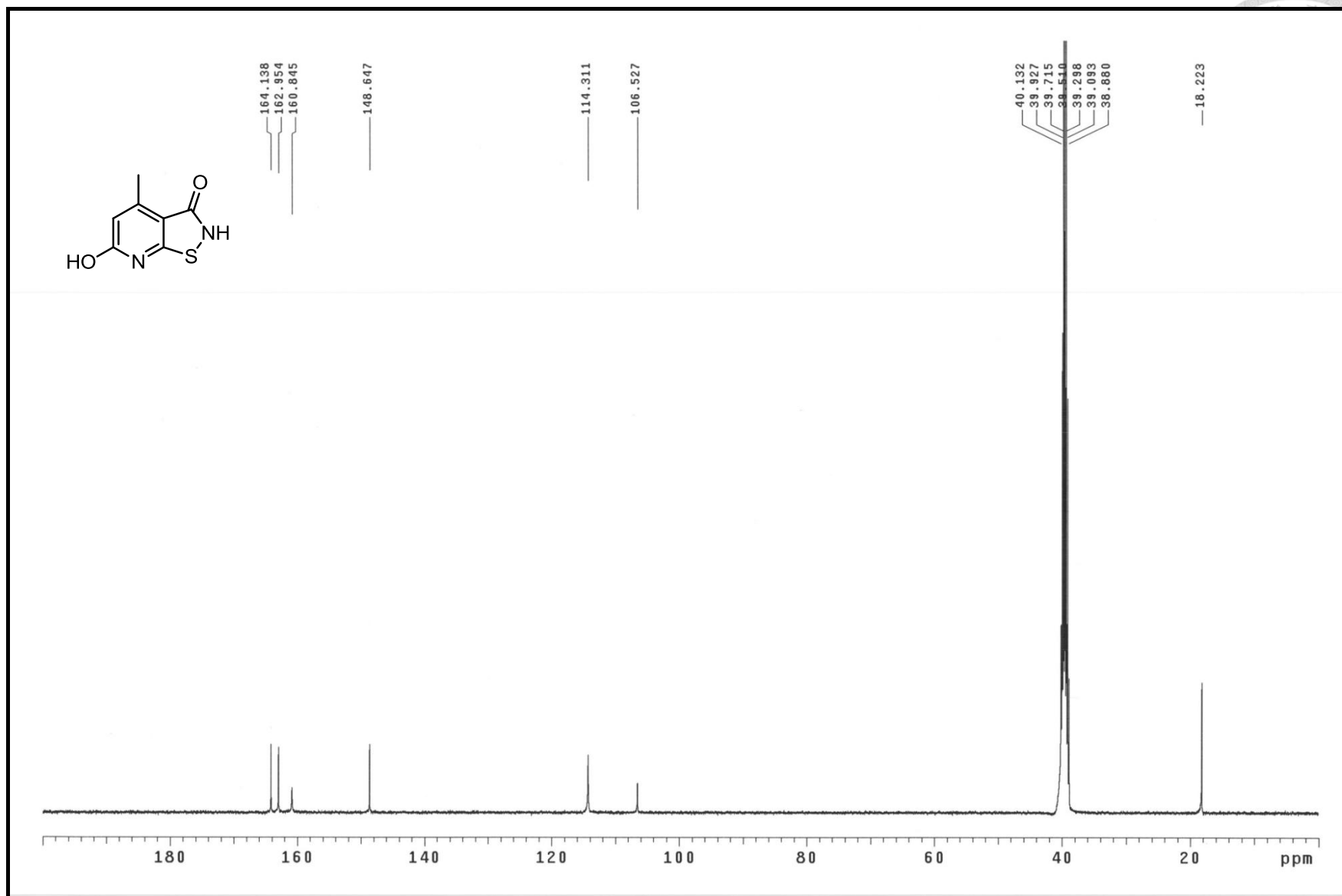
¹H NMR spectrum of compound **20** (400MHz, DMSO-*d*₆)



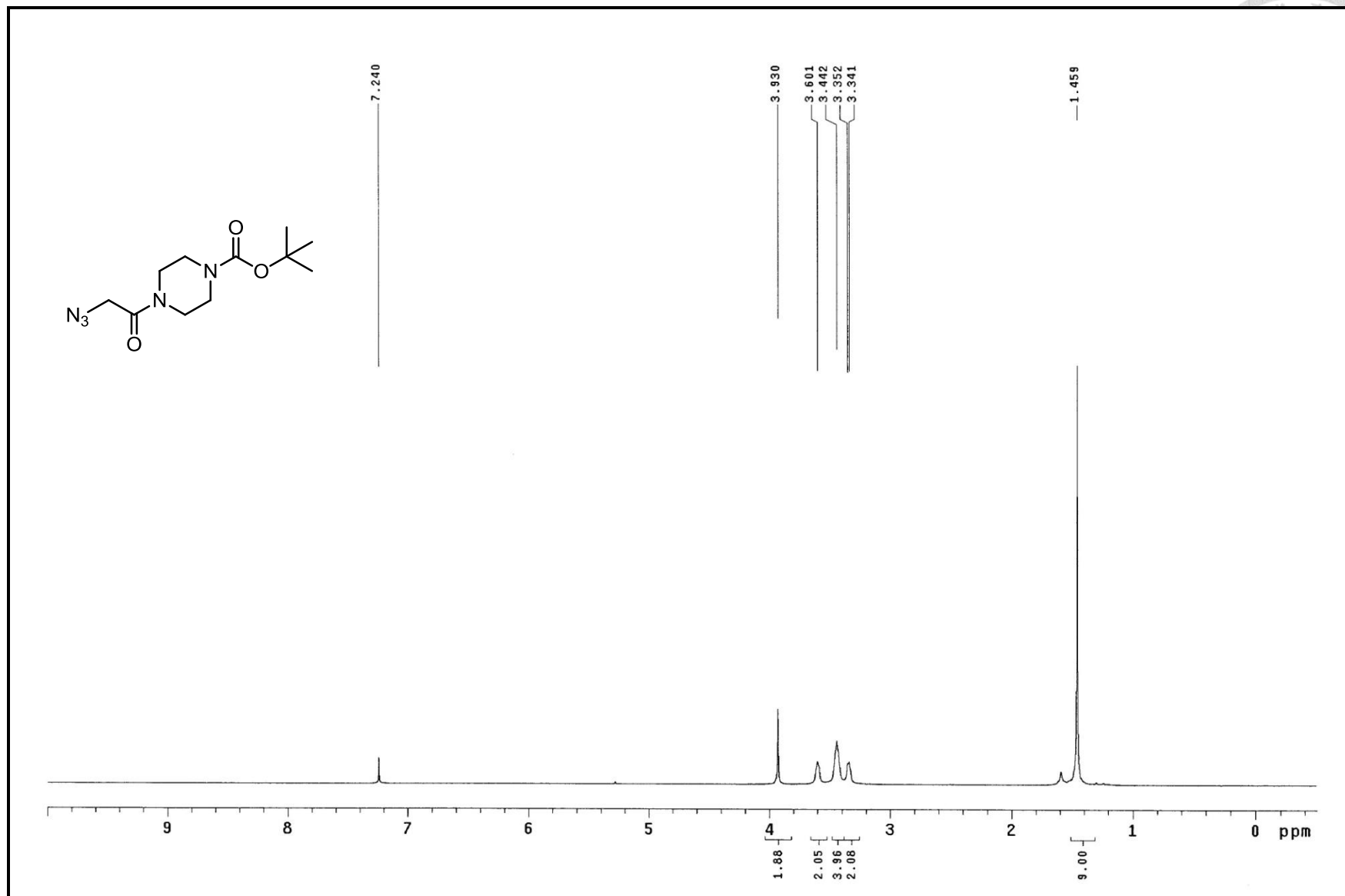
^{13}C NMR spectrum of compound **20** (100MHz, $\text{DMSO-}d_6$)



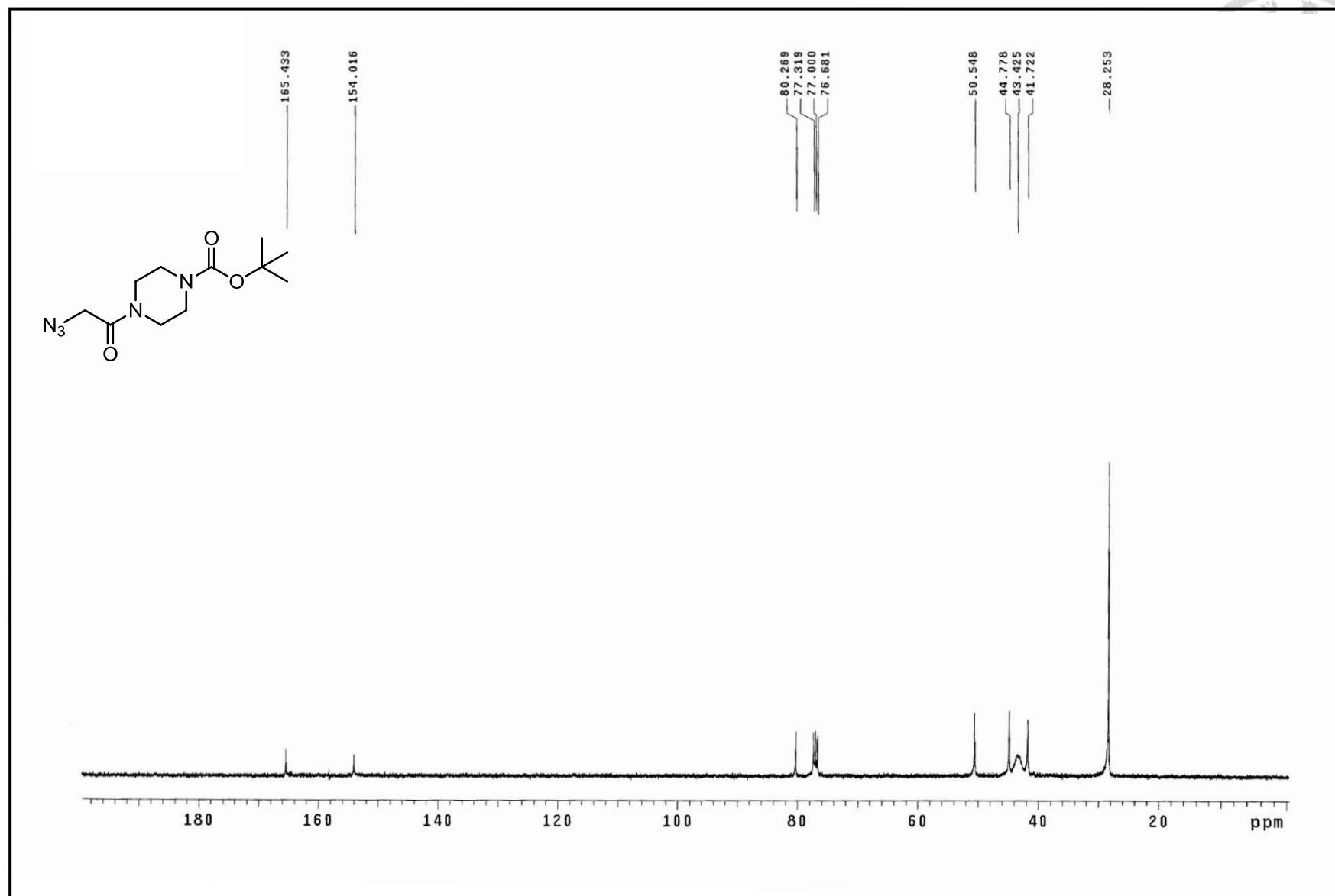
^1H NMR spectrum of compound **22** (400MHz, $\text{DMSO-}d_6$)



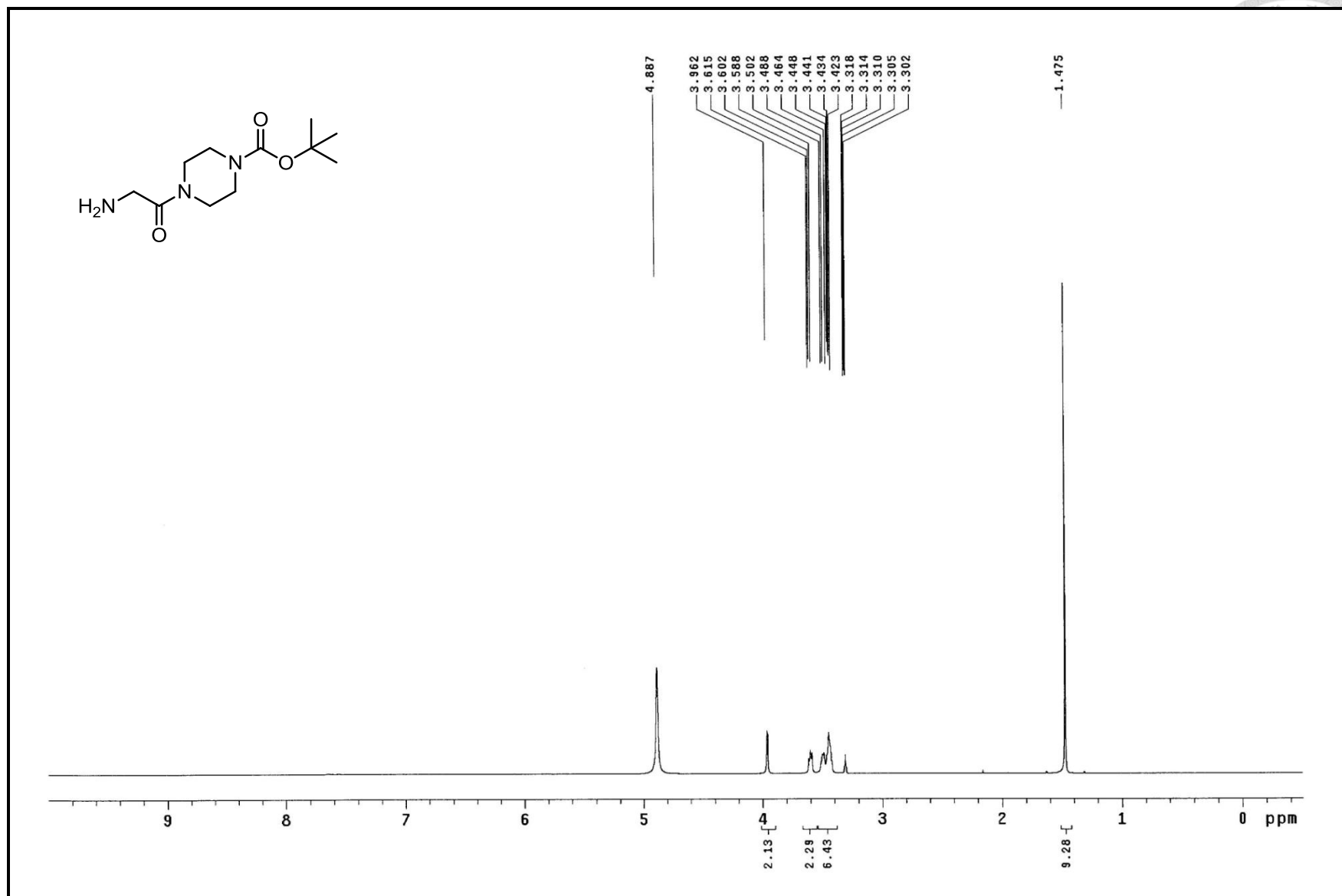
^{13}C NMR spectrum of compound **22** (100MHz, $\text{DMSO-}d_6$)



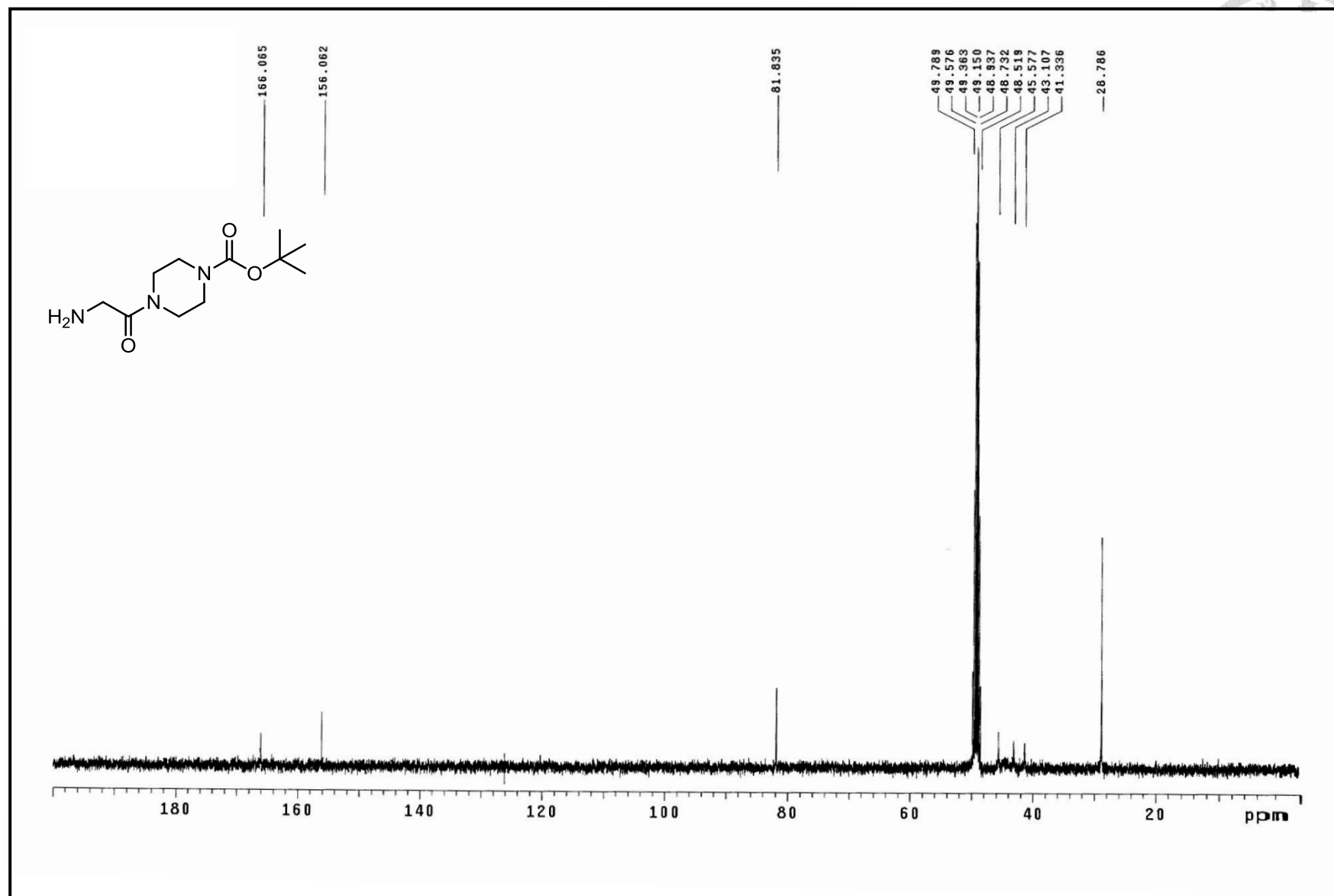
^1H NMR spectrum of compound **23** (400MHz, CDCl_3)



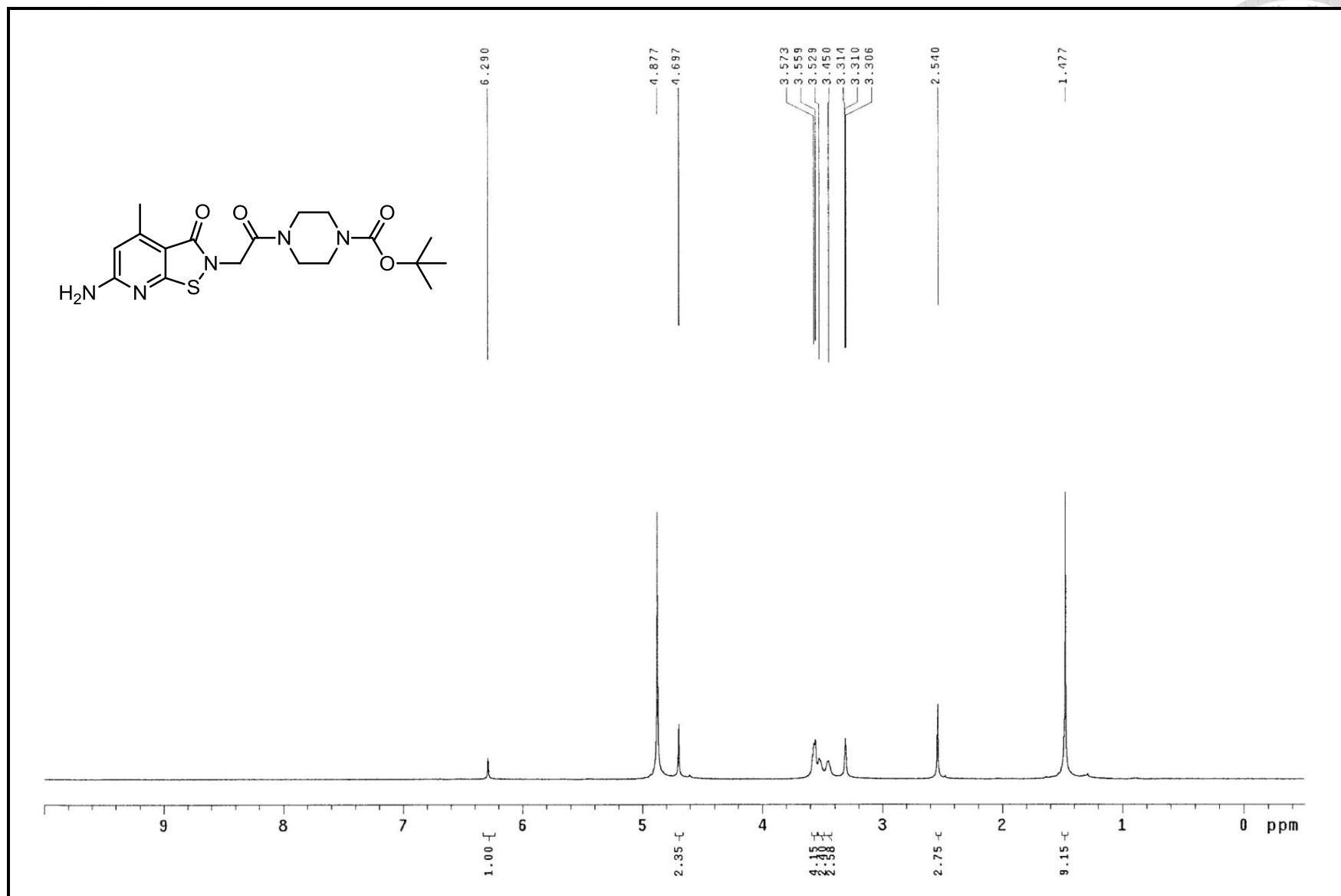
^{13}C NMR spectrum of compound **23** (100MHz, CDCl_3)



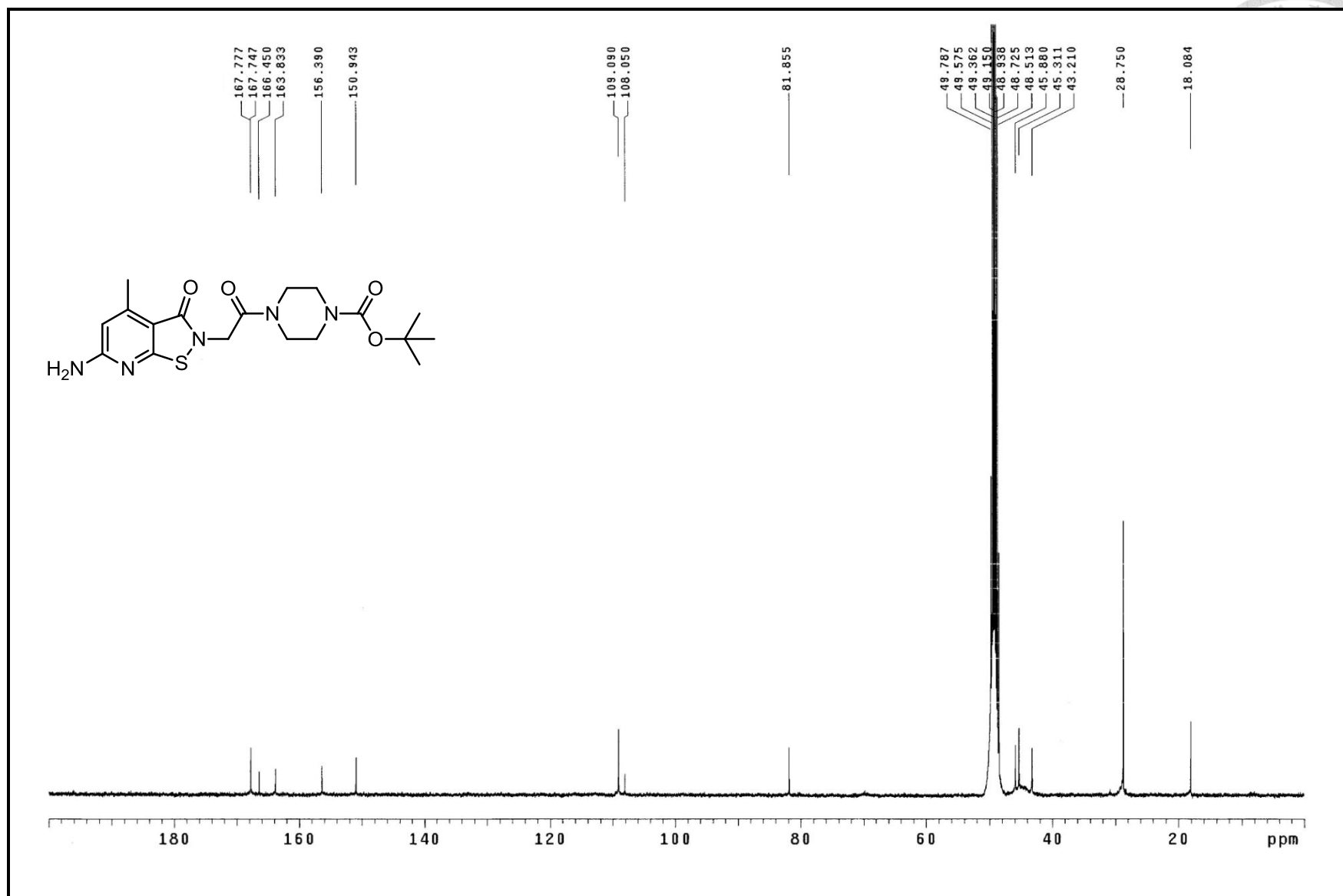
^1H NMR spectrum of compound **24** (400MHz, CD_3OD)



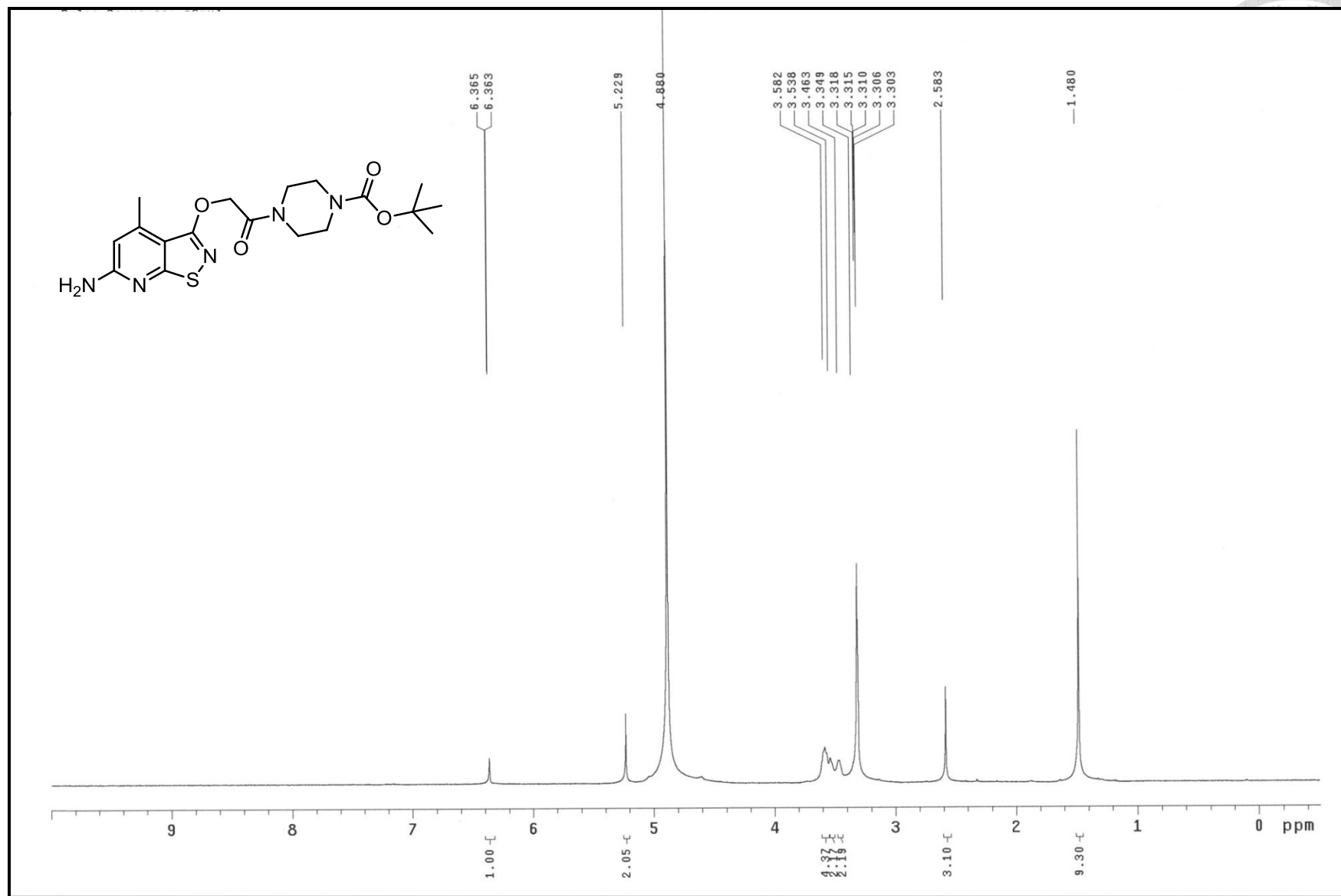
^{13}C NMR spectrum of compound **24** (100MHz, CD_3OD)



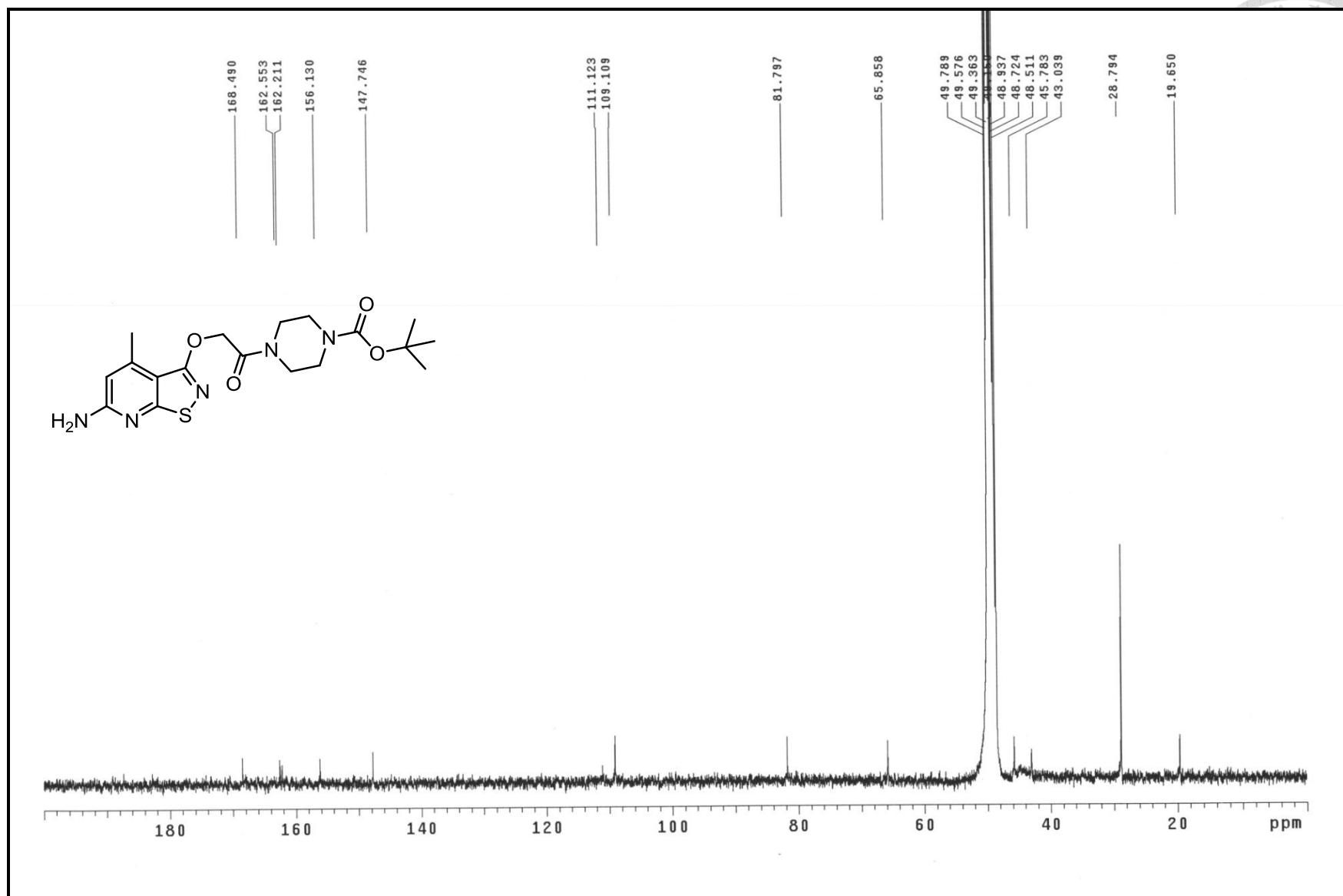
^1H NMR spectrum of compound **25** (400MHz, CD_3OD)



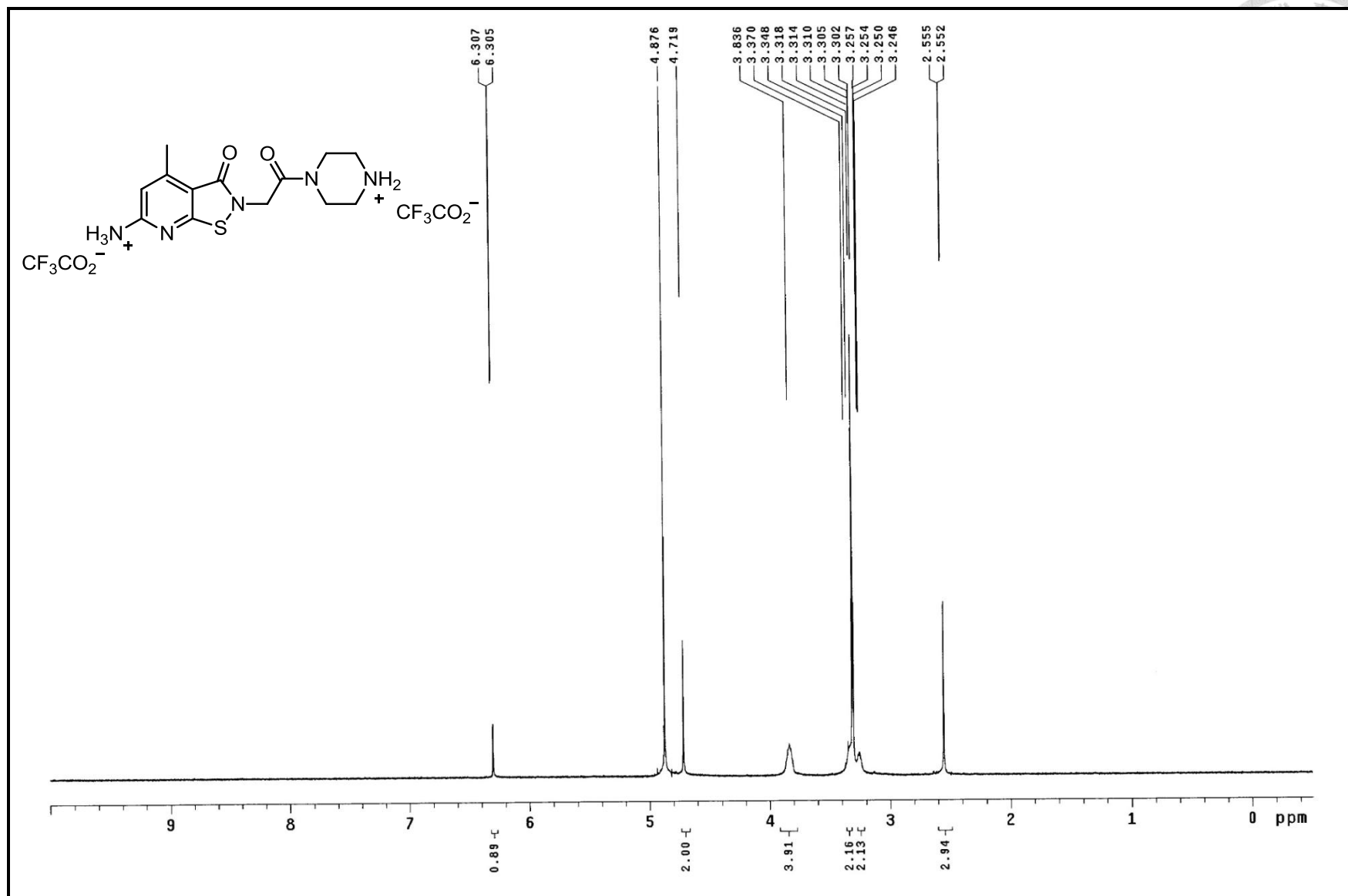
^{13}C NMR spectrum of compound **25** (100MHz, CD_3OD)



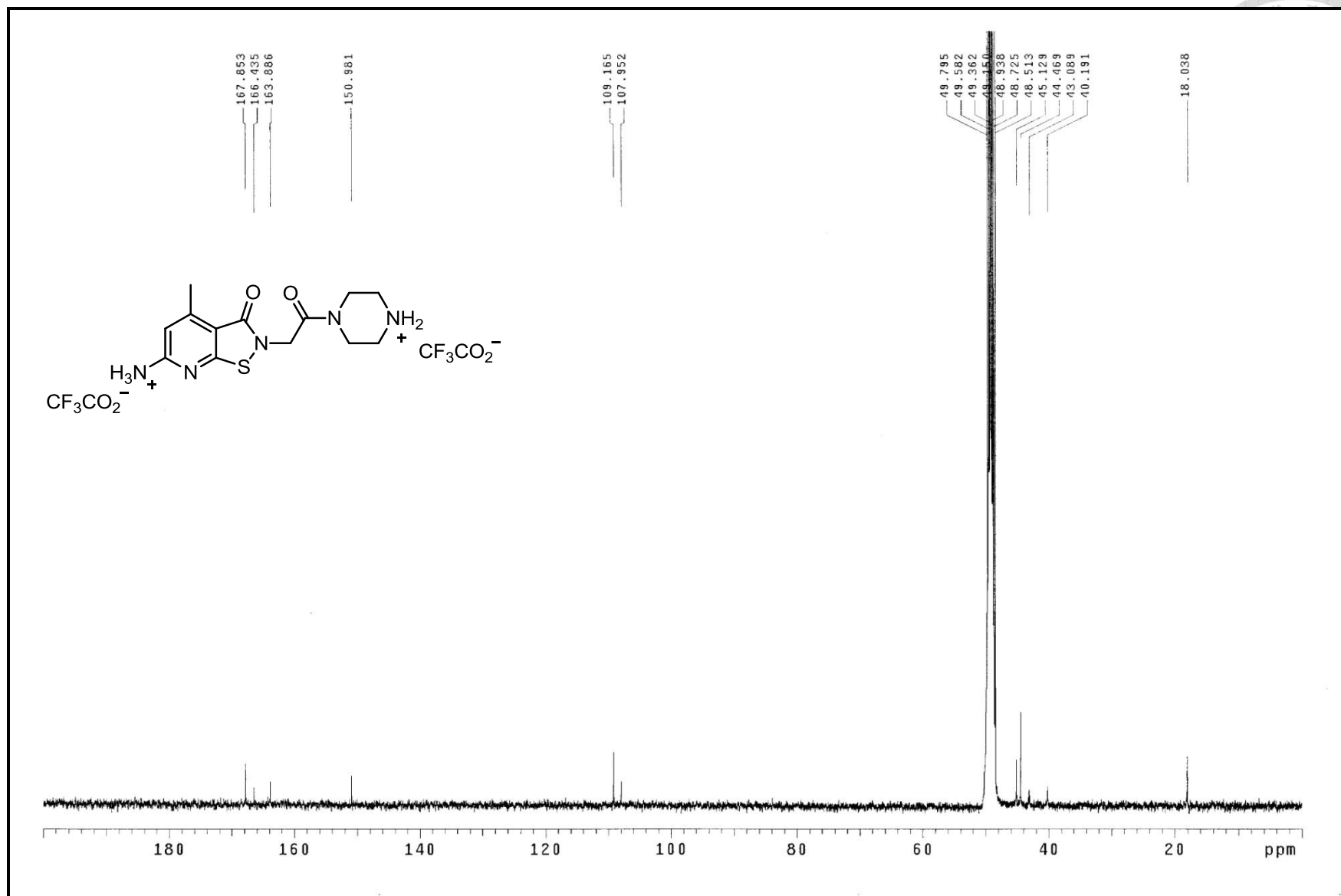
^1H NMR spectrum of compound **26** (400MHz, CD_3OD)



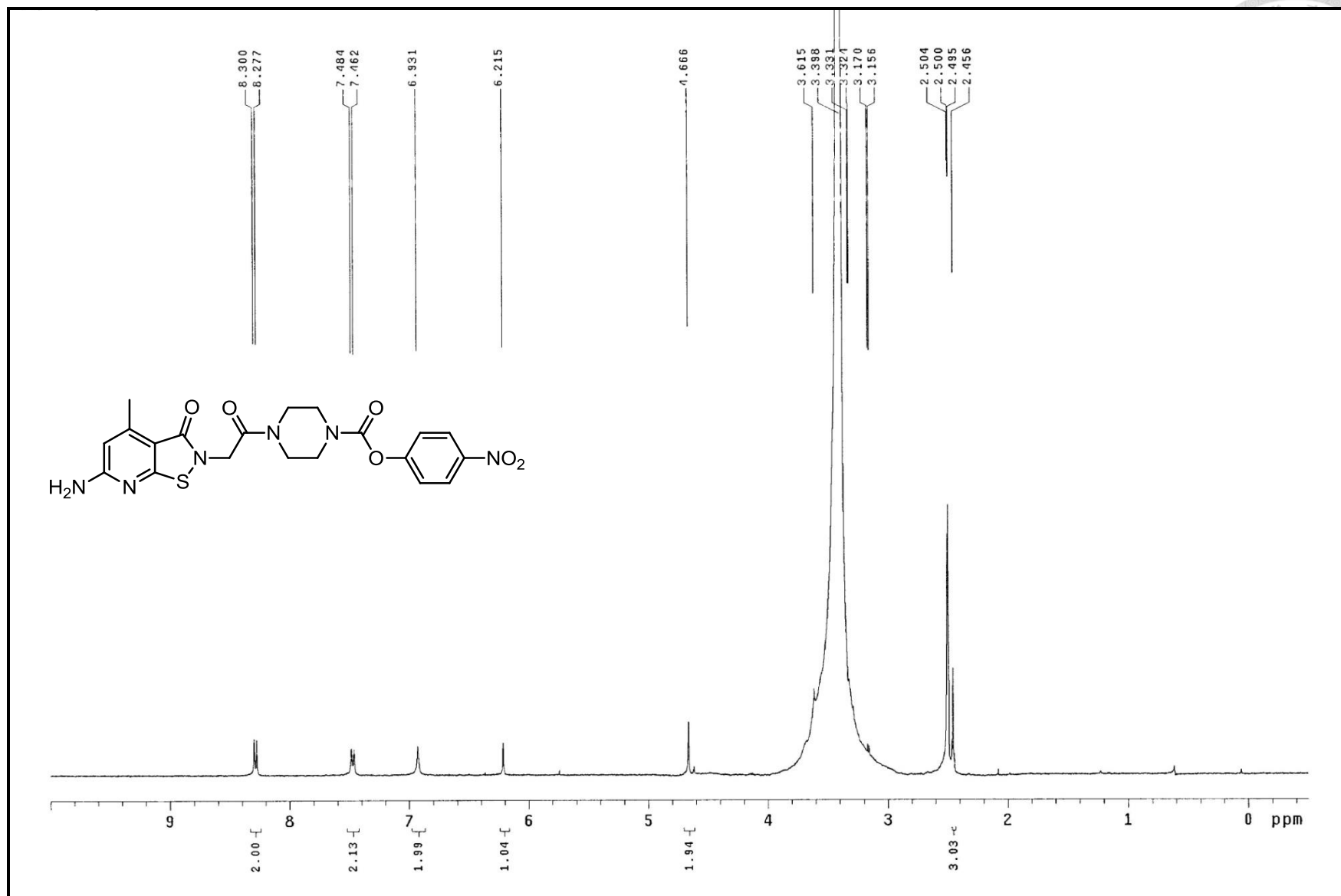
^{13}C NMR spectrum of compound **26** (100MHz, CD_3OD)



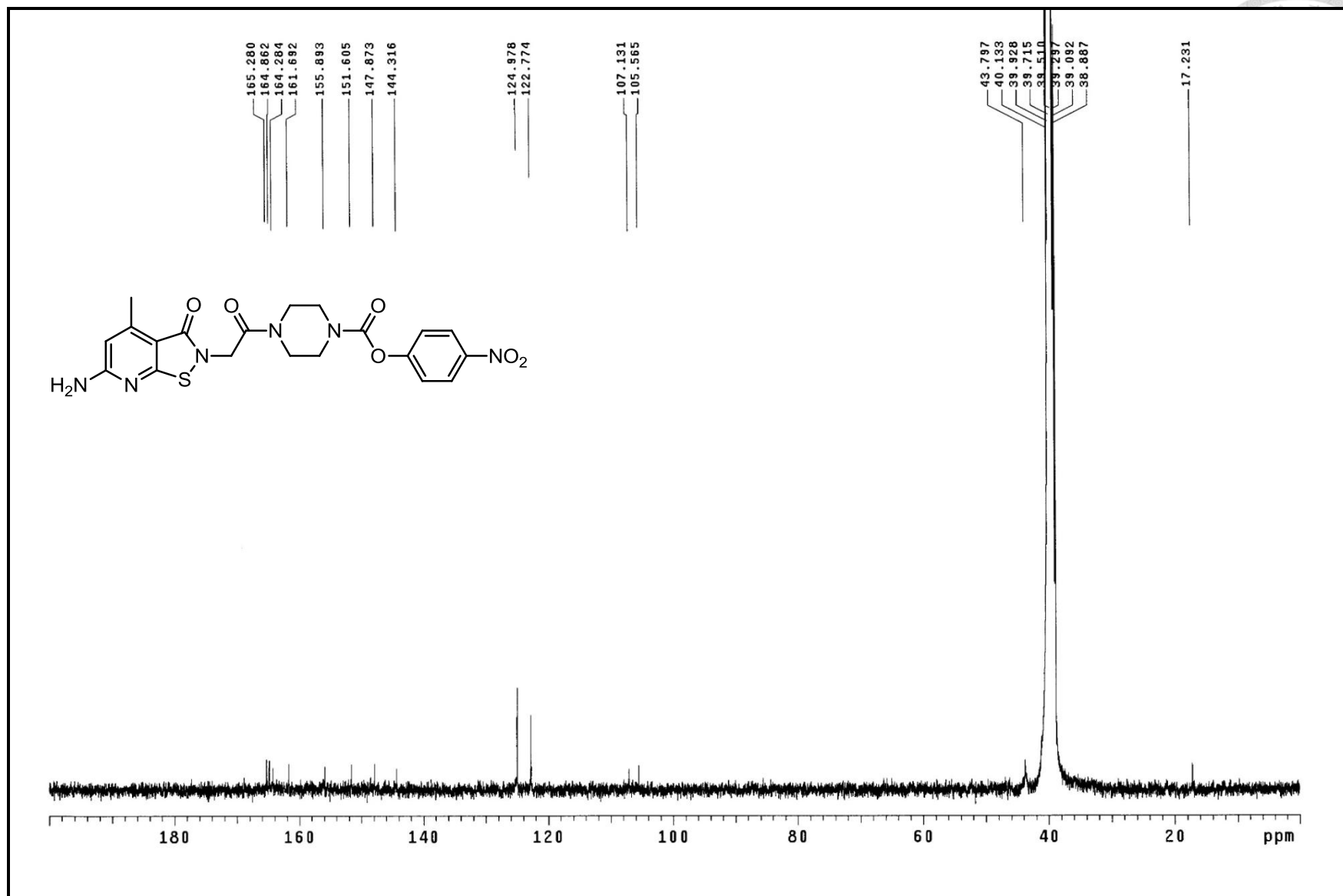
^1H NMR spectrum of compound **27** (400MHz, CD_3OD)



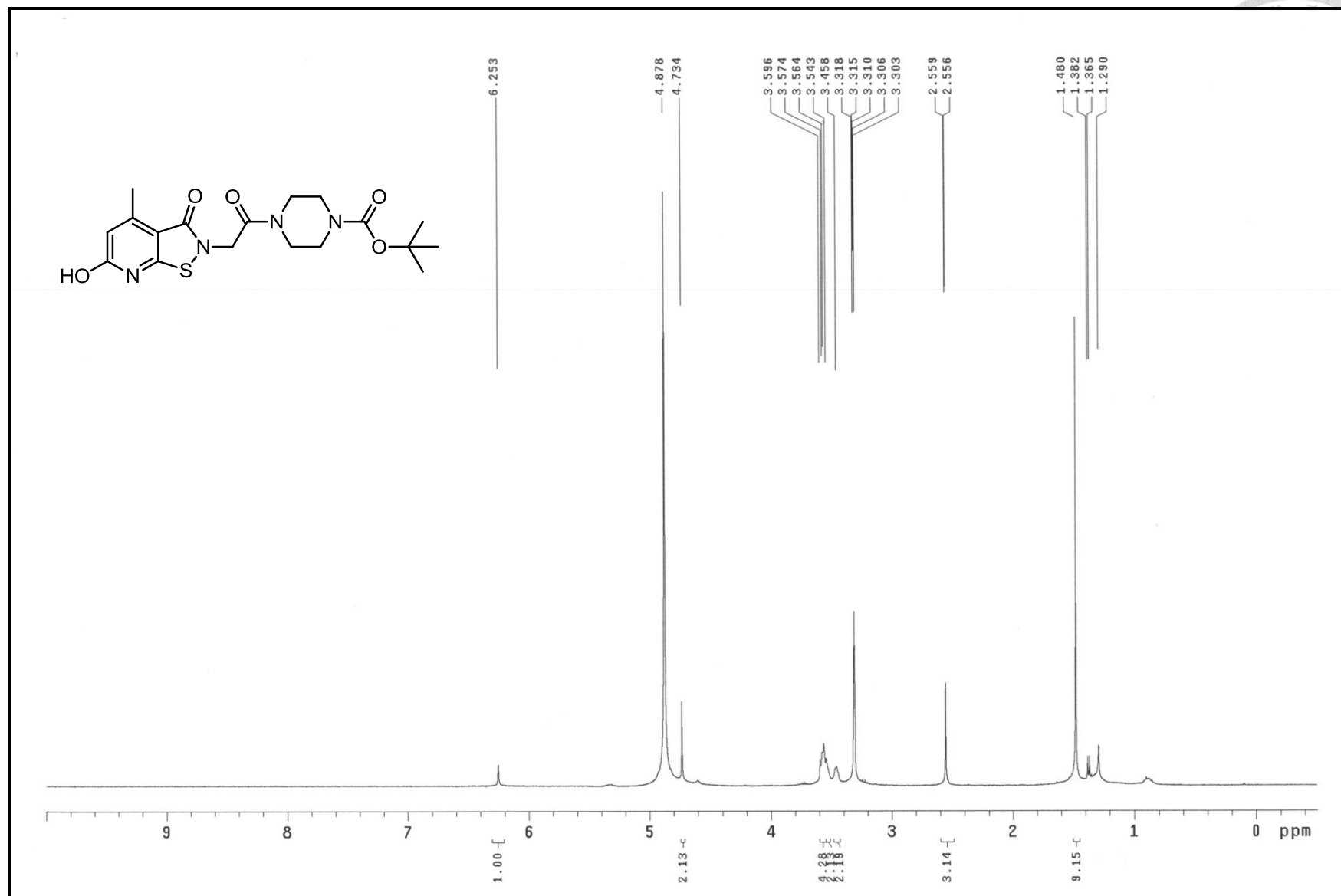
^{13}C NMR spectrum of compound **27** (100MHz, CD_3OD)



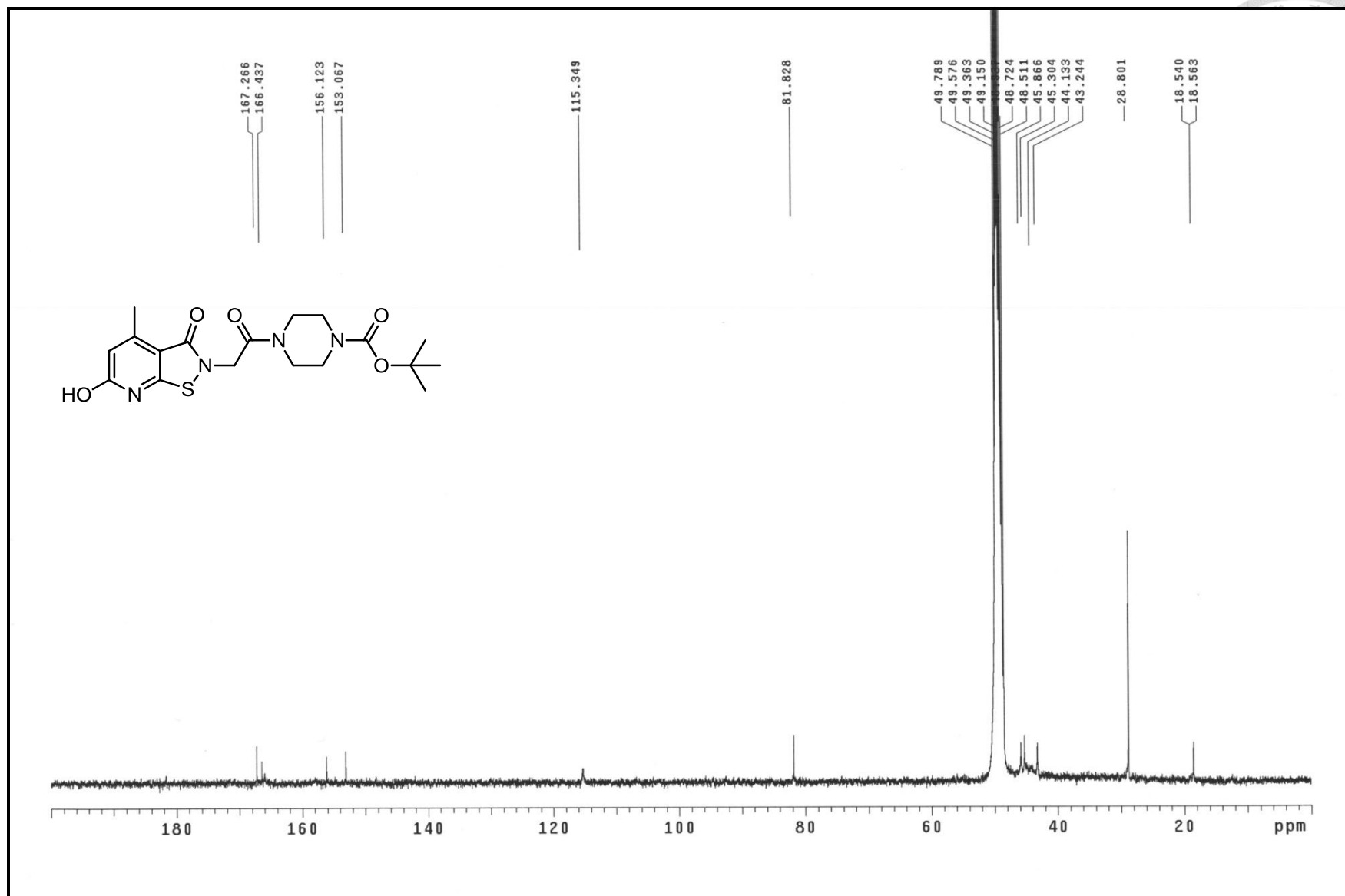
^1H NMR spectrum of compound **28** (400MHz, $\text{DMSO-}d_6$)



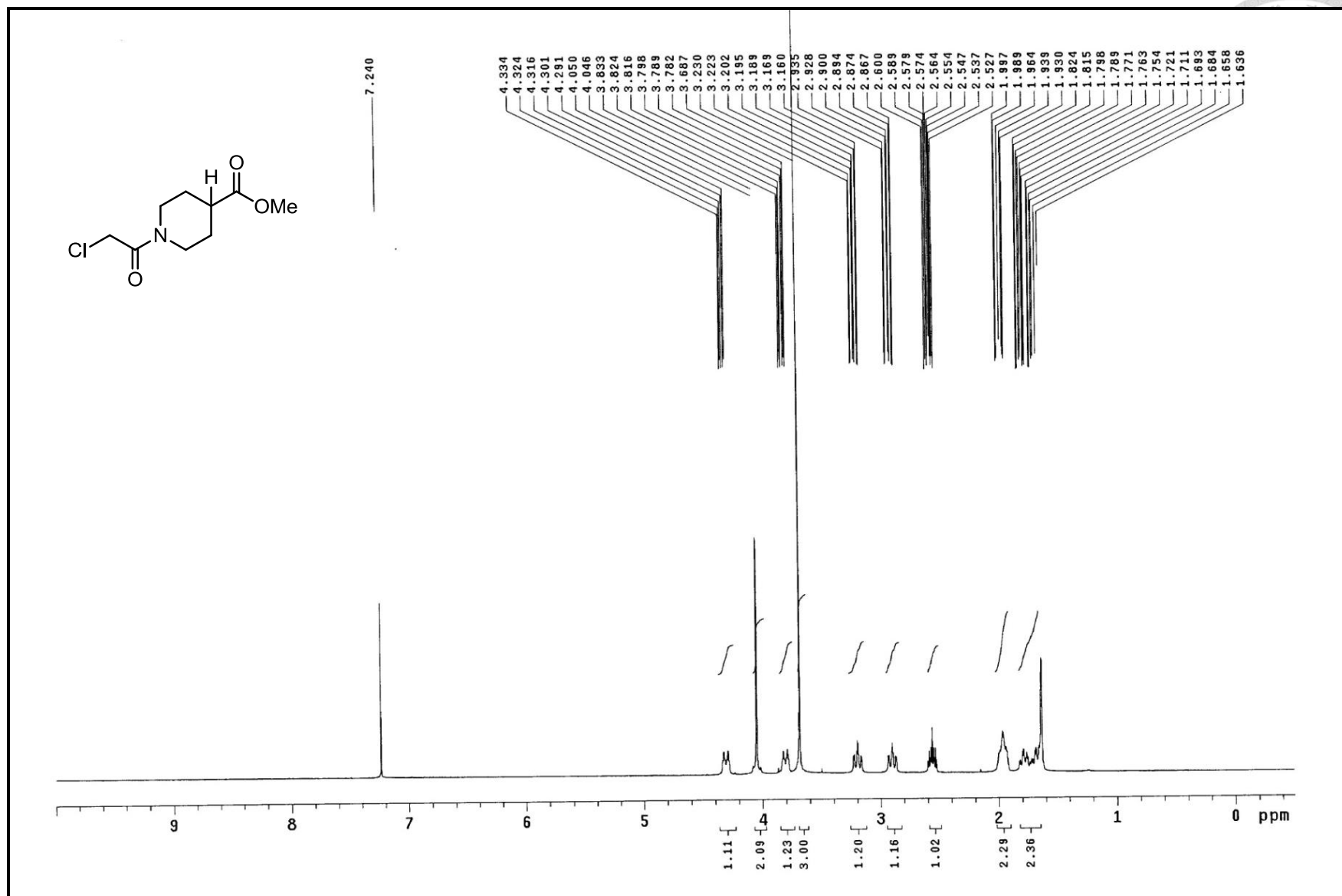
^{13}C NMR spectrum of compound **28** (100MHz, DMSO- d_6)



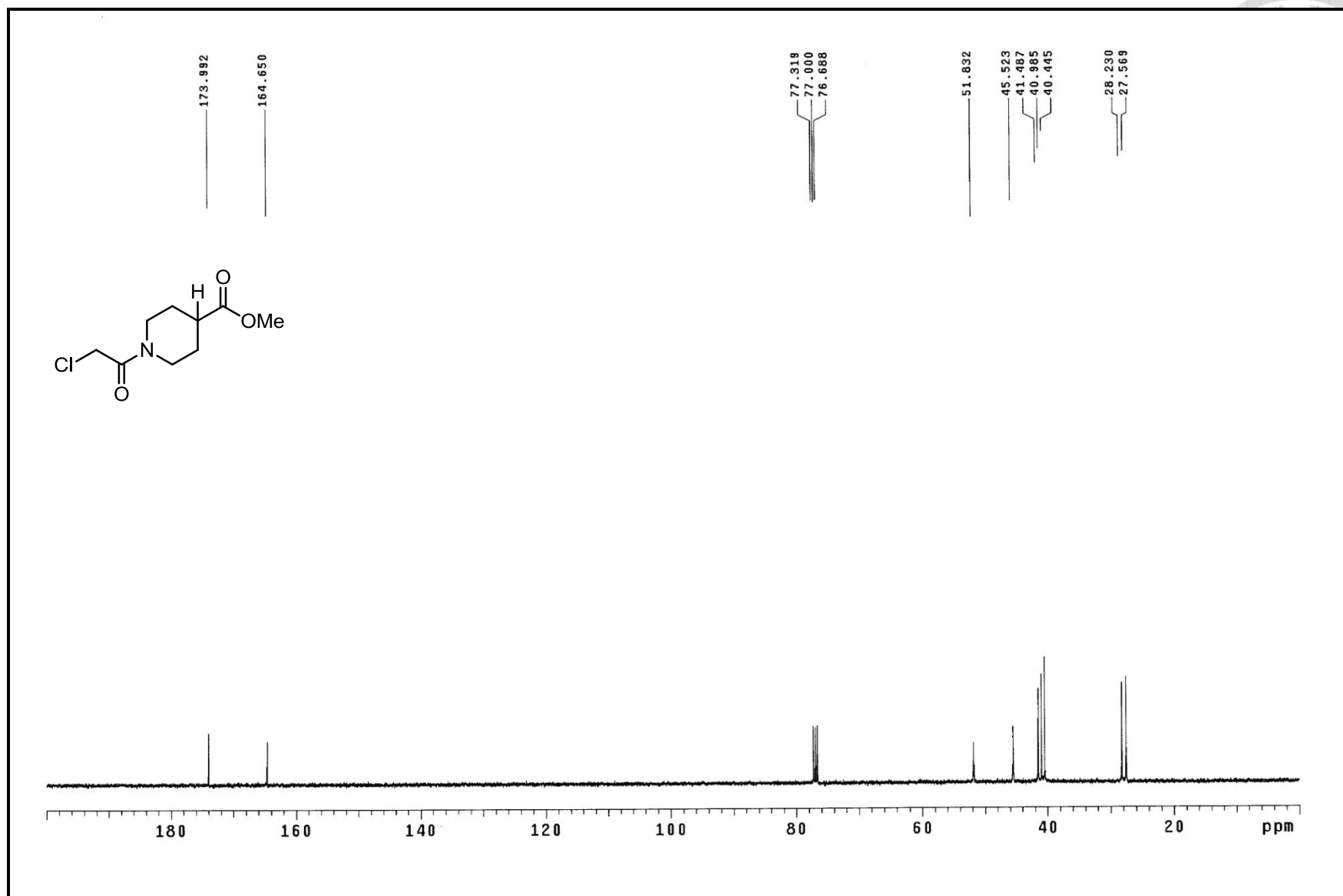
^1H NMR spectrum of compound **29** (400MHz, CD_3OD)



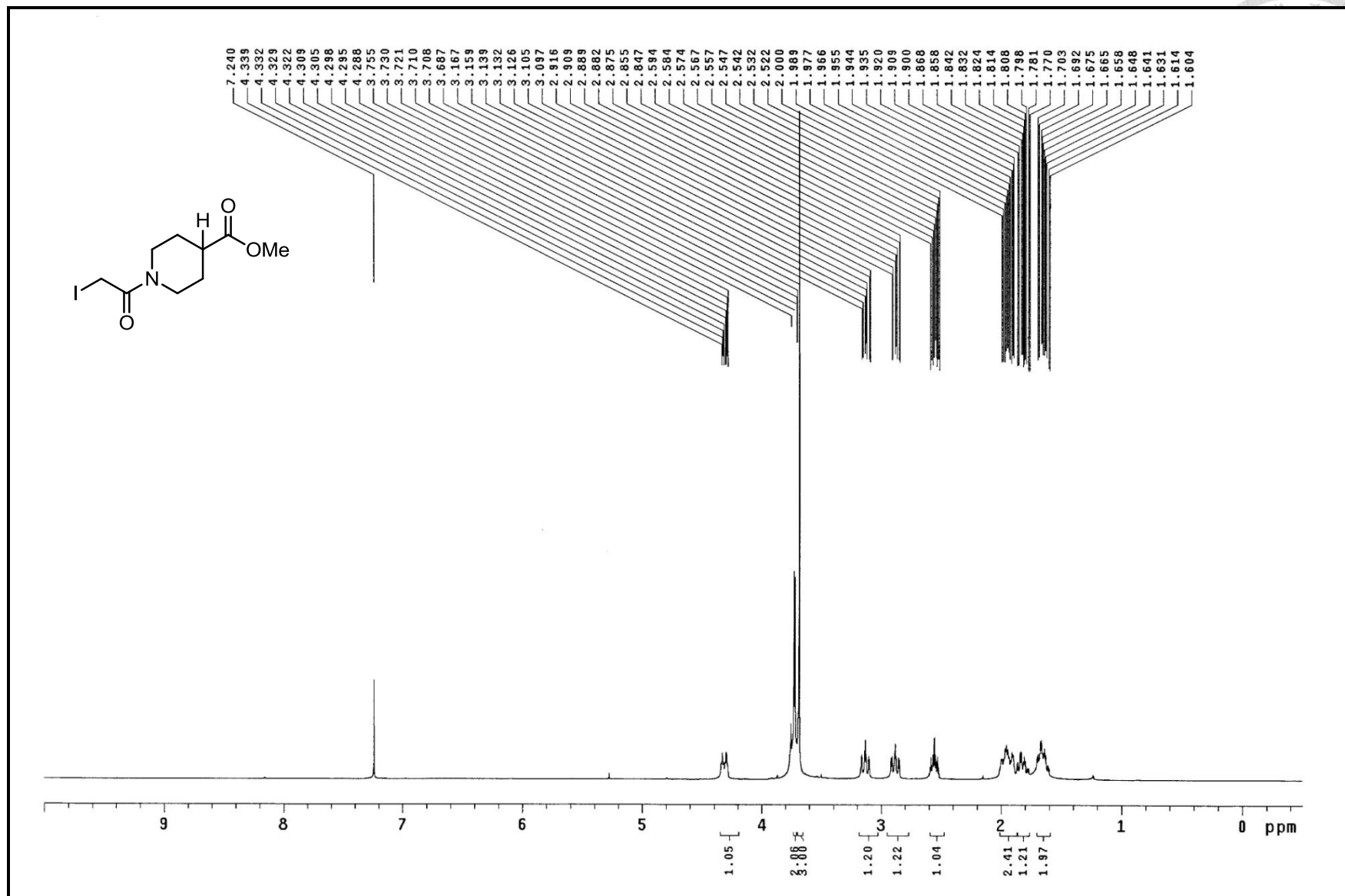
^{13}C NMR spectrum of compound **29** (100MHz, CD_3OD)



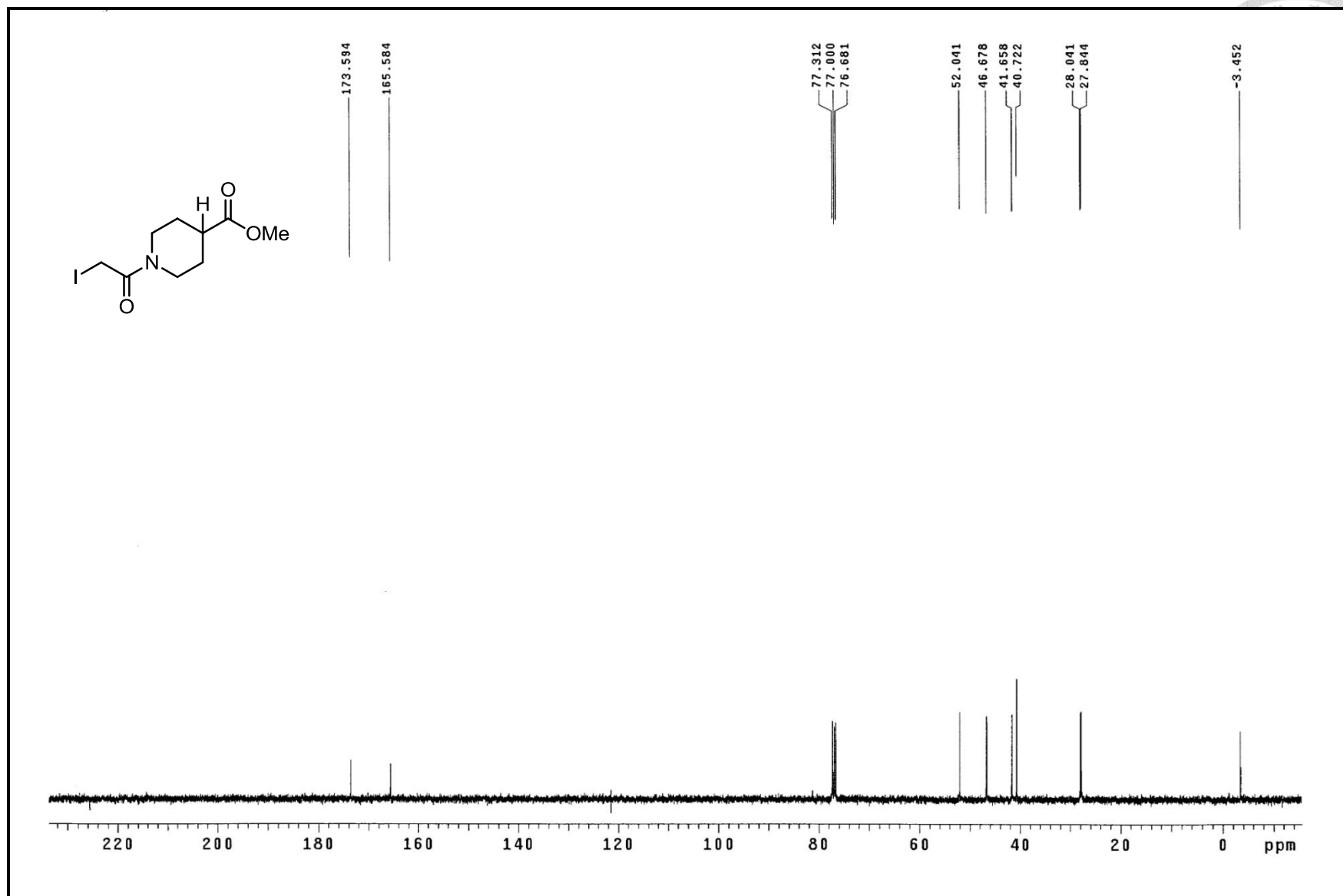
^1H NMR spectrum of compound **31** (400MHz, CDCl_3)



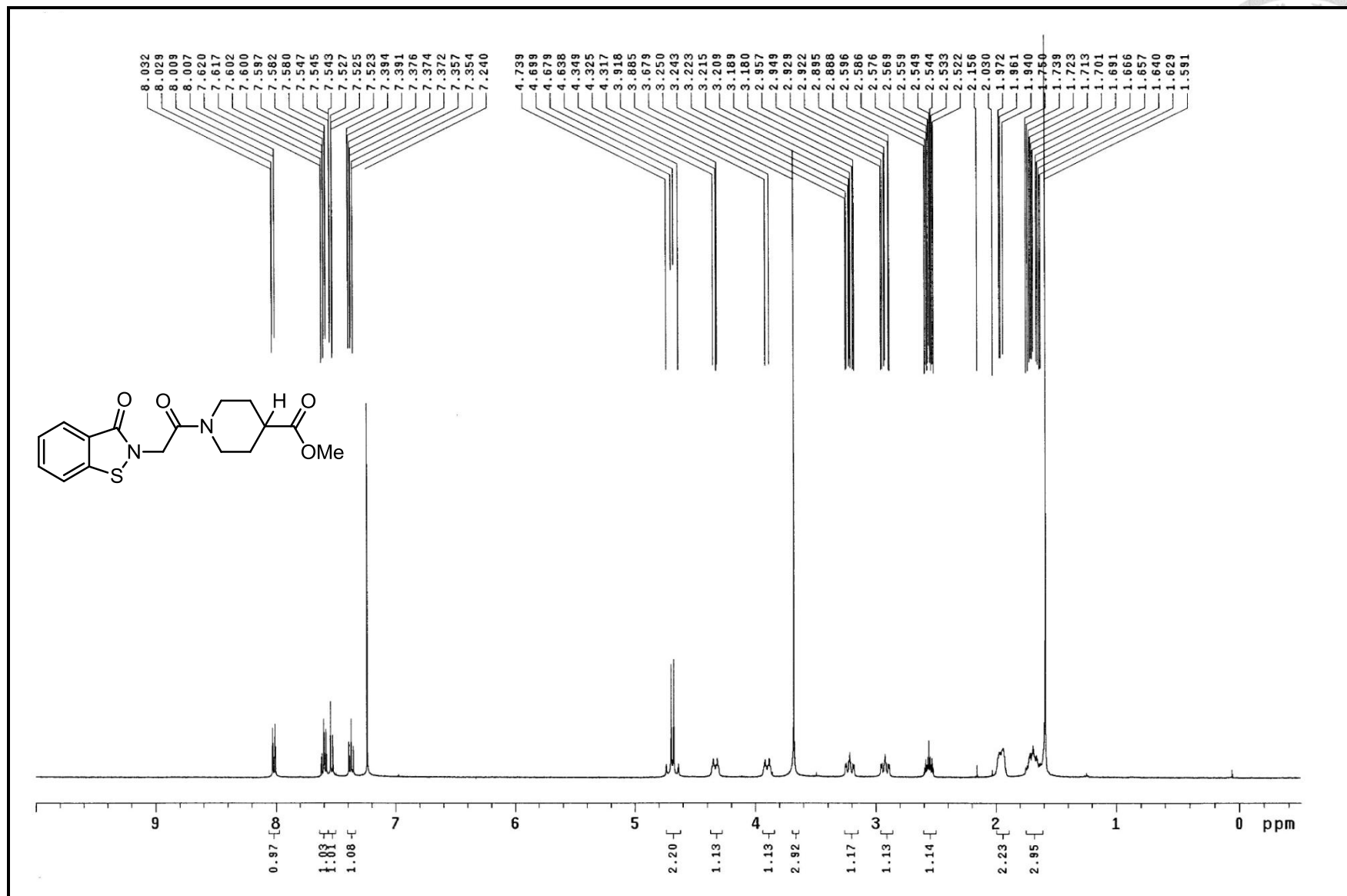
^{13}C NMR spectrum of compound **31** (100MHz, CDCl_3)



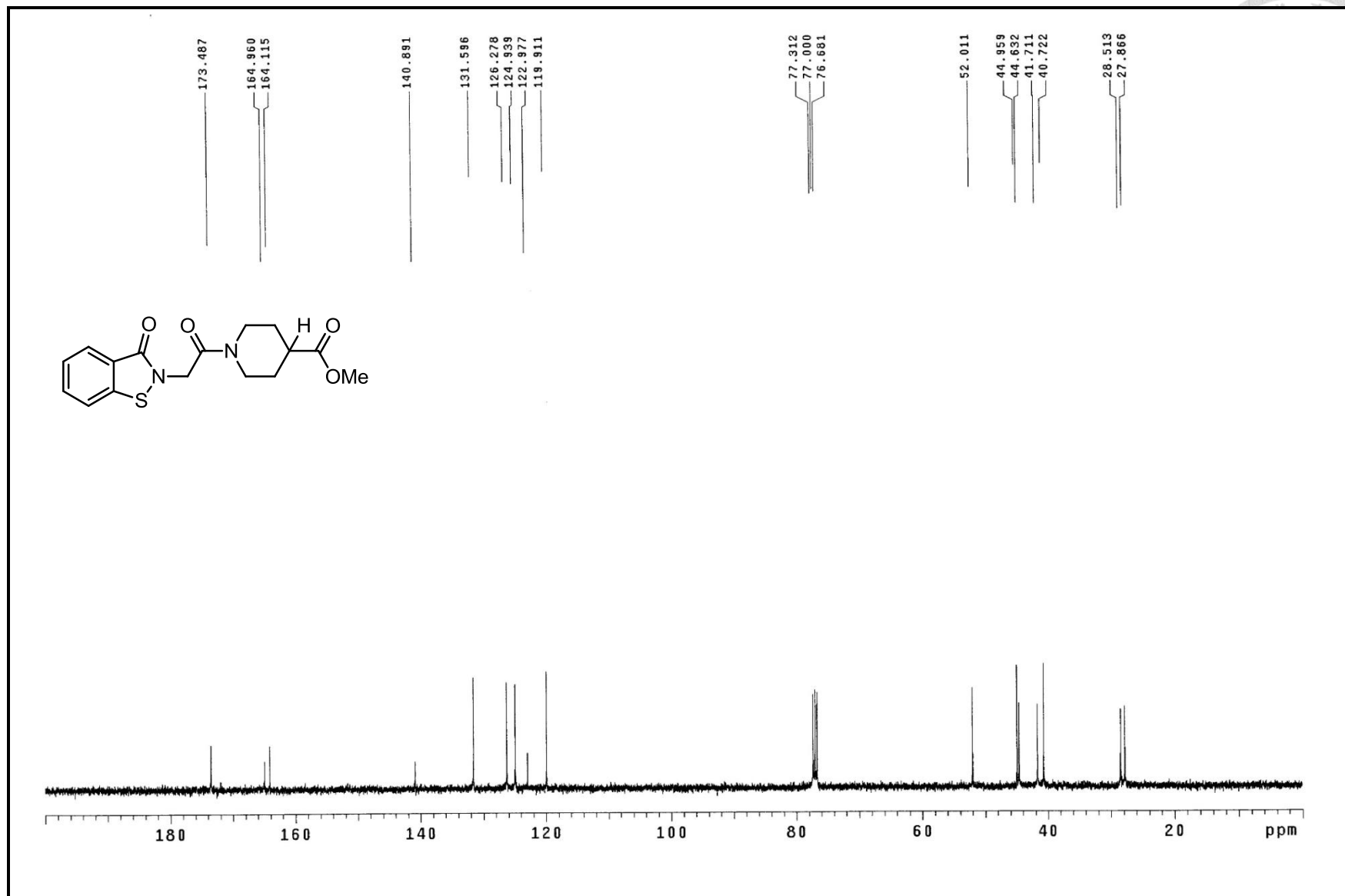
¹H NMR spectrum of compound **32** (400MHz, CDCl₃)



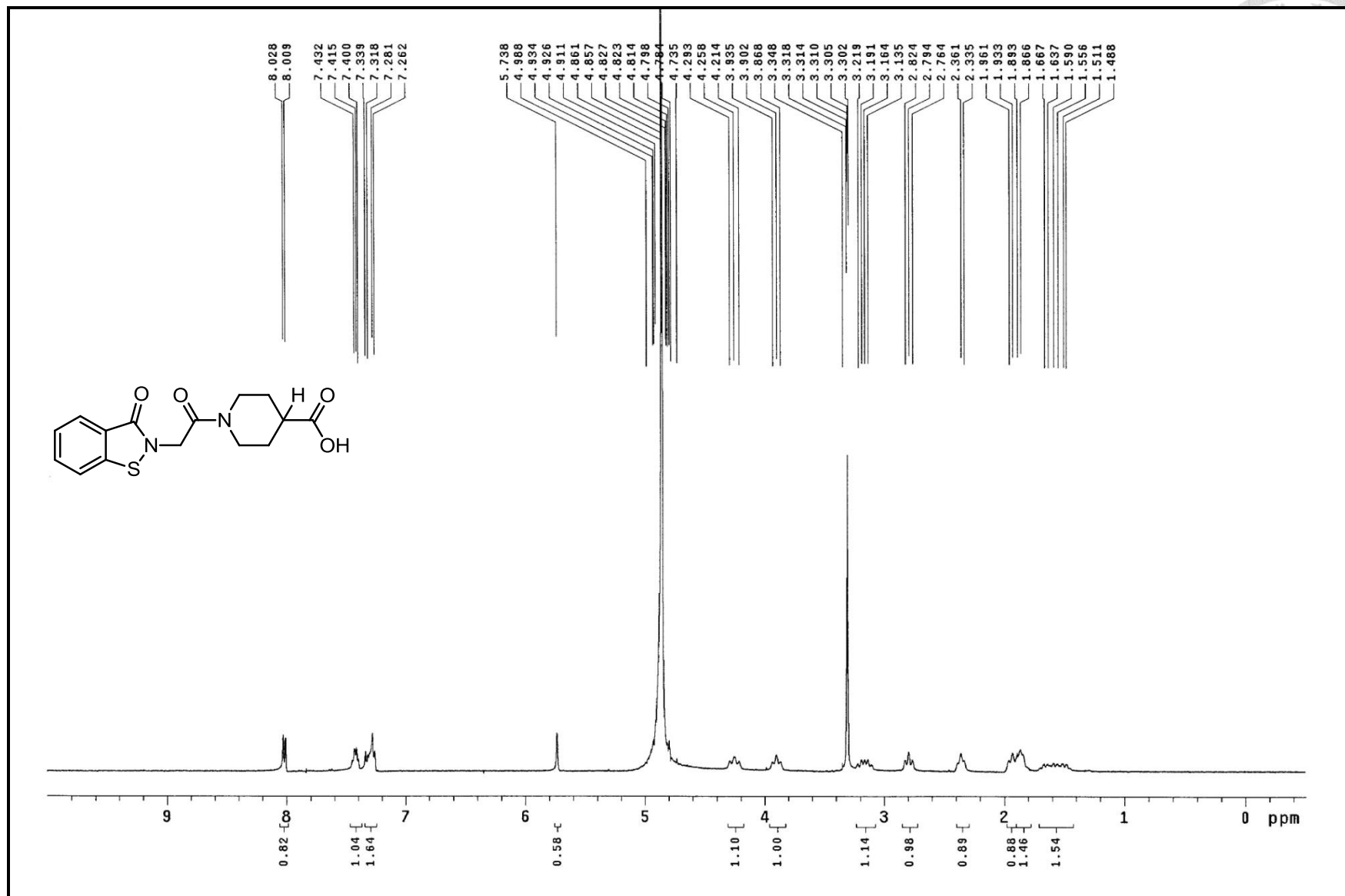
^{13}C NMR spectrum of compound **32** (100MHz, CDCl_3)



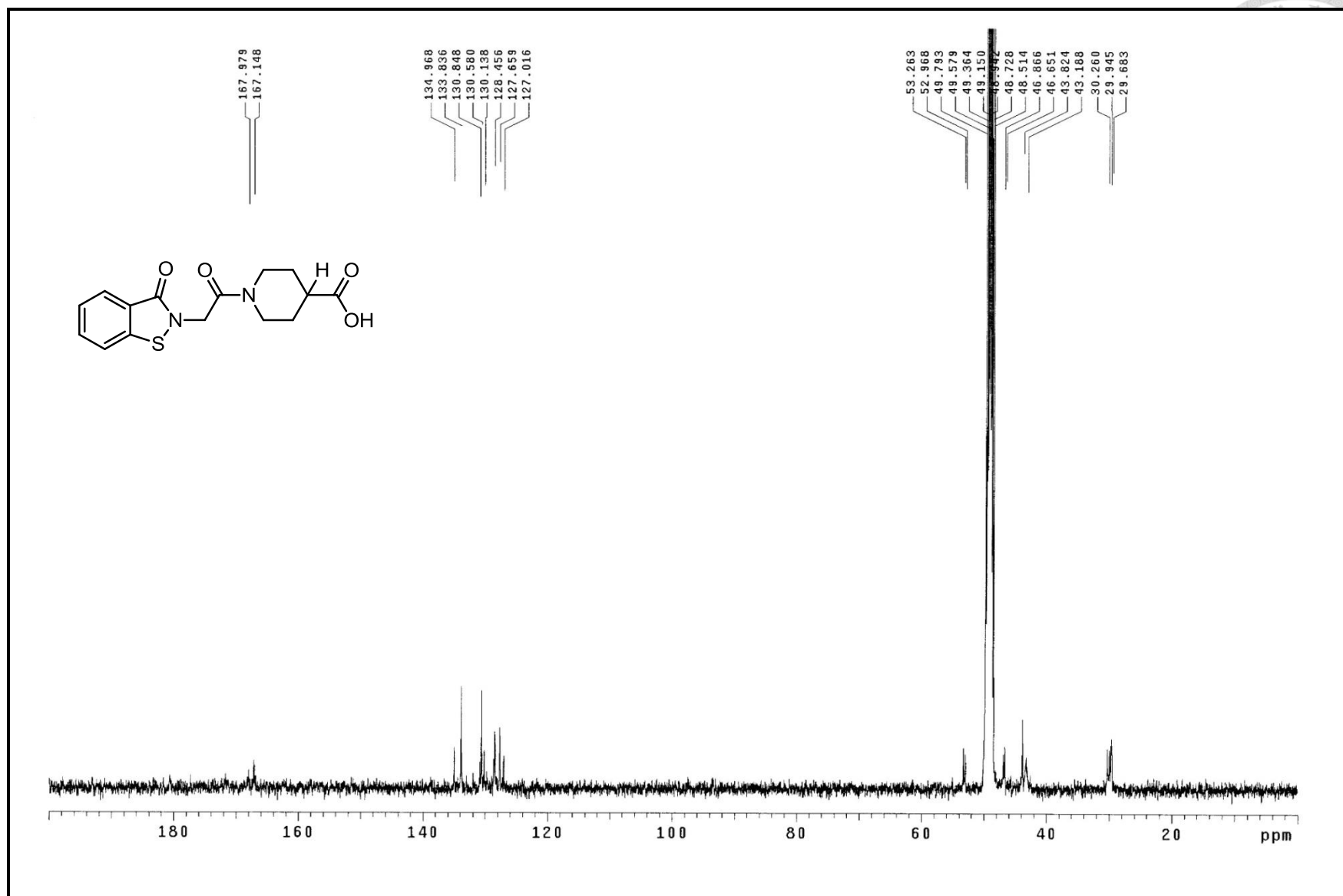
¹H NMR spectrum of compound **33** (400MHz, CDCl₃)



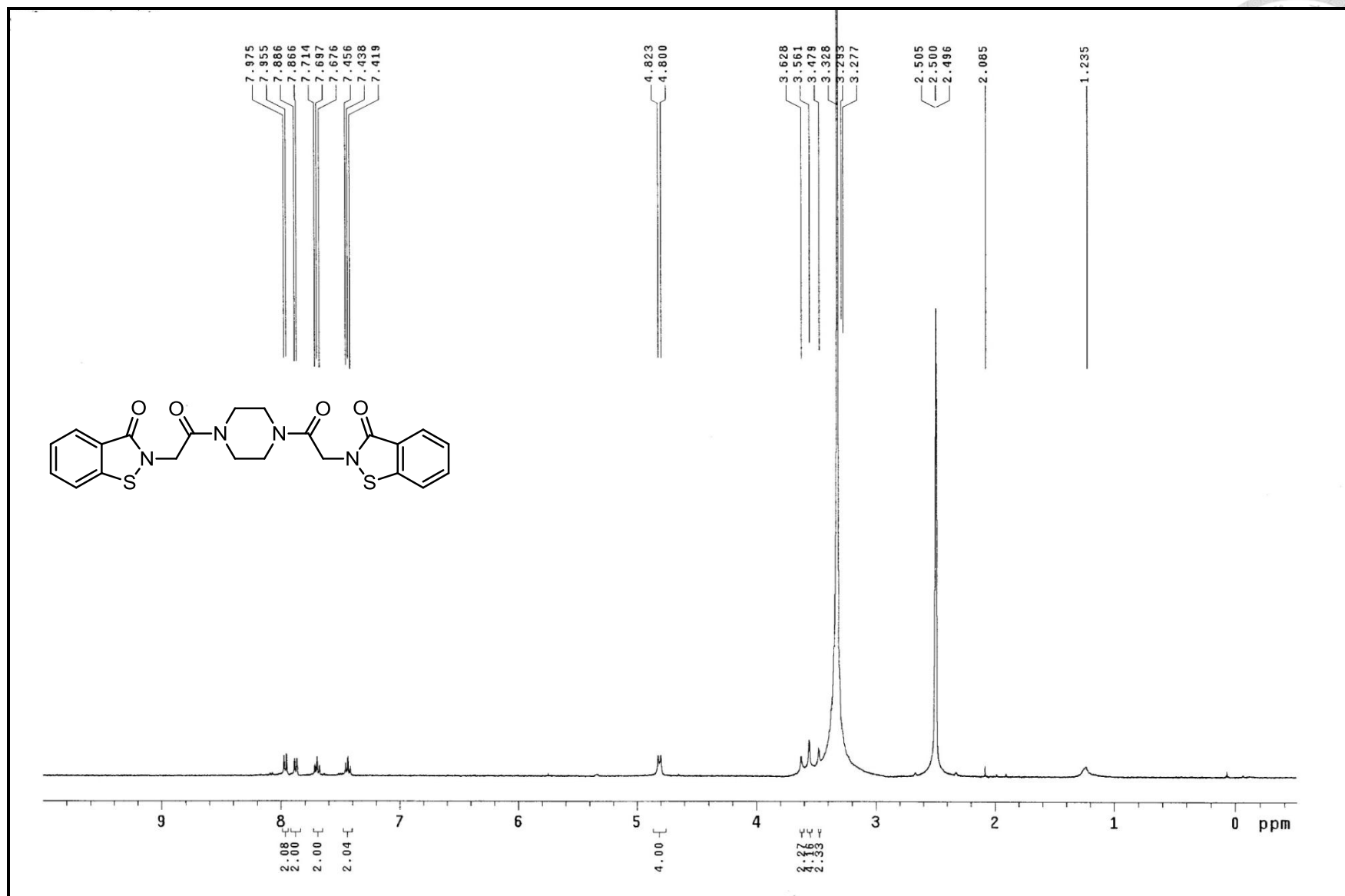
^{13}C NMR spectrum of compound **33** (100MHz, CDCl_3)



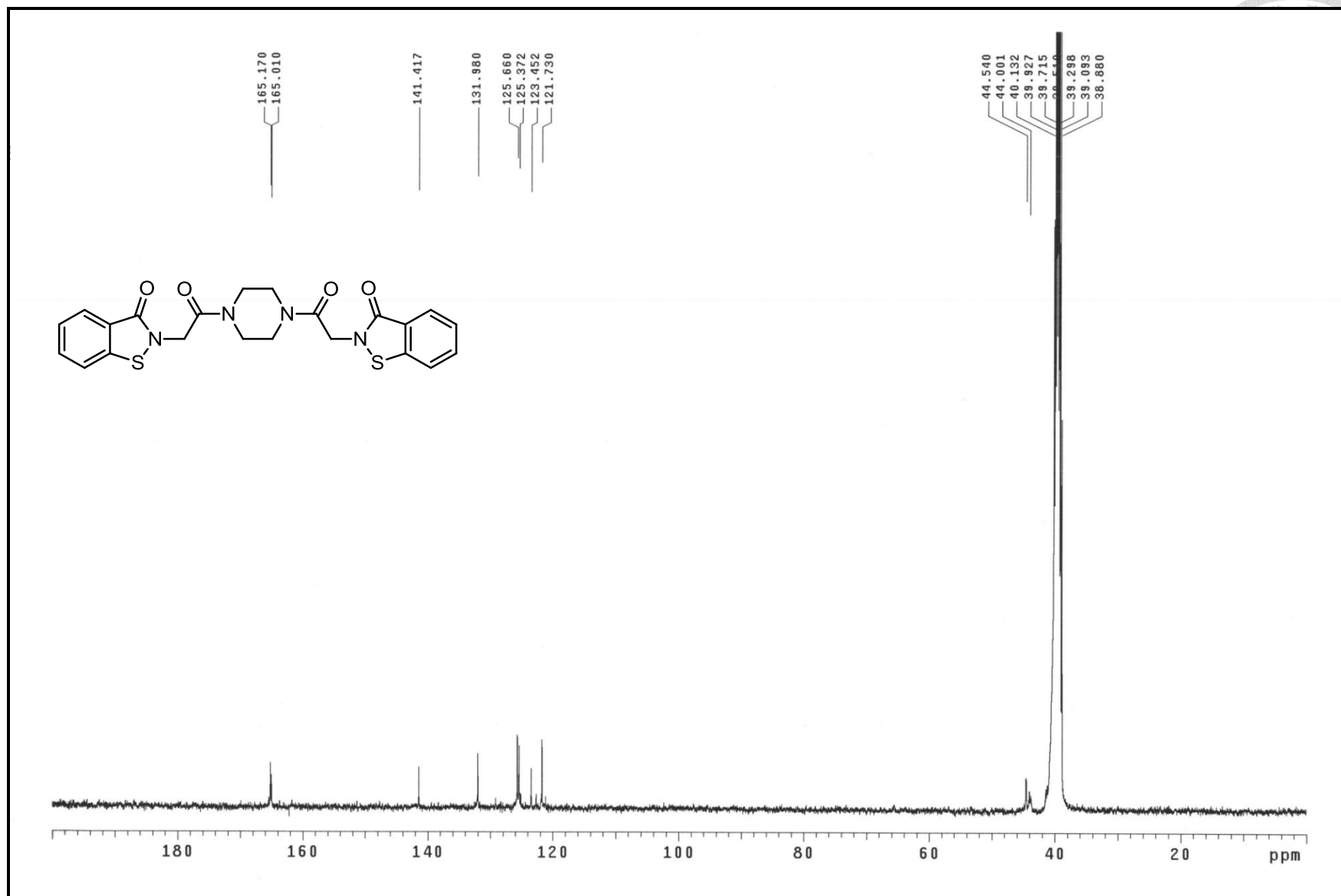
¹H NMR spectrum of compound 34 (400MHz, CD₃OD)



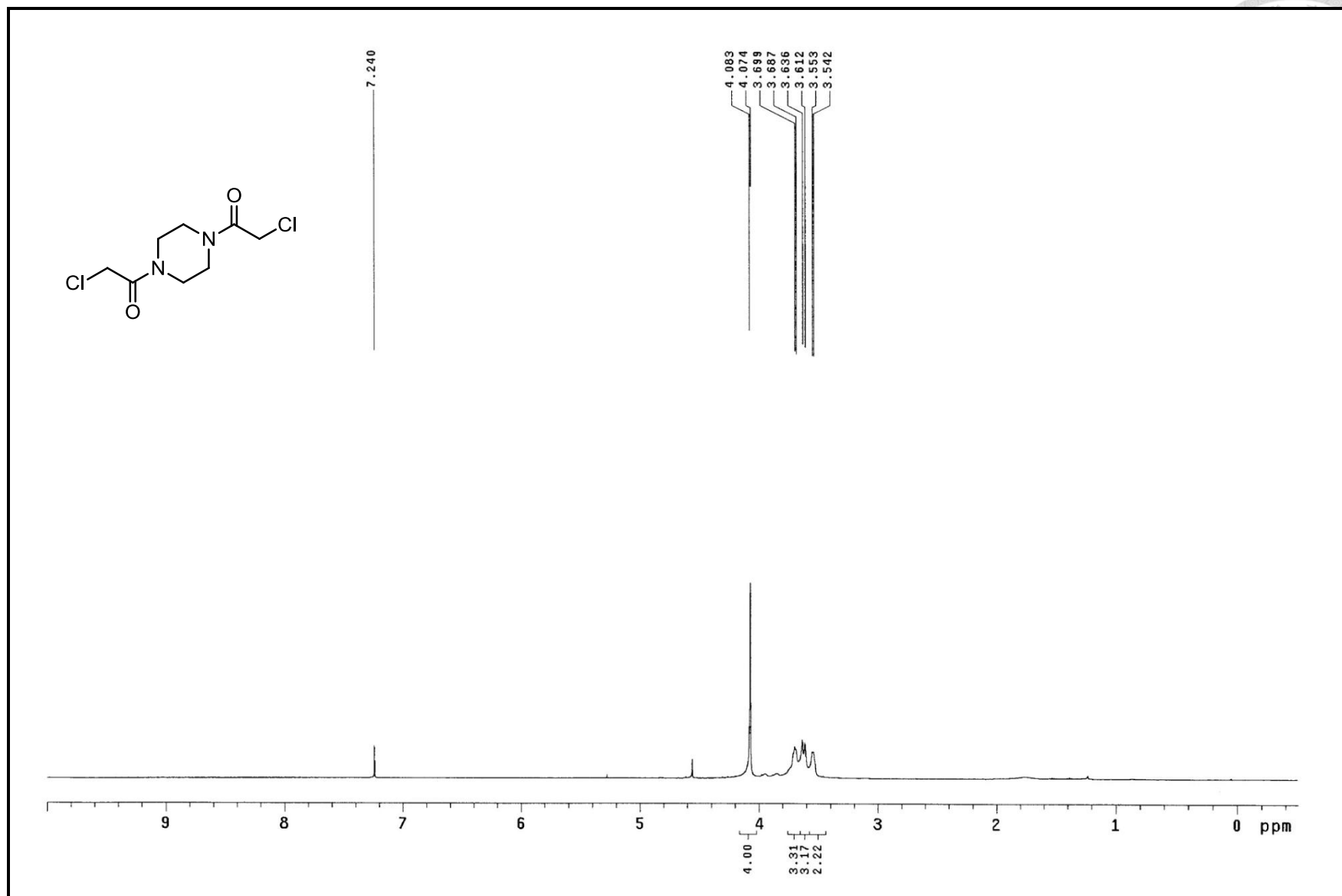
^{13}C NMR spectrum of compound **34** (100MHz, CD_3OD)



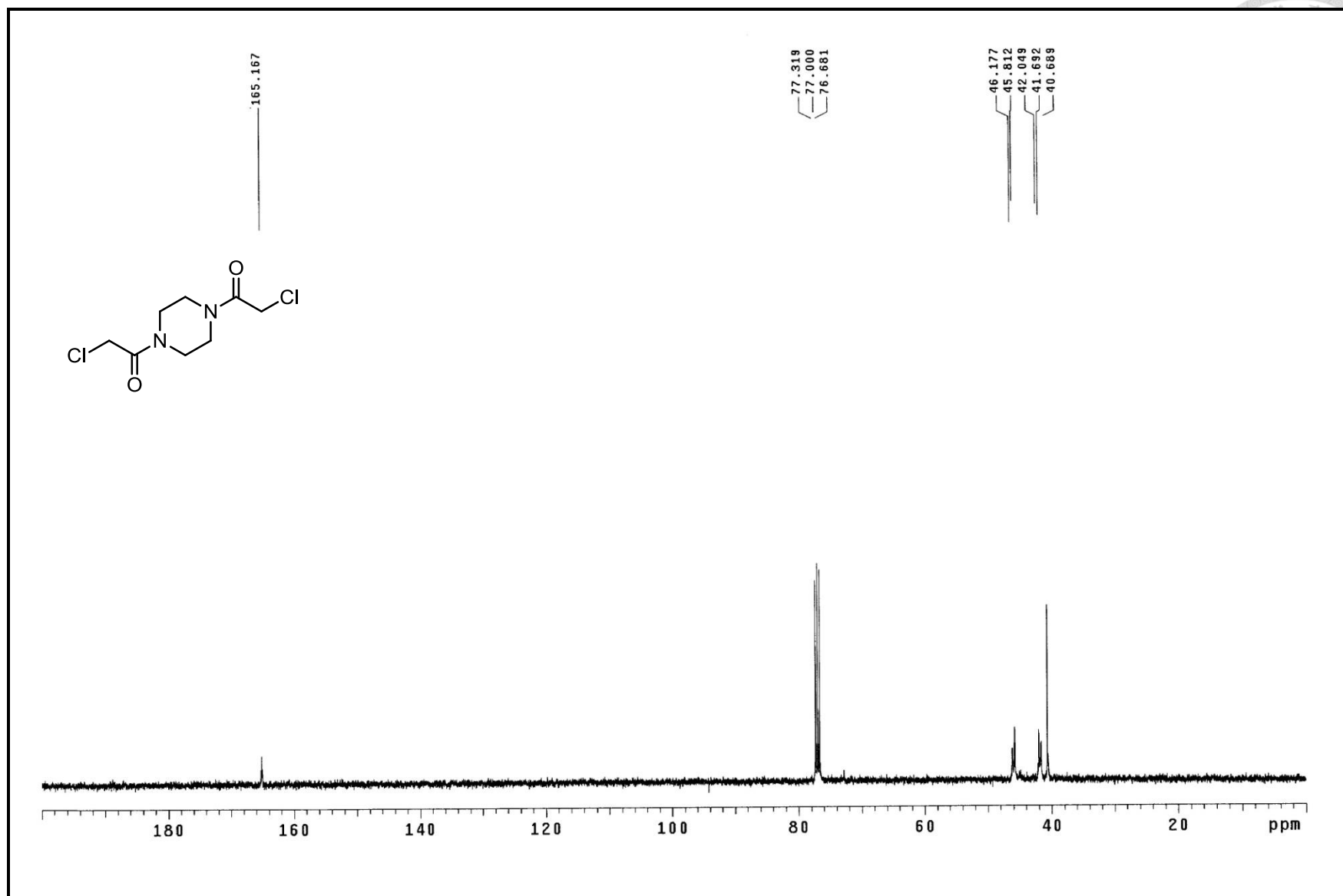
^1H NMR spectrum of compound **35** (400MHz, $\text{DMSO-}d_6$)



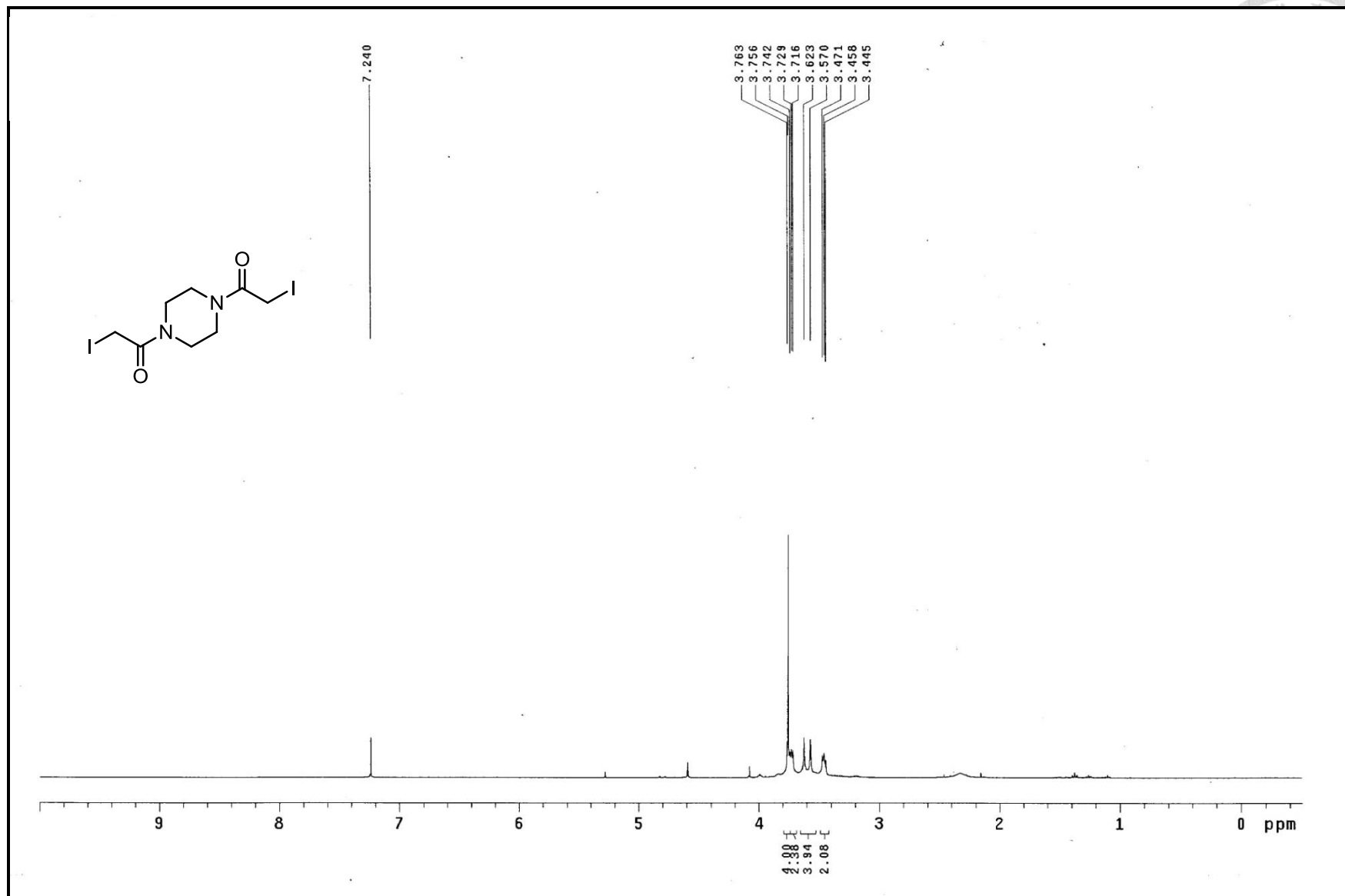
^{13}C NMR spectrum of compound **35** (100MHz, DMSO- d_6)



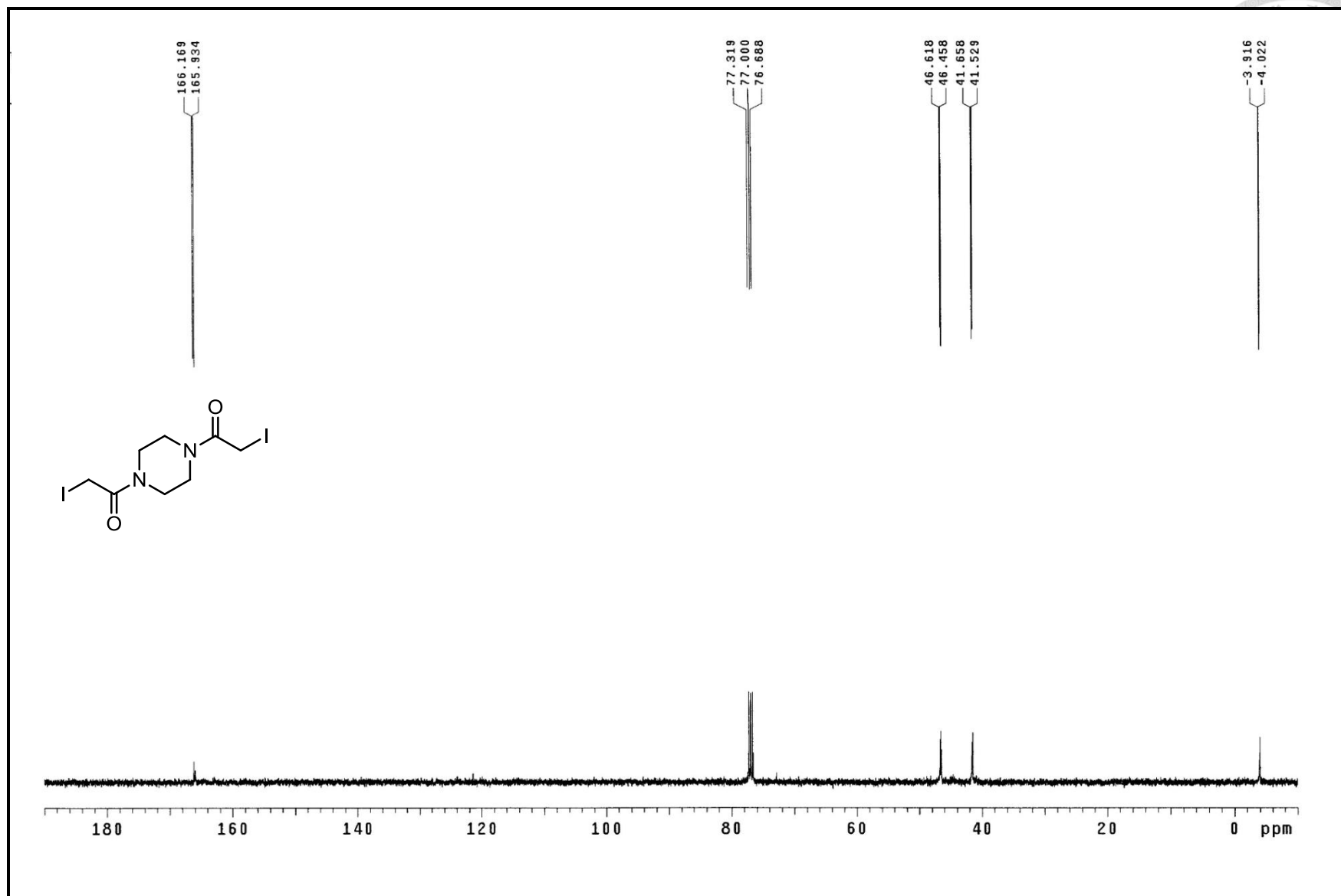
^1H NMR spectrum of compound **36** (400MHz, CDCl_3)



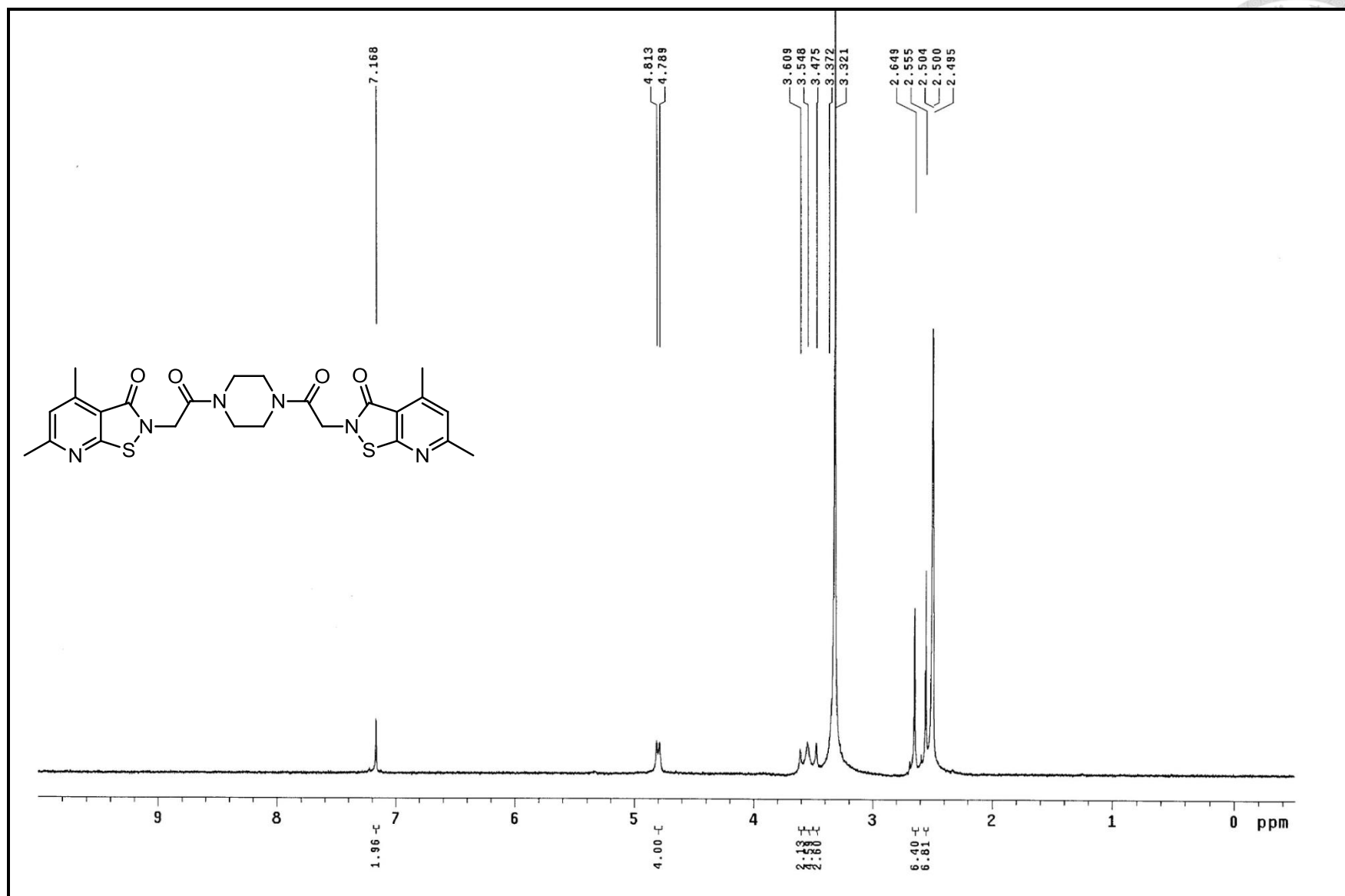
^{13}C NMR spectrum of compound **36** (100MHz, CDCl_3)



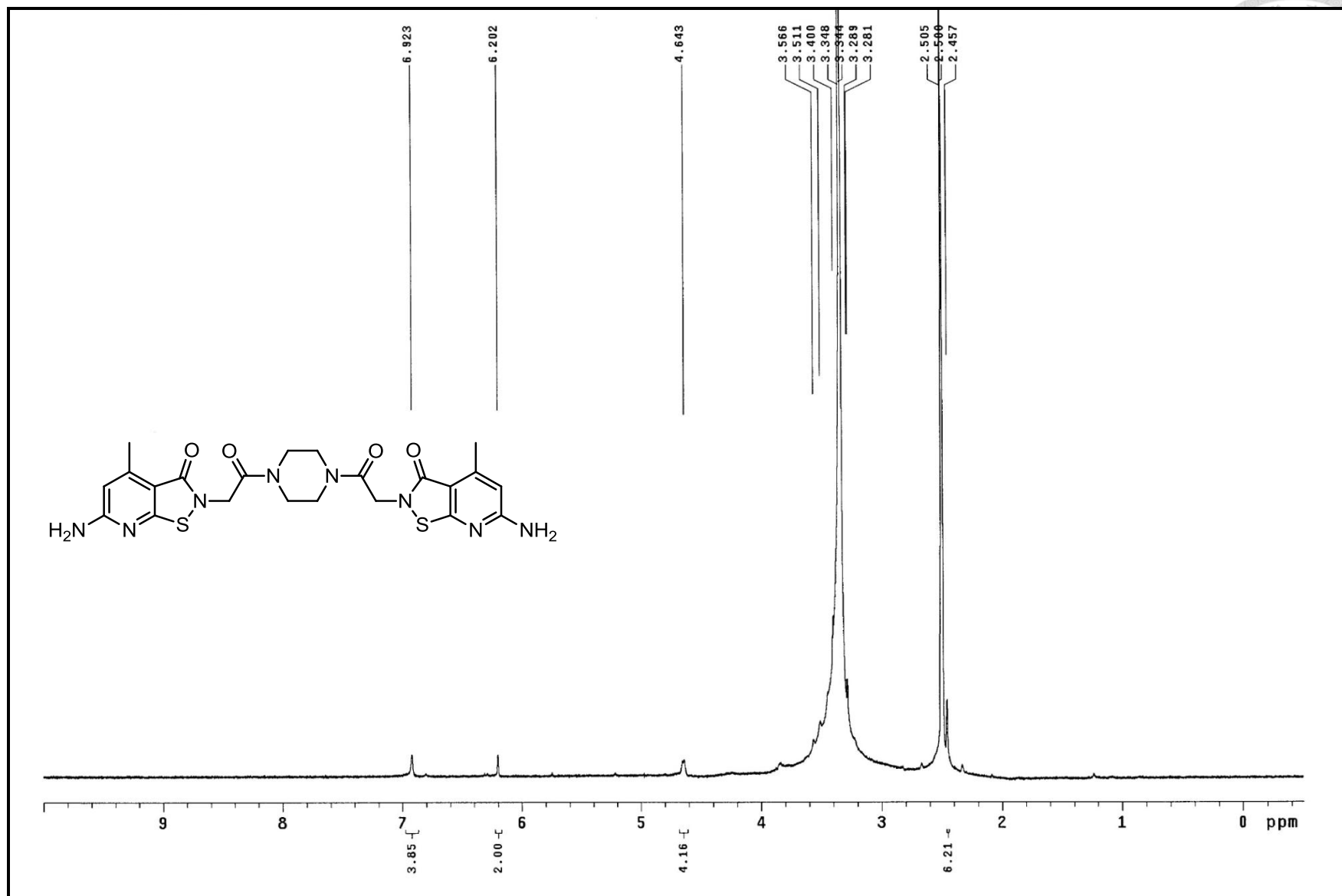
^1H NMR spectrum of compound **37** (400MHz, CDCl_3)



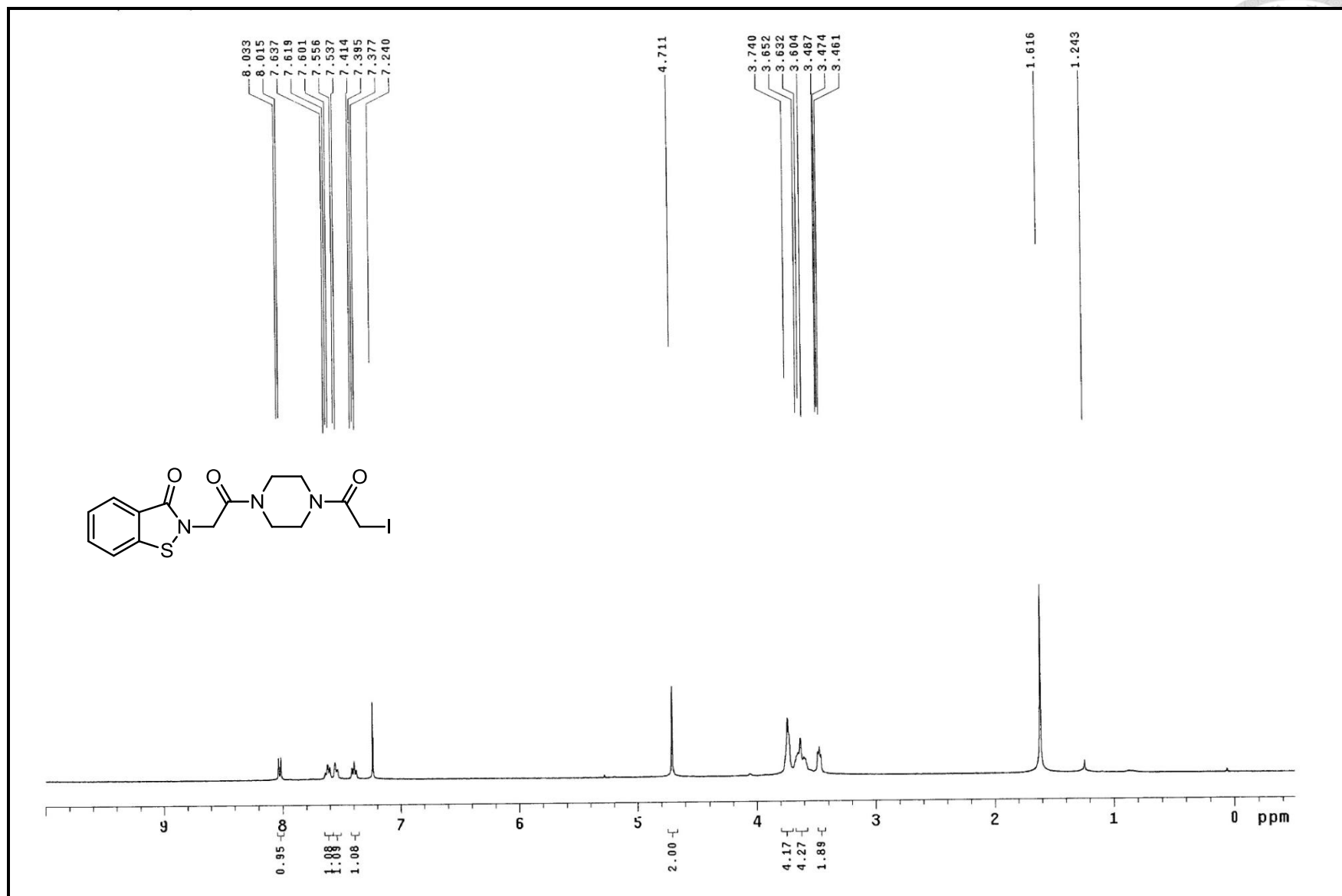
^{13}C NMR spectrum of compound **37** (100MHz, CDCl_3)



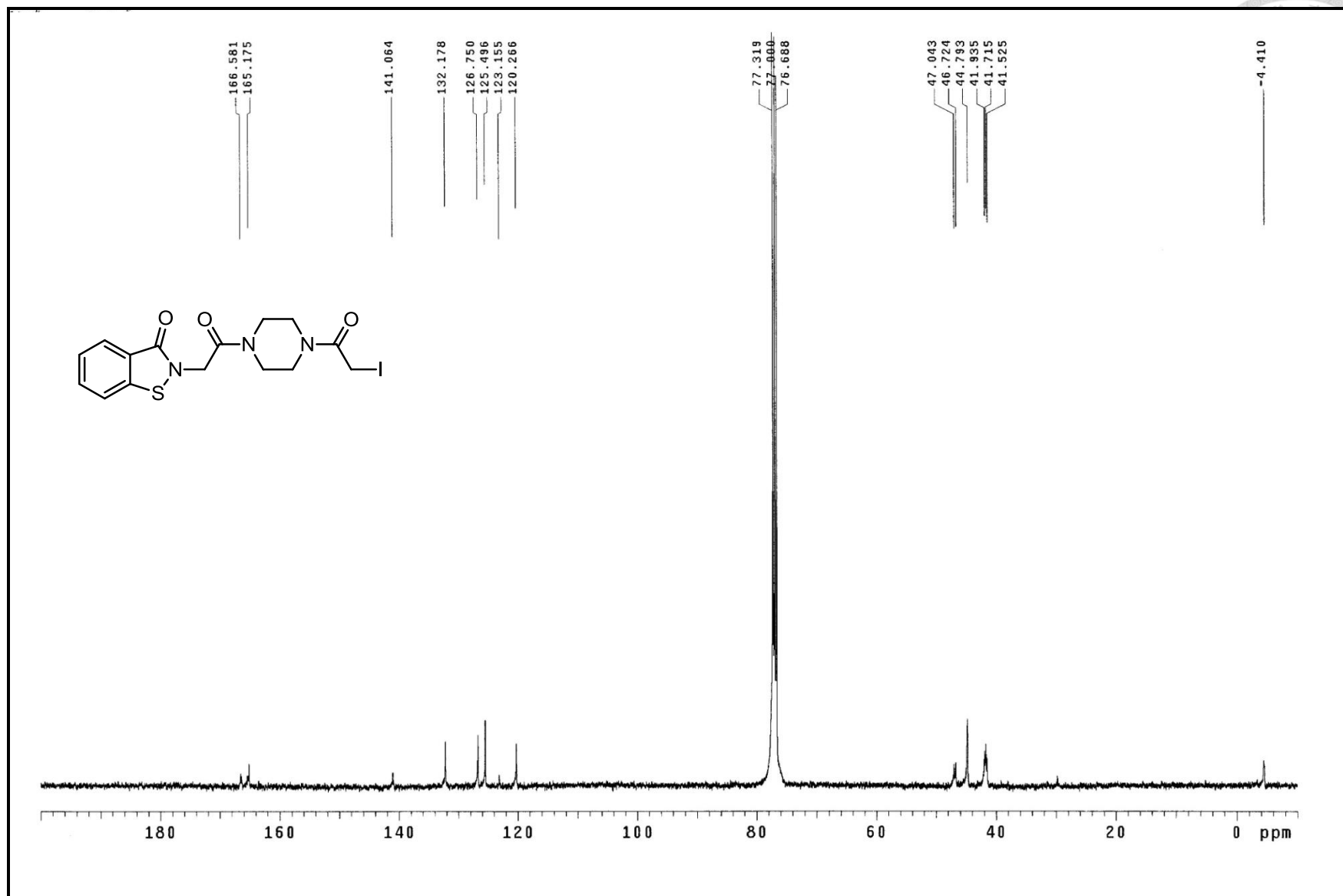
^1H NMR spectrum of compound **38** (400MHz, $\text{DMSO-}d_6$)



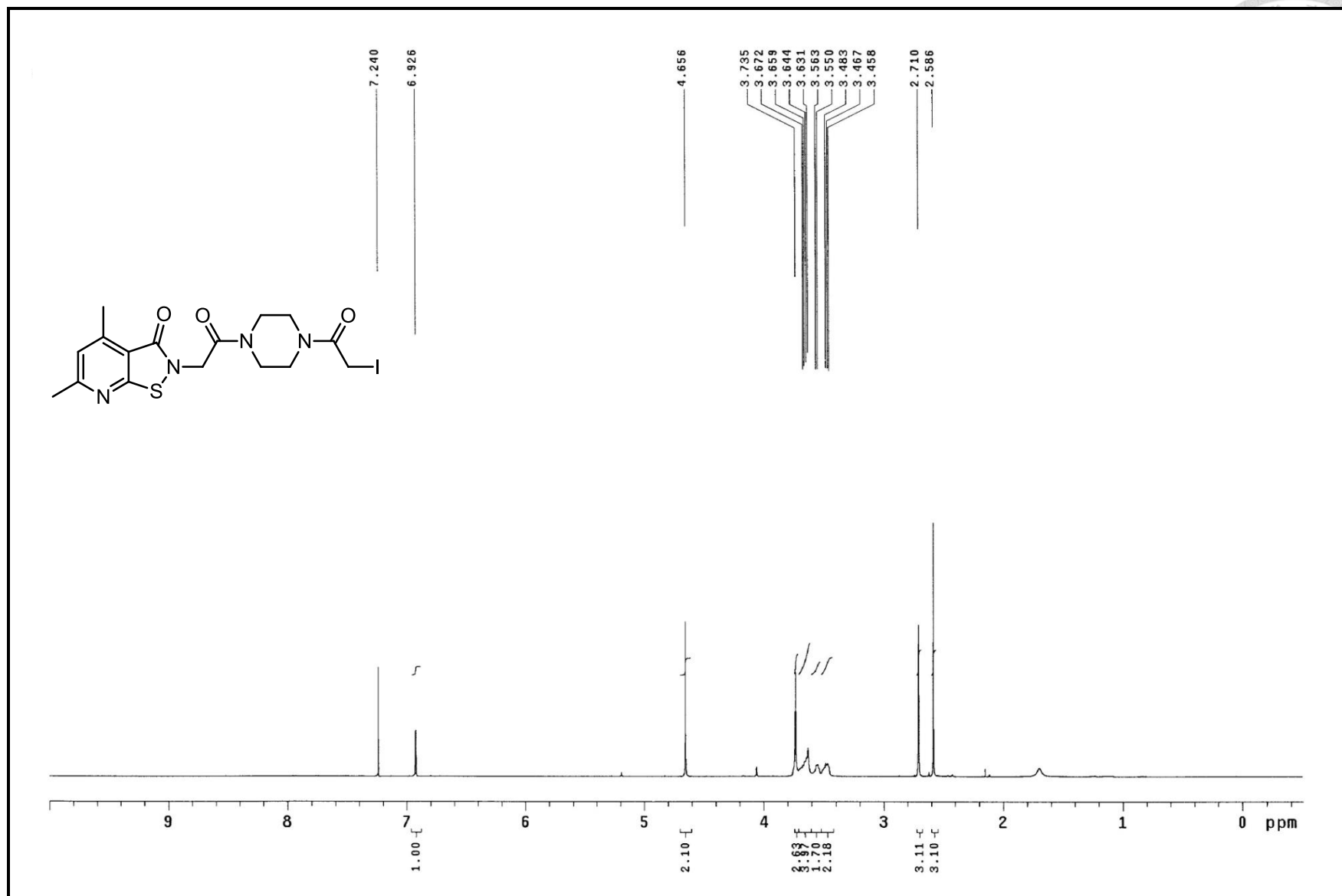
^1H NMR spectrum of compound **39** (400MHz, $\text{DMSO-}d_6$)



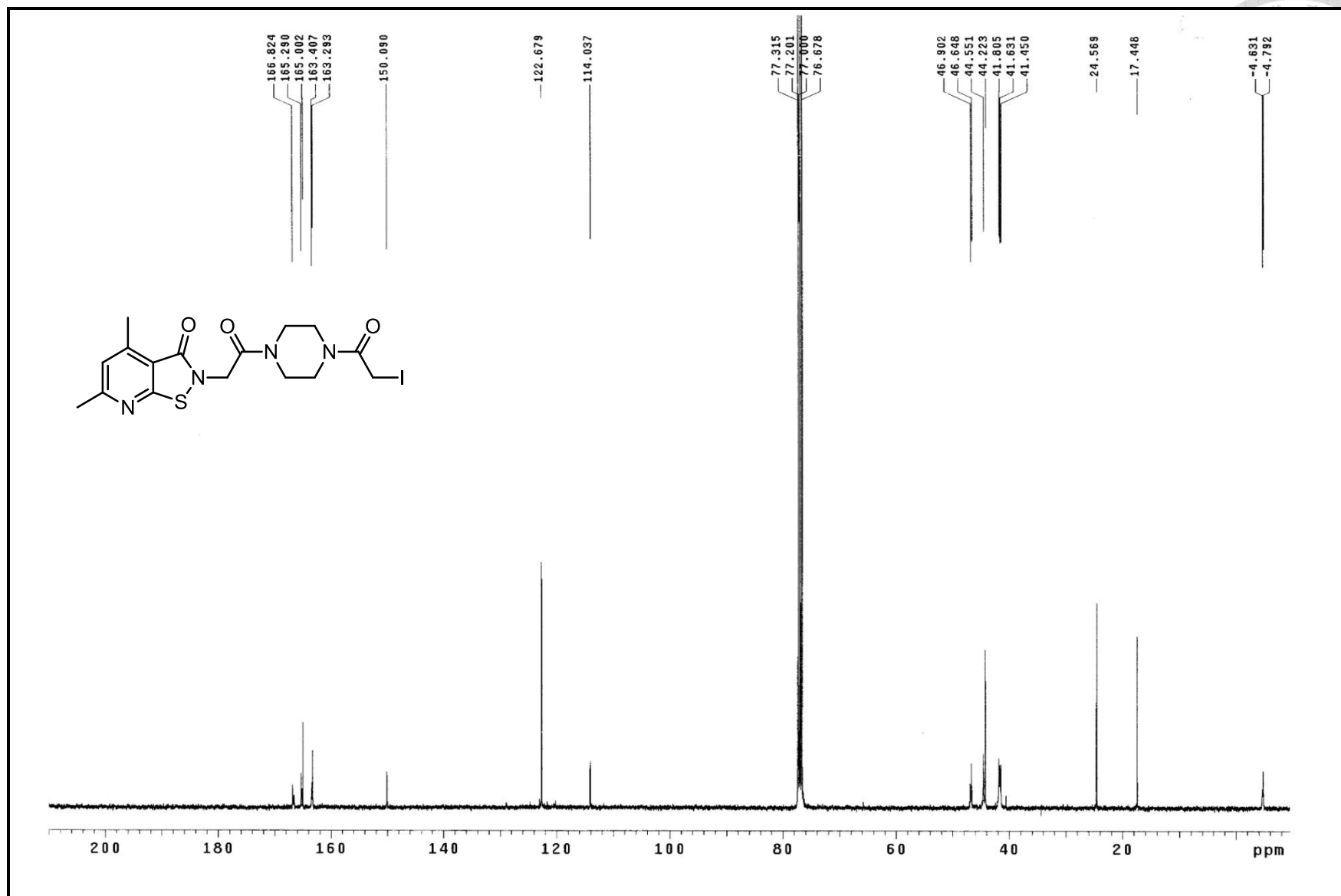
¹H NMR spectrum of compound **40** (400MHz, CDCl₃)



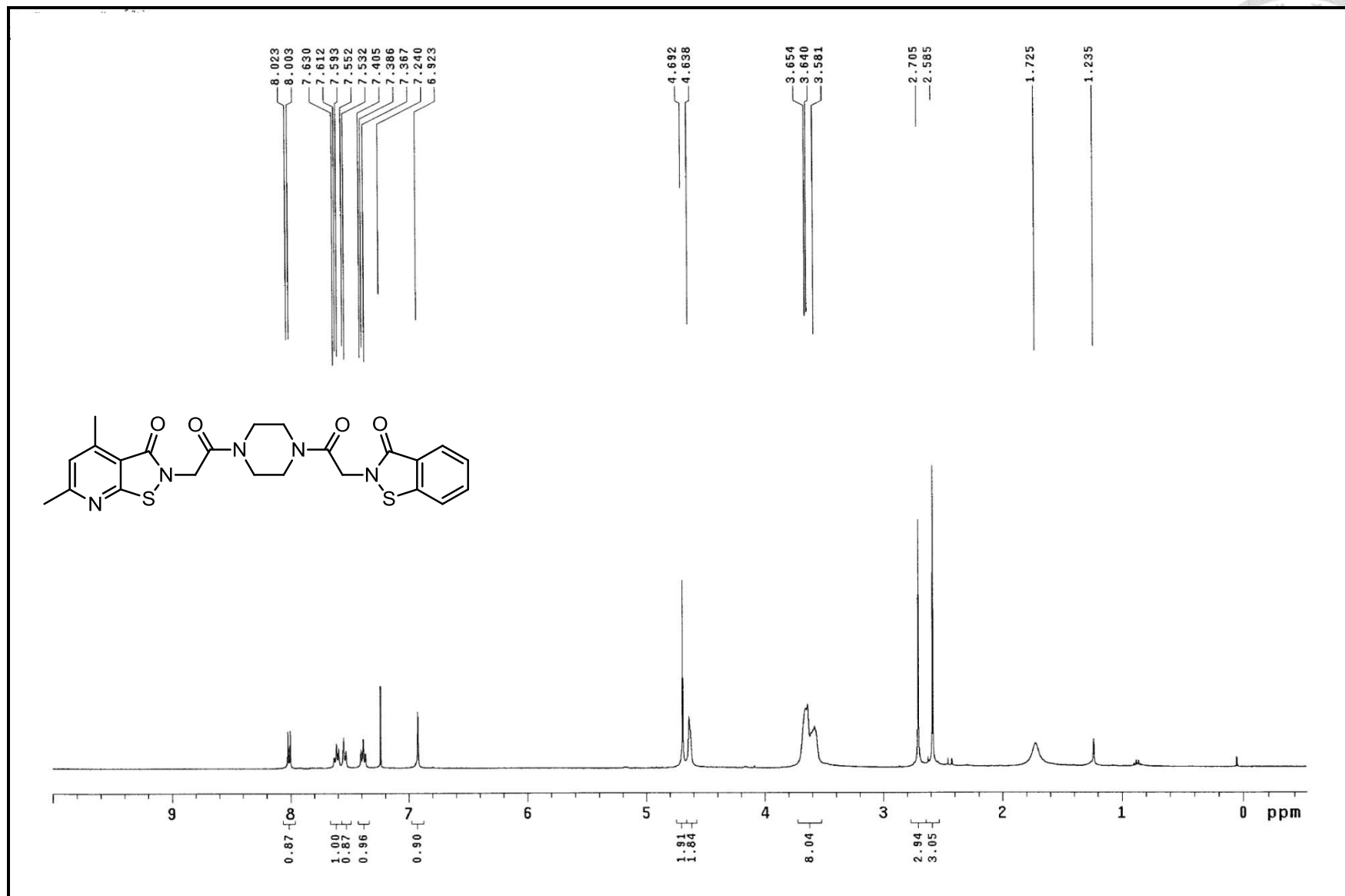
^{13}C NMR spectrum of compound **40** (100MHz, CDCl_3)



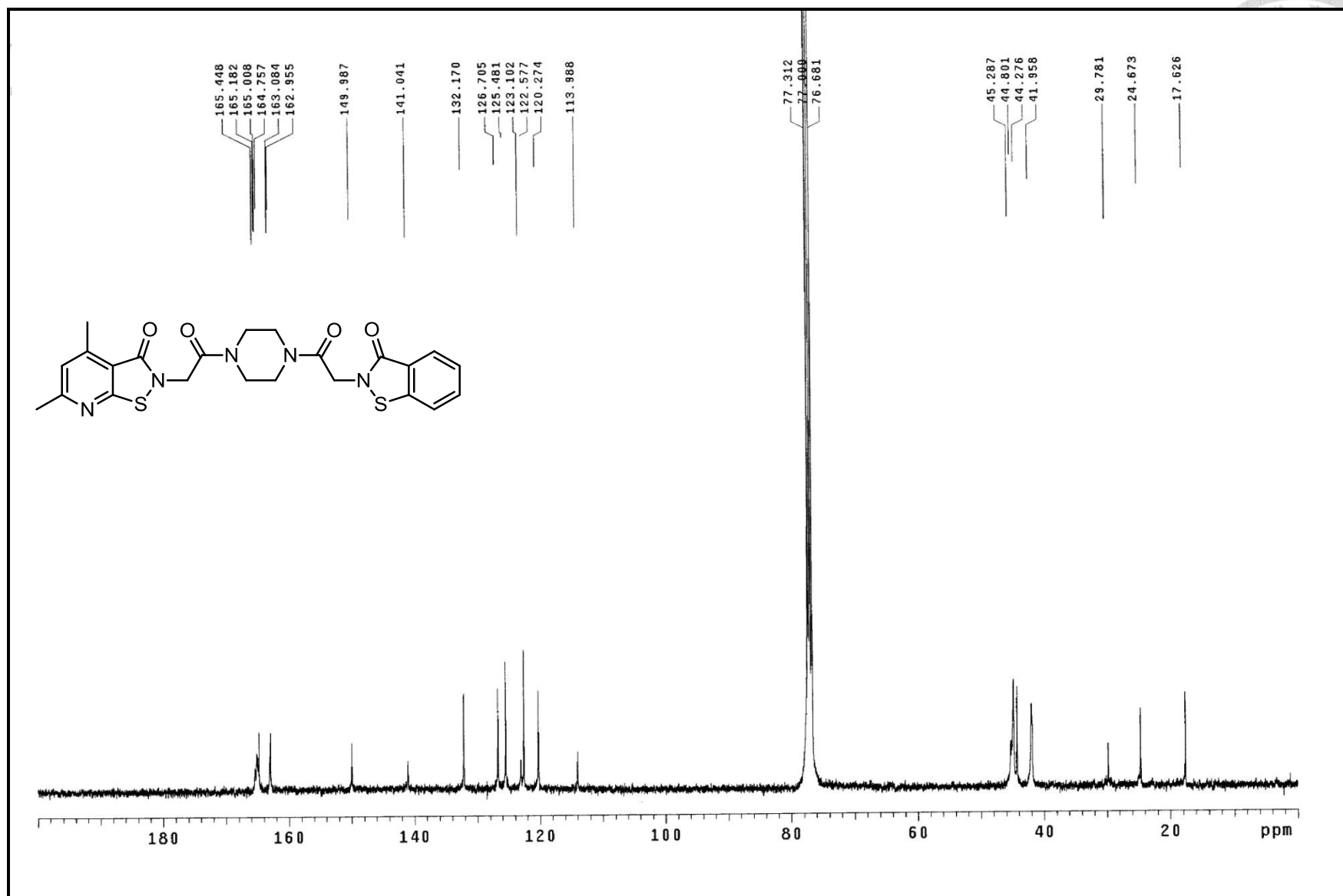
^1H NMR spectrum of compound **41** (400MHz, CDCl_3)



^{13}C NMR spectrum of compound **41** (100MHz, CDCl_3)



¹H NMR spectrum of compound **42** (400MHz, CDCl₃)



^{13}C NMR spectrum of compound **42** (400MHz, CDCl_3)